FAKULTÄT FÜR MEDIZIN
DER TECHNISCHEN UNIVERSITÄT MÜNCHEN
INSTITUT FÜR PHARMAKOLOGIE UND TOXIKOLOGIE

Molecular and computational characterization of microRNA/target interactions

ANDREA RINCK

Vollständiger Abdruck der von der Fakultät für Medizin der Technischen Universität München zur Erlangung des akademischen Grades eines

DOKTORS DER NATURWISSENSCHAFTEN (DR. RER. NAT.)

genehmigten Dissertation.

VORSITZENDER:

Univ.-Prof. Dr. Heribert Schunkert

PRÜFER DER DISSERTATION:

Univ.-Prof. Dr. Dr. Stefan Engelhardt
Univ.-Prof. Dr. Dr. Fabian J. Theis

Die Dissertation wurde am 04.12.2014 bei der Technischen Universität München eingereicht und durch die Fakultät für Medizin am 11.03.2015 angenommen.

Voici mon secret. Il est très simple:
on ne voit bien qu'avec le cœur.
L'essentiel est invisible pour les yeux.

— Antoine de Saint Exupéry [81]

ABSTRACT

MicroRNAs (miRNAs) are endogenous small non-coding RNAs with the potential to post-transcriptionally regulate hundreds of target genes. Upon loading into an Argonaute effector protein, they guide the so-called 'miRNA-Induced Silencing Complex (miRISC)' to binding sites on corresponding target messenger RNAs (mRNAs). Due to their pivotal role in the coordination of virtually all cellular processes, miRNAs have evolved as interesting therapeutic targets. However, they often function in multiple biological pathways within different tissues or cells and are dynamically regulated over time. To develop novel diagnostic and therapeutic strategies, profound knowledge of context-dependent miRNA functions is required. The key to understand the cellular roles of disease-related miRNAs is to identify the complete set of target genes each miRNA regulates. Unfortunately, target gene identification is challenging. In animals, miRNA/mRNA annealing is often limited to short stretches of complementary pairing, leading to incorrect computational target prediction. As the miRNA-mediated effect on a particular target is generally modest, experimental approaches need to identify the whole phenotype-defining network of regulated targets rather than individual miRNA/mRNA pairs. Biochemical methods based on UV Cross-Linking and ImmunoPrecipitation (CLIP) of protein/RNA complexes in living cells have enabled transcriptome-wide probing of high confidence miRISC/target interactions at nucleotide resolution.

This work aimed at combining experimental identification of heart-specific targets of important miRNA candidates with theoretical analysis of the general concept of miRISC cooperativity to generate further insight into the role of miRNAs and the mechanistic details of miRNA-mediated targeting in cardiac biology and disease.

In the experimental part, comprehensive Argonaute CLIP methods were applied to the cardiac system. The Photo-Activatable Ribonucleoside enhanced-CLIP (PAR-CLIP) protocol was adapted to adult rat primary myocardial cells and human whole heart tissue cultures as starting material. It was demonstrated that cultivatable human tissue slices are in principle accessible for PAR-CLIP studies, providing an optimistic outlook for future projects.

The computational part was based on previous reports of amplified target repression for adjacent miRISC binding sites. As a starting point, a global inter-site distance analysis was conducted on published data of predicted as well as experimentally identified target sites. The obtained distance distributions revealed an enrichment of adjacent binding sites when compared to two control models. Furthermore, the fraction of targets featuring miRISC sites in a binding cooperativity-permitting distance was increased for co-expressed or co-regulated miRNAs.

In summary, the combination of molecular and computational approaches for characterizing miRNA/target interactions represents a profound step towards understanding cardiac miRNA function as the fundament for developing new miRNA-based diagnostic and therapeutic strategies.

CONTENTS

INTERDEPENDENCY OF THE CHAPTERS

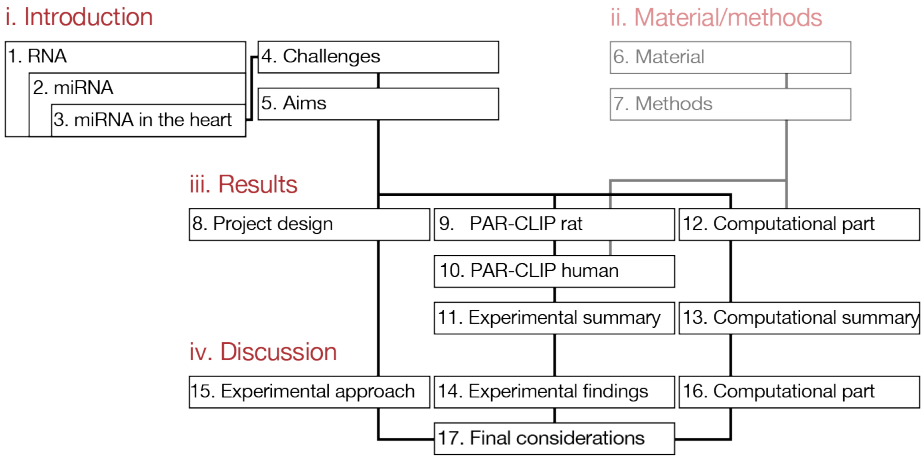

FIGURE 0.1. Graphical overview of the structural interdependency of parts (red) and chapters (black) of the thesis to facilitate navigation through the work.

LIST OF FIGURES

LIST OF TABLES

ACRONYMS

3′-UTR	three prime end UnTranslated Region
4SU	4-thio(S)-Uridine
6SG	6-thio(S)-Guanine
A	Adenosine
AAV	Adeno-Associated Virus
AM	Adult Mouse
AMCF	Adult Mouse Cardiac Fibroblasts
AMCM	Adult Mouse Cardiac Myocytes
AMO	Anti-MiRNA Oligonucleotides
AR	Adult Rat
ARCF	Adult Rat Cardiac Fibroblasts
ARCM	Adult Rat Cardiac Myocytes
C	Cytidine
cDNA	complementary DNA
CF	Cardiac Fibroblasts
circRNA	circular RNA
CLASH	Cross-linking, Ligation And Sequencing of Hybrids
CLIP	Cross-Linking and ImmunoPrecipitation
CM	Cardiac Myocytes
DGCR8	DiGeorge syndrome critical region gene 8
DNA	DeoxyriboNucleic Acid
dsRNA	double-stranded RNA
EC	Endothelial Cells
ECL	Enhanced ChemiLuminescence
eRNA	enhancer RNA
G	Guanosine
HITS-CLIP	HIgh-Throughput Sequencing of RNA isolated by CLIP
HPLC	High-Performance Liquid Chromatography
i.p.	intra-peritoneal injection
iCLIP	individual nucleotide resolution CLIP
IP	ImmunoPrecipitation
kb	kilobases
kDa	kiloDaltons
LNA	Locked Nucleic Acid

lncRNA	long non-coding RNA
miRISC	miRNA-Induced Silencing Complex
miRNA	microRNA
mRNA	messenger RNA
ncRNA	non-coding RNA
nm	nanometers
ORF	Open Reading Frame
PABP	Poly(A)-Binding Protein
PAR-CLIP	Photo-Activatable Ribonucleoside enhanced-CLIP
PCR	Polymerase Chain Reaction
piRNA	PIWI-interacting RNA
PLS	Photo-Stimulated Luminescence image
PNK	PolyNucleotide Kinase
pre-miRNA	precursor miRNA
pri-miRNA	primary miRNA
RBP	RNA Binding Protein
RNA	RiboNucleic Acid
RNAi	RNA interference
RNP	RiboNucleoProtein
rRNA	ribosomal RNA
RT	Reverse Transcription
SDS-PAGE	Sodium Dodecyl Sulfate PolyAcrylamide Gel Electrophoresis
SILAC	Stable Isotope Labeling with Amino acids in Cell culture
siRNA	small interfering RNA
snoRNA	small nucleolar RNA
snRNA	small nuclear RNA
T	Thymidine
TNRC6	Tri-Nucleotide Repeat-Containing proteins 6
tRNA	transfer RNA
U	Uridine
UV	UltraViolet
XPO_5	eXPOrtin-5

I

INTRODUCTION

1 FIRST INSIGHT INTO THE RNA UNIVERSE

Only about three decades ago, RiboNucleic Acid (RNA) was considered merely a template of DeoxyriboNucleic Acid (DNA) needed to convey genetic information into proteins.
This first chapter points at the fact that RNAs are now also recognized as functional end products in themselves, which control and coordinate almost every cellular process [250]. Not only did the unanticipated discovery that RNAs can act as both genetic material and enzymes [225, 145] revive the RNA world hypothesis [137], but also advanced technologies continue to reveal the enormous diversity of the still expanding RNA universe [157].

1.1 RIBONUCLEIC ACID

RNA belongs, together with DNA and protein, to the three major macromolecules that provide the basis for all known forms of life. It is usually transcribed from a DNA template by RNA polymerases, forming a mainly single-stranded polymer of nucleotides, which very often undergoes post-transcriptional modification.
Rooting from bacterial molecular genetics, genes were long used synonymously with proteins, and RNA was presumed to only take the role of a transitional intermediate state between those two. Thereby a DNA gene is transcribed into messenger RNA (mRNA), which then carries the genetic information to the ribosome, where the nucleotide sequence is translated into an amino acid chain of the corresponding protein.
However, RNAs are a large family of molecules performing versatile and vital roles within the cell. They started to expand their status with the discovery of catalytic RNAs (ribozymes). The discovery of endogenous RNA interference (RNAi) (see Section 1.2) and the still ongoing detection of new members of the non-coding RNA (ncRNA) family emphasizes their versatility and importance for cellular processes.

1.2 RNA INTERFERENCE

Early studies indicated that introducing antisense RNA into a plant cell could lead to transcriptional inhibition of the respective target gene [101]. Another phenotypic description of RNA-mediated gene silencing were unexpected outcomes in experiments performed in *Petunia hybrida* [301]. The researchers overexpressed chalcone synthase, a key enzyme for flower pigmentation, and expected darkening of the normally violet blossoms. However, the introduced transgene blocked pigmentation, resulting in variegated pigmentation with fully or partially white petunias. This indicates that chalcone synthase activ-

ity had been substantially decreased. However, both research groups did not understand the process by which this had happened.
In 1998, Fire, Mello (both shared the 2006 Nobel Prize in Physiology/Medicine for their discovery) and colleagues studied the specific requirements for antisense RNA activity in the nematode worm *Caenorhabditis elegans* [124]. They discovered that, in response to introducing double-stranded RNA (dsRNA), sequence-specific gene silencing results in reduction of both mRNA and protein levels. The phenomenon was called RNA interference (RNAi). Unexpectedly, only few dsRNA molecules per cell were able to systemically silence gene expression throughout the whole worm. Moreover, the effect also persisted into the progeny of the injected animals.
The term 'RNAi' became commonly used after a publication of Tuschl and colleagues in 2001 [104]. Using an *in vitro* system of *Drosophila melanogaster*, they could show that 21 and 22 nucleotides long dsRNAs with short 3'-overhangs, which they referred to as small interfering RNA (siRNA) (see Section 1.3), are sequence-specific mediators of target mRNA degradation.
RNAi might have evolved as a cellular defense mechanism against invading nucleotide sequences such as RNA viruses. During their replication, they temporarily exist in a dsRNA-form. This intermediate would trigger RNAi and thereby inactivate the expression of virus genes. Later it was shown that also dsRNA of endogenous origin can generate siRNA (endo-siRNA), which was able to silence selfish genetic elements, called transposons, and to regulate gene expression during development in both, plants and animals [7, 411, 2, 118]. Transposons spread by forming additional copies of themselves within the genome which sometimes causes mutations that can lead to cancer or other diseases. Similar to RNA viruses, transposons can take on a dsRNA-form that would trigger RNAi to arrest the potentially harmful jumping. Thus, RNAi could further have developed as a way to combat the potentially detrimental spread of transposons.
Another class of endogenous small non-coding RNA (see Section 1.3), called microRNA (miRNA), has been found to confer target degradation, similar to RNAi. However, upon incorporation into a comparable silencing complex, miRNAs do not only cleave, but also (and more often) repress the translation and induce exonucleolytic degradation of their target RNAs [22] (see Section 2).
RNAi and miRNA-mediated gene silencing have soon become valuable tools in research and therapy. For instance, the introduction of synthetic siRNAs into cells offers an effective way to selectively and robustly repress specific target genes of interest. Conversely, introducing, e. g., miRNA inhibitors may lead to a release of specific targets from miRNA-mediated repression [95, 26, 287, 431, 55].

1.3 NON-CODING RNA

High-throughput transcriptome analyses disclosed that, while about 90% of eukaryotic genomes are transcribed [75], only 1 to 2% of all transcriptional output is protein-coding [272]. Thus, the majority of cellular transcripts are either fragments spliced out in the process of mRNA maturation or they are copies of

their own RNA genes. Both are referred to as non-coding RNA (ncRNA).
The plethora of ncRNAs can be functionally classified into infrastructural and regulatory ncRNA [200].
The most prominent examples of infrastructural ncRNA are transfer RNA (tRNA) and ribosomal RNA (rRNA), which perform housekeeping functions during the process of mRNA translation (see Figure 1.1A). Other examples are small nuclear RNA (snRNA), which was identified as component of spliceosomal RiboNucleoProtein (RNP) complexes [53] and small nucleolar RNA (snoRNA), which was isolated from nucleoli and attributed roles in rRNA processing or modification [106].
Prominent representatives of regulatory ncRNAs are miRNA, siRNA, PIWI-interacting RNA (piRNA), circular RNA (circRNA), and long non-coding RNA (lncRNA) (see Figure 1.1B and below). In addition to infrastructural and regulatory ncRNAs, a novel class of promoter-associated RNA (PAR) and enhancer RNA (eRNA) has been described [82, 212, 307].
However, hardly all members of the stated groups have been identified yet and new classes of ncRNA continue to be discovered.

MIRNA The first miRNA was discovered in 1993 as *lin-4* regulatory RNA in *Caenorhabditis elegans* [241]. The authors found that the 22 nucleotides *lin-4* is processed from a 61 nucleotides precursor RNA and contains sequences that are partially complementary to multiple sites in the three prime end UnTranslated Region (3′-UTR) of mRNA *lin-14*. 3′-UTRs can extend over several kilobases (kb) and generally contain binding sites for various regulators acting in a dynamic and combinatorial way to control, e. g., mRNA translation, localization, and stability. It was shown that miRNA *lin-4* negatively regulates two identified target genes, *lin-14* [426] and *lin-28* [294]. It took seven years until a second miRNA, *let-7*, was characterized [338] and soon found to be highly conserved among bilaterally symmetrical animals [320], indicating a more general phenomenon of miRNA-mediated target gene regulation. Since then, the number of known miRNAs has escalated exponentially and constituted a rapidly evolving new research area. Only one year later, the presence of large numbers of miRNAs in *Caenorhabditis elegans* [240, 238], invertebrates and vertebrates [233] was reported. Release 20 (June 2013) of the miRNA database *miRBase* [222] holds over 30,000 mature miRNA sequences from about 200 species. MiRNAs are transcribed as longer hairpin structured precursors which undergo consecutive processing [30, 242]. Mature miRNAs are between 20 and 24 nucleotides in length. They interact with AGO proteins to form the miRNA-Induced Silencing Complex (miRISC), which, in the classical view, binds within the 3′-UTR of a target mRNA, leading to its translational repression or degradation [241, 426, 179].

SIRNA As mentioned above, siRNAs were first observed in plants [101, 301, 155] and the canonical siRNA is a perfectly complementary dsRNA of 20 to 24 nucleotides. In mammals, the afore named endo-siRNAs have only been found in mouse oocytes and embryonic stem cells [17, 387, 378].

PIRNA PIWI-associated small RNA were first discovered as repeat-associated siRNA (rasiRNA) in *Drosophila melanogaster*, possessing complementarity to a

variety of transposable and repetitive elements [13, 12]. Evolutionary conservation of this type of ncRNA was demonstrated by identification of rasi-like RNA in testes and ovaries of zebrafish [170]. Also in mammalian testes, small RNA interacting with PIWI proteins were revealed and termed piRNA [214]. Although there are some substantial differences between rasiRNA and piRNA, they are both referred to as piRNA with rasiRNA being one specialized subclass [11]. Generally, they are about 24 to 31 nucleotides long and carry a uridine 5'-end as well as a 2'-O-methyl modification at the nucleotide of the 3'-terminus [371]. The primary function of piRNAs has been supposed to lie in the suppression of transposon activity during germ line development [48, 146].

CIRCRNA Early occasional evidence for the formation of circular RNAs, often thought to represent transcriptional noise or artifacts, has recently been overrun by the demonstration of their widespread and substantial presence within eukaryotic transcriptomes [353, 188, 280, 352, 445]. Even though the often detected evolutionary conservation of circRNA speaks in favor of relevant cellular functions of these covalently closed RNA loops, evidence as to their exact mechanisms of action is still missing. First steps were made by the discovery of circRNAs acting as competitive miRNA inhibitors [158, 280]. Further plausible functions include a role as delivery vehicle for miRNA or RNA Binding Protein (RBP) [159], they could be involved in the storage, sorting or assembly of RBP, act as a kind of an allosteric group, directly regulate mRNA expression by partial base pairing or even form a template for translation into proteins themselves [165].

LNCRNA The majority of ncRNA belong to the group of long non-coding RNA, which are to some extent arbitrarily distinguished from the small ncRNAs (miRNAs, siRNAs, and piRNAs) by possessing a length larger than 200 nucleotides [329]. One of the most well-described examples of lncRNAs is the human X(Inactive)-Specific Transcript (*XIST*), which has been attributed a role in chromatin structure mediating X-chromosome inactivation [16].

Although proteins, derived from the Greek word *proteios* for 'primary', are the chief actors within the cell, the basis of eukaryotic complexity and phenotypic versatility may lie primarily in the highly regulated networks established by ncRNA. In particular, whereas the proteomes of higher organisms have remained relatively static, the amount of non-coding sequences and the complexity of the organism seem to possess a direct dependency [5]. It is therefore a prime goal of contemporary molecular biology to further identify and understand the regulatory roles of ncRNA. The pathways of the three major classes of small ncRNA, miRNA, siRNA and piRNA, are intertwined in that they cross-regulate each other and share or compete for common substrates or effectors at several levels [136].

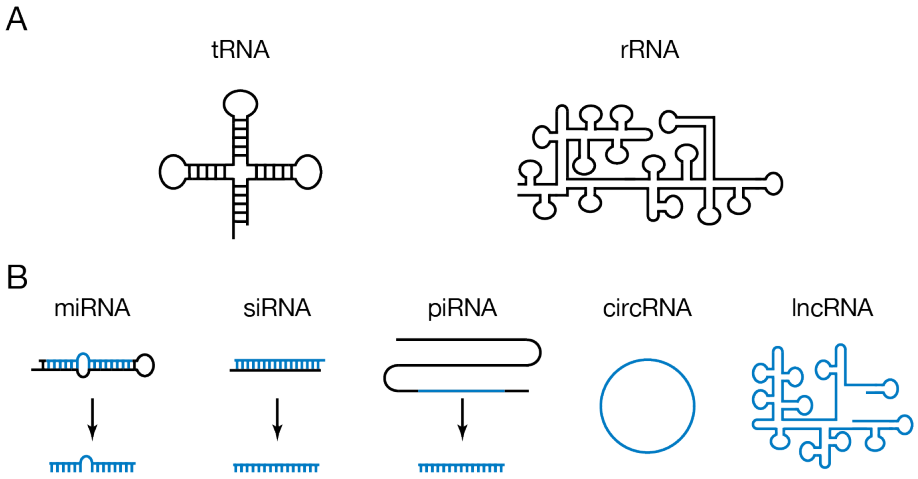

FIGURE 1.1. Classification of exemplary non-coding RNA species. A: infrastructural non-coding RNA, transfer RNA (tRNA), ribosomal RNA (rRNA); B: regulatory non-coding RNA, microRNA (miRNA), small interfering RNA (siRNA), PIWI-interacting (piRNA), circular RNA (circRNA), long non-coding RNA (lncRNA).

1.4 MIRNAS, THE OBJECTS OF INVESTIGATION

The present thesis focuses predominantly on the miRNA pathway. In mammals, miRNAs have been predicted to post-transcriptionally regulate (and thereby generally repress) more than 50% of all mRNAs [127, 224]. Due to the sequential production of proteins, with first gene transcription into mRNA and second mRNA translation into an amino acid sequence, a block in protein synthesis lags behind a block in gene transcription. Even if the mRNA supplies are cut off, transcripts that have been synthesized already can still be translated. In contrast, miRNA can stop protein production very rapidly and may even have the potential to reverse the translational repression if the protein is needed again [143]. Besides the promptness of the response, the often short and imprecise nature of target hybridization enables individual miRNAs to target transcripts coding for different proteins acting within the same or related metabolic pathways. Thereby they receive the potential to coordinate cellular processes at a higher level. This circumvents the need for transcriptional regulation of each individual gene and facilitates synchronization of the repressive effects. Further, multiple miRNAs targeting the same transcript, might fine-tune its expression. They thereby establish a buffering system guarding gene expression and conveying robustness to cellular homeostasis. Thus, investigating their cellular roles and the mechanistic details of target regulation will help to unveil the complexity of post-transcriptional gene regulation and reach a molecular understanding of phenotypic observations.

2 CURRENT KNOWLEDGE ON MIRNA BIOLOGY

Since their discovery about 20 years ago, miRNA research has brought to light profound knowledge about their genomics, biogenesis, regulation, and biological function.
The present chapter aims to summarize generally accepted concepts and to introduce key players involved in animal miRNA-mediated target silencing.

2.1 MIRNAS: ENDOGENOUSLY SYNTHESIZED SINGLE-STRANDS

Proper maturation of miRNAs as well as their correct assembly into the miRISC (see Section 2.2) are among the key steps in miRNA-mediated gene silencing allowing them to act as guides leading the miRISC effector to available target transcripts.
Canonical miRNA biogenesis starts in the nucleus, where they are encoded in the genome as intergenic long non-coding transcripts or as part of protein-coding host genes (see Figure 2.1). According to their intragenic location, the latter may be further divided into intronic, exonic, 3'-UTR, and 5'-UTR miRNA. The majority belongs to intergenic as well as to intronic encoded miRNAs [421]. Hence, most miRNAs are transcribed either independently or as part of their hosting protein-coding transcripts by RNA polymerase II or III [244, 42]. Initial transcripts of intergenic miRNAs can reach over 1,000 nucleotides in length, are 5'-capped, spliced, and poly-adenylated [77, 213]. They are termed primary miRNA (pri-miRNA) and contain single or clustered double-stranded hairpins with distal loops [351]. The generation of mature miRNAs occurs in two steps. First, the pri-miRNA is endonucleolytically cropped by the so-called 'Microprocessor' resulting in an approximately 65 to 70 nucleotides long stem loop precursor miRNA (pre-miRNA) (see Figure 2.1). The Microprocessor complex comprises the RNase III enzyme 'Drosha' (DROSHA) and the dsRNA binding protein DiGeorge syndrome critical region gene 8 (DGCR8). DGCR8 recognizes junctions of stem and single-stranded regions on the pri-miRNA. As kind of a molecular ruler, it helps to position DROSHA for endonucleolytic cleavage of the stem about 11 nucleotides from the junction [156]. After nuclear processing, the pre-miRNA associates with the transport receptor eXPOrtin-5 (XPO_5) in complex with RAN/GTP. This GTPase facilitates the export through nuclear pores into the cytoplasm and may also protect the pre-miRNA against nuclear digestion [438, 38, 264]. In the cytoplasm, the precursor has to undergo a second processing step before it can be assembled into the miRISC and guide it to its mRNA targets. Both, processing and loading are accomplished by the 'RISC Loading Complex' (RLC, see Figure 2.1). It consists of another RNase III family enzyme called 'Dicer' (DICER1), the dsRNA-binding domain proteins TARBP2P (also known as TRBP) and/or PRKRA (also known as PACT), and one of the AGO clade Argonaute proteins [141, 148, 243, 267].

The exported pre-miRNA only joins the RLC after assembly of a ternary complex consisting of DICER1, TARBP2P and AGO [268]. Deletion of DICER1 decreases or abolishes miRNA biogenesis [177] with lethal consequences [31]. DICER1 is a large endoribonuclease, which contains two different RNA-binding sites. One of them was shown to position long dsRNA for cleavage and the other one to re-bind the cropped duplex after cleavage, assisted by TARBP2P [304]. Cleavage removes the precursor loop of the pre-miRNA to generate an about 21 to 25 nucleotides long duplex intermediate consisting of the mature miRNA and the corresponding counterpart called miRNA star (miRNA*) [30]. Typically, these double-stranded intermediates are 5'-phosphorylated and bear 2 nucleotides overhangs at each 3'-end. Loading of the miRNA/miRNA* duplex onto the AGO protein was confirmed to be facilitated by large complexes such as of the Hsc70/Hsp90 chaperone machinery, which may (by an ATP-dependent mechanism) stabilize newly synthesized, unloaded AGO proteins and keep them at an open state [184]. To obtain an active miRISC, the miRNA/miRNA* duplex needs to be unwinded. Theoretically both, miRNA and miRNA*, could end up as a mature miRNA. However, usually only one strand is selected and incorporated into a miRISC [362]. This so-called 'guide strand' later guides the miRISC to (often only partially) complementary mRNA regions and thereby determines the targets of the respective miRISC. The counterpart, called 'passenger strand', is degraded.

One important determinant in guide strand selection lies in the thermodynamic stability of the base pairs at the two ends of the miRNA/miRNA* duplex. The strand with the less stably paired 5'-terminus is preferentially loaded into the AGO protein of the miRISC [210, 362]. The structural basis of this so-called 'asymmetry rule' has been suggested to lie in the fact that 5'-phosphate of the guide strand can only be bound by the 5'-end binding pocket (between the MID and PIWI domain, see Section 2.3), if the first base pair of the 'guide stand' with the complementary passenger strand is dissociated. Therefore, the terminus that can be denatured more easily would be thermodynamically preferred [316, 419, 41, 107, 357]. The actual unwinding might be achieved by 'wedging' of the N domain of the AGO protein edging it in between the two duplex strands [232]. Putative DEXD/H RNA helicases, such as RNA helicase A (DHX9) [344] or MOV10 [277], might not be generally required [141, 268, 267, 368], but are likely to facilitate efficient separation of both strands [277, 344]. When the passenger strand is removed, the loaded AGO protein is released from the RLC to form the active miRISC (see Figure 2.1).

In contrast to the linear miRNA processing pathway outlined above, numerous evidence accumulates supporting a rather differential expression and processing of individual miRNAs [427].

For example intron-derived so-called 'mirtrons' were shown to completely bypass the first processing step by the Microprocessor, if the spliced out intron has the appropriate size to form a pre-miRNA hairpin [29, 63, 347] (see Figure 2.1). MiRNAs generated from snoRNA also seem to be DROSHA-independent [108, 385, 363].

Also the second processing step seems rather heterogeneous for individual miRNAs. For instance, pre-miRNAs with a high degree of complementarity along the hairpin stem were observed to pass through an additional cleavage step be-

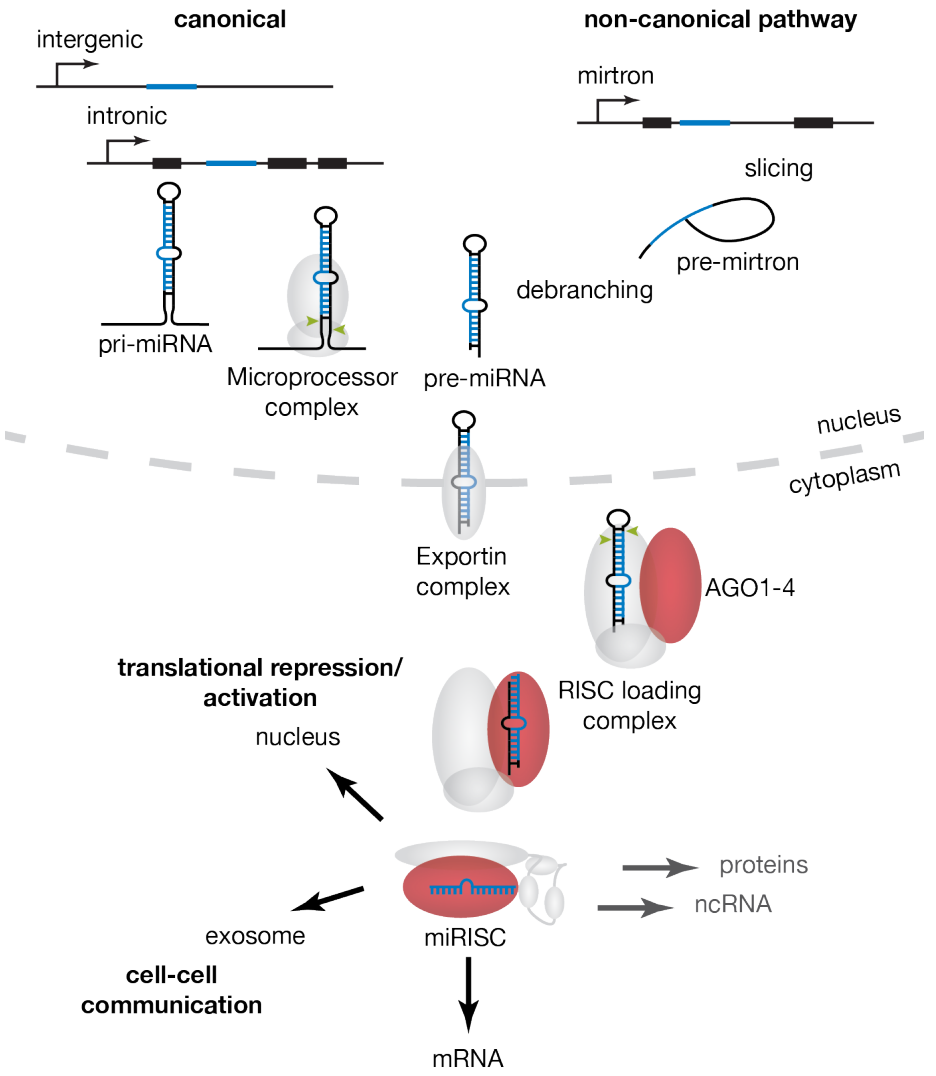

FIGURE 2.1. Schematic representation of canonical and non-canonical miRNA biogenesis pathways. Canonical miRNA genes are transcribed as primary transcripts (pri-miRNA). The initial processing step (cropping) is mediated by the Microprocessor, a complex of DROSHA and DGCR8, generating 65 to 70 nucleotides long pre-miRNA which are exported from the nucleus. The cytoplasmic RISC loading complex, consisting of DICER1, TARBP2P and one of the four AGO proteins (depicted in red), catalyzes the second processing step (dicing) into a miRNA/miRNA* duplex and loading of the mature miRNA (remaining on the AGO) into the miRISC. Non-canonical intron-derived mirtrons may bypass Microprocessor cropping by being produced from spliced introns and debranching. See main text for additional non-canonical pathways. Drawn on the basis of [215] Figure 2a and 2c.

fore dicing, at which AGO2 slices the 3′-arm of the stem (passenger strand) to generate a nicked hairpin, termed AGO2-cleaved pre-miRNA (ac-pre-miRNA) [86]. In the case of *miR-451*, biogenesis has been shown to be completely independent of DICER1. AGO2 cleaves the *pre-miR-451* leading to the mature miRNA [66, 73].

Recent examinations further revealed that some miRNAs are actually re-

imported into the nucleus after their cytoplasmatic processing. For example, mature human *miR-29b* is predominantly localized in the nucleus [180].
Next to the increasing knowledge about miRNA biogenesis and processing, surprisingly little is known about the stability and regulation of individual miRNAs.
Mature miRNA are generally expected to be rather stable, as indicated by a mostly long persistency after depletion of processing enzymes. For example, tracking of miRNA levels upon conditional DICER1 ablation in mouse embryonic fibroblasts revealed a half-life between 28 and 220 h [132]. This is about double to 20-fold longer than for mRNA with an approximate half-life of 10 h. One line of argumentation explaining the observed increased ribonuclease resistance follows the fact that AGO proteins have been shown to potentially act as enhancing factors regarding miRNA stability. An increase of any of the four AGO paralogs resulted in a general up-regulation of mature miRNA levels [86]. In contrast, loss of AGO2 diminished the expression and activity of mature miRNAs [308, 87]. This shielding effect might be explained by structural data of AGO in complex with small RNA, which revealed that both, 5'- and 3'-end of the small RNA are covered and thereby protected against degrading enzymes by the Argonaute [419, 107, 357] (see Section 2.3).
However, while miRNAs generally seem rather stable, individual examples of accelerated or more tightly controlled miRNA turnover have been reported. Interestingly, sequences present at the human *miR-29b* 3'-end do not only account for its predominant localization in the nucleus (see above), but they have also been shown to direct an accelerated decay of that miRNA in cycling cells [180]. Further, in the case of the interferon β-induced *miR-122*, its significant decrease within only one hour after treatment of liver cells with IFNB suggests a specific control mechanism regulating the turnover of particular miRNAs [321].

2.2 MIRISC: A TRIPARTITE COMPLEX

The miRISC is the executor of miRNA-guided target gene silencing. In mammals, this RNP complex contains at its core the target-determining miRNA loaded into one out of four AGO proteins (AGO1-AGO4) and an AGO-bound member of the Tri-Nucleotide Repeat-Containing proteins 6 (TNRC6) protein family. Mammals express three different TNRC6 proteins (A-C), with TNRC6A also known as glycine(G)-tryptophan(W) repeat-containing protein of 182 kiloDaltons (kDa) (GW182).

AGO Inside the miRISC, the AGO protein (see Section 2.3) is the main effector protein mediating mRNA translational inhibition, destabilization or 'slicing' [179, 256, 276, 437, 80, 398, 123]. Knock-down of AGO proteins was shown to result in impaired repression of gene expression [358] and miRNA-independent tethering of AGO2 to mRNA 3'-UTR using artificial hairpins seems sufficient to induce silencing [326] (see Figure 2.2 red sphere).

MIRNA MiRNA (see Section 2.4) anneal with partial complementarity to mRNA and thereby designates it as a specific target of the miRISC. Thus, the

miRNA dictates the potential targets of a miRISC within a given transcriptome (see Figure 2.2 blue line).

FURTHER EFFECTORS AGO proteins do not only contain a guiding miRNA, they also serve as a platform for interacting proteins assisting and mediating downstream effects of target gene silencing (see Section 2.5). For example, AGO proteins in the miRISC directly interact with a TNRC6 protein (see Figure 2.2 connected gray spheres), to perform target mRNA repression. Multiple lines of evidence imply that without TNRC6 AGO proteins fail to silence target gene expression [27, 397, 113, 116]. TNRC6 proteins, in turn, interact with several other silencing effectors [442, 175, 192, 47, 65].

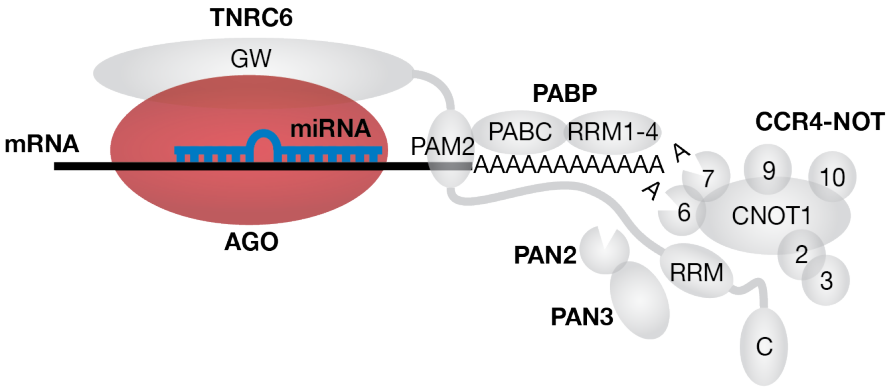

FIGURE 2.2. Schematic representation of the miRNA-Induced Silencing Complex, a tripartite composition of AGO, miRNA and TNRC6. Argonaute (AGO, red sphere) forms the core protein component. It harbors the miRNA (blue), which guides the miRISC to its target transcripts (black) and interacts with further effector proteins (gray spheres). TNRC6 proteins directly interact with AGO through their N-terminal GW-rich domain (GW). The C-terminal part contains a major effector domain called the silencing domain, comprised of multiple sequence motifs such as a PABP-interacting motif 2 (PAM2) and an RNA-recognition motif (RRM). It is therefore able to interact with cytoplasmic poly(A)-binding proteins (PABP) via their C-terminal (PABC) domain. As they are in turn bound to the mRNA poly(A) tail (via RRM1-4), the miRISC might interfere with the closed-loop formation mediated by the Eukaryotic translation Initiation Factor complex/PABP interaction and thus repress the initiation of mRNA translation. Furthermore, the silencing domain has been shown to recruit deadenylase complexes such as CCR4/NOT and PAN2/PAN3, which could thus initiate miRISC-mediated target poly(A) tail deadenylation and subsequent mRNA degradation (see Section 2.5 and Figure 2.6). Drawn on the basis of [115] Figure 5 and [185] Figure 1.

2.3 AGO: THE KEY PROTEIN OF THE MIRISC

PHYLOGENY AND AGO ORTHOLOGS

Eukaryotic Argonaute proteins are classified into three clades: AGO proteins (homologous to AGO1 of *Arabidopsis thaliana*), PIWI proteins (similar to PIWI of *Drosophila melanogaster*), and WAGO proteins (all in *Caenorhabditis elegans*). While AGO proteins, as direct binding partners of miRNAs and siRNAs, mainly

mediate post-transcriptional gene silencing in the cytoplasm [322, 178], PIWI proteins interact with piRNAs in the nucleus to silence transposable elements [372]. In *Caenorhabditis elegans* Argonaute proteins seem to function sequentially to mediate target gene silencing [439] with primary Argonaute proteins loading the small RNA into the species-specific WAGO proteins, which then perform secondary steps [275].
AGO proteins are highly conserved among eukaryotes, with *Saccharomyces cerevisiae* as an exception [96]. Even some prokaryotes have been shown to express Argonaute genes [398] (see Figure 2.3B).

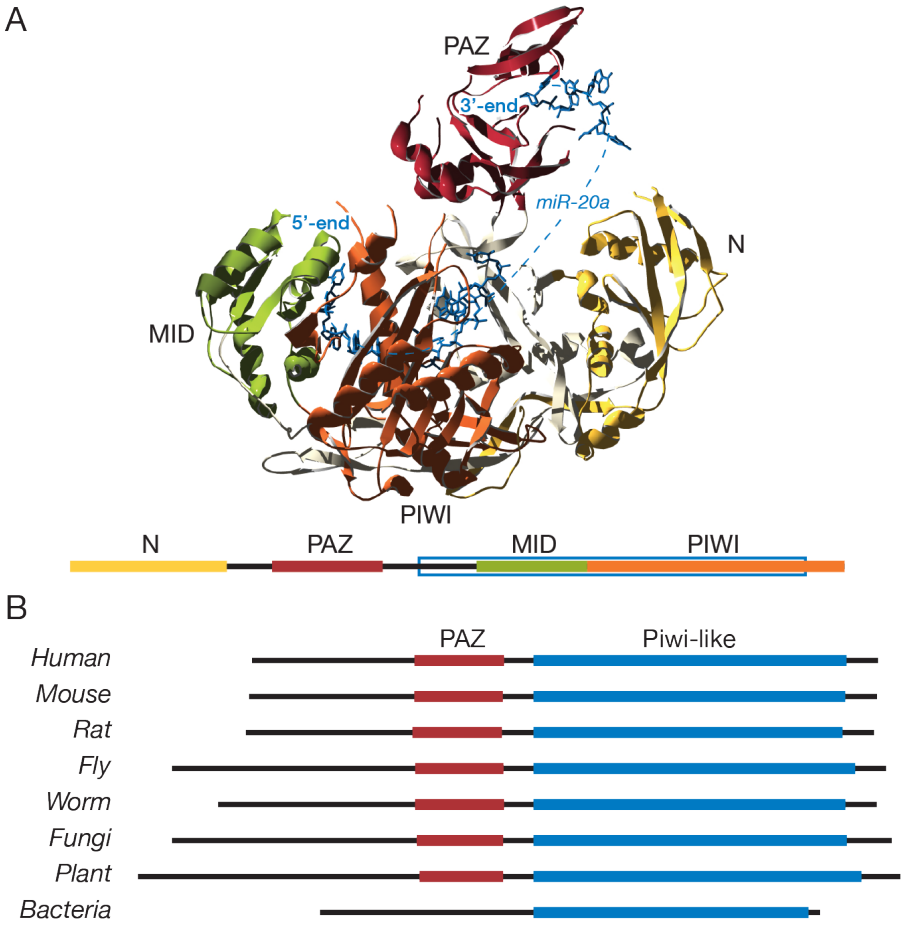

FIGURE 2.3. Structure and conservation of hAGO2. A: structural representation of hAGO2 and its domain architecture in complex with *miR-20a* (PBD:4F3T) [107], N domain (yellow), PAZ domain (red), MID domain (green) and PIWI domain (orange) are depicted as ribbon, the miRNA is shown in stick representation (Swiss-PdbViewer, POV-Ray rendering); B: schematic representation of AGO protein orthologs, *Homo sapiens* (NCBI:NP_ 036286.2, 859 amino acids), *Mus musculus* (NCBI:NP_ 694818.3, 860 amino acids), *Rattus norvegicus* (NCBI:NP_ 067608.1, 863 amino acids), *Drosophila melanogaster* (NCBI:NP_ 725341.1, 984 amino acids), *Caenorhabditis elegans* (NCBI:NP_ 871992.1, 910 amino acids), *Neurospora crassa* (NCBI:XP_ 958586.1, 989 amino acids), *Arabidopsis thaliana* (NCBI:NP_ 001185169.1, 1050 amino acids), *Thermus thermophilus* (PDB:3DLB_ A, 685 amino acids), PAZ and PIWI-like domain superfamilies are indicated (derived from the Conserved Domain Database [269]).

STRUCTURAL DOMAINS AND AGO PARALOGS

Structural studies revealed that the domain organization of eukaryotic AGO proteins is very similar to that of prokaryotic Argonautes [357]. For human AGO2, they disclosed a bilobal architecture with each lobe containing two evolutionary conserved domains and both lobes connected by a hinge region which allows for structural rearrangements upon RNA binding. The overall shape was likened to a duck [107]. While the lobe of middle (MID, see Figure 2.3A green) and carboxy terminal PIWI (see Figure 2.3A orange) domain forms a crescent body, the PIWI-Argonaute-Zwille (PAZ, see Figure 2.3A red) domain serves as the duck's head with the 3'-end of the miRNA held in its bill. The amino terminal (N, see Figure 2.3A yellow) domain has been suggested as a wing folding over the miRNA/mRNA duplex [107].

Functionally, the N domain is required for small RNA loading into the Argonaute protein and it assists in small RNA duplex unwinding [232].

The PAZ domain anchors the 3'-end of the small RNA by providing a pocket to accommodate 2 nucleotides of the 3'-terminus [433, 254, 265]. PIWI clade Argonaute PAZ domains specifically anchor methylated piRNA 3'-ends [370].

In contrast to the 3'-end binding, 5'-terminus recognition between the MID and PIWI domain tends to be sequence-specific and to be dependent on the identity of the Argonaute protein [203]. The electrostatic environment of the MID domain allows for specific contacts with Adenosine (A) and Uridine (U), but is rather incompatible with Cytidine (C) and Guanosine (G) [30, 126]. The 5'-terminal base is kinked and buried by this interaction, which makes it unavailable for base-pairing. This explains the unimportance of the identity of the miRNA's first nucleotide in target recognition [246].

The PIWI domain adopts an RNase H-like fold. This implicates it as the catalytic domain providing endonucleolytic activity, which has been shown for specific Argonaute proteins, guided by a small RNA with complete complementarity to its target RNA [377, 191]. Structural analyses of yeast Argonaute revealed that the catalytic center might be formed by four residues (DEDX) resembling the catalytic tetrad of RNase H (DEDD) [299]. However, only a small subset of Argonaute proteins carries this so-called 'Slicer' activity. In mammals, only AGO2 possesses cleavage activity [179, 256, 276, 437, 80, 398, 123]. Therefore, AGO2 may not only act as the major protein component of the miRISC, but also of the siRNA-Induced Silencing Complex (siRISC), that mediates RNAi. Further, its Slicer activity appears essential in neonatal processing of *miR-451* [66, 73] (see Section 2.1). However, similar to the non-catalytic paralogs in human (AGO1, AGO3, and AGO4), AGO2 is able to mediate gene silencing independently of endonucleolytic activity, directed by small RNA with only partial complementarity to their target RNA. AGO1 and AGO3 are expressed broadly, while AGO4 seems to be more tissue-specific [324]. It has been observed that mammalian AGO proteins differ in their efficiency to repress target gene expression when tethered to mRNA. This could lead to cell or tissue-specific strength of miRISC-mediated repression according to the relative abundance of individual AGO paralogs [430]. Further, AGO3 has been suggested to act in stem cell proliferation accompanying mRNA decay [172], while AGO4 seems to be required for spermatogenesis [286]. This suggests a non-redundant nature of the mam-

malian AGO proteins [275]. However, miRNAs do not seem to be specifically sorted into the four AGO homologs [276, 382, 56, 97]. It though requires further examination, if all miRNAs target the same mRNA when bound to different AGO proteins [162].

2.4 MIRNA: GUIDE OF THE MIRISC

Once embedded into the miRISC, a miRNA determines the available target sites and thus the area of influence of a certain miRISC. Target recognition principles and the mechanisms of miRISC-induced target repression are of particular interest to predict individual miRISC 'targetomes' and eventually allow for ameliorative intervention in case of pathological malfunction.

SEQUENCE DETERMINANTS OF TARGET SITES

Most target mRNA studied thus far are regulated through miRISC binding sites located within their 3'-UTR [22]. In contrast to plants, where most miRNAs align to their targets with nearly perfect complementarity (see Figure 2.4A), mammalian miRNAs usually bind to only partially complementary sites. Experimental and bioinformatic analyses within the last ten years have determined that miRISC/target interaction follows a set of canonical rules [91, 49, 246, 142]. The most common rule might be a contiguous and fully complementary Watson-Crick base pairing between nucleotide 2 to 7 or 8 of the miRNA, the so-called 'seed sequence', and the target (see Figure 2.5 and 2.4B). The seed region often shows the best conservation among the miRNA sequences, indicating functional relevance. It has first been introduced as a successful criterion in early attempts of bioinformatic target prediction [247] and soon became experimentally verified by comparative profiling studies, which showed that genes with changed expression after miRNA over-expression or depletion were enriched in corresponding seed matches [227, 252, 18, 364]. On a molecular level, the seed interaction is believed to nucleate the miRNA/mRNA duplex association by largely contributing to the energy required for the miRISC/target binding [154, 8, 420, 107, 357]. In some experimental contexts it has been shown to be both, necessary and sufficient for miRISC-mediated target repression [91]. However, from other experiments it was concluded that perfect seed pairing cannot generally be used as a reliable predictor for effective miRNA/target interactions [84, 162]. An A across nucleotide 1 of the miRNA and an A or U opposite to nucleotide 9, has been suggested to improve the repressive effect [246].

A second rule consists in the presence of unpaired bulges or mismatches within the central region of the miRNA/mRNA duplex (see Figure 2.5). In rare cases in which there is prefect hybridization between miRNA and mRNA binding site, and if the AGO protein component consists of AGO2, endonucleolytic cleavage in the middle of the miRNA/mRNA duplex would take place at exactly this position, inducing mRNA degradation in an RNAi-like mechanism [278, 437, 80].

Another rule is that complementarity of the miRNA's 3'-half, specifically nucleotides 13 to 16, to the mRNA stabilizes miRISC interaction (see Figure 2.5). This might be of particular importance for target interactions in which base

pairing of the seed region is suboptimal [49, 142]. For example, the imperfect pairing of the 5'-end of miRNA *let-7* with the 3'-UTR of mRNA *lin-41* might be compensated by extensive 3'-interaction [338, 374] (see Figure 2.4C).
However, exceptions to these rules have been discovered. As many as 40 to 60% of all seed interactions have been proposed to occur non-canonical, containing bulged or mismatched nucleotides [258, 162]. Another exceptional base pairing pattern constitute so-called 'centered sites', at which 11 to 12 consecutive Watson-Crick base pairs between the miRNA middle sequence (around nucleotides 4 to 15) and the mRNA lead to target regulation, for instance shown for the interaction between human *miR-124* and mRNA *RPTOR* [366] (see Figure 2.4D). Many other functional miRISC target sites have been discovered, which deviate significantly from the above mentioned rules [196, 389, 234] (see Figure 2.4E). A recent experimental study even revealed that almost one fifth of transcriptome-wide identified miRNA/target interactions show somehow 'seedless' binding pattern with little evidence of 5'-contacts [162]. This flexibility in animal miRISC/target recognition rules suggests that also determinants other than position-specific miRNA/mRNA duplex complementarity mediate efficient target regulation.

SEQUENCE CONTEXT OF TARGET SITES

Some features that have emerged as indicators of potential miRISC binding sites include an unstructured and A/U-rich neighborhood [22] and a position that is not too far away from the poly(A) tail or the ribosome stop codon [129, 142, 302]. Both leads to an enhanced accessibility of the mRNA, a factor that has been shown to be critical for miRNA-mediated regulation [207, 260]. However, the region immediately after the translational termination codon, that would fall into the ribosome shadow, seems to be avoided [142].
But, many questions are still unsolved. For example, approximately half of the miRISC binding sites identified by recent transcriptome-wide biochemical analyses align to coding regions within the Open Reading Frame (ORF) of the mRNA targets [70, 151, 450, 245, 335, 162]. To which degree these sites are effective in target repression remains to be determined.
Moreover, AGO proteins were shown to associate with RNA fragments of diverse origin [56] and one study revealed that only 70% of the so-called 'miRNA interactome' represent mRNA. Other identified interaction partners include rRNA, tRNA, pseudogenes, miRNA and long-intergenic ncRNA [162].
Further, often multiple miRISC target sites are predicted for a single mRNA and for effective repression generally more than one site for the same or different miRNA are required [91, 49, 246, 142, 302]. It is therefore interesting to study, how two or more miRISCs interact at these sites and with which consequences. Some combinations of sites have been shown to require a specific configuration, e. g., a separation by a particular length, for efficient repression [412]. One explanation could be that close sites tend to act cooperatively, meaning their repressive effect exceeds that expected from the independent contributions of single sites [91, 142, 350, 51] (see Section 2.6).
Further, it needs to be elucidated why miRISC interaction efficiency for identical binding sites varies on different mRNA targets [85]. Here RNA-binding pro-

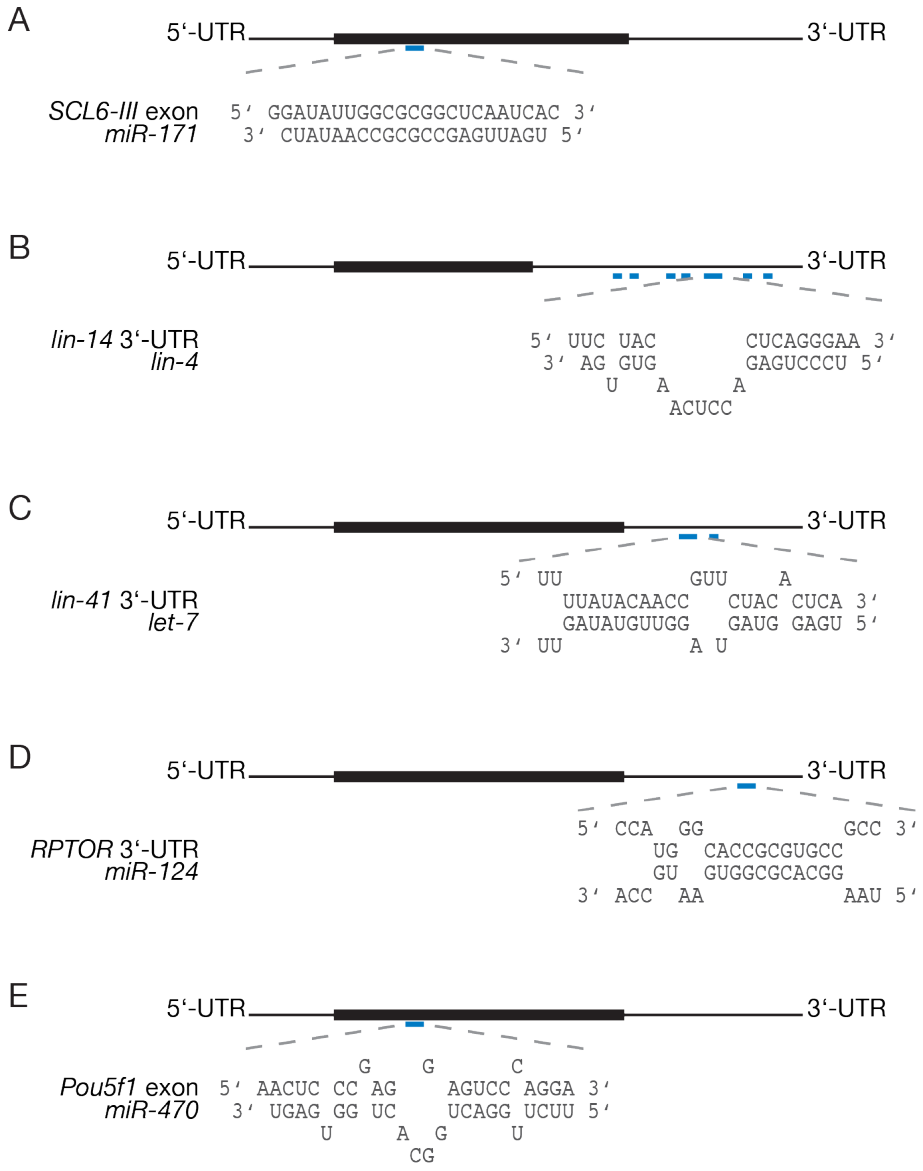

FIGURE 2.4. Selection of functional miRISC target sites on transcripts of following genes. A: *Arabidopsis thaliana SCL6-III*; B: *Caenorhabditis elegans lin-14*; C: *Caenorhabditis elegans lin-41*; D: *Homo sapiens RPTOR*; E: *Mus musculus Pou5f1*. In B, additional *lin-4* target sites are indicated below the *lin-14* 3'-UTR, not all of which exhibit seed pairing. In C, an additional *let-7* target site lies immediately downstream of the depicted duplex. ORFs are depicted in a thicker line. Blue lines indicate miRISC target sites. Drawn on the basis of [319] Figure 2.

teins might come into consideration, which potentially interfere with miRISC binding or function (see below).

COMPETITORS AND ENHANCERS OF TARGET SITES

In higher organisms, gene expression is extensively regulated at the post-transcriptional level. Global mRNA interactome studies capturing all proteins cross-linked to poly-adenylated RNA upon UltraViolet (UV) irradiation identi-

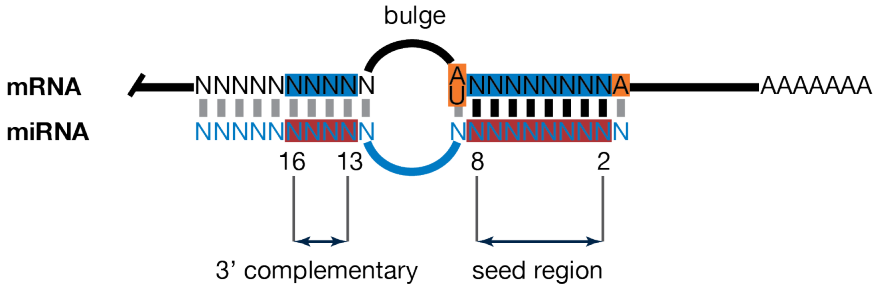

FIGURE 2.5. Schematic representation of sequence regions that determine miRISC/target interaction following canonical binding rules. Animal miRNAs generally base pair with their targets imperfectly. Watson-Crick alignment is often only observed between nucleotides 2 to 7 or 8 (seed region) and sometimes also between nucleotides 13 to 16 (3′ complementary) of the miRNA (red boxes) and the corresponding region on the target mRNA (blue boxes). Further, frequently an A across nucleotide 1 of the miRNA and an A or U opposite to nucleotide 9 (orange boxes) can be observed. See main text for additional information. Drawn on the basis of [123] Box 2.

fied almost [20] or even more than 800 [62] different RBP in eukaryotic cells. Similar to miRISCs, they often fine-tune maturation, stability, transport, and translation of target RNA [270, 290, 376]. The binding sites of most RBPs are known to reside in the 3′-UTR of their target mRNA. These untranslated transcript ends frequently comprise many kb with various adjacent or overlapping binding sites on the level of primary or secondary sequence. Thus, multiple RBPs potentially attenuate or enhance the miRISC-mediated effect on mutual target mRNAs and the identification of transcriptome-wide interactions between them seems essential to understand eukaryotic post-transcriptional regulatory networks [250].
One of the first reported examples of an RBP that antagonizes miRISC target regulation was the interference of ELAVL1 (also known as 'Hu antigen R' or HuR), a member of the Embryonic Lethal Abnormal Vision (ELAV) family proteins, with *miR-122*-mediated repression of mRNA *SLC7A1* [36]. ELAVL1 is a mostly nuclear RBP. However, certain stress conditions induce its re-localization to the cytoplasm. Here it is able to interacts with A/U-rich sequences in the 3′-UTR of *SLC7A1* mRNA, and thereby relieves it from *miR-122*-induced repression. Interestingly, the ELAVL1 binding site is located hundreds of nucleotides downstream of the *miR-122* interacting region. Possibly, the secondary structure of the 3′-UTR allows for spatial vicinity of ELAVL1 to the *miR-122*-loaded miRISC, interfering with miRISC binding or its mediated regulation [319]. Further experimental studies identified a potentially more general role of ELAVL1-mediated target competition. More than 75% of 3′-UTR with miRISC interaction sites simultaneously contained ELAVL1 binding regions [295]. However, ELAVL1 might not only interfere antagonistic to the repressive effect of miRNA-mediated regulation. At the 3′-UTR of *MYC*-mRNA (coding for a protein also known as c-Myc), ELAVL1 binding appears necessary for effective repression mediated by the miRNAs *let-7b* and *let-7c* [211]. Here, ELAVL1 is presumed to unmask the respective miRISC target site or to stabilize miRISC association with the mRNA target [319].
DND1 is another RPB shown to relieve mRNAs from miRISC-mediated reg-

ulation. For example, in *Danio rerio*, DND1 interaction on the mRNAs of *nanos1* or *tdrd7* in vicinity to *miR-430* binding sites might lead to reduced *miR-430*/miRISC accessibility [285] and thus reduced target repression. In mammalian cells it impedes *miR-221*-mediated repression of *CDKN1B* [204]. As *DND1* is expressed in primordial stem cells, but not in somatic cells, the antagonizing effect is virtually cell-specific [204]. In contrast to ELAVL1 binding sites, which have been found to be only close to miRISC binding sites, DND1 sites have been shown to actually overlap with the latter, interdicting miRISC accessibility [239, 295].
In contrast, PUF proteins represent RBP that have been reported to facilitate the miRISC-mediated target repression. For instance, in *Caenorhabditis elegans* PUF-9 collaborates with miRNA *let-7* to synergistically repress mutual targets [305]. A systematic analysis of human PUF proteins further disclosed that miRISC binding sites are enriched in the vicinity of PUF binding regions [130]. Interestingly, the human PUF protein PUM1 has been shown to be able to interact with a subunit of the 'CCR4/NOT' complex [139] (see Section 2.5). However, whether PUF-mediated silencing augments miRISC-mediated silencing remains to be answered.
Further, it has been shown that AGO proteins are recruited to target mRNA by other mRNA binding proteins, independently of miRNA-mediated guidance [328]. Such a model could also explain orphan Argonaute binding regions often found in AGO Cross-Linking and ImmunoPrecipitation (CLIP) experiments, which do not contain miRNA binding sites [275].
In either case, RBPs might not only modulate the miRISC effect, but the miRISC may also interfere with the RBP-mediated target regulation by competing for or blocking of mutual binding sites. To give an example, *miR-328*-loaded miRISCs, next to acting as genuine miRISCs, have been shown to relieve mRNA *CEBPA* form translational repression mediated by the RBP PCBP2 [102].

2.5 EFFECTOR PROTEINS: THE EXECUTORS OF THE MIRISC

MiRNA expression underlies stringent spatial and temporal regulation and, in general, shows an inverse correlation between the expression of its target transcripts. The negative regulation of target gene expression has been attributed to an inhibition of mRNA translation into functional proteins and a miRNA-promoted target mRNA degradation. However, also miRNA-mediated target gene activation has been observed. The complete collection of mechanisms leading to miRNA-coordinated regulation of target gene expression remains to be elucidated.

MIRISC-MEDIATED TARGET REPRESSION

Similarly to the siRNA-mediated cleavage of fully complementary targets (RNAi), perfectly pairing miRNA targets are cleaved at the miRISC binding site by the endonucleolytic Slicer activity of AGO2 [179, 256, 276, 437, 80, 398, 123] (see Figure 2.6B green arrowhead), leading to an RNAi-like silencing of the corresponding gene expression. However, in animals, miRNAs more often bind to their target mRNA with only partial complementarity [247, 333, 49, 144, 223,

246], which can hardly be cleaved [154]. Thus, miRISC interaction must result in more diverse mechanisms of target repression. In a general consensus, miRISCs have been proposed to mediate the silencing effect on target gene expression through translational repression and the promotion of mRNA deadenylation with subsequent degradation of the targets. But the relative contribution, coupling and timing of both, i.e. inhibition and decay, are not completely understood to date.

TRANSLATIONAL INHIBITION The translation of mRNA comprises three steps: initiation, elongation, and termination. The initiation phase describes all processes needed to assemble the complete ribosome at the start codon of the mRNA. It starts with the recognition of the mRNA 5'-terminal 7-methylguanosine (m^7G) cap by the Eukaryotic translation Initiation Factor (EIF) 4E subunit of the initiation factor EIF4F, which also contains an RNA helicase EIF4A and a large multi-domain protein that functions as an important scaffold for the assembly of the ribosome initiation complex, termed EIF4G. The ability of EIF4G to simultaneously interact with the Poly(A)-Binding Protein (PABP)C3, which is, as named, associated with the poly(A) tail, leads to pseudo-circularization of the mRNA [424, 199]. Circularized mRNA is efficiently translated and protected against degradation [83].
In principle, target inhibition has been suggested to occur in four possible ways: inhibition of initiation of translation, interference with translational elongation, induction of co-translational protein degradation, and premature termination of translation [112, 123, 429, 61] (see Figure 2.6A).
Some studies revealed that mRNA translated through m^7G cap independent mechanisms could escape miRNA-mediated repression, providing an indication for an inhibiting mechanism at the initiation of target mRNA translation [173, 327]. It has been shown that human AGO2 has the potential to directly interact with the m^7G cap and might therefore compete with EIF4E for cap binding [216]. However, since the m^7G affinity for AGO is apparently lower than for EIF4E [216], multiple AGO proteins would be necessary to prevent initiation of mRNA translation [123]. This would also provide an explanation for the reported frequent requirement of multiple miRISCs for effective target repression [90, 91, 326].
Early studies in *Caenorhabditis elegans* demonstrated that mRNA *lin-14* and mRNA *lin-18* are both repressed by *lin-4* without major changes at the mRNA level, speaking in favor of miRNA-mediated repression of target translation [426, 310]. However, both mRNAs were identified within polysomes, the functional units of protein synthesis consisting of several ribosomes attached along a translated mRNA, indicating a repression after initiation of translation.
As an explanation for such findings it was proposed that the nascent amino acid chain might be co-translationally degraded [306]. Alternatively, a miRISC-mediated premature drop off of ribosomes may occur [323].

TRANSCRIPT DESTABILIZATION On the other hand, several biochemical studies have collected evidence that target mRNA degradation is a widespread mechanism of miRNA-mediated silencing. First, there are experiments, in which induction of a miRNA led to decrease of transcripts with complemen-

tary binding sites [252, 18, 364, 164, 147]. Second, comparative transcriptome profiling and proteome analyses have reported a relative increase of binding site-containing mRNA after miRNA depletion [227, 18, 364]. Third, deletion of essential mediators of miRNA maturation (for example DICER1, AGO or TNRC6) increased target mRNA abundance [27, 337, 358]. Further, multiple studies have emphasized a reciprocal expression of miRNAs and their targets [120, 380].

Eukaryotic mRNA decay mainly follows two pathways, both of which initiated by deadenylase complexes trimming the 3'-poly(A) tail. Subsequently, degradation is either catalyzed by the exosome in 3'-to-5' direction or after 5'-decapping, exonucleolytic digestion in 5'-to-3' direction is mediated by the cytoplasmatic exonuclease XRN1 [318] (see Figure 2.6B).

The mechanism of miRNA-mediated target degradation was shown to resemble the 5'-to-3' mRNA decay pathway and is thought to occur in 'GW-bodies', cytoplasmatic granules containing proteins involved in mRNA catabolism and translational repression [10, 111, 317]. They are enriched in and named after their initial marker protein, GW182 (later named TNRC6A). TNRC6 protein interaction with the AGO protein component of the miRISC was suggested to be crucial for miRISC-mediated silencing of target miRNAs [386, 435]. The interaction has been shown to take place between the C-terminal AGO lobe and the N-terminal TNRC6 segment containing multiple GW, WG or GWG repeats [27, 103, 249, 386, 435]. Not only that multiple miRISCs are able to bind next to each other on one TNRC6 protein, potentially enhancing occupancy of a target mRNA, TNRC6 proteins also recruit and bind further effector proteins involved in target silencing. For example, it has been shown that TNRC6 proteins act as platform for interaction with the deadenylase complexes CCR4/NOT and PAN2/PAN3 [116, 47, 65, 115, 231] (compare Figure 2.2), suggesting them to be responsible for miRNA-mediated mRNA poly(A) tail deadenylation. Further, knock-down of the decapping enzyme DCP2 and co-factors like DCP1A/B prevents target mRNA degradation and leads to accumulation of deadenylated mRNAs [27, 114] indicating that 5'-decapping might be an essential step in miRISC-mediated target decay.

Importantly, the above mentioned studies do not rule out that target decay is caused by an initial inhibition of translation [176]. Interestingly, the C-terminal silencing domain of TNRC6 proteins further contains several short binding motifs including a Poly(A)-binding protein-interacting Motif 2 (PAM2) and an RNA Recognition Motif (RRM), which both interact with PABPs (compare Figure 2.2). This association has been suggested to actually trigger translational repression through interfering with the EIF complex/PABP association and thus mRNA circularization during translational initiation [116, 442] (see above). Further, PABPs and the poly(A) tail might stimulate miRISC/target association which would explain why the length of the poly(A) tail and thus the number of PABPs positively correlate with the silencing effect [292]. In addition to this repression of translation, the PABP interaction could enhance target mRNA deadenylation by placing the miRISC-recruited deadenylase complexes next to the poly(A) tail [116]. However, artificial tethering of CCR4/NOT complexes to mRNA reporter constructs that lack a poly(A) tail has been shown to induce translational repression of the mRNA independent of mRNA deadenyla-

tion, indicating that the CCR4/NOT complex may simultaneously contribute to translational repression [65]. Moreover, TNRC6 proteins have been reported to interact with an E3 ubiquitin ligase, UBR5 (also known as EDD) [381]. This interaction might also lead to (E3 ligase-independent) translational repression with subsequent mRNA destabilization [117].
In summary, the relative contribution of either inhibition or decay appears context-dependent. Another solution may be provided by a sequential model of miRISC-mediated target gene repression in animals [117, 185] that has been proposed based on further studies addressing the kinetics of miRNA-mediated regulation [34, 89]. First, the ternary complex of a miRNA, target transcript and AGO protein recruits a member of the TNRC6 family. This interaction leads to a decreased initiation of translation in a deadenylation-independent manner. Second, the TNRC6 protein interacts with members of deadenylase complexes inducing deadenylation of the translationally repressed mRNA. Depending on the individual cell type and/or particular target, these deadenylated transcripts may be stored or alternatively decapped and consequently degraded by XRN1, enabling a differentiated regulation. Thereby, the recruitment of the deadenylase complex potentially triggers both, translational repression and target degradation. However, this reflects just one of many models and the precise mechanisms remain to be identified.

2.6 MIRISC COOPERATIVITY: AN OPERATING PRINCIPLE?

Biochemical cooperativity describes a phenomenon at which the measured output is greater than what might be expected when only accounting for the additive effect of multiple elements. Figuratively, such an effect would result in a dose-response curve being sigmoidal rather than hyperbolic.
For instance, binding cooperativity may be observed for the assembly of multimolecular complexes at which binding of one or more units enhances the affinity for subsequent units. A classical example is the cooperative binding of oxygen to hemoglobin, already described in 1904 [40]. The tetrameric hemoglobin features four oxygen binding sites (heme groups). 3-oxy-hemoglobin has a several hundreds-fold higher oxygen affinity than deoxy-hemoglobin. Compared to the monomeric myoglobin, a plot of oxygen-concentration versus fraction of oxygen-saturated complex would result in a more sigmoidal curve for hemoglobin in contrast to a more hyperbolic shape for myoglobin.
The concept of cooperative target repression by multiple miRISCs on a mutual mRNA target has already been considered with the first miRNA/target interaction discovered, when the 3'-UTR of mRNA *lin-14* was shown to contain multiple binding sites for miRNA *lin-4* [426, 241]. Later, many mRNAs were reported to contain multiple potential miRISC binding sites for the same or different miRNA species within their 3'-UTRs [338, 253, 23, 142, 127] and the repressive effect seemed to positively depend on their number [90, 91, 326, 49, 142, 302].
To explain the molecular basis of such observations, at least three different mechanisms have been proposed [51]. First, the enhanced effect might be attributed to a cooperative binding of multiple miRISCs, where through mutually stabilizing interactions the affinity of subsequent miRISCs is increased (similar

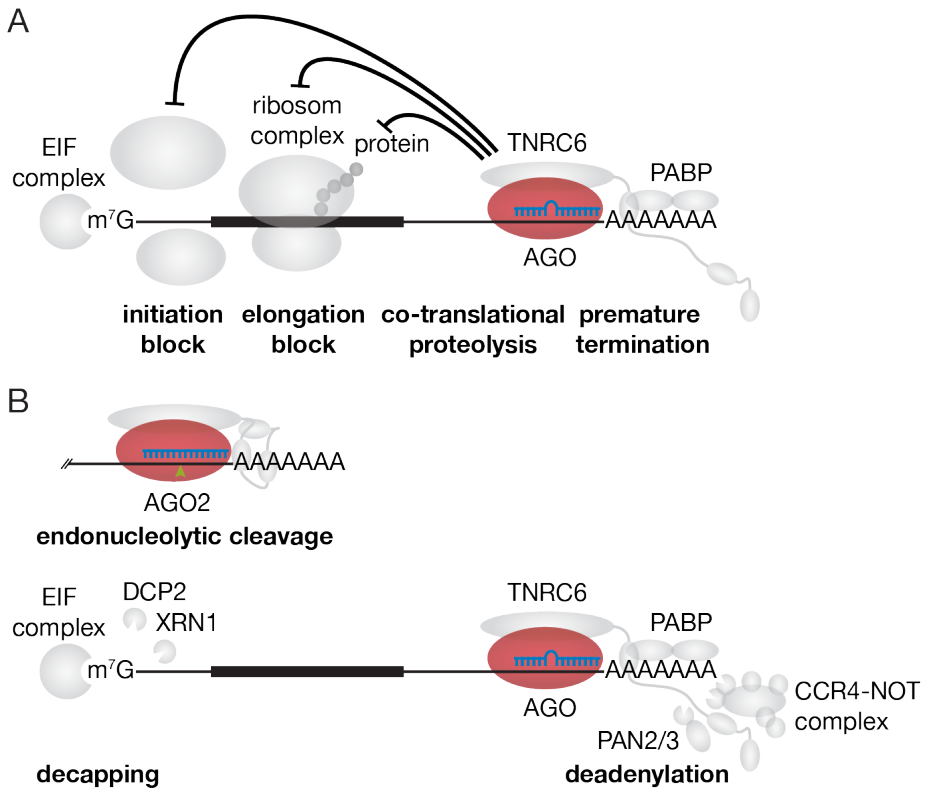

FIGURE 2.6. Schematic representation of the mechanisms of miRISC-mediated post-transcriptional repression. Negative regulation of target gene expression by miRISC has been attributed to both, translational repression and target mRNA degradation. A: translational inhibition has been suggested to occur in four possible ways: block of initiation of translation, interference with translational elongation, induction of co-translational proteolysis, and premature termination of translation; B: miRISC-mediated mRNA decay might follow two pathways: RNAi-like endonucleolytic slicing of the target at the miRISC binding site (AGO2-dependent) or mRNA 3′ poly(A) tail deadenylation (potentially by TNRC6 interaction with the deadenylase complexes CCR4/NOT and/or PAN2/PAN3) and 5′ 7-methylguanosine (m^7G) cap removal by the decapping enzyme DCP2 followed by exonuclease XRN1-mediated 5′-to-3′ digestion of the target. The relative contribution of both mechanism appears context-dependent and may as well occur sequentially. See main text for additional information. ORFs are depicted in a thicker line. Drawn on the basis of [185] Figure 1 and [319] Figure 3.

to oxygen binding to hemoglobin). Thus, more robust repression could follow from increased site occupancy. Second, functional cooperativity is considerable, at which miRISC interaction at multiple sites would trigger an increased recruitment or efficiency of repressive effector proteins. Or third, combined regulation might simply follow an additive model with increased repression due to the sum of individual miRISC-mediated effects.

As indicated above, miRISC cooperativity would be traceable by a steeper miRNA (dose) to target repression (response) curve for a target mRNA with multiple miRISC binding sites. Until now, only one study characterized reporter repression as a function of applied small RNA concentration in a quantitative manner [51]. The authors tested the influence of the identity of the Argonaute paralog, the pairing geometry of the small RNA/reporter duplex, the number

of target sites and the distance between two binding sites on the steepness of the measured dose-response curves. They proposed that cooperative repression by multiple RISCs can indeed be observed, that it requires AGO1, AGO3 or AGO4 and, importantly, that it depends on directly adjacent binding sites. This would speak in favor of binding cooperativity with stabilizing interactions between adjacent silencing complexes rather than the cooperative recruitment of effector proteins involved in subsequent steps that lead to enhanced target repression. Consistently, the importance of the distance between miRISC binding sites in order to cause cooperative targeting has already been emphasized in previous experimental studies [142, 350] (see Figure 2.7C). Determined cooperative inter-site distances (see Table 2.1) encircle the length of a miRNA (20 to 24 nucleotides) corroborating the concept of binding cooperativity as the source of amplified target repression.

SMALL RNA SITES	REPORTER	TESTED DISTANCES	ADDITIVE EFFECTS	COOPERATIVITY	REFERENCE
2 - 6 × *CXCR4* siRNA	luciferase reporter, HeLa	20	20	n.a.	[90]
4 × *CXCR4* siRNA	luciferase reporter, HeLa	11, 16, 20, 24	16, 20, 24	n.a.	[91]
2 × *let-7* (2 × 2 × *let-7*/ 3 × *let-7*/ *mir-25*, *miR-106b* & *miR-93*)	luciferase reporter, HeLa/ HEK293	9, 13, 17, 21, 24, 35, 70	13, 17, 21, 24, 35, 70	n.a.	[350]
2 × *miR-124*/ 2 × *miR-1*/ *miR-1* & *miR-133*	luciferase reporter, HeLa	11, 15, 17, 26, 39, 41, 46, 63, 156, 200, 336, 414, 495, 547, 791	11, 15, 17, 26, 39, 41, 46, 63, 156, 200, 336, 414, 495, 547, 791	15, 17, 26, 39, 41, 200	[142]
artificial siRNA (2 - 6 × perfect/ bulged/ seed & 13 to 16/ seed)	luciferase reporter, HeLa	21, 40	21, 40	21	[51]

TABLE 2.1. Cooperativity-permitting inter-site distances: Summary of a selection of studies investigating the dependency of binding site distances on the effect of reporter regulation mediated by multiple small RNAs. To allow comparison, nucleotide distances were re-determined to be always counted between two miRNA 5'-end complementary nucleotides within a particular reporter construct. If the reported repressive effect of a particular pairwise binding site distance was detected stronger than for a single target site, it was listed as 'additive effects'. Some authors [142, 51] showed repression significantly greater than expected from additive effects. Such inter-site distances were indicated as 'cooperativity'.

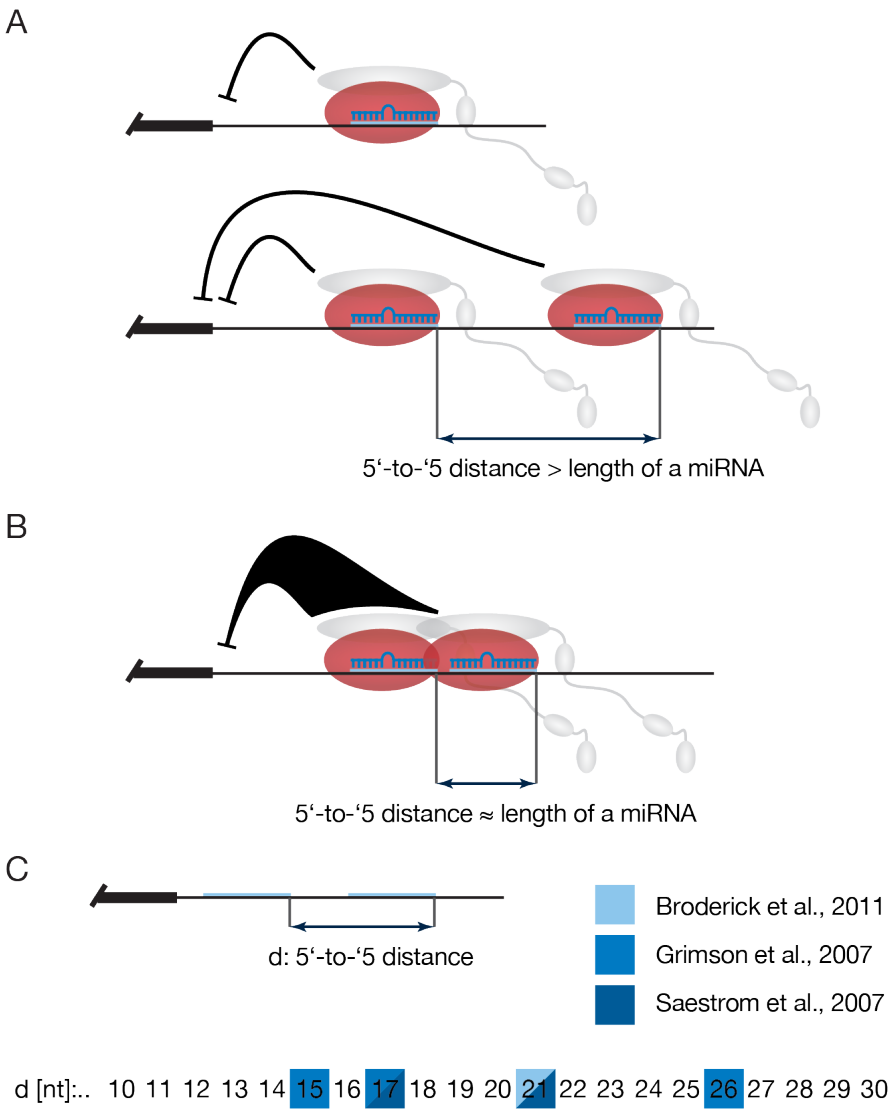

FIGURE 2.7. Schematic representation of the concept of miRISC binding cooperativity at multi-binding site targets. Target regulation by the miRISCs may be described by independent or cooperative activities. A: targets possessing only one miRISC binding site or multiple but distant sites have been described to show an independent mode of repression with a rather linear response on the number of target sites; B: activity-enhancing or cooperative interactions with an repressive effect greater than expected from additive regulation could be observed for miRISCs, whose binding sites on a specific mRNA target are approximately contiguously arranged; C: experimental studies investigating distance-dependency of cooperative target repression revealed inter-site distances (between adjacent miRNA 5’-ends on the respective mRNA target) of 15 to 26 nucleotides (blue squares) corresponding approximately to the length of a miRNA. However, also more distant sites could show synergistic regulation, potentially due to secondary structure formations of the target sequence and rather spatial miRISC adjacency. See Table 2.1 and main text for additional information. ORFs are depicted in a thicker line. Drawn on the basis of [341] Figure 1.

3 RELEVANCE OF MIRNAS FOR CARDIAC HEALTH

Deregulated expression of miRNAs has been associated with a variety of diseases, including cardiac disease [406, 395], developmental malformations [425, 161], lung cancer [133], leukemia [44], neurological disorders such as Alzheimer's disease [134], metabolic abnormalities like diabetes mellitus [197] or rheumatoid arthritis [25], and viral disease [229].
As miRNAs frequently mediate the repression of not only a single mRNA, but of numerous transcripts encoding multiple often functionally related components of complex intracellular networks, the manipulation of miRNA abundance or function can have strong impact on the cellular phenotype in health and disease. Therefore, miRNAs emerged as candidates in the development of novel therapeutic strategies to treat various kinds of disorders.
This chapter emphasized the importance of miRNAs in cardiac health and how they might be used to anticipate harmful deregulations.

3.1 CARDIAC CELLS

Heart tissue is built up of several types of distinct cells, which all bear specific features. They include, e. g., Cardiac Myocytes (CM), Cardiac Fibroblasts (CF), Endothelial Cells (EC), smooth muscle cells, pacemaker cells, Purkinje cells, and immune cells.
Even though the exact percentages might be quite species-specific with, for instance, adult mouse hearts containing about 56% myocytes, 27% fibroblasts, 7% endothelial cells, and 10% vascular smooth muscle cells [21] and adult rat cardiac cell populations being distributed to about 30% myocytes, 64% fibroblasts, and 6% other cells [298, 21], CM account for most of the cardiac mass and tissue volume.

3.2 CARDIOVASCULAR DISEASE

Diseases of the cardiovascular system are versatile, but they often result in a similar final phenotype, heart failure [168]. Generally, heart failure is preceded by cardiac stress, such as hemodynamic alterations caused by, e. g., Myocardial Infarction (MI) due to coronary artery occlusion, hypertension, aortic stenosis or valvular dysfunction, leading to myocardial hypertrophy. This is characterized by an enlargement of CM and increased protein synthesis. Physiological hypertrophy, which serves the purpose of enhancing the cardiac muscle power subsequent to heavy exercise, is not associated with cardiac damage. In contrast, prolonged cardiac stress may lead to maladaptive pathological increase of heart size in order to adapt to altered workloads (for example through aortic stenosis) and compensate for impaired cardiac function (for instance after MI).

It is characterized by an induced assembly of sarcomeres and the re-expression of 'fetal' cardiac genes [71, 94, 273]. On a molecular level, chronic stimulation of cardiac β1-adrenergic receptors (ADRB1) has been identified as one of the major elicitors contributing to CM hypertrophy [259, 109]. The activation of receptor coupled heterotrimeric (stimulatory) G proteins provokes the induction of a defined set of downstream effectors such as adenylyl cyclase (ADCY) and cAMP-dependent protein kinase (PRKA). Ultimately, it may provoke an irreversible loss of CM and a subsequent remodeling of the cardiac muscle. During this process, fibroblasts become activated leading to an increase in their proliferation, growth factor secretion, and an inappropriate production of ECM proteins. Dead CM are replaced by a non-contractile scar tissue with adjacent so-called 'interstitial fibrosis', which further impairs cardiac function [168]. Not only that the resulting increased mechanical stiffening eventually leads to systolic dysfunction and heart failure, but also the increased diffusion distance to the CM impairs the myocardial supply with nutrients and oxygen. Additionally, fibrosis may break the electrical connection between CM, which increase the risk of arrhythmia [52]. Therefore, alterations of fibroblasts and also of endothelial cells have strong impact on CM function. Diminished vascularization (lack of nourishment) and progressive inflammation (contributing to atherosclerosis) further deteriorate the diagnosis towards heart failure and sudden death [166].

3.3 EXPERIMENTAL MODELS IN CARDIAC MIRNA RESEARCH

Inherent to many fields of research and in particular to drug development is the requirement of relevant experimental models. MiRNA-mediated regulation is highly cell type-specific and thus, also cardiovascular miRNA research depends on model cells, tissues or organisms, which ideally allow for the extrapolation to the human situation.

PRIMARY CELLS

Primary cells and in particular isolated CM and CF have emerged as useful models to conduct research on myocardial mechanisms. Already in 1976, viable Adult Rat Cardiac Myocytes (ARCM) have been shown to be isolatable by an *in vitro* perfusion approach based on collagenase-induced cell separation [330]. Unfortunately, although these methods could be developed further [392], adult CM can only be cultivated for a few days. Further, the cultivation of isolated cardiac cells often drives them into strong alterations and a general remodeling, leading to a rather inappropriate representation of the *in vivo* cell physiology. Albeit the isolated examination of only a single cardiac cell type does provide the opportunity to study cell type-specific mechanisms, it may as well neglect potentially important hetero-cellular cross-talk between the individual strains [345].

SLICE CULTURES

Apparently, the use of for instance perfusion strategies to perform cardiac cell preparations is restricted to model organisms, preventing direct transfer of the research results to the human cardiovascular system [263]. Interestingly, it has been shown that whole tissue slices (~300 µm thick) of human adult myocardium cut from specimens of therapeutic myectomies maintain vital and functionally intact under organotypic culturing conditions throughout a month [46]. Therefore, these slices seem to represent an attractive, adequately available, and multi-cellular model of the human myocardium.
However, the supply and quality of these slices can be subject to heavy variations and individual patient information regarding the kind and state of disease may be protected. Obviously, tissue samples only allow for the analysis of the combined targetome of cardiac miRNAs. An unambiguous assignment of cell type-specific miRNA/mRNA associations based on computational analysis might be rather complicated.

3.4 IDENTIFICATION OF MIRNAS INVOLVED IN CARDIAC DISEASES

MiRNAs are implicated in the regulation of various pathological processes within the cardiovascular system such as CM hypertrophy, cardiac fibrosis, arrhythmia, angiogenesis, and heart failure.

KNOCK-OUT APPROACH One strategy for studying the comprehensive role of miRNAs in the heart has been the creation of model systems lacking central processing enzymes required for miRNA maturation. A mouse model carrying a conditional cardiac *Dicer1* knock-out, was shown to develop heart failure upon recombinase induction. While younger mice died within one week after cardiac *Dicer1* knock-out, in adult mice loss of DICER1 activity was accompanied by strong alterations of the myocardium with CM hypertrophy, ventricular fibrosis, and induction of fetal gene expression. This emphasizes an essential role of miRNAs to account for the correct morphology and function of the heart [78]. Another model with a muscle-specific deletion of *Dgcr8* (see Section 2.1) confirmed the critical role of miRNA to maintain cardiac function [334]. An endothelial cell-specific, conditional *Dicer1* knock-out mice showed, upon induction, reduced postnatal angiogenic response to various stimuli including exogenous vascular endothelial growth factor, which emphasizes the importance of miRNA in angiogenesis [383].

CARDIAC HYPERTROPHY MODEL Pathological hypertrophy was the first [406] and since then has been one of the most studied phenotype with respect to miRNA in cardiovascular diseases [311]. Such work includes the examination of miRNA deregulation in stress models inducing pathological cardiac remodeling. Both, mice with 'Transverse Aortic Constriction' (TAC), which induces CM hypertrophy by increased afterload on the heart [167] and a mouse model, in which transgenic expression of activated calcineurin A results in severe hypertrophy [288], were shown to develop a deregulation of miRNA expression, similar to that observed during pathological cardiac remodeling. Further, *in*

vitro transfection of the identified stress-inducible miRNAs, for instance *miR-195*, into cultured CM was sufficient to promote hypertrophic growth. In contrast, *in vitro* over-expression of down-regulated miRNAs such as *miR-150* or *miR-181b* reduced the size of cultured CM [406].
These findings suggest that deregulation of miRNA in the context of cardiac hypertrophy may as well be a cause rather than simply a consequence of cardiac remodeling [311] (see below).

ISCHAEMIA/REPERFUSION MODEL Further, MI and loss of CM subsequent to ischaemia or oxidative damage upon reperfusion has been modeled to determine miRNA expression pattern in ischaemic hearts. Thereby, *miR-320* has been identified to be consistently deregulated and knock-down of *miR-320* was shown to protect CM against ischaemia/reperfusion injury [339]. In the early phase after MI, in rat hearts expression of *miR-21* has been shown to be significantly down-regulated in infarcted areas, but up-regulated in the border zone. Further, adenoviral over-expression of *miR-21* was reported to decrease the myocardial infarct size and mediate a protective effect on ischaemia-induced CM loss [93].

DIFFERENTIAL EXPRESSION PROFILING A comparative study directed at miRNA alterations in failing left ventricles of the human heart, revealed over 60 significantly up- and over 40 down-regulated miRNAs. Interestingly, more than 80% of them have been shown to be similarly different in fetal human hearts compared to healthy adult control left ventricular tissue [394]. Many other profiling studies also revealed a differential expression of a large number of miRNAs in the failing heart [68, 182, 388, 98, 181].

In general, though, only a couple of targets are known for each miRNA and the precise link between them and the disease phenotype is often missing. This this probably due to the finding that individual miRNA-mediated effects on target gene expression are rather low and only the combined impact of small alterations on the expression level of multiple targets can be made responsible for the grave phenotypic outcome of deregulated miRNAs [404].
Further, miRNAs are frequently cell-specifically expressed and regulated in response to developmental or disease processes, mediating the repression of only a distinct set of available targets. From an experimental view, it is therefore interesting to examine isolated cardiac cell populations, meaning to separate CM, CF, endothelial cells, and maybe also smooth muscle cell fractions.

3.5 INTRODUCTION OF PROMISING MIRNA CANDIDATES IN THE HEART

A clear classification of miRNAs according to a specific cell type or cardiac disease is rather unfeasible. In the following, a short selection of exemplary miRNAs is sorted according to their predominant cell type (of either CM or CF) and introduced in the context of associated disease phenotypes.

CARDIAC MYOCYTES

MIR-1 One of the most abundant miRNAs in heart and skeletal muscle is *miR-1* [447]. It has been shown to be involved in the regulation of cardiogenesis [447, 303, 446] by repression of *Hand2* gene expression coding for a cardiac transcription factor [447]. Further, *miR-1* is among the earliest miRNAs that are down-regulated during TAC-induced hypertrophy [354]. *In vivo* studies suggest a causality between the decrease of *miR-1* levels and the subsequent increase in CM size and mass [60]. Validated targets include the transcripts of prohypertrophic substances like, insulin-like growth factor 1 (mRNA *Igf1*) [105], calmodulin (mRNA *Calm*), myocyte enhancer factor 2A (mRNA *Mef2a*), and GATA binding protein 4 (mRNA *Gata4*) [181], which are de-repressed upon *miR-1* down-regulation (see Figure 3.1).
The pool of mature *miR-1* comprises identical mature sequences derived from two distinct genomic loci, each encoding a different precursor sequence. Therefore, they are differentiated by labeling them as *miR-1-1* and *miR-1-2*.

MIR-133 Both *miR-1* precursors are transcribed from bisictronic gene clusters with *miR-133*, which is also a muscle-specific miRNA and likewise down-regulated during cardiac hypertrophy [406, 60, 68]. While mice lacking either *miR-133a-1* or *miR-133a-2* are normal, double-mutants showed lethal defects in about 50% of embryos or neonates. Survivors were prone to dilated cardiomyopathy and heart failure [257]. Further, silencing of *miR-133* by chemically modified antisense oligonucleotides, so-called 'antagomirs' [227] (see Section 3.6) or expression of tandem repeat antisense sequences, so-called 'miRNA sponges' [100] (see Section 4.4) sensitized the myocardium to pathological cardiac growth. Conversely, *in vitro* over-expression of *miR-133* (or *miR-1*) attenuated agonist-induced cardiac hypertrophy [60]. Mechanistically, de-repression of potential targets of this miRNA, such as family members of the Rho kinase family, mRNA *Rhoa* and mRNA *Cdc42*, as well as mRNA *Nelfa*, encoding a negative regulator of RNA polymerase II, was demonstrated to play a role in cardiac growth response downstream of *miR-133* [105] (see Figure 3.1).

MIR-208 As mentioned above, hypertrophic growth response is also characterized by a re-activation of fetal gene expression, which includes the replacement of the primary contractile protein of the rodents heart, myosin heavy polypeptide 6 (MYH6, also known as α-MHC) by myosin heavy polypeptide 7 (MYH7, also known as β-MHC) [261, 300]. This so-called 'α/β-MHC switch', which mainly accounts for decreased cardiac contractility, is regulated by *miR-208* [407]. It is not only a cardiac-enriched but a cardiac-restricted miRNA [35], which comes in two isoforms, *miR-208a* and *miR-208b*. Both are contained within the introns of the myosin encoding genes *Myh6* and *Myh7*, respectively. Knock-out mice of *miR-208a* developed normally with regard to the MYH6/MYH7 levels, but they did not show hypertrophy of CM or fibrosis in response to TAC. The animals were unable to up-regulate MYH7 [407]. Both isoforms are predicted to mirror the expression pattern of their host genes with *miR-208a* being the main contributor to the *miR-208* pool in adult mouse hearts and *miR-208b* mainly expressed during fetal cardiac development.

However, also *miR-208b* knock-out mice showed no evidently defective phenotype during development [405]. Apparently, while *miR-208* is not necessary for the synthesis of MYH7 during cardiac development, it is required for the switch to MYH7 observed during cardiac hypertrophy [1]. Therapeutic inhibition of *miR-208a* in a hypertension-induced rat heart failure model was shown to prevent the pathological α/β-MHC switch and cardiac remodeling, emphasizing the potential of miRNA-based therapies to intervene in heart disease progression [289]. Two studies identified mRNA *Med13* (also known as *Thrap1*), a negative regulator of hypertrophy, as targeted transcript of *miR-208*-loaded miRISC [407, 59] (see Figure 3.1).

MIR-378 Another miRNA strongly expressed in the mammalian heart, which decreases in cardiac disease is *miR-378*. A broad examination of the hypertrophy-inducing effect of synthetic miRNA libraries on isolated ARCM, identified *miR-378* among the group of anti-hypertrophic miRNAs [189]. Interestingly, *miR-378* has been shown to control cardiac hypertrophy by the combined repression of four distinct regulators within the pro-hypertrophic MAPK pathway, encoded by mRNAs *Igf1r*, *Grb2*, *Kar1*, and *Mapk1* (see Figure 3.1). Adeno-Associated Virus (AAV)-mediated (see Section 3.6) restoration of *miR-378* levels has therefore been suggested as a promising therapeutic strategy to ameliorate pathological cardiac hypertrophy and thus myocardial disease [131].

CARDIAC FIBROBLASTS

MIR-21 One of the most highly up-regulated miRNAs during cardiac hypertrophy is *miR-21* [406, 68, 354, 388] and its up-regulation in CF was suggested to be much more pronounced than in CM [395]. Further, sprouty homolog 1 mRNA (*Spry1*) was identified as a direct target of *miR-21* which in turn acts as an inhibitor of MAPK signaling. Increased *miR-21*-mediated repression was made responsible for an enhanced phosphorylation (activation) of MAPK3/1 (also known as Erk1/Erk2) potentially resulting in increased fibroblast survival and thus indirectly in increased cardiac fibrosis during hypertrophy [395] (see Figure 3.1). Conversely, antagonizing *miR-21* was reported to reduce myocardial fibrosis in the same mouse model of pressure overload-induced cardiac hypertrophy [395, 393].

MIR-29 In a group of miRNAs identified as down-regulated upon MI, members of the *miR-29* family have been shown to target several transcripts encoding proteins involved in fibrosis, which include multiple collagens (for example mRNA *Col1a1*), fibrillins, and elastin [408]. Therefore, down-regulation of *miR-29* was expected to de-repress theses mediators of cardiac fibrosis. Conversely, over-expression of *miR-29* in fibroblasts has been shown to reduce collagen expression *in vitro*, elevating this miRNA family as promising therapeutic option to prevent the fibrotic response upon MI [408] (see Figure 3.1). However, it has not yet been finally clarified whether *miR-29* inhibition can indeed lead to cardiac fibrosis *in vivo*. Down-regulation of *miR-29* has even been found protective against myocardial ischaemia/reperfusion injury [436]. The observed anti-apoptotic effect of *miR-29* inhibition has been attributed to an increase of the po-

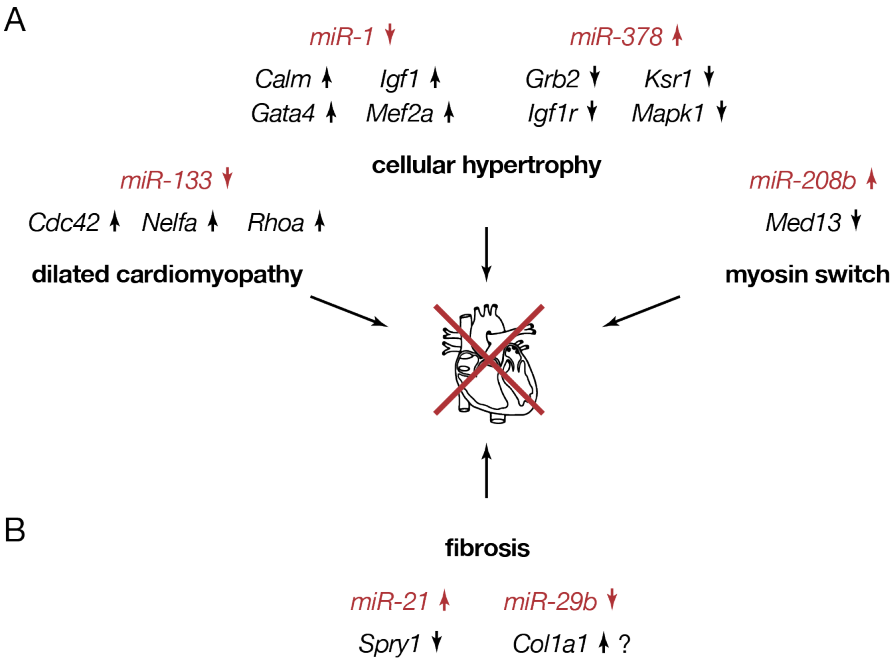

FIGURE 3.1. Selection of miRNAs and exemplary targets in the cardiac system. MiRNAs were separated according to their predominant cell type of action. A: cardiac myocytes; B: cardiac fibroblasts. Targets are referred to by mouse symbols of mRNAs encoding: calmodulin (*Calm*), cell division cycle 42 (*Cdc42*), collagen, type I, alpha 1 (*Col1a1*), GATA binding protein 4 (*Gata4*), growth factor receptor bound protein 2 (*Grb2*), insulin-like growth factor 1 (*Igf1*), insulin-like growth factor I receptor (*Igf1r*), kinase suppressor of ras 1 (*Ksr1*), mitogen-activated protein kinase 1 (*Mapk1*), mediator complex subunit 13 (*Med13*), myocyte enhancer factor 2A (*Mef2a*), negative elongation factor complex member A (*Nelfa*), ras homolog gene family, member A (*Rhoa*), sprouty homolog 1, Drosophila (*Spry1*). The question mark behind *Col1a1* indicates controversial results. See main text for additional information.

tential target mRNA *Mcl1* encoding an anti-apoptotic BCL2 family member. It has been suggested that *miR-29* inhibition-dependent activation of pro-survival pathways may actually lead to both, fibrosis and hypertrophy when considering long-term effects and protection against ischaemia/reperfusion injury in short-term observation [436]. Further studies regarding the role of *miR-29* in cell types other than CF and during cardiac disease are needed to ultimately define its role in the heart.

3.6 OPPORTUNITIES AND OBSTACLES OF CLINICAL APPLICATION

Cardiovascular disease remains the leading cause of morbidity and mortality worldwide. It causes about 47% of all deaths in Europe (European Heart Network, CVD Statistics 2012) and about 32% of deaths in the United States[138]. Therefore, new therapeutic strategies to prevent and/or treat cardiovascular disorders are clearly needed.

Most therapeutic agents currently on the market are small molecule drugs targeting proteins such as enzymes (for example 3-hydroxy-3-methylglutaryl-CoA

reductase or angiotensin I converting enzyme, HMGCR or ACE) or receptors (for instance β1-adrenergic receptor, ADRB1).
By contrast, therapeutic strategies based on ncRNA act one level higher by targeting mRNA molecules before their translation into proteins and may therefore potentially regulate many proteins in parallel. In principle ncRNA therapeutics operating in an antisense mechanism may be divided in two sub-groups. On the one hand siRNA-mediated RNAi can be used to silence specific genes of interest (for example of pro-inflammatory cytokines) and on the other hand, miRNA alterations may serve to modulate and thereby normalize complex gene expression pattern by simultaneously addressing multiple targets.
Focusing on miRNA modulations, they can be sub-divided into strategies for the inhibition of pathologically up-regulated miRNAs and methods to re-express undesirably depleted miRNAs. However, due to major challenges in their delivery and design, miRNA mimicry lags behind the development of miRNA inhibitors [404].
Antisense oligonucleotides designed for high-affinity interaction with target miRNAs ('antimiR' chemistries), prevent miRNA/mRNA interaction and thereby miRNA-mediated repression. Such Anti-MiRNA Oligonucleotides (AMO) are often chemically modified to enhance their miRNA affinity, nuclease resistance or cellular uptake. For example, the afore mentioned antagomirs are conjugated to cholesterol in order to increase their delivery and *in vivo* stability [227, 226]. They are complementary to the full length of their target miRNA and contain several phosphorothioate moieties to further enhance their stability. Locked Nucleic Acid (LNA) contain an artificial 2'-O-,4'-C methylene bridge, that locks the ribose in a C3'-endo confirmation, which dramatically increases their affinity (dsRNA duplex melting temperature +2 to +8°C per each LNA moiety) [404].

EFFICACY Highly expressed miRNAs can reach up to tens of thousands of copies per cell [64]. Further, many miRNA genes share the same seed region and may therefore compensate for the loss of one member of such a family, because residual sequence divergence may prevent a collective inhibition of the complete family by a single antisense construct. Thus, inhibition of potential miRNA candidates may only come into question, if a relatively modest increase in the expression of their regulated targets is sufficient to evoke therapeutic benefits (i.e. where miRNAs act as switches rather than fine-tuners of gene expression [296]).

DELIVERY Further attention should be paid to the challenge of delivery. Until the advent of AAV vector systems, cardio-specific targeting has been extremely difficult. The discovery of cardio-tropic AAV serotypes like AAV9 [183, 312] and the ability to re-engineer them for therapeutic purposes [248, 15] ameliorated the situation, but tissue-specific and regulable expression of miRNA-based drugs remains one of the most crucial issues. This is of particular importance for miRNA candidates with a broad tissue-distribution as they are expected to control multiple networks and perform different functions in different cell types.

SPECIFICITY Consequently, next to efficacy and delivery, potential 'off-target' effects and toxicity (often hepatotoxicity) of therapeutic agents based on miRNA biology need to be considered, especially since doses used in most animal studies may not even be therapeutically feasible [404]. Here, the initially mentioned mechanistic difference between classical drugs specifically acting on a single target and miRNA-mediated regulation potentially affecting multiple and not necessarily functionally related targets, may not only be a blessing. Unless the complete set of targets regulated by a particular miRNA is discovered, miRNA manipulation possibly leads to unexpected and potentially adverse changes in gene expression [404].

With respect to miRNAs as diagnostic targets, first successes have become apparent. In order to develop new strategies for the early recognition of MI, miRNA present in circulating blood included in exosomes and microparticles [403, 174] might represent an option. Such circulating miRNA have been detected in patients with MI [416] and as they may reflect tissue damage, they have been proposed as interesting new biomarkers [3, 69, 79].
Importantly, the fundamental basis for powerful miRNA-based medical strategies against cardiovascular disease is the comprehensive understanding of the cellular function of potential miRNA candidates.

4 CHALLENGES AND APPROACHES IN THE FIELD

4.1 TARGET IDENTIFICATION TO DETERMINE MIRNA FUNCTIONS

In general, the design and use of miRNA and miRNA-based strategies as valuable tools in molecular biology and medicine is highly dependent on a better understanding of the cellular function of miRNAs. The as yet most successful way to decipher the function of a miRNA is to look at the gene transcripts it regulates [391]. Therefore, the identification and validation of the complete set of miRNA-regulated targets, the miRISC targetome, including the functions of the encoded proteins and the tissue-specific availability of the target transcripts are required [404]. However, the identification of direct miRNA targets is challenging. First, miRNA/target interactions are complex. The current *miRBase* [222] release 20 lists more than 2,500 mature human miRNA sequences which renders them as one of the most abundant classes of regulatory genes. Each miRNA is expected to regulate multiple (up to even hundreds of) targets [57, 235] and in turn, each mRNA is likely to underlie the combined regulation of multiple miRNAs [223]. Second, the short and only partially complementary binding sites, the often small effects, and the fact that we still do not fully understand the molecular mechanisms of miRNA/target interaction, avoid an easy forecasting of individual miRNA targets. Even though theoretical predictors (see Section 2.4) for effective miRISC-mediated target repression have been incorporated in numerous dedicated computational algorithms, disruptive factors like competing regulators, cell type-specific target or miRNA expression, and statistics (due to the short interaction sites) make such software approaches quite error-prone.
Finally, also biochemical high-throughput methods, which easily disclose the complete and correct set of mRNAs each miRNA-guided silencing complex directly regulates are not yet available.
Therefore, the knowledge concerning each miRNA's targetome and its mediated cell-specific functions is sill rather limited.

4.2 COMPUTATIONAL TARGET PREDICTION

Bioinformatic miRNA target identification algorithms, such as *TargetScan* [246, 142, 127], *PicTar* [223], *miRanda* [194] or *RNAhybrid* [336], which base their predications with variable emphasis on indicators such as seed pairing, evolutionary conservation of the binding region on the mRNA, free energy of the miRNA/mRNA duplex, mRNA sequence features outside the miRISC binding site, and target site accessibility have emerged as interesting attempts for miRNA target prediction.
However, the short length of the seed region intrinsically retrieves a multi-

tude of potential target site hexa- or heptamers and thus such *in silico* predictors often identify huge amounts of targets accompanying large fractions of false-positives [18, 4]. Further, non-conserved (10-times more frequent than conserved [223, 246]) or non-canonical target recognition sites and interactions outside the often exclusively examined 3′-UTR sequences cause a considerable amount of false-negatives [391]. Moreover, all algorithms face the obstacle of variations in the sequence annotation among the databases used for the predictions leading to inconsistent outcomes. For example, the results of the same prediction method applied to two different databases (*UCSC* and *Ensembl*) overlapped by less than 50% [342]. Further, tissue-, development- or disease-specific mRNA isoforms [415] due to alternative splicing and differential 3′-end processing are not yet taken into account. In summary, there is no universally applicable computational algorithm for effective (specific and sensitive) target prediction [428].

4.3 GENETIC TARGET IDENTIFICATION

The first miRNA/target interaction of *lin-4* with mRNA *lin-14* was identified by forward genetics, characterized by, first, screening for mutants with interesting phenotypes and, second, conducting research regarding their origins on a genotypic level [6]. Here, the advantage lies in the immediate identification of phenotypically and hence biologically meaningful targets [391].
However, the reverse approach involving the examination of the functional consequences of specific genetic manipulations has also proved useful in the identification of miRNA/target pairs. This is especially true, if the approach is combined with computational predictions or biochemical methods which may comprise comparative profiling studies upon miRNA manipulation or isolation of mRNAs bound to miRISCs (see below).

4.4 COMPARATIVE TARGET INFERENCE AFTER MIRNA MANIPULATION

Based on the generally repressive effect of miRNA-mediated regulation on target gene expression, inverse correlation between miRNA and mRNA levels indicates potential interaction partners. Therefore, artificially perturbing of the cellular levels of a miRNA of interest (reverse genetics) is a generally accepted approach to study its function.

MIRNA MANIPULATION

MiRNA manipulation strategies are manifold and widely used *in vivo* and *in vitro*.
To experimentally deplete a miRNA of interest, similar strategies as describe for the therapeutic application (see Section 3.6) come into question. Next to AMO and LNA chemistries, inhibitors designed as miRNA scavengers comprising multiple miRNA binding sites to competitively keep a miRNA from its cellular target sites have been proposed. These include miRNA sponges [100], 'erasers' [355], 'decoys' [60], and 'tough decoys' [160].

Also for the deliberate mimicry or over-expression of miRNAs multiple options are conceivable. Synthetic miRNA mimics are RNA duplexes of a guide stand identical to the endogenous miRNA and a passenger strand (see Section 2.1). Theses mimics are often modified to increase their nuclease stability and cellular uptake. Further, the cellular level of the miRNA of interest may be increased by virus-mediated expression of cytoplasmatic pre-miRNA precursors in order to account for proper miRNA maturation and loading into the miRISC [262, 131].

COMPARATIVE PROFILING

In principle, reciprocal miRNA/target correlation can be observed on both, mRNA and protein level.
For the profiling of differential target gene expression, ectopic over-expression of a particular miRNA [252, 195] as well as artificial depletion of the miRNA of interest [227, 255] has been applied. The increase in mRNA expression subsequent to miRNA knock-down has been reported to be rather low compared to the decrease upon ectopic over-expression. However, artifacts might be generated by supra-physiological levels of miRNAs, which may even lead to an increased expression of endogenous miRNA targets due to the occupation of available miRISCs [208]. Importantly, profiling mRNA expression fails to identify targets that are translationally repressed.
Alternatively, proteomic analyses can be used to identify an inverse relation of the levels of miRNAs and proteins encoded by predicted target transcripts. Stable Isotope Labeling with Amino acids in Cell culture (SILAC) followed by mass spectrometry has been applied to measure the effect of manipulated miRNA expression on the whole cellular proteome [18, 364] (compare Section 2.5). In both studies, transcripts corresponding to responsive proteins were enriched in seed matches to the manipulated miRNAs. However, changes of the transcriptome correlated well with proteome alterations. Thus, due to their comparably lower demands regarding resources and costs, transcriptomic analyses might be preferable.
Albeit seed matches may provide an indication, both strategies (mRNA profiling and proteomics) cannot distinguish direct from indirect target molecules.

4.5 UTILIZATION OF THE PHYSICAL MIRISC/TARGET CONTACT

Several experimental studies have aimed to identify direct miRNA targets by taking advantage of the physical interaction between the target mRNA and protein components of the miRISC. Thereby biochemical purification strategies are employed to enrich for miRISC-associated mRNA populations prior to their profiling.

CO-IMMUNOPRECIPITATION (CO-IP)

In a first approach, RNA co-ImmunoPrecipitation (RIP) of often epitope-tagged miRISC proteins (for example AGO [28, 99, 202, 163, 169] or TNRC6 proteins [444, 236]) has been used to co-precipitate miRISC-associated targets from cultured cell or tissue extracts. Simultaneous depletion [99] or over-expression

[202] of the miRNA of interest has been combined to facilitate target identification. To profile the co-isolated RNA population, quantitative Reverse Transcription Polymerase Chain Reaction (qRT-PCR) or array hybridizations assays (microarrays) have been used [193, 390, 99, 202, 163, 236, 169]. The latter approach is referred to as RIP-Chip.
Unfavorably, AGO proteins have been shown to also unspecifically associate with RNA after cell lysis [282, 202], indicating the potential of false-positive targets. This is aggravated by the shortcoming that purification conditions subsequent to the ImmunoPrecipitation (IP) have to be rather mild in order to not destabilize the protein/RNA interactions of interest [282, 205]. Hence, these methods either identify too many (false-positives) or only relatively stable miRISC/mRNA interactions failing to detect transient contacts (false-negatives). Besides, it is inherent to these methods to not allow for the disclosure of individual miRISC binding sites. However, the precise knowledge and the distribution of binding sites rather than only the identity of the isolated RNA is crucial to understand, e. g., the combinatory regulation of a particular target.

CROSS-LINKING AND IMMUNOPRECIPITATION (CLIP)

Substantial progress towards a higher resolution and specificity of binding site identification has been made by the CLIP technique. The introduction of an initial cross-linking step establishes a covalent connection between the miRISC and the associated RNA species enabling to quasi 'snapshot' and preserve RBP/RNA interactions in living cells.
Already before miRNA have been discovered, UV light was shown to cross-link proteins to RNA in living cells [413, 325]. In contrast to formaldehyde-based cross-linking often used to study protein/DNA interaction in so-called 'CHromatin ImmunoPrecipitation (CHIP) assays' [230], protein/RNA cross-linking is performed by irradiating the cells with short-wave UV light of 254 nanometers (nm). Thereby protein/protein cross-links are avoided, which could potentially lead to large protein/RNA complexes that may contain RNA not directly or not even functionally associated to the RBP of interest. The exact mechanism of UV-induced protein/RNA cross-linking is not fully understood yet, but UV irradiation is suggested to elevate the energy states of electrons within the ribonucleotide bases, which are thereby enabled to form new covalent bonds to, e. g., aromatic amino acids in direct contact [50, 122].
This phenomenon was first combined with the IP of an RBP other than a member of the miRISC (a splicing regulator) to study its RNA targets (see Table 4.1 #1). The method was termed CLIP [401, 400]. Thereby, the immunoprecipitate is subjected to partial RNA digestion to digest RNA which is not bound (and thus not protected) by the RBP and to decrease the size of the cross-linked transcripts to fragments of about 50 nucleotides. Subsequently, the RNA is radioactively labeled and the RNA/protein complexes are size-fractionated by Sodium Dodecyl Sulfate PolyAcrylamide Gel Electrophoresis (SDS-PAGE). After transfer to a nitrocellulose membrane, the radioactive signal at the expected size of the protein complex is excised in order to separate it from still indirectly associated, non-cross-linked RNAs, which are expected to migrate faster [14]. The protein component is digested with proteinase K, and the RNA still carrying

the covalently bound amino acids or oligopeptides are recovered. Such isolated RNA fragments are ligated to 5'- and 3'-adaptor sequences to enable Reverse Transcription (RT) and Polymerase Chain Reaction (PCR) amplification of the obtained complementary DNA (cDNA). Originally, the amplificates have been used for Sanger-sequencing, resulting in a set of sequence reads. Alignment to the reference genome and/or transcriptome and identification of clusters of overlapping reads ideally lead to true RBP binding sites within the corresponding transcripts.
Compared to RIP or RIP-Chip, the covalent linkage enables to apply more stringent purification conditions after the immunoprecipitation, such as high salt washing buffers with stronger detergents and denaturing SDS-PAGE, reducing the detection of post-lysis false-positive associations. Further, also transient interactions may be preserved, if a direct contact at the time of UV irradiation enabled the formation of a covalent linkage. The partial RNase-mediated digestion increases the resolution of detected binding sites.
However, the actual miRISC binding region at these sites still needs to be predicted. Further, the small number of sequences obtained by conventional Sanger-sequencing limited the full potential of early CLIP studies.

HIGH-THROUGHPUT SEQUENCING OF RNA ISOLATED BY CLIP (HITS-CLIP)

During the last decade, sequencing technologies have improved tremendously, allowing for massively parallelized generation of millions of sequencing reads [37]. Compared to other high-throughput methods such as microarray analysis they offer a larger dynamic range of target identification and are not limited to the detection of known transcripts [422]. Hence, they allow for the examination of, e. g., alternative splice products [314], 3'-terminal differentially processed [415], and novel RNA species [58].
In combination with the CLIP approach the so-called 'HITS-CLIP technique' enables a less biased and more exhaustive sequencing of cross-linked RNA species and to systematically map transcriptome-wide binding patterns of the RBP of interest [251] (see Figure 4.1 middle).
The first application of HITS-CLIP for the large-scale identification of AGO-associated RNA fragments identified nearly 500 different cross-linked miRNA and mRNA reads that mapped to almost twice as many transcripts in murine brain tissue [70] (see Table 4.1 #2). A second HITS-CLIP study to examine the tripartite complexes of AGO protein, miRNA and target transcript *in vivo* was performed in *Caenorhabditis elegans* [450] (see Table 4.1 #3). Another study based on AGO2-specific immunoprecipitation compared binding sites detected for wild-type and *Dicer1*-depleted mouse embryonic stem cells, which enabled a differentiation between miRNA-dependent and -independent AGO2 targets [245] (see Table 4.1 #4). HITS-CLIP has also helped to resolve viral miRNA binding sites on a genome-wide scale. A study with Epstein-Barr Virus (EBV)-transformed B cells identified that most transcripts targeted by the top 12 viral miRNAs (almost exclusively non-viral transcripts) are simultaneously co-targeted by cellular miRNAs at distinct binding sites [340] (see Table 4.1 #6). The targetome of Kaposi's Sarcoma-associated HerpesVirus (KSHV) and cellular miRNAs was approached by AGO HITS-CLIP with two latently KSHV-

infected murine cell lines [149] (see Table 4.1 #7). Also these viral miRNAs were identified to predominantly target cellular transcripts and especially ones with products involved in multiple pathways central for KSHV biology. By a combination of genetic modification (*miR-155* knock-out) with differential HITS-CLIP (dCLIP) and mRNA expression analysis, transciptome-wide targets of a single miRNA have been approached [258] (see Table 4.1 #8). Interestingly, about 40% of *miR-155*-dependent miRISC binding occurred at sites lacking perfect seed matches, confirming non-canonical miRNA binding as a widespread phenomenon. To identify which miRNAs participate in liver regeneration and which targets they regulate, the original HITS-CLIP protocol [70] was transferred to liver tissue of mice [360] (see Table 4.1 #9). Upon induction of hepatocyte proliferation with a partial hepatectomy model, expression-weighted AGO footprinting identified a dynamic recruitment of miRNAs to target transcripts within the regenerating tissue. An AGO2 HITS-CLIP study with human brain tissue revealed more than 7,000 binding sites across over 3,300 brain transcripts with more than 1,800 target sites corresponding to the top 20 human brain miRNAs [43] (see Table 4.1 #10). Interestingly, an intersection of human and mouse brain AGO HITS-CLIP data [70] showed an overlap of less than 10% of the human clusters with the murine data set. In spite of obvious differences between mice and humans, the use of slightly different IP antibodies and the comparison of developing (mouse) versus adult (human) tissue, these extensive disparities appear rather unexpected. Probably different peak-calling and data evaluation procedures have contributed to this result, indicating the strong dependency of CLIP data on the computational analysis. Moreover, this study was one of the first building a bridge from a feasibility study to clinical relevance. It emphasized impressively how Single Nucleotide Polymorphisms (SNP) can alter miRNA binding sites with disease-relevant consequences.
These large-scale assays showed not only that CLIP studies allow for narrowing down the binding regions through RNase treatment of the target transcripts, but also that cross-linking induces indicatory single nucleotide mutations. Presumably introduced during reverse transcription of the more bulky cross-linked ribonucleotides (still covalently connected to one or more amino acids), such specific point mutations have proved helpful in localizing the exact RBP binding site [39, 140, 217, 443, 291]. Further, these so-called 'Crosslinking-Induced Mutation Sites' (CIMS) [443] provide an opportunity to distinguish true binding events from ubiquitous background noise of unspecific associations. However, cross-linking efficiency of nucleic acids (DNA) to binding proteins by short-wave UV irradiation has been shown to saturate within the range of only 2 to 7% (depending on the protein) [122]. Thus, cross-linking-induced formation of covalent protein/RNA (or DNA) connections might be rather inefficient.

PHOTO-ACTIVATABLE RIBONUCLEOSIDE ENHANCED-CLIP (PAR-CLIP)

Another method for comprehensive profiling of RNA covalently bound to an RBP of interest has been termed PAR-CLIP [151] (see Figure 4.1 left). For this CLIP approach, previously to cross-linking and harvesting, cells are grown in a medium containing photo-activatable nucleoside analogs, such as thione-containing 4-thio(S)-Uridine (4SU) or 6-thio(S)-Guanine (6SG) [121]. Both are

readily taken up by mammalian cells [279] with no apparent alterations of transcript levels (determined by microarrays) [151]. 4SU and 6SG can randomly substitute during transcription for U and G, respectively. The incorporation rate may vary substantially, depending on factors such as the identity of the nucleoside analog, its concentration, the labeling time or the metabolism of the used cell type [14]. Upon successful transcriptome-wide incorporation of these substances into nascent transcripts, the RNA is generally more efficiently covalently cross-linked to RBPs as compared to the previous CLIP methods using the same irradiation dose [151, 217]. Importantly, photo-activatable ribonucleotides are exited with long-wave UV light (365 nm), which is not sufficient to cross-link unmodified nucleotides. Photo-activated bases predominantly cross-link to aromatic amino acids but also to lysines and cysteines [274]. Similar to the (HITS-)CLIP approach, electronic orbitals of exited nucleotides and reactive amino acid sides chains need to overlap to trigger photo-addition [14]. Thus, cross-linking efficiency may be variable, depending on the sequence composition of the binding site (for instance the number of U), the type of amino acids in close proximity, and the spatial orientation of the participating reaction partners. However, compared to HITS-CLIP, the use of replicate experiments of cells labeled with different photo-activatable nucleosides may control for such bias. Likewise, immunoprecipitated protein/RNA complexes are used to generate cDNA libraries for deep sequencing analysis. In contrast though, reverse transcriptase apparently specifically mis-incorporates for example a G or Thymidine (T) opposite to cross-linked 4SU or 6SG residues, leading to diagnostic T-to-C or G-to-A mutations, respectively. As HITS-CLIP-induced CIMS, these indicatory base transitions can be used to pinpoint RBP binding sites resulting in a near-nucleotide resolution. Interestingly, PAR-CLIP of the AGO members revealed that the regions downstream of the prominent cross-linking sites (indicated by T-to-C transitions) are enriched in sequences complementary to the seed regions of the top expressed miRNAs placing the cross-link near the center of the miRISC/target RNA complex [151]. As for CIMS, these diagnostic mutations simultaneously provide a valuable feature to distinguish cross-linked (signal) from non-cross-linked sequence reads (noise). Typically, clusters of reads corresponding to cross-linked RBP binding sites show 50 to 70% T-to-C transitions, while background reads are basically free of indicatory mutations [151, 14].

In the initial study, several RBPs have been isolated from human cell cultures to identify their binding sites on associated RNA targets including the four AGO paralogs and TNRC6 A to C (all epitope-tagged) [151] (see Table 4.1 #12). Each individual AGO protein yielded on average 4,000 clusters of sequenced reads. Since they essentially overlapped, the sequence reads of all four AGO proteins were combined resulting in more than 17,000 clusters of more than five reads each. They mapped to more than 4,600 (about 21%) of all annotated transcripts defining the targetome of more than 500 identified miRNAs. Interestingly, a quantitative comparison of HITS-CLIP and PAR-CLIP for two kinds of RBPs including human AGO2 (in its native form) revealed only small differences in the accuracy of both methods [217] (see Table 4.1 #13). Also, the PAR-CLIP technique has already been applied to examine the targets of virus-encoded miRNAs [373] (see Table 4.1 #16). By precipitating either tagged or

endogenous AGO2 from EBV-infected lymphoblastoid cell lines, this study comprehensively identified viral and cellular miRNA binding regions (about 7,800 miRISC binding sites on almost 3,500 transcripts). Another one of the few CLIP studies recently trying to reach beyond proof-of-principle analysis towards their application in the context of human diseases is the use of PAR-CLIP to identify differential miRNA targeting dependent on distinct breast cancer molecular subtypes [119] (see Table 4.1 #17). Through integration of high confidence target data revealed by PAR-CLIP of a breast cancer cell line (MCF7) with patient-paired miRNA/mRNA expression data and computational modeling, the authors identified subtype-associated regulatory miRNAs as potential therapeutic targets and prognostic markers in breast cancer.
Certainly, the need for previous RNA labeling involves the disadvantage of generally depending on cells in culture and cells which are metabolically active enough to regenerate their complete transcriptome within the labeling period. Further, the modified nucleotides potentially interfere with biogenic processes and may provoke cellular stress or even apoptosis with unpredictable bias on the final results [206, 54]. Moreover, the transfer of RNA fragments into a cDNA library and finally sequenced reads is quite lossy. Not only that the PAR-CLIP protocol for the library preparation is based on two (3′ and 5′) inefficient terminal linker ligations allowing only a fractional amount of transcripts to be at all reverse transcribed. It is also that in most cases reverse transcriptase encounters a cross-linked nucleotide, the enzyme probably drops off leaving a truncated cDNA without the second primer binding site needed for amplification and sequencing [384] (see below).

INDIVIDUAL NUCLEOTIDE RESOLUTION CLIP (ICLIP)

Similar to the above mentioned HITS- and PAR-CLIP techniques, iCLIP allows for the identification of RBP binding sites on the target RNA at nucleotide resolution [221] (see Figure 4.1 right). However, it differs from the previous methods in that it takes advantage of the observation that reverse transcriptase rarely reads through the obstacle introduced by the photo-adduct of ribonucleotide and peptides that remain after Proteinase K digestion at the position of the cross-link. This effect has already been used in an early version of the CLIP protocol in which, during RT with a primer extension assay, reverse transcriptase has been observed to stall at the cross-linking position [402]. With the standard library preparation method used for previous CLIP assays, all truncated cDNAs are lost due to the lack of RT of the 5′-adaptor sequence needed for PCR amplification prior to sequencing. The iCLIP method employes an alternative strategy to prepare the cDNA library. Thereby an intra-molecular circularization step replaces one of the inefficient inter-molecular sequencing adapter ligations previously required on both ends of the isolated RNA fragments. Only the 3′-end is ligated to an adaptor containing the reverse transcriptase primer binding site, a specific restriction site, a barcode, and the 5′-primer binding site needed for sequencing. After the generation of the complementary second strand, the then double-stranded reverse transcripts are circularized and subsequently re-opened at the introduced restriction sites, positioning the barcode next to the presumed cross-link position and one adaptor sequence on both

sides of the fragments (see Figure 4.1F right). The introduced barcode, which contains a randomized sequence, enables to evaluate the complexity of the library. Reads originating from the same cDNA template (PCR duplicates) will also share the same barcode and can therefore be distinguished from unique, independent cDNAs [221]. Certainly, this approach can also be applied to the previously mentioned CLIP techniques in order to detect amplification artifacts [218]. However, as it is difficult to assess the fraction of cross-linked reads, it might be challenging to distinguish signal form noise during iCLIP data analysis [14].

'TANDEM AFFINITY PURIFICATION-CLIP (TAP-CLIP)'

For the sake of completeness it should be mentioned that, next to cross-linking and library preparation, also immunoprecipitation represents a key point for variation and optimization of the original CLIP protocol. As both variants are base on a Tandem Affinity Purification (TAP) protocol of the RBP of interest (subsequent to short-wave UV cross-linking), they are listed together. In a technique termed CRoss-linking and Analysis of CDNA (CRAC) [39, 140], modified RBPs containing a C-terminally 6 $\times$ histidine (H) - Tobacco Etch Virus (TEV) protease site - protein A tag are applied. Double affinity purification includes the initial use of immunoglobulin G beads followed by TEV protease treatment and denaturing Immobilized Metal-ion Affinity Chromatography (IMAC) of the first eluate. For individual nucleotide resolution Cross-Linking Affinity Purification (iCLAP), the RBPs are previously engineered to contain a Strep-tag and a poly(H)-epitope [423]. After purification on streptavidin beads, likewise IMAC is performed. In contrast, isolated RNA targets are converted into a cDNA library and sequenced similar to the iCLIP protocol.

CONSIDERATIONS REGARDING THE CLIP TECHNIQUES

All variants of AGO CLIP experiments provide elegant and comparably promising biochemical methods to identify miRNA targets.
Both HITS-CLIP [450] and PAR-CLIP [198] have even been shown to not only capture transcriptome-wide RBP binding sites in living cells, but also in whole (transparent) animals such as *Caenorhabditis elegans*. However, there are a few drawbacks which need to be considered right from the start.

MATERIAL CHALLENGES First, these methods always involve a technically challenging protocol with numerous steps at which precious input material may get lost. Thus, they have so far predominantly been designed as kind of proof-of-concept studies, based on rather easily accessible cellular material (for example stable cell lines). In order to capture context-dependent interactions under physiological conditions, biologically interesting but possibly scarce starting material (for instance primary cells) will be required. Moreover, parameters such as the RBP expression level, cross-linking efficiency, cell lysability etc. may be different. Hence, it might be difficult to collect sufficient input to obtain cDNA libraries that contain the complete set of RBP binding sites. Even in case of adequate biological availability, it should be mentioned that

such experiments easily get quite resource-intensive. More starting material is only helpful, if purifications are scaled up in order to preserve optimal signal-to-noise ratios. If PAR-CLIP is the method of choice, not only the expenses of, e. g., 4SU, but also the necessary incorporation of the photo-activatable nucleosides prior to cross-linking could represent a limitation (for instance for *in vivo* studies).

EXPERIMENTAL CHALLENGES Second, the multi-step protocols comprise many enzymatic reactions that may potentially bias the detection of binding sites. For example, the kind of RNA ligase used for adaptor ligation was shown to potentially influence the cDNA library composition of small RNAs [153]. Likewise, the choice and extent of the RNase treatment may critically influence the obtained results. The desired RNA fragment length ranges between 25 and 30 nucleotides [14]. Such relatively short reads are preferable as fragmentation increases IP efficiency and reduces the risk of isolating and detecting RNA-dependent interactions of other RBPs. Further, the small size avoids substantial spreading of the expected RBP band during SDS-PAGE, the adapter ligation is more efficient and reads can be obtained by a short-read sequencing approach. Moreover, it confines the search space for putative miRISC binding sites. However, over-digestion may decrease the number of identified binding sites. The use of sequence-specific RNases such as RNase T1, which specifically cuts after G residues [313], minimizes the risk of over-digestion but may as well led to a bias towards a depletion of G-rich clusters. The mentioned comparative study of HITS-CLIP versus PAR-CLIP addressed not only the effect of metabolic labeling with photo-activatable nucleoside analogs and cross-linking at the two different wavelengths (254 nm and 365 nm), but also the use of different RNases [217]. Interestingly, while both CLIP approaches revealed only minor differences in the identified binding sites, an unexpectedly strong impact was observed by the degree of RNase-mediated digestion. Probably due to an insufficient protection of the RBP-bound RNA fraction, extensive digestion strongly biased recovered binding sites.

COMPUTATIONAL CHALLENGES Third, the computational effort of analysis and interpretation of the large amount of data generated by CLIP experiments should not be underestimated. Bioinformatic data analysis comprises another complex multistep protocol not easy to be standardized. Even though a couple of online software packages implement the workflow and provide web-based visualization tools for the definition of RBP binding sites based on experimental CLIP data (for example *CLIPZ* [209], *PARalyzer* [76], *miRTarCLIP* [72], *PARma* [110] and *PIPE-CLIP* [67] or *dCLIP* [417] for the comparison of multiple CLIP data sets), they may not always provide out of the box solutions.
In general, the first step is to filter out low-quality reads and then to map the remaining sequence reads to the reference genome. As a detected binding site may span an exon-exon junction, the mapping should either also be done against the transcriptome or by splicing-aware algorithms such as *TopHat* [399]. Multi-copy genes are another challenge, which may be bypassed by the use of non-redundant reference data sets [140]. Importantly, one needs to think about the number of allowed mismatches to account for cross-link-induced mutations.

Next, the actual binding sites need to be identified by read clustering and normalization steps. Provided that the sequencing library is of sufficient complexity, highly occupied binding sites are expected to appear as clusters of reads. However, read counts are not necessarily interpretable as a direct measure of the affinity of the RBP of interest. The number of reads within one cluster may also depend on factors such as transcript abundance and nuclease stability or cross-linking efficiency of the particular sequence bound by the RBP. Thus, quantitative binding affinity cannot directly be inferred from the peak hight of the CLIP clusters. Therefore replicate experiments and/or normalization strategies need to be applied in order to identify true target sites.
Depending on the CLIP protocol applied, further determinants such as, e. g., CIMS (HITS-CLIP) or T-to-C mutations (PAR-CLIP) indicating the position of cross-linked nucleotides may be used to increase the signal-to-noise ratio and pinpoint the exact binding sites. Therefore, statistical analysis needs to clarify whether a particular mutation occurs at higher frequency than expected by chance. However, this can as well be complicated by the existence of, e. g., SNP or RNA-editing sites [291].
In case of read clusters corresponding to miRISC binding sites, the next step is to identify potential miRNA binding sites. This is typically implemented by algorithms searching for the enrichment of certain sequence stretches of defined length or particular binding motifs and comparing them to the seed sequences of the top n expressed miRNAs [367, 19]. However, if a particular miRNA is not among this number n of most expressed miRNAs, not even identified yet or, which is in fact quite likely [162], does not hybridize to the target with a canonical seed region, it will not be matched. Therefore, it must be emphasized that all CLIP techniques do not allow for a direct miRNA/mRNA matching. The search space is narrowed, however it is still a prediction of binding sites according to predetermined (and thus biasing) binding rules.

Taken together, binding sites identified by CLIP techniques not necessarily correspond to biologically relevant miRISC/mRNA interaction sites making it indispensable to validate and prioritize the large lists of potentially interacting pairs.

4.6 VALIDATION AND PRIORITIZATION OF MIRNA TARGETS

With respect to the initially mentioned intention, to identify target molecules in order to disclose the cellular function of a miRNA, CLIP derived large lists of potential miRNA/target interactions need to be verified and possibly sorted based on their cellular relevance.

VALIDATION

To test individual miRNA/target pairs for direct and functionally relevant interactions, multiple validation approaches have been developed [410].
Often these methods involve a disturbance of the miRNA/target interaction and a subsequent abrogation of the interference to test for loss and recovery

#	PROTOCOL	RBP	CELLS	4SU LABELING	UV [J/CM^2]
Short-wave UV CLIP					254 nm
1	CLIP	NOVA1	mouse brain tissue	no	3 × 0.4 (10 ml, 10 cm plate)
2	HITS-CLIP	mAGO	mouse brain tissue	no	3 × 0.4 (10 ml, 10 cm plate)
3	CLIP-seq	ALG-1	*Caenorhabditis elegans*	no	0.3 (empty plate)
4	HITS-CLIP	mAGO2	2E6 mESC	no	0.004 (4 ml, 10cm plate)
5	iCLIP	HNRNPC	mouse brain tissue	no	4 × 0.1 (5 ml, 10 cm plate)
6	HITS-CLIP	hAGO, hAGO2	Jijoye (EBV$^+$)	no	2 × 0.3 (10 ml, 10 cm plate)
7	HITS-CLIP	mAGO	BCBL-1, BC-3 (KSHV$^+$)	no	0.4 + 0.2 (10 cm plate)
8	dCLIP	mAGO2	mouse T cells (WT, *miR-155* KO)	no	0.4 + 2 × 0.2 (1 ml, 3.5 cm plate)
9	HITS-CLIP	mAGO	mouse liver tissue	no	3 × 0.4 (10 ml, 10 cm plate)
10	HITS-CLIP	hAGO2	human postmortem brain tissue	no	*
11	CLASH	hAGO1	HEK293 T-REx Flp-In (hAGO1)	no	0.4 (10 ml, 10 cm plate)
Long-wave UV CLIP					365 nm
12	PAR-CLIP	F/H-hAGO1-4 (i.a.)	HEK293 T-REx Flp-In (hAGO1-4)	0.1 mM, 16 h	0.15 (empty plate)
13	PAR-CLIP	hAGO2 (i.a.)	HEK293	0.1 mM, 16 h	0.15 (empty plate)
14	PAR-CLIP	ELAVL1	HeLa	0.1 mM, 12 h + 4 h	0.15 (empty plate)
15	PAR-CLIP	GLD-1-G/F	*Caenorhabditis elegans*	2 mM, ca. 48 h	2.0 (empty plate)
16	PAR-CLIP	hAGO2, F/H-hAGO2-G	5 LCL (EBV$^+$)	*	*
17	PAR-CLIP	hAGO2	MCF7	0.1 mM, 24 h	*

TABLE 4.1. Selection of published CLIP studies. Cross-Linking and ImmunoPrecipitation (CLIP), HIgh-Throughput Sequencing of RNA isolated by CLIP (HITS-CLIP), individual nucleotide resolution CLIP (iCLIP), differential CLIP (dCLIP), Cross-linking, Ligation And Sequencing of Hybrids (CLASH), Photo-Activatable Ribonucleoside enhanced-CLIP (PAR-CLIP), Flag/HA-hAGO1-4 (F/H-hAGO1-4), GLD-1-GFP/Flag (GLD-1-G/F), Flag/HA-hAGO2-GFP (F/H-hAGO2-G), RNase A (A), MNase (MN), RNase I (I), RNase A+T1 (RNace-IT, A+T1), RNase T1 (T1), bridged antibody (#2 rabbit anti-mouse IgG, #6 rabbit anti-mouse IgG (2A8) and rabbit anti-rat IgG (11A9), brd.), protein (prot.), sepharose (seph.), * indicates details have not been withdrawable but authors reference original study: short-wave UV CLIP: [70], long-wave UV CLIP: [151].

#	RNASE [MU/µL]	ANTIBODY	INPUT	BEADS	REF.
Short-wave UV CLIP					
1	A: 0.04/ 2, 37°C, 10 min	anti-Nova	20 mg	400 µl (prot. A)	[400]
2	A: 0.02/ 2, 37°C, 10 min	brd. anti-mAGO (2A8/ 7G1-1)	20 mg	400 µl (prot. A)	[70]
3	MN: (1 ng), 4°C, 10 min	anti-ALG-1	40,000 worms (L4)	100 µl (prot. G, seph.)	[450]
4	A. 2, 37°C, 10 min	anti-mAGO2 (2D4)	8 × 10 cm plates	100 µl (prot. G)	[245]
5	I: 1, 37°C, 3 min	anti-Hnrnpc	50 mg	100 µl (prot. A)	[219]
6	*	brd. anti-mAGO (2A8)/ brd. anti-hAGO2 (11A9)	*	*	[340]
7	A: 0.02 - 0.04, 37°C, 10 min	anti-mAGO (2A8)	*	*	[149]
8	I: ~9, 37°C, 5 min	anti-mAGO (polyclonal)	65 × 10^6 cells	90 µl (prot. G)	[258]
9	*	anti-mAGO (2A8)	*	*	[360]
10	*	anti-hAGO2 (3148)	~60 mg	*	[43]
11	A+T1: 1, 20°C, 7 min	rabbit IgG (PTH tag)	4 × 15 cm plates	20 mg (epoxy)	[162]
Long-wave UV CLIP					
12	T1: 1,000 + 100,000, 22°C, 15 + 15 min	anti-FLAG (F1804)	3 ml pellet	120 µl (prot. G)	[151]
13	T1: 1,000 + 100,000, 22°C, 15 + 15 min/ T1: 5 + 20,000, 22°C, 15 + 15 min/ MN: 50 + 200, 37°C, 5 + 5 min	anti-hAGO2 (11A9)	*	*	[217]
14	T1: 1,000 + 50,000 22°C, 15 + 8 min	anti-HuR (sc-5261)	60 - 100 × 15 cm plates	360 - 600 µl (prot. G)	[239]
15	T1: 1,000 + 100,000, 22°C, 15 + 12 min	anti-FLAG (F3165)	250,000 worms	300 µl (prot. G)	[198]
16	*	anti-hAGO2 (9E8.2)/ anti-FLAG (F1804)	10^9 cells	*	[373]
17	*	anti-hAGO2 (9E8.2)	*	*	[119]

(cont.)

of the miRNA-mediated regulation, respectively. In general, highly sensitive but pairwise reporter assays have to be traded off against comprehensive but consumptive high-throughput assays.

REPORTER ASSAYS Among the first approaches to validate putative miRNA/mRNA interactions (and still serving as an efficient and routinely used strategy) were reporter assays, usually involving luciferase [223, 284]. These are based on expression vectors containing parts (including the miRNA binding site(s)) or the entire 3'-UTR of genes of interest behind a reporter gene. Transient transfection of cells with the reporter constructs followed by measurement of the reporter activity upon simultaneous modification of the expression level of the miRNA candidate allows for the validation of an expected inverse relationship between the gene product and the miRNA. Direct target regulation by the miRNA is confirmed by mutating residues within the miRISC binding site in the reporter and testing for restored expression [247, 196]. If the reporter gene can be shown to be regulated by physiologically relevant levels of the miRNA candidate, additional evidence regarding a biologically important miRNA/mRNA interactions rather than, e. g., an artifact due to miRISC saturation by the over-expressed miRNA is inferable. MiRNA inhibitors on the other hand need to be designed to exclusively repress the function of the candidate miRNA, which may be difficult in case of miRNA families with common seed regions.
Even though reporter assays represent a rather easy approach to test individual target interactions, the finding that a potential miRISC target site is effective upon placing it within the 3'-UTR of a reporter gene, not necessarily means that the site in question will be available when it is part of the naturally folded and regulated transcript. Further, the pairwise assay does not allow for a high-throughput verification of the entire set of CLIP-identified targets. Thus, it cannot account for the issue that quite likely the combined effect on many targets rather than a single miRNA/target interaction accounts for the phenotypic consequence of miRNA-mediated regulation. Therefore, it might be of great value to combine different high-throughput approaches for target verification [220, 281]. However, the significant advantage of high-throughput profiling approaches, the large-scale format, also entails higher expenses of time and money.

INVERSE PROPORTIONALITY PROFILING As previously introduced (see Section 4.4), the generally inverse correlation between miRNA and target mRNA levels can be utilized to determine (or validate) potential interaction partners. Microarray profiling [252, 418] and quantitative proteomics [18, 364] allow to quantify changes in mRNA and protein synthesis after miRNA manipulation for thousands of genes simultaneously. However, for the microarray approach it has to be considered that potentially not all miRNA/mRNA interactions may be discovered, if miRNA-mediated regulation is based on translational repression rather than transcript degradation, and proteome analysis based on SILAC followed by quantitative mass spectrometry is quite labor-intensive. Again, both methods share the limitation, that the results of direct miRISC binding to targeted transcripts cannot be distinguished from indirect effects.

REPLICATES AND COMPARISON TO PUBLISHED TARGET DATA SETS As with all experiments, CLIP data need to be statistically confirmed. Technical and biological replicates are essential and need to be taken into account during experimental design and budgeting. Further, obtained data can be compared to an increasing amount of published CLIP results. To collect, curate and integrate such data, dedicated open-access databases allow for the transcriptome-wide exploration and comparison of, e. g., miRNA/mRNA interactions (*CLIPZ* [209], *starBASE* [434] or *doRiNA* [9]). Besides, experimentally validated miRNA/mRNA interactions are also gathered in databases such as *TarBase* [315], *MiRecords*[432], *Argonaute* [365], and *miRNAMap* [171].

DEGRADOME SEQUENCING Another transcriptome-wide analysis that has been suggested to determine miRISC interaction sites is called degradome sequencing (Degradome-Seq). It analyses RNA degradation pattern to specifically detect miRNA-determined cleavage sites, which was originally shown to be successful in the identification of miRISC-cleaved targets in plants [2, 135]. The method is a modified version of 5'-Rapid Amplification of cDNA Ends (RACE), where mRNA fragments possessing 5' monophosphate termini are specifically selected (adaptor ligation), amplified and analyzed by high-throughput sequencing. Even though eukaryotic slicing might reflect a relatively rare event, Degradome-Seq of cultured mammalian cells and tissue extracts identified several new cleavage sites on potential target transcripts [201, 366, 45].

CROSS-LINKING, LIGATION AND SEQUENCING OF HYBRIDS A recent refinement of the library preparation subsequent to CLIP-like isolation of miRISC-associated transcripts allowed, for the first time, the direct detection of miRNA/mRNA pairs [228, 162]. Thus, this method, referred to as Cross-linking, Ligation And Sequencing of Hybrids (CLASH), offers a fundamentally new approach to directly monitor inter-RNA interaction by an additional base-paired RNA ligation step to establish an inter-molecular linkage between, e. g., the miRNA and its corresponding target RNA.
The application of the CLASH technique to human AGO1 has identified more than 18,000 direct miRNA/mRNA interactions and in addition a multitude of binding sites on other types of RNA (for example on rRNAs, tRNAs or even on other miRNAs) [162] (see Table 4.1 #11). It may represent one of the most reliable transcriptome-wide data sets published so far. Next to these thousands of high-confidence interactions, CLASH of human AGO1 also revealed new interaction rules. For example, about 60% of seed interactions have been determined to occur non-canonical, containing bulged or mismatched nucleotides. In contrast to the often cited seed pairing rule, ~18% of identified miRNA/mRNA interactions appeared to involve exclusively the miRNA 3'-end with little or no evidence for 5'-contacts.
However, as miRNA/mRNA chimeras have only been observed in 1% of the ligated RNA/RNA hybrids, the amount of input material required to obtain a cDNA library of sufficient complexity to ideally draw quantitative conclusions might be high.

PRIORITIZATION

Ranking of miRNA/target interactions in order to, e. g., explain a particular phenotype or to evaluate their therapeutic potential is highly desirable but not trivial.
In principle, validation of targets already provides a good indication of cellular importance. Hence, the above mentioned validation strategies are certainly helpful in prioritizing miRNA/mRNA interactions. For example, as endonucleolytic cleavage reflects a rather definitive type of regulation, Degradome-Seq identified targets might be quite effectively repressed. Further, CLASH-derived direct targets may be rated more valuable in the pursuit to determine the function of a miRNA than potentially indirect relations identified by microarrays.
Alternatively, target lists may be narrowed down by coupling experimental identification to further experiments or computational modeling.

EXPERIMENTAL SERIES The coupling of comprehensive top-down RBP-specific CLIP techniques with bottom-up strategies such as cross-linked RNA bait assays [20, 62, 297] or RNA digests [369] profiling RBP occupancy could enable the generation of high-resolution maps representing the concerted regulation of different RBPs on particular target RNAs [359]. Together with high-throughput quantitative proteomics data, the spatiotemporal resolution of these interactions could be increased, which would greatly facilitate the identification of the physiologically most relevant targets.

COMPUTATIONAL MODELING In turn, the computational combination of cell type-specific and context-dependent RBP/RNA interaction maps with systemic data or predictions revealing stability, modifications or secondary structures of the whole transcriptome [346, 88, 128, 271] might allow for the evaluation of the contacts according to their availability and occupancy under physiological conditions.
Further, the concept of miRISC cooperativity could provide a predictor to identify more effectively regulated and thus biologically important target candidates (see Section 2.6).

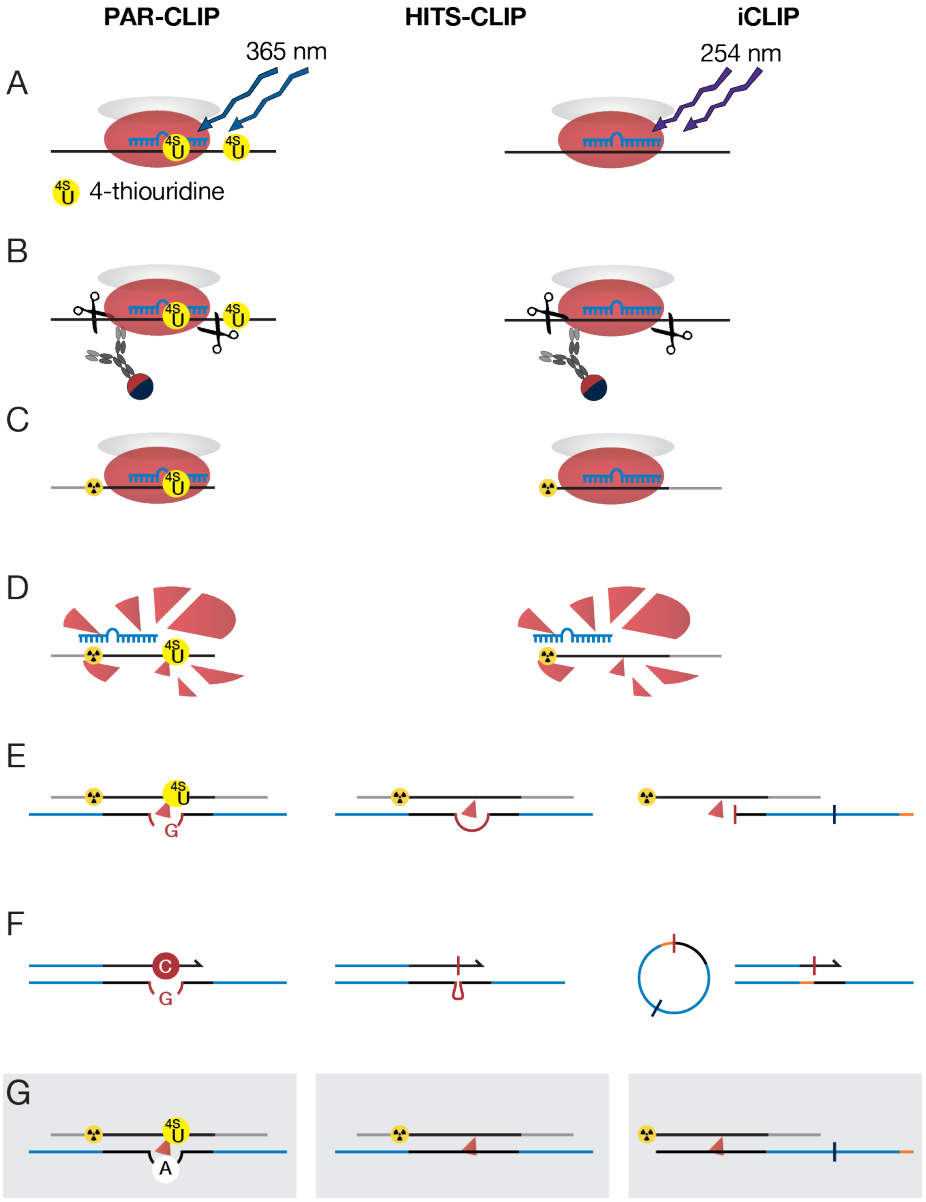

FIGURE 4.1. Schematic representation of different AGO CLIP strategies. The experimental approaches pictured are, from left: Photo-Activatable Ribonucleoside enhanced-Cross-Linking and ImmunoPrecipitation (PAR-CLIP), HIgh-Throughput Sequencing of RNA isolated by CLIP (HITS-CLIP), and individual nucleotide resolution CLIP (iCLIP). A and B: AGO CLIP; C to F: cDNA library preparation. A: RNA labeling with photo-activatable nucleoside analogs such as 4SU (only PAR-CLIP) and UV cross-linking of living cells (PAR-CLIP: 365 nm, HITS-CLIP, iCLIP: 254 nm); B: bead preparation, lysate preparation, AGO immunoprecipitation and partial RNA digest; C: dephosphorylation of RNA 3′-ends, linker ligation and ^{32}P-γ-ATP labeling of the RNA; D: AGO elution, SDS-PAGE, western blotting and RNA isolation, 3′-linker ligation (only PAR-CLIP); E: primer ligation, reverse transcription and gel purification; F: circularization followed by restriction digest (only iCLIP), high-throughput sequencing. G: reverse transcriptase events not leading to cross-link indicatory positions upon computational evaluation of the sequencing data (PAR-CLIP: transcription of 4SU with A or drop off, HITS-CLIP: accurate transcription or drop off, iCLIP: no drop off). See main text for additional information. Drawn on the basis of [220] Figure 1 and [14] Figure 2.

5 AIMS OF THIS PROJECT

Cardiac miRNA research may provide a solution to cardiovascular disease remaining the leading cause of morbidity and mortality worldwide. The basis for designing innovative and powerful miRNA-based medical strategies to prevent and treat cardiovascular disease is to understand the function and regulatory mechanisms of potential miRNA candidates. However, biochemical miRNA target identification methods and computational prediction algorithms are far from smoothly producing useful results. To determine the function of a miRNA candidate in its particular cellular context, biochemical target identification ideally needs to be carried out in primary cells excluding the use of stable cell lines. However, high-throughput experimental target identification often requires large amounts of input material which might be difficult to obtain from freshly isolated cells or tissue. Moreover, the detected targets should reflect the situation under physiological conditions and of one cell type only. This represents a real challenge, as input material may need to be pre-treated (Photo-Activatable Ribonucleoside enhanced-CLIP (PAR-CLIP)) or will be difficult to obtain in pure cell fractions prior to the experiment. Computational prediction, on the other hand, can only be as good as the biochemical data on which the algorithm was designed and must therefore be subject to some kind of iterative process. In summary, cardiac miRNA research is confronted with the following issues:

1. The as yet most successful way to decipher the function of a miRNA is to look at the gene transcripts it regulates (see Section 4.1)
2. All variants of AGO CLIP experiments provide elegant and comparably promising biochemical methods to identify miRNA targets (see Section 4.5)
3. BUT: Binding sites identified by CLIP techniques not necessarily correspond to biologically relevant miRISC/mRNA interaction sites making it indispensable to validate and prioritize large lists of potentially interacting pairs (see Section 4.5)
4. The concept of miRISC cooperativity could provide a predictor to identify more effectively regulated and thus biologically important target candidates (see Section 4.6)

In order to establish a foundation for the development of new miRNA-based therapeutic and diagnostic strategies to ameliorate cardiovascular disease, the first part of this PhD project aimed at the transfer of the CLIP approach to the cardiac system in order to facilitate the identification of targets directly regulated by functionally important miRNAs within the heart. In particular, the PAR-CLIP method was aimed to be applied to rodent primary CM and CF as well as to human myocardial slice cultures as a first step towards the

elucidation of the function of highly expressed cardiac miRNAs.
Not least in order, to better evaluate the therapeutic relevance of thereby identified miRNA/target interactions, a second part of the present project aimed at a deeper understanding of the mechanistic basis of miRNA-mediated target regulation. In particular, the objective was to theoretically address the concept of miRISC cooperativity. Previous experimental studies reported amplified target repression for adjacent miRISC binding sites (see Section 2.6). If cooperative target regulation was required for effective miRNA-mediated gene repression and thus a common principle, one would expect genomic evidence. Hence, transcriptome-wide computational screens with the objective to elucidate a potential genomic enrichment of miRISC binding sites in cooperativity-permitting adjacency were planned. Thereby, it was aimed for an answer to the question whether miRISC cooperativity reflects a general regulation principle and could thus serve as predictor to evaluate large sets of target transcripts based on their cellular relevance.

In summary, within the scope of the present PhD project, the following aims were set:

1. Transfer of the CLIP approach to individual cardiac cell cultures or total heart tissue
2. Biochemical identification of the transcriptome-wide set of potential miRNA/target interactions of highly expressed cardiac miRNAs by AGO2 CLIP experiments
3. Computational analysis of the concept of binding site distance-dependent miRISC cooperativity
4. Evaluation of identified miRNA/target interactions

II

MATERIAL AND METHODS

6 MATERIAL

6.1 EQUIPMENT, CONSUMABLES AND AGENTS

DEVICE	TYPE	MANUFACTURER
CCD camera	ImageQuant™ LAS 4000mini	GE Healthcare
centrifuge, table	microcentrifuge 5417R	Eppendorf AG
disperser	T 10 basic ULTRA-TURRAX®	IKA®-Werke GmbH & Co. KG
GE chamber (agarose gels)	PerfectBlue Gelsystem Mini M	PEQLAB Biotechnologie GmbH
GE chamber (SDS-PAGE)	XCell SureLock® Mini-Cell	Thermo Fisher Scientific Inc.
GE chamber (western blot)	Mini-PROTEAN® Tetra Cell	Bio-Rad Laboratories, Inc.
magnetic separator	DynaMag™-2	Thermo Fisher Scientific Inc.
micro scales	CP225D	Sartorius AG
PCR cycler	Mastercycler® pro	Eppendorf AG
perfusion system	Peristaltic Pump P-1	GE Healthcare
pH meter	pH211R	HANNA Instruments
phosphor imager	Cyclone Plus Phosphor Imager C431200	PerkinElmer Life and Analytical Sciences
phosphor imager screen	MultiSensitive Phosphor Screens, Small	PerkinElmer Life and Analytical Sciences
pipettes	0.1-2.5 µl, 2-20 µl, 20-200 µl, 100-1000 µl	Eppendorf AG
pipettor	accu-jet® pro	BRAND GmbH & Co. KG
power supply electrophoresis	EPS 1001 Power Supply	GE Healthcare
rotating wheel	Intelli-Mixer™ RM-2S	ELMI Ltd.
sonifier	SONOPULS HD 3100	BANDELIN electronic GmbH & Co. KG
thermoshaker	Thermomixer comfort	Eppendorf AG
tumbling table	Biometra® WT12	Biometra GmbH
UV cross-linker	Stratalinker® UV Crosslinker 1800	Stratagene
vibratome	VT1200 S	Leica Mikrosysteme Vertrieb GmbH
vortexer	Vortex-Genie 2, 230V	Scientific Industries, Inc.

TABLE 6.1. Devices

MATERIAL	NAME	PRODUCT ID	MANUFACTURER
1 ml syringe plunger	Omnifix®-F, 1 ml	9161406V	B. Braun Melsungen AG
1.5 ml siliconized tube	DNA LoBind Tube	22431021	Eppendorf AG
1.5 ml tubes	Micro tube 1.5 ml	72.690.001	SARSTEDT AG & Co.
2 ml tubes	Micro tube 2.0 ml	72.695.400	SARSTEDT AG & Co.
2 ml Phase Lock tube	Phase Lock Gel Heavy 2 ml	2302830	5 PRIME GmbH
15 ml Falcon	Tube 15ml	62.554.502	SARSTEDT AG & Co.
50 ml Falcon	Tube 50ml	62.547.254	SARSTEDT AG & Co.
4-12% NuPAGE Bis-Tris Gel	NuPAGE® Novex® 4-12% Bis-Tris Gels, 1.0 mm, 10 well	NP0321PK2	Thermo Fisher Scientific Inc.
5% TBE gel	5% Mini-PROTEAN® TBE Precast Gel, 15 Well	456-5016	Bio-Rad Laboratories, Inc.
6% TBE/Urea gel	Novex® TBE-Urea Gels, 6%, 10 Well	EC6865BOX	Thermo Fisher Scientific Inc.
cell strainer	BD Falcon™ Cell Strainer, 100 µm, yellow	352360	BD Biosciences
Costar SpinX column	Costar Spin-X® Centrifuge Tube Filter	8161	Sigma-Aldrich Corporation
glass prefilters	Filter Circles, 10 mm	1823-010	GE Healthcare
Hybond N membrane	Amersham Hybond-N	RPN203N	GE Healthcare
nitrocellulose membrane	Protean BA 85	10401197	GE Healthcare
slice filter	Millicell Cell Culture Insert, 30 mm, hydrophilic PTFE, 0.4 µm	PICM0RG50	Merck KGaA

TABLE 6.2. Material

SUBSTANCE	NAME	PRODUCT ID	MANUFACTURER
10× FastDigest Buffer	10× FastDigest Buffer	B64	New England Biolabs
^{32}P-γ-ATP	^{32}P-γ-ATP (10 µCi/µl)	SPR-501	Hartmann Analytic GmbH
AccuPrime SuperMix I	AccuPrime™ SuperMix I	12342-010	Thermo Fisher Scientific Inc.
BSA	Bovine Serum Albumin, Molecular Biology Grade (20 mg/ml)	B9000S	New England Biolabs
chloroform	Trichloromethane/Chloroform	3313.1	Carl Roth GmbH & Co. KG
DMEM	Dulbecco's Modified Eagle's Medium (DMEM)	41966-029	Thermo Fisher Scientific Inc.
DMSO	Dimethyl sulfoxide BioChemica	A1584	AppliChem GmbH
dNTP	dNTP-Set 1 (100 µM)	K039.1	Carl Roth GmbH & Co. KG
ethanol	Ethanol ⩾99.5%, Ph.Eur., reinst	5054.3	Carl Roth GmbH & Co. KG
FCS	Fetal Bovine Serum	3302-P103105	PAN-Biotech GmbH
GlycoBlue	GlycoBlue™ Coprecipitant	AM9515	Thermo Fisher Scientific Inc.
hsa-miR-1	Pre-miR™ *hsa-miR-1*	AM17150	Thermo Fisher Scientific Inc.
isoamyl alcohol	Isoamyl alcohol p. A.	A3611	AppliChem GmbH
isopropanol	2-Propanol BioChemica	A3465	AppliChem GmbH
M199	Medium 199	11150-059	Thermo Fisher Scientific Inc.
magnetic beads	Dynabeads® Protein G	10009D	Thermo Fisher Scientific Inc.
MEM	Minimum essential medium (MEM), 1X (with Hanks' salts and L-glutamine)	M1018	Sigma-Aldrich Corporation
MOPS Running Buffer	NuPAGE® MOPS SDS Running Buffer (20×)	NP0001	Thermo Fisher Scientific Inc.
NEBuffer 2	NEBuffer 2 (10×)	B7002S	New England Biolabs
NuPAGE Loading Buffer	NuPAGE® LDS Sample Buffer (4×)	NP0007	Thermo Fisher Scientific Inc.

TABLE 6.3. Substances

SUBSTANCE	NAME	PRODUCT ID	MANUFACTURER
PBS	Dulbecco's Phosphate-Buffered Saline (DPBS)	14190-094	Thermo Fisher Scientific Inc.
PEG 400	PolyEthylene Glycol (PEG), Mn 400	202398	Sigma-Aldrich Corporation
PenStrep	Penicillin/Streptomycin (penicillin: 10.000 U/ml, streptomycin: 10 mg/ml)	P06-07100	PAN-Biotech GmbH
peqGOLD RNAPure	peqGOLD RNAPure	30-1010	PEQLAB Biotechnologie GmbH
protease inhibitor	Halt Protease Inhibitor Cocktail, EDTA-Free (100×)	78428	Thermo Fisher Scientific Inc.
pyridyldithiol-biotin	EZ-Link HPDP-Biotin	21341	Thermo Fisher Scientific Inc.
RNA phenol/$CHCl_3$	Acid Phenol:Chloroform	AM9722	Thermo Fisher Scientific Inc.
Sigma FCS	Fetal Bovine Serum	F7524	Sigma-Aldrich Corporation
sodium acetate	3 M Sodium Acetate Solution, pH 5.5	AM9740	Thermo Fisher Scientific Inc.
streptavidin-HRP	High Sensitivity Streptavidin-HRP	21130	Thermo Fisher Scientific Inc.
Super Bond	Super Bond Gel	86068	KENT Deutschland GmbH
SYBR Green I	SYBR® Green I Nucleic Acid Gel Stain	S7563	Thermo Fisher Scientific Inc.
SYBR Green II	SYBR® Green II RNA Gel Stain	S7564	Thermo Fisher Scientific Inc.
TBE Loading Buffer	Novex® Hi-Density TBE Sample Buffer (5×)	LC6678	Thermo Fisher Scientific Inc.
TBE/Urea Loading Buffer	Novex® TBE-Urea Sample Buffer (2×)	LC6876	Thermo Fisher Scientific Inc.
water	Distilled Water	10977-035	Thermo Fisher Scientific Inc.

(cont.)

ENZYME	ACTIVITY	PRODUCT ID	MANUFACTURER
CircLigase™ II ssDNA Ligase	100 U/µl	CL9021K	Epicentre Biotechnologies
Collagenase Type II, Lot: 40S12366	280 U/mg	LS004179	Worthington Biochem. Corp.
FastDigest BamHI	(4-30 U/µl)	FD0054	Thermo Fisher Scientific Inc.
Proteinase K	0.05 U/µl	3115887001	Roche Diagnostics GmbH
RNase I	100 U/µl	AM2295	Thermo Fisher Scientific Inc.
RNase T1	1,000 U/µl	EN0542	Thermo Fisher Scientific Inc.
SUPERaseIn	20 U/µl	AM2694	Thermo Fisher Scientific Inc.
SuperScript® III Reverse Transcriptase	200 U/µl	18080-044	Thermo Fisher Scientific Inc.
T4 Polynucleotide Kinase (PNK)	10 U/µl	M0201S	New England Biolabs
T4 RNA Ligase 1	10 U/µl	M0204S	New England Biolabs
T4 RNA Ligase 2 truncated K227Q	200 U/µl	M0351S	New England Biolabs
Turbo DNase	2 U/µl	AM2238	Thermo Fisher Scientific Inc.

TABLE 6.4. Enzymes

ANTIBODY	TYPE	CLONE	PRODUCT ID	USE (IP)	MANUFACTURER
anti-AGO1-4	polyclonal	H-300	sc-32877	0.2 µg/µl	Santa Cruz Biotechnology Inc.
anti-AGO2	monoclonal	C34C6	2897S	0.15 µg/µl	New England Biolabs
anti-hAGO2	monoclonal	11A9	SAB4200085	0.1 µg/µl	Sigma-Aldrich Corporation
anti-mAGO2	monoclonal	2D4	018-22021	0.15 µg/µl	Wako Chemicals GmbH
goat anti-rat	polyclonal	goat anti-rat	112-035-068	0.3 µg/µl	Jackson ImmunoResearch Laboratories Inc.
mouse IgG	polyclonal	mouse IgG	015-000-003	0.15 µg/µl	Jackson ImmunoResearch Laboratories Inc.

TABLE 6.5. Antibodies

MARKER	NAME	PRODUCT ID	MANUFACTURER
1 kb DNA Ladder	1 kb DNA Ladder (0.5 µg/µl)	N3232S	New England Biolabs
100 bp DNA Ladder	100 bp DNA Ladder (0.5 µg/µl)	N3231S	New England Biolabs
Low Range DNA Ladder	O'GeneRuler Low Range DNA Ladder	SM1203	Thermo Fisher Scientific Inc.
Protein Ladder	Full-Range Rainbow Molecular Weight Markers	RPN800E	GE Healthcare

TABLE 6.6. Size markers

NAME	SEQUENCE
Linker	
Ap^{32}p-TL3	rAp^{32}pCTGTAGGCACCATCAAT-ddC
^{32}P-TL3	^{32}pCTGTAGGCACCATCAAT-ddC
acceptor	GAATTCTAATACGACTCACTATC
bridge	GATTGATGGTGCCTACAGTATAGTGAGTCGTATTAGAATTC
RT Primer	
RT_AGGT	NNAGGTNNNAGATCGGAAGAGCGTCGTGGATCCTGAACCGC
RT_ATTG	NNATTGNNNAGATCGGAAGAGCGTCGTGGATCCTGAACCGC
RT_CATT	NNCATTNNNAGATCGGAAGAGCGTCGTGGATCCTGAACCGC
RT_CCGG	NNCCGGNNNAGATCGGAAGAGCGTCGTGGATCCTGAACCGC
RT_CGCC	NNCGCCNNNAGATCGGAAGAGCGTCGTGGATCCTGAACCGC
RT_GACC	NNGACCNNNAGATCGGAAGAGCGTCGTGGATCCTGAACCGC
RT_GGTT	NNGGTTNNNAGATCGGAAGAGCGTCGTGGATCCTGAACCGC
RT_TATT	NNTATTNNNAGATCGGAAGAGCGTCGTGGATCCTGAACCGC
RT_TGCC	NNTGCCNNNAGATCGGAAGAGCGTCGTGGATCCTGAACCGC
RT_TTAA	NNTTAANNNAGATCGGAAGAGCGTCGTGGATCCTGAACCGC
Oligos	
CutOligo	GTTCAGGATCCACGACGCTCTTCAAAA
P3 Solexa	ACGAGATCGGTCTCGGCATTCCTGCTGAACCGCTCTTCCGATCT
P5 Solexa	AATGATACGGCGACCACCGAGATCTACACTCTTTCCCTACACGACGCT CTTCCGATCT
Elution peptide	
hAGO2 peptide	MYSGAGPPAPPCPALA

TABLE 6.7. Oligonucleotide and peptide sequences

KIT	PRODUCT ID	MANUFACTURER
ECL Detection	32106BID	Thermo Fisher Scientific Inc.
Pierce 660 nm Protein Assay	22662	Thermo Fisher Scientific Inc.
RNeasy Mini	74104	QIAGEN GmbH

TABLE 6.8. Kit systems

6.2 CELLULAR MATERIAL AND ANIMAL STRAINS

All animal studies were carried out with the prior consent of local authorities and according to the German law of animal protection.

NOMENCLATURE	DISTRIBUTOR
Cell lines	
Escherichia coli SURE® (200238)	Thermo Fisher Scientific Inc.
human embryonic kidney HEK293	Thermo Fisher Scientific Inc.
human embryonic kidney HEK293-T	American Type Culture Collection (ATCC)
murine embryonal fibroblast NIH/3T3	American Type Culture Collection (ATCC)
Mice	
FVB/NCrl	Charles River Laboratories International Inc.
C57BL/6NCrl	Charles River Laboratories International Inc.
Rats	
SPAGUE DAWLEY RjHan/SD	JANVIER LABS

TABLE 6.9. Cell lines and animal strains

6.3 BUFFERS AND REACTION MIXES

NAME	COMPOSITION
10× TE Buffer	100 mM Tris-HCl, pH 7.4 10 mM EthyleneDiaminTetraacetic Acid (EDTA) pH 7.4
Blocking Solution	10% (w/v) Sodium Dodecyl Sulfate (SDS) 1 mM EDTA in PBS
Citrate Phosphate Buffer [151]	65 mM Na_2HPO_4 25 mM citric acid 0.01% (v/v) NP40 substitute pH 5.0
Flag Lysis Buffer	50 mM HEPES-KOH, pH 7.5 150 mM NaCl 1 mM EDTA 1 mM NaF 0.5 mM DiThioThreitol (DTT) 3% Triton X-100 0.5% (v/v) NP40 substitute 1% (v/v) protease inhibitor pH 7.5
High Salt Wash Buffer [151]	50 mM HEPES-KOH, pH 7.5 500 mM NaCl 0.5 mM DTT 0.05% (v/v) NP40 substitute 1% (v/v) protease inhibitor pH 7.5
IP Wash Buffer [151]	50 mM HEPES-KOH, pH 7.5 300 mM NaCl 0.5 mM DTT 0.05% (v/v) NP40 substitute 1% (v/v) protease inhibitor pH 7.5
Meister Lysis Buffer [348]	20 mM Tris-HCl, pH 7.5 150 mM NaCl 2 mM EDTA 1 mM NaF 0.5% (v/v) NP40 substitute 0.5 mM DTT 1% (v/v) protease inhibitor pH 7.5

NAME	COMPOSITION
Membrane Wash 1	10% (w/v) SDS in PBS
Membrane Wash 2	1% (w/v) SDS in PBS
Membrane Wash 3	0.1% (w/v) SDS in PBS
PAR-CLIP Lysis Buffer [151]	50 mM HEPES-KOH, pH 7.5 150 mM NaCl 1 mM EDTA 1 mM NaF 0.5 mM DTT 0.5% (v/v) NP40 substitute 1% (v/v) protease inhibitor pH 7.5
TBE Running Buffer	89 mM Tris 89 mM boric acid 2 mM EDTA pH 8.3
TE Buffer	10 mM Tris-HCl, pH 7.4 1 mM EDTA pH 7.4
Ule Lysis Buffer [221]	50 mM Tris-HCl, pH 7.4 100 mM NaCl 1 mM $MgCl_2$ 0.1 mM $CaCl_2$ 1% (v/v) NP40 substitute 0.1% (w/v) SDS 0.5% (v/v) sodium DeOxyCholate (DOC) 1% (v/v) Protease Inhibitor pH 7.4

TABLE 6.10. Buffers and reaction mixes used in Section 7.1

NAME	COMPOSITION
Circularization Mix [221]	3.75 U/µl CircLigase™ II ssDNA Ligase 33 mM Tris-CH_3COOH, pH 7.5 66 mM KCH_3CO_2 2.5 mM $MnCl_2$ 0.5 mM DiThioThreitol (DTT) pH 7.5
Dephosphorylation Mix [221]	0.25 U/µl T4 PNK 1 U/µl SUPERaseIn 70 mM Tris-HCl, pH 6.5 10 mM $MgCl_2$ 5 mM DTT pH 6.5
dNTP Mix	10% (v/v) dNTP
Flag Elution Mix	0.15 mg/ml 3X FLAG peptide 50 mM Tris-HCl, pH 7.5 50 mM NaCl 10 mM $MgCl_2$ 0.01% (v/v) NP40 substitute pH 7.5
Hot PNK Mix [221]	0.5 U/µl T4 PNK 1 U/µl SUPERaseIn 167 nM ^{32}P-γ-ATP (1 µCiµl) 70 mM Tris-HCl, pH 7.6 10 mM $MgCl_2$ 5 mM DTT pH 7.6
L3 Linker Ligation Mix [221]	10 U/µl T4 RNA Ligase 2 truncated K227Q 1 U/µl SUPERaseIn 1.5 µM App-L3 50 mM Tris-HCl, pH 7.4 10 mM $MgCl_2$ 10 mM DTT 20% (v/v) PEG 400 pH 7.4
Oligo Annealing Mix [221]	0.33 µM CutOligo 10% (v/v) 10X FastDigest Buffer

NAME	COMPOSITION
Peptide Elution Mix	4 mg/ml hAGO2 peptide 50 mM Tris-HCl, pH 8.0 300 mM NaCl 5 mM $MgCl_2$ 0.05% (v/v) NP40 substitute pH 8.0
Phosphatase Wash Buffer [151]	50 mM Tris-HCl, pH 7.5 20 mM Ethylene Glycol Tetraacetic Acid (EGTA) 0.5% (v/v) NP40 substitute pH 7.5
PK K Buffer [221]	100 mM Tris-HCl, pH 7.5 50 mM NaCl 10 mM EthyleneDiaminTetraacetic Acid (EDTA) pH 7.5
PK U Buffer [221]	100 mM Tris-HCl, pH 7.5 7 M urea 50 mM NaCl 10 mM EDTA pH 7.5
PolyNucleotide Kinase (PNK) Buffer [151]	50 mM Tris-HCl, pH 7.5 50 mM NaCl 10 mM $MgCl_2$ 0.01% (v/v) NP40 substitute pH 7.5
Primer Mix P5/P3 Solexa	10 µM P5 Solexa 10 µM P3 Solexa
RT Mix	18 U/µl SuperScript® III Reverse Transcriptase 182 mM Tris-HCl, pH 8.3 273 mM KCl 18 mM DTT 11 mM $MgCl_2$ pH 8.3
TE Buffer	10 mM Tris-HCl, pH 7.4 1 mM EDTA pH 7.4
Transfer Buffer	25 mM Tris 192 mM glycine 10% (v/v) methanol

TABLE 6.11. Buffers and reaction mixes used in Section 7.2

NAME	COMPOSITION
10% CF Plating Medium	MEM 12 mM $NaHCO_3$ 10% (v/v) FCS 1% (v/v) PenStrep 0.1% (v/v) vitamin B12
293-T Medium	DMEM 10% (v/v) Sigma FCS 1% (v/v) PenStrep
AMCM Culture Medium	MEM 2mM L-glutamine 0.1 mg/ml BSA 1% (v/v) PenStrep
AMCM Plating Medium	MEM 10 mM 2,3-ButaneDione-Monoxime (BDM) 2mM L-glutamine 5% (v/v) FCS 1% (v/v) PenStrep
ARCM Culture Medium	M199 10 mM BDM 2mM L-glutamine 0.1 mg/ml BSA 1% (v/v) PenStrep 0.01% (v/v) ITS supplement (10 mg/l insulin, 5.5 mg/l transferrin, 5 mg/l selenium)
AM Digestion Buffer	1.5 mg/ml collagenase type II (280 U/mg) 12.5 µM $CaCl_2$ in 10 ml Perfusion Buffer per heart
AR Digestion Buffer	3.5 mg/ml collagenase type II (280 U/mg) 12.5 µM $CaCl_2$ in 20 ml Perfusion Buffer per heart
DMEM++	DMEM 10% (v/v) FCS 1% (v/v) PenStrep
glucose-free Modified Tyrode's Solution (MTS)	5 mM HEPES-KOH, pH 7.4 30 mM BDM 136 mM NaCl 5.4 mM KCl 1 mM MgH2PO4 0.9 mM CaCl2 pH 7.4

NAME	COMPOSITION
Modified Tyrode's Solution (MTS)	5 mM HEPES-KOH, pH 7.4 30 mM BDM 10 mM glucose 136 mM NaCl 5.4 mM KCl 1 mM MgH_2PO_4 0.9 mM $CaCl_2$ pH 7.4
Perfusion Buffer	10 mM HEPES-KOH, pH 7.46 30 mM taurine 10 mM BDM 5.5 mM glucose 113 mM NaCl 12 mM $NaHCO_3$ 10 mM $KHCO_3$ 4.7 mM KCl 1.2 mM $MgSO_4$ 0.6 mM KH_2PO_4 0.6 mM Na_2HPO_4 32 µM phenol red pH 7.46
Slice Culture Medium	M199 1% (v/v) ITS supplement (10 mg/l insulin, 5.5 mg/l transferrin, 5 mg/l selenium) 1% (v/v) PenStrep
Stop Buffer 1	12.5 µM $CaCl_2$ 10% (v/v) FCS in Perfusion Buffer
Stop Buffer 2	12.5 µM $CaCl_2$ 5% (v/v) FCS in Perfusion Buffer

TABLE 6.12. Buffers and reaction mixes used in Section 7.3

6.4 DATABASES AND SOFTWARE

NAME	URL	REF.
Conserved Domain Database	`http://www.ncbi.nlm.nih.gov/Structure/cdd/wrpsb.cgi`	[269]
mimiRNA	`http://mimirna.centenary.org.au/mep/`	[343]
PhenomiR	`http://mips.helmholtz-muenchen.de/phenomir/`	[349]
starBASE	`http://starbase.sysu.edu.cn/starbasev1/`	[434]

TABLE 6.13. Databases

NAME	VERSION	APPLICATION
DeVision G	2.0	UV transillumination
LAS4000IR	2.1	western blot detection
Multi Gauge	3.2	western blot analysis
ND-1000	3.5.2	nucleic acid quantification
OptiQuant^{TM}	5.0	PLS image detection
POV-Ray	3.7	graphical rendering
Python	2.7.3	bioinformatic analysis
R	2.14	statistical computing and data plotting
Swiss-PdbViewer	4.1	molecular visualization
Tecan i-control	1.6.19.0	protein quantification

TABLE 6.14. Software

7 METHODS

7.1 AGO CLIP

In principle, two types of CLIP protocols have been combined, PAR-CLIP [151] and individual nucleotide resolution CLIP (iCLIP) [221]. The PAR-CLIP method has become an established tool to identify miRNA targets [152]. However, it had to be adapted for using primary cells or tissue cultures as an input source. The preparation of cDNA libraries was transferred from the iCLIP protocol [219]. Further, for some of the experiments AGO protein elution has been changed to a competitive approach [348] in order to circumvent the SDS-PAGE purification step. In the following, the steps of the protocols are described in modular, but sequential, order. Alternatives and protocol-specific procedures are indicated.

THIO-NUCLEOSIDE LABELING (ONLY PAR-CLIP)

The RNA of all samples used for PAR-CLIP experiments were labeled using the photo-activatable nucleoside analog 4SU (kindly provided by the Tuschl Lab). However, various 4SU concentrations as well as incubation times were applied. HEK cells were grown in medium supplemented with 0.1 mM 4SU for 16 h prior to harvesting (according to the original protocol [151]). Primary cardiac cell cultures were labeled with 4SU concentrations from 0.1 mM to 1 mM for 16 h up to 24 h. Slice cultures were incubated with 0.1 mM to 20 mM 4SU for 24 to 72 h. Adult mice were tested for *in vivo* labeling by intra-peritoneal injection (i.p.) administration of 4SU in PBS with either 10 mg -12 h, 5 mg -8 h and 5 mg -4 h or 7.5, 2.5 and 5 mg at -8, -4 and -1 h prior to sacrifice (per 20 g of body weight).

TESTING THE 4SU LABELING EFFICIENCY (ONLY PAR-CLIP)

To analyze the ratio of 4SU incorporated into cellular RNA, the RNA can be completely digested to mono-nucleotides and the solution subjected to reverse-phase High-Performance Liquid Chromatography (HPLC). By calculating the integral over each nucleotide's elution peak and determining their relative proportion on the total area, the 4SU incorporation rate can be estimated [151, 14]. To avoid laborious HPLC techniques, it is also possible to get a rough estimate regarding the relative 4SU labeling efficiency by visualizing the incorporated 4-thio-nucleotides and comparing the signal to that of a reference sample. One way to visualize the nucleotide analogs is to first thiol-specifically biotinylate isolated total RNA and to perform a dot-blot assay with it. Subsequent detection of introduced biotin residues by streptavidin-coupled HorseRadish Peroxidase (HRP) together with Enhanced ChemiLuminescence (ECL) detection reagent allows to compare the amount of detectable thiol-groups (corresponding to integrated 4SU) [92, 198].

The first approach (HPLC) has kindly been conducted by the Tuschl Lab. The latter (dot-blot) was applied in the Engelhardt Lab (based on [92]) with characteristics as follows. First, total RNA was isolated using peqGOLD RNAPure and purified with the RNeasy Mini Kit. Per ~50 mg deep frozen sample (cells or tissue) 1 ml peqGOLD was added to a 1.5 ml tube. The sample was dispersed, incubated at room temperature for 5 min and pre-cleared (12,000 × g, room temperature, 10 min). The supernatant was transferred to a pre-spun (15,000 × g, room temperature, 20 s) 2 ml Phase Lock tube and ~300 µl chloroform were added. After shaking the sample gently for 15 s it was incubated on ice for 5 min. Phase separation was achieved by centrifugation (12,000 × g, 4°C, 5 min). The upper phase was transferred to a 1.5 ml siliconized tube, 0.5 µl GlycoBlue were added and, after mixing, also one volume isopropanol was added. Subsequent to a precipitation step on ice for 15 min the RNA was collected (~21,000 × g, 4°C, 15 min), the supernatant was removed completely, the pellet washed with 0.5 ml 80% (v/v) ethanol and again centrifuged (~21,000 × g, 4°C, 15 min). The precipitate was resuspended in 100 µl water. To that, 350 µl Buffer RLT (RNeasy Mini Kit) were added and the solution mixed. After the addition of 250 µl ethanol the sample was directly transferred to an RNeasy Mini spin column (RNeasy Mini Kit), centrifuged (12,000 × g, room temperature, 20 s), washed with 500 µl Buffer RPE (RNeasy Mini Kit), centrifuged (12,000 × g, room temperature, 20 s), and again washed with 500 µl Buffer RPE. Next, the column was dried by centrifugation (12,000 × g, room temperature, 2 min), placing it in a new collection tube and centrifuging it again (20,000 × g, room temperature, 1 min). To elute the RNA, two times after each other 25 µl water (heated to 50°C) were added to the column, it was incubated at room temperature for 3 min and centrifuged (12,000 × g, room temperature, 2 min) in the same 1.5 ml siliconized tube. Second, the biotinylation reagent was prepared by dissolving pyridyldithiol-biotin in DMSO to a concentration of 1 µg/µl, heating the solution to 37°C for 5 min and vortexing it rigorously. The input RNA was denatured at 70°C for 3 min and then directly put on ice. For setting up the biotinylation mix, it was ensured that it fulfills both, 2 µl biotinylation reagent should be used per each µg RNA and the volume of the biotinylation reagent should account for ~30% of the total volume. For example, to biotinylate 15 µg of total RNA, the RNA was diluted to 60 µl, followed by an addition of 10 µl 10× TE Buffer and 30 µl biotinylation reagent to obtain a final volume of 100 µl. The biotinylation mix was incubated in the dark at room temperature for 3 h. From now on the sample was exposed to light as little as possible. Third, the RNA was purified from unbound biotin by a chloroform/isoamyl alcohol extraction step. The biotinylation reaction was mixed with an equal volume of chloroform/isoamyl alcohol (24/1) and transferred to a 2 ml Phase Lock tube. Phases were separated at 12,000 × g, 4°C, 5 min and the upper phase was transferred to a 1.5 ml siliconized tube. After addition of 0.5 µl GlycoBlue and approximately 0.1 volume of sodium acetate, mixing, then adding one total volume isopropanol and again mixing the RNA was precipitated at -20°C overnight. The RNA was collected by centrifugation (~21,000 × g, 4°C, 15 min), the supernatant was removed completely, the pellet washed with 0.5 ml 80% (v/v) ethanol and again centrifuged (~21,000 × g, 4°C, 15 min). The precipitate was resuspended in TE Buffer and the concentration was adjusted

to 1 µg/µl. Finally, the RNA was again linearized by incubation at 65°C for 10 min and rapid cooling on ice for 5 min prior to dotting it on a Hybond N membrane. Typically, 1 µl or 2 × 1 µl were dotted on each spot. After air-drying the membrane, the RNA was cross-linked to the membrane by short-wave UV light of 254 nm (0.15 J/cm²). Subsequently, the membrane was incubated in Blocking Solution on a tumbling table for 20 min and then probed with a 1/4,000 dilution of streptavidin-HRP in Blocking Solution for 15 min. Before detecting the signal, the membrane was washed 6 × for 10 min (2 × Membrane Wash 1, 2 × Membrane Wash 2, 2 × Membrane Wash 3). The signal of the streptavidin-HRP bound to thio-coupled biotins was visualized using the ECL Detection Kit and a chemiluminescence detecting CCD camera.

UV CROSS-LINKING (PROTOCOL-DEPENDENT)

The PAR-CLIP approach takes advantage of the fact that previously integrated, photo-activatable 4-thio-nucleotides can be efficiently cross-linked with long-wave UV light at a wavelength of about 365 nm.
For cell cultures, cells were grown in 10 to 15 cm cell culture plates. After removal of the cell culture medium cells were washed once with ice-cold PBS. Subsequently, PBS was removed completely and cells were irradiated on ice with a dosage between 0.15 J/cm² and 0.6 J/cm². Afterwards, cells were scraped off with a cell scraper in 1 ml PBS per plate, collected by centrifugation (500 × g, 4°C, 5 min), shock frozen and stored at -80°C until use. Tissue slices were cultured on slice filters in 6-well plates. They were subjected to UV cross-linking immediately (without removing the culturing media). The plates were put on ice (without lid) for cross-linking with a dosage of 0.3 J/cm². Subsequently, slices were collected with a pair of tweezers, shock frozen and stored at -80°C until use.
For the iCLIP protocol, RNA does not have to be previously labeled. Hence, cells were directly irradiated with short-wave UV light of 254 nm to covalently cross-link proteins to close-by RNA using a dosage between 0.15 and 0.6 J/cm².

BEAD PREPARATION

Based on the amount of input material, different volumes of magnetic beads (protein G, 30 mg Dynabeads®/mL) have been used per CLIP experiment (total range: 10 to 360 µl 'bead volume', typically about 100 µl per sample). Beads were washed twice with 1 ml Citrate Phosphate Buffer. Depending on the antibody used, beads were resuspended in 1 volume Citrate Phosphate Buffer containing 0.15 µg/µl anti-mAGO2 (2D4) or 0.1 µg/µl anti-hAGO2 (11A9). Incubation was performed on a rotating wheel at 4°C overnight. Subsequently, beads were washed twice with 1 ml Citrate Phosphate Buffer, once with Lysis Buffer and were then added to the lysate.

LYSATE PREPARATION (PROTOCOL-DEPENDENT)

Pellets of frozen samples were thawed on ice and resuspended in 3 volumes of published [151, 245] (or slightly adapted) ice-cold lysis buffers (for example PAR-CLIP Lysis Buffer). If not otherwise indicated, samples were kept on ice

or in the cold room (4°C) from now on. The suspension was homogenized by repetitive pipetting or by using a disperser and incubated on ice for 10 min. Afterwards, the lysate was cleared by centrifugation (13,000 × g, 4°C, 15 min) followed by filtering it through a 5 µm membrane syringe filter. The protein concentrations was determined using the Pierce 660 nm Protein Assay Kit (by mixing 10 µl sample with 150 µl Pierce 660 nm Protein Assay Reagent and measuring the absorbance at 660 nm after 5 min). Now, the lysate was subjected to partial RNA digestion by treatment with RNase T1 added at a final concentration of 1 U/µl and incubation in a water bath at 22°C for 15 min [151].
Alternatively, RNase I was added (final concentration: 1 mU/µl) together with Turbo DNase (final concentration: 2 mU/µl) before centrifugation. The lysates were incubated in a thermoshaker at 1,100 rpm and 37°C for exactly 3 min. Subsequently, samples were cleared (13,000 × g, 4°C, 15 min, no filtering) and the protein concentration was determined [221].

AGO IMMUNOPRECIPITATION (PROTOCOL-DEPENDENT)

According to the volume of the lysate, a sample was either split to multiple 2 ml Eppendorf tubes or one 15 or 50 ml Falcon tube. Beads were added and IP was carried out on a rotating wheel at 4°C for 4 h or overnight. Afterwards, beads were collected in a fresh 1.5 ml tube using a magnetic separator. Next, they were washed 2 × with either 1 ml PAR-CLIP Lysis Buffer (2D4) or 1 ml IP Wash Buffer (11A9) in the cold room (4°C) and taken up in 1 bead volume of the same buffer. For those samples that were subjected to a second RNase-mediated digest (PAR-CLIP) RNase T1 was added at a final concentration of 100 U/µl and the suspension was again incubated in a water bath at 22°C for 15 min with subsequently cooling on ice for 5 min. Next, all samples were washed 3 × with either 1 ml PAR-CLIP Lysis Buffer (2D4) or 1 ml High Salt Wash Buffer (11A9) in the cold room.

7.2 CDNA LIBRARY PREPARATION

The preparation of the cDNA libraries was initially performed at the Tuschl Lab [150, 151].
At the Engelhardt Lab, cDNA libraries were prepared as follows, based on the library preparation protocol used at the Ule Lab [221, 219].

DEPHOSPHORYLATION OF RNA 3'-ENDS

After washing the supernatant was removed and the beads were resuspended in one fifth of the original bead volume of Dephosphorylation Mix. The samples were incubated at 1,000 rpm and 37°C for 20 min. In contrast to the published protocol [221, 219] the beads were now washed twice with 1 ml of Phosphatase Wash Buffer and twice with PolyNucleotide Kinase (PNK) Buffer in the cold room (4°C).

linker ligation to rna 3′-ends

The supernatant was removed from the beads, they were resuspended in one fifth of the original bead volume of L3 Linker Ligation Mix and ligation was performed in a thermoshaker at 16°C overnight (>16 h). Afterwards, beads were either subjected to radioactive labeling of the RNA and/or subsequent protein denaturation prior to SDS-PAGE purification or directly to competitive peptide elution.

^{32}p-γ-atp labeling of rna 5′-ends

After removing the supernatant, the beads were taken up in PNK Buffer and one fifth of each sample was transferred to a separate 1.5 ml tube. The supernatant was removed and the beads were resuspended in one fifth of their bead volume of Hot PNK Mix. The reaction was incubated at 500 rpm and 37°C for 5 min. The supernatant was removed and the 'hot' beads were resuspended in 20 µl NuPAGE Loading Buffer. The suspension was transferred to the remaining 'cold' beads and the mix incubated at 500 rpm and 70°C for 5 min (protein denaturation).

sds-page and western blotting

The eluate of the beads was loaded and run on a 4-12% NuPAGE Bis-Tris Gel in MOPS Running Buffer at 4°C using the XCell SureLock® Mini-Cell electrophoresis chamber. A Protein Ladder which has been shown to run as expected on NuPAGE gels was used. The power settings applied were 70 V for 20 min and 180 V for 2 h. Subsequently, protein/RNA complexes were transferred from the gel to a Protean BA 85 nitrocellulose membrane using the Mini-PROTEAN® Tetra Cell electrophoresis chamber filled with Transfer Buffer at 4°C and 380 mA for 1 h 30 min. After transfer the membrane was wrapped in a fitted plastic waste bag and adjusted on a previously marked dark frame on a phosphor imager screen. Exposure was performed at 4°C for 1 h up to overnight. Protein/RNA complexes identified by their molecular weight and radioactive signal (AGO2 runs at ~100 kDa, AGO2/miRNA at ~110 kDa, molecular weight of 70 nucleotides RNA (~50 nucleotides + 21 nucleotides linker) equals ~20 kDa, tags of sufficient lengths are thus expected at ~130 kDa) were isolated by cutting the respective region out of the nitrocellulose membrane using the phosphor screen autoradiograph as a mask. The membrane piece was sometimes divided in an upper (H), middle (M) and lower (L) portion and placed into separate 1.5 ml siliconized tubes. Finally, 200 µl of PK K Buffer were added to each tube.

competitive ago2 elution

SDS-PAGE and subsequent Blotting on nitrocellulose are very effective purification steps but their consumption of input material is rather high. Therefore, an alternative purification strategy was applied by competitive elution of native hAGO2 with a competing peptide of 16 amino acids [348] (for sequence see Table 6.7). Subsequent to the washing steps after dephosphorylation the beads

were resuspended in two thirds bead volume of Peptide Elution Mix and incubated at 600 rpm and 25°C for 90 min (11A9). The eluates were separated from the beads and diluted and/or adjusted to obtain 100 mM Tris-HCl, 50 mM NaCl and 10 mM EDTA (PK K Buffer).

RNA ISOLATION

To each tube, a twentieth part of the PK K Buffer volume of Proteinase K was added (final concentration of 2.5 mU/µl). The reaction was incubated at 1,100 rpm and 37°C for 20 min. Afterwards, one volume of PK U Buffer was added and each sample was again incubated at 1,100 rpm and 37°C for 20 min. The solution was collected and together with one total volume RNA phenol/$CHCl_3$ transferred to one or multiple 2 ml Phase Lock tubes. After incubation at 1,100 rpm and 30°C for 5 min phases were separated by centrifugation (~18,000 × g, room temperature, 5 min). The aqueous layer was carefully (without touching the gel matrix with the pipette) transferred to one or multiple fresh 1.5 ml siliconized tubes. RNA was precipitated by addition of 0.5 µl GlycoBlue and approximately 0.1 volume of sodium acetate per tube, mixing, then adding about 2.5 volumes ethanol, again mixing and incubation at -20°C overnight. The precipitate was collected by centrifugation (~21,000 × g, 4°C, 15 min), the supernatant was removed completely, each pellet washed with 0.5 ml 80% (v/v) ethanol and collected (~21,000 × g, 4°C, 15 min). The supernatant was again removed completely and the pellets were dried for exactly 3 min. Each RNA sample was taken up in 6.25 µl water.

REVERSE TRANSCRIPTION

To the resuspended RNA, 0.5 µl dNTP Mix and 0.5 µl RT_# primer (0.5 µM) where added. The # is a placeholder for the individual four letter barcode sequence used for each sample (for sequences used see Table 6.7 RT Primer). After an initial denaturing step, 2.75 µl RT Mix were added per reaction and RT was performed as indicated (see Table 7.1).

TEMPERATURE	TIME
70°C	5 min
25°C	hold (until addition of RT Mix)
Addition of 2.75 µl RT Mix per sample	
25°C	5 min
42°C	20 min
50°C	40 min
80°C	5 min
4°C	hold

TABLE 7.1. RT Thermal Conditions

Subsequently, samples that were intended to be sequenced together were mixed. Transcripts were precipitated by addition of TE Buffer to 100 µl, 0.5 µl GlycoBlue and 15 µl sodium acetate, mixing, then adding 300 µl ethanol, again mixing and incubation at -20°C overnight.

gel purification of cDNA

The precipitate was again collected by centrifugation (~21,000 × g, 4°C, 15 min), the supernatant removed completely and the pellet washed with 0.5 ml 80% (v/v) ethanol. The supernatant was again removed completely and each pellet dried for exactly 3 min. Transcripts were resuspended in 6 µl water. After addition of 6 µl TBE/Urea Loading Buffer, each cDNA solution was incubated at 80°C for 3 min directly before loading it on a 6% TBE/Urea gel. Electrophoresis was performed in TBE Running Buffer at 180 V and room temperature for 40 min using the XCell SureLock® Mini-Cell apparatus. The last lane containing Low Range DNA Ladder was cut off and stained by shaking in 10 ml TBE Buffer containing 2 µl SYBR Green II for 10 min. The gel piece was washed once in TBE Buffer and the marker bands were visualized by UV transillumination. Guided by the size marker, three bands (approximately 70 to 85, 85 to 120 and 120 to 200 nucleotides) were cut out of each sample lane. Gel pieces were placed into separate 1.5 ml siliconized tubes. To each tube, 400 µl TE Buffer were added and the gel piece crushed with a 1 ml syringe plunger. Subsequently, the mixture was incubated at 1,100 rpm and 37°C for 2 h with a 2 min cooling period on dry ice after 1 h of incubation. The liquid portion of the supernatant was transferred to a Costar SpinX column into which two glass prefilters had been placed. The cDNA solution was collected by centrifugation (~18,000 × g, room temperature, 1 min) of the columns. After addition of 0.5 µl GlycoBlue and 40 µl sodium acetate, the solution was mixed. Then, 1 ml ethanol was added and after a second mixing step, the cDNA was precipitated at -20°C overnight.

primer ligation to cDNA 5′-ends

The cDNA was collected by centrifugation (~21,000 × g, 4°C, 15 min), the supernatant removed and the pellet washed with 0.5 ml 80% (v/v) ethanol. The supernatant was again removed completely and the pellet dried for exactly 3 min. The precipitate was resuspended in 8 µl Circularization Mix and incubated at 60°C for 1 h. Subsequently, 30 µl Oligo Annealing Mix were added and annealing of the oligonucleotide (for sequence see Table 6.7 Oligos) to its cleavage site was performed after heating at 95°C for 2 min by successive temperature decrease from 95°C to 25°C with 20 s per each 1°C step. At 25°C, 2 µl FastDigest BamHI were added and the mix incubated at 37°C for 30 min. The cDNA that had been re-linearized, and hence carried linker sequences on both ends, was precipitated by addition of 50 µl TE Buffer, 0.5 µl GlycoBlue and 10 µl sodium acetate, mixing, then adding 250 µl ethanol, again mixing and incubation at -20°C overnight.

PCR AMPLIFICATION

Precipitated cDNA was collected again by centrifugation (~21,000 × g, 4°C, 15 min), the supernatant was removed and the pellet washed with 0.5 ml 80% (v/v) ethanol. Again, the supernatant was removed completely, the pellet dried for 3 min and then resuspended in 13 µl water. To test for the optimal number of required PCR cycles, three to five test PCRs with increasing numbers of cycles were run prior to the preparative PCR (see Table 7.2 and 7.3). Each test PCR reaction (10 µl) was mixed with 2.5 µl TBE Loading Buffer and loaded on a 5% TBE gel. Electrophoresis was performed in a Mini-PROTEAN® Tetra Cell apparatus filled with TBE Buffer at 100 V and room temperature for 60 min. Subsequently, the gel was stained by shaking in 10 ml TBE Buffer containing 2 µl SYBR Green I for 10 min. It was washed once in TBE Buffer and the PCR product bands were visualized by UV transillumination. The minimum number of cycles required for the test PCRs was estimated by the test PCR cycle number sufficient to get a visible band on the gel minus one cycle (starting with a two-fold higher cDNA concentration, see Table 7.2). Subsequently, 10 µl of the final PCR products were mixed with 2.5 µl TBE Loading Buffer and DNA bands were detected as for the preparative PCR. This step was included, as samples in which sharp bands are detected below 145 nucleotides (P5/P3 Solexa Primers and the barcode sequences account for 128 nucleotides) have to be gel purified.

COMPONENT	TEST PCR	PREPARATIVE PCR
cDNA	0.50 µl	5.0 µl
water	4.25 µl	42.5 µl
Primer Mix P5/P3 Solexa	0.25 µl	2.5 µl
AccuPrime SuperMix I	5.00 µl	50.0 µl

TABLE 7.2. PCR Mix

TEMPERATURE	TIME	
94°C	2 min	
94°C	15 s	16 to 34 cycles
65°C	30 s	
68°C	30 s	
68°C	3 min	
25°C	hold	

TABLE 7.3. PCR Thermal Conditions

HIGH-THROUGHPUT SEQUENCING

10 µl of the final library would have been sent for Solexa Sequencing.

7.3 PREPARATION OF CLIP INPUT MATERIAL

CELL LINE CULTURING

Stable cell lines derived from Human Embryonic Kidney 293 (HEK293) or murine embryonal fibroblast cells (NIH/3T3) were cultured in DMEM++. Cells were grown in a humidified atmosphere at 5% CO_2 and 37°C. They were only used between passage 5 and 15 after thawing and split twice weekly as well as 24 h before starting 4SU labeling.

ISOLATION AND CULTURING OF PRIMARY CARDIAC CELLS

Adult Mouse (AM) and Adult Rat (AR) CM and CF were prepared by adhering (with minor adjustments) to a anterograde heart perfusion protocol [309], which is in principle based on very early preparation methods already described in the 19th century [237, 449].
Briefly, the animal was heparinized and anesthetized, fixated, and the chest opened up. Subsequently, the heart was removed and cleaned in a dish with PBS. Next, the aorta was connected to a cannula (with a clip and twine) and initially perfused with Perfusion Buffer (AM: 1 ml, AR: 2 ml) using a syringe. Now, the cannula was connected to a perfusion system and the heart perfused for 3 min with Perfusion Buffer at a flow rate of 3 ml/min. Subsequently, the buffer was switched to Digestion Buffer and the heart was digested (AM: 7.5 min, AR: 27 min) at the same flow rate. Afterwards, the heart was detached from the perfusion system, the atria were removed and the ventricles were gently minced into small pieces in (AM: 2.5 ml, AR: 15 ml) Digestion Buffer using a fine pair of tweezers. The digestion was stopped with (AM: 2.5 ml, AR: 15 ml) Stop Buffer P1 and the dissociation of the heart tissue was continued using pipette tips. The suspension was filtered through a 100 µm cell strainer into a 50 ml Falcon tube and transferred into (AM: 1, AR: 2) 15 ml Falcon tubes. The tubes were put at 37°C (water bath) and CM were allowed to sediment by gravity for 10 min. Subsequently, the supernatant was transferred into a new 15 ml Falcon tube and remaining CM were collected by centrifugation (~55 × g, room temperature, 1 min). Again, the supernatant was transferred to another tube and CF were collected (~75 × g, RT, 5 min). Sediment(s) and pellet(s) of CM were combined in 10 ml Stop Buffer P2 and the suspension was transferred into a 25 ml conical flask (sterile). Now, CM were incrementally re-introduced to increasing calcium concentrations from 12.5 µM to 1 mM by repeated adding of $CaCl_2$ solutions: 50 µl 10 mM $CaCl_2$, 4 min; 50 µl 10 mM $CaCl_2$, 4 min; 100 µl 10 mM $CaCl_2$, 4 min; 30 µl 100 mM $CaCl_2$, 4 min; 50 µl 100 mM $CaCl_2$. The suspension was transferred into a 15 ml Falcon tube and CM were allowed to sediment at 37°C (water bath) for 10 min. Again, remaining cells in the supernatant were collected after transfer by centrifugation (~55 × g, room temperature, 1 min). The sediment and the pellet were pooled (in AM: 5 ml Plating Medium, AR: 10 ml AR Culture Medium), transferred to a laminin-coated culture dish (AM: 5 cm, AR: 10 cm) and the medium was exchanged after 2 h (AM: 5 ml Culture Medium, AR: 10 ml AR Culture Medium). Adult Mouse Cardiac Myocytes (AMCM) and ARCM were cultured in a humidified atmosphere at 5% CO_2 and 37°C. The pelleted CF were taken up in 10%

CF Plating Medium (AM: 5-10 ml, AR: 10-20 ml) and transferred to untreated culture dishes. The cells were washed 2 × with PBS after pre-plating for 2 h and then again covered with 10% CF Plating Medium. Adult Mouse Cardiac Fibroblasts (AMCF) and Adult Rat Cardiac Fibroblasts (ARCF) were cultured in a humidified atmosphere at 1% CO_2 and 37°C. They were used after splitting them once 1 to 2 24 h before starting 4SU labeling.

MYOCARDIAL SLICE CULTURING

Myocardial samples obtained from human patients (subjected to cardiac surgery) were transferred into slice cultures according to [46]. In summary, the myocardial tissue was diced and embedded in 4% low-melting agarose dissolved in glucose-free Modified Tyrode's Solution (MTS) of 37°C and subsequently glued (Super Bond) to the sample holder of a vibratome. The tissue was immersed in ice-cold MTS and cut into slices of 300 µm with an advance rate of 0.06 mm/s and 81 Hz vibration of 1 mm amplitude. After slicing, the tissue samples were kept in MTS for approximately 20 min, before they were transferred onto semi-porous slice filters for culturing. Slices were cultured at a liquid/air interface by placing the loaded slice filters into six-well culture plates with 1 ml Slice Culture Medium. Slices were cultured in a humidified atmosphere at 5% CO_2 and 37°C. The medium was exchanged daily or every second day (for labeling).

7.4 COMPUTATIONAL ANALYSIS OF MIRISC COOPERATIVITY

Based on previous experimental studies reporting amplified target repression for adjacent miRISC binding sites, the aim of the second computational part of this project consisted in a theoretical approach to answer the general question whether miRNA-loaded miRISCs act on their own or cooperate for effective target regulation. Therefore, a human transcriptome-wide analysis of pairwise inter-site distances of miRISC binding regions on 3'-UTRs containing multiple predicted or experimentally validated target sites of miRNAs was conducted.
This sub-project was done in close collaboration with Martin Preusse (Lickert Lab), who shares co-authorship in the publication of the collected data [341]. All computational analyses were performed with *Python* [409] programs combined with data plotting using *R* [331].

DISTRIBUTION OF PAIRWISE INTER-SITE DISTANCES

First, all distances between multiple predicted binding sites of one miRNA species were calculated on all human 3'-UTRs and for all human miRNAs considered to obtain a distribution of pairwise distances.
The miRNA target sites were computationally predicted using *TargetScan* (release 6.2) [246, 142, 127]. This release contained 1,536 conserved human miRNAs and the prediction was performed on a multiple sequence alignment of 18,413 3'-UTRs from 23 species. For the prediction, only evolutionary conserved miRNAs and targets were used.
The spacing of two miRNA binding sites was measured as the distance between

the two nucleotides within the 3′-UTR opposite to the 5′-ends of two hypothetical miRNAs aligned to two predicted binding sites on the same target (5′-to-5′). All pairwise site combinations (more than two target sites per 3′-UTR) were taken into account for measuring the distances between them.
Next, all distances between binding sites predicted for groups of multiple miRNA species were determined on all human 3′-UTRs (retrieved from *TargetScan*). In particular, these groups consisted of two or five miRNA sequences, which were sampled randomly (1,000 ×) from the complete set of species (without recurrence).

COMPARISON TO CONTROL DISTANCE DISTRIBUTIONS

The obtained frequencies of inter-site distances (plotted against the pairwise binding site distances) were now compared to distance distributions obtained from two types of control models. Pairwise distances were either calculated for a random composition of arbitrarily placed sites ('random sites') or determined for predicted sites of scrambled sequences reflecting the length of a miRNA but not matching to the sequence of any mature human miRNA available at the *miRBase* [222] release 18 ('scrambled').
In the first case, control site positions were randomly selected within the complete set of human 3′-UTRs available at the *Ensembl Genome Browser* [125] (*BioMart*, assembly GRCh37.p10). The number of sites per 3′-UTR was normalized to lie within the range of *TargetScan* predictions. This process was repeated 1,000 × on the 3′-UTR sequences (to obtain a data set equivalent to that of 1,000 miRNAs). As this first control model does not involve any binding site prediction algorithm, it is completely independent of miRNAs, their binding sequence requirements or other pairing determinants. Thus, the distance distribution derived from this control represents the most basic null model for binding site allocation, which does not rely on any prior knowledge.
A second control based on random miRNA-like sequences was set up to augment the basic random position model. For this, 1,000 completely arbitrary 22 nucleotides long sequences were generated. However, only sequences which neither matched to any known human miRNA sequence nor contained any human miRNA seed sequence (nucleotides 2 to 8) were considered. Target sites of such randomly generated 'seed sequences' were predicted using the *TargetScan* software (6.2) on the 3′-UTR data provided by *TargetScan*. For the analysis of pairwise inter-site distances, only such sequences that produced comparable numbers of 'targets' as human miRNAs (between 10 and 2,719 hits) were taken into account.
To compare the obtained distributions of pairwise distances for one, two and five miRNAs to the corresponding control distributions (also sampled randomly 1,000 × from the two control sets of 1,000 species each), the difference in frequency of a particular inter-site distance (real miRNA data minus control model) was plotted against each pairwise distance.

COOPERATIVITY-PERMITTING DISTANCE

Previous experimental studies showed amplified reporter repression to levels significantly greater than expected from additive effects of multiple binding

sites, especially if they were located in close proximity to each other (see Section 2.6 and Table 2.1). Based on these reports indicating that directly adjacent miRISCs (with certain variations) have the highest potential to repress a common target in a cooperative manner and taking into account the outcome of the above analysis revealing a peak of human miRNA binding site distances within that range (see Section 12.1), a window of inter-site distances between 15 and 26 nucleotides (5′-to-5′) was defined as cooperativity-permitting distances.

PROPORTION OF COOPERATIVE TARGETS

In contrast to the pairwise distance distributions, the proportion of cooperative targets indicates the fraction of 3′-UTRs with miRNA binding sites in cooperativity-permitting distance (see above).
More precisely, all binding sites of a given set of miRNAs were acquired for each 3′-UTR first. If at least one pair of binding sites on a common mRNA target fulfilled the criterion of having a 5′-to-5′ distance within the cooperativity-permitting range, the target was considered to be potentially regulated in a cooperative manner and hence counted as cooperative. All data sets were stored in a MySQL database containing tables for genes, miRNAs and binding sites as well as their relations. Again, data for individual miRNA species and groups of two or five kinds of miRNAs were gathered. Further, both above mentioned control models were analyzed accordingly.

VALIDATION OF TARGET SITES

To confirm the *TargetScan* predicted distance data, first an alternative prediction algorithm was applied by using *miRanda/mirSVR* (release August 2010) [194, 33, 32]. This release contained 249 conserved human miRNAs. Only predictions for conserved miRNAs were considered.
Furthermore, the predicted data was aimed to be confirmed by published experimentally identified target sets, which were expected to be of higher specificity. Therefore, data sets obtained by two different biochemical CLIP protocols (HITS-CLIP and PAR-CLIP) were analyzed. The HITS-CLIP data set [70] is available at `http://ago.rockefeller.edu/` and includes the mapping of miRNA binding sites onto genomic positions. The authors of this study used neocortex of P13 mouse brain tissue, cross-linked RNA to RBPs with short-wave UV irradiation (254 nm) and immunoprecipitated murine RNA/AGO1-4 complexes using anti-pan-mAGO antibodies (see Table 4.1 #2). Upon cDNA library preparation of the isolated RNA and high-throughput sequencing, computational analysis produced a miRNA/mRNA interaction map. The data set used was the mapping on mouse genome assembly *mm9*. The PAR-CLIP data set applied [151] is available through the *starBASE* [434] database providing gene mappings for a wide range of CLIP experiments. The authors of the study analyzed binding sites on isolated RNA fragments of (amongst others) epitope-tagged human AGO1-4 in a HEK cell line upon 4SU labeling and long-wave UV irradiation (see Table 4.1 #12).
To compare the different data sets, the proportion of cooperative targets was determined as before.

FUNCTIONALLY RELATED MIRNA SUBSETS

In case cooperativity between miRISCs could indeed be referred to as a common principle, one may expect an enrichment of miRNA binding sites in cooperativity-permitting distance for miRNAs either acting within the same cell (or tissue) or which are regulated in the same disease context.
To test the first hypothesis, the proportion of cooperative targets for miRNAs co-expressed within one tissue and miRNAs not expressed within that tissue was analyzed. The miRNA expression data were obtained from the dedicated *mimiRNA* database [343].
The second point, to compare the fraction of potentially cooperatively targeted transcripts for miRNA subsets co-regulated (or not) within the same disease context, was addressed by employing the database *PhenomiR* [349] providing data on differential miRNA expression based on certain disease phenotypes. For all miRNAs in both databases targets were retrieved from *TargetScan* as described above. Again, the analysis was done for individual miRNA species as well as groups of two or five miRNAs.

STATISTICAL ANALYSIS

The distributions of pairwise distances (within a particular distance window) as well as the percentage of cooperative targets were analyzed for a significant difference between miRNA and control models with a one-sided Wilcoxon rank-sum test [24]. The *wilcox.test* function in the *stats* package of the *R* statistical computing software [331] was applied with a confidence interval of 0.95 to calculate p-values. P-values $< 2.2 \times 10^{-16}$ are always displayed as such due to the limits in floating point precision in *R*.

III

RESULTS

8 OVERVIEW OF THE PROJECT DESIGN

The following chapter outlines the design of this two-part PhD project (see Figure 8.1) to provide an overview of the results and of their assignments to either of the two parts.
The experimental part (see Figure 8.1B) aimed at the transfer of AGO CLIP technologies to the cardiac system in order to identify targets that are directly regulated by functionally important miRNAs within the heart. Two sub-projects were pursued: PAR-CLIP with either cultured primary rat cardiac cells (see Section 9) or with myocardial cells of human slice cultures (see Section 10).
The computational part (see Figure 8.1C) addressed the concept of miRISC cooperativity in general and as a potential predictor to identify biologically most relevant miRISC targets in particular. As previous experimental studies reported amplified target repression for adjacent miRISC binding sites, this part comprised analyses based on the inter-site distance of miRNA binding sites on transcripts potentially targeted by multiple miRISCs (see Section 12).
The results of the second were part obtained in close collaboration with Martin Preusse (Lickert Lab) and have for the most part been published prior to this thesis in *RNA Biology* (2013) with Martin Preusse as a shared first author [341].

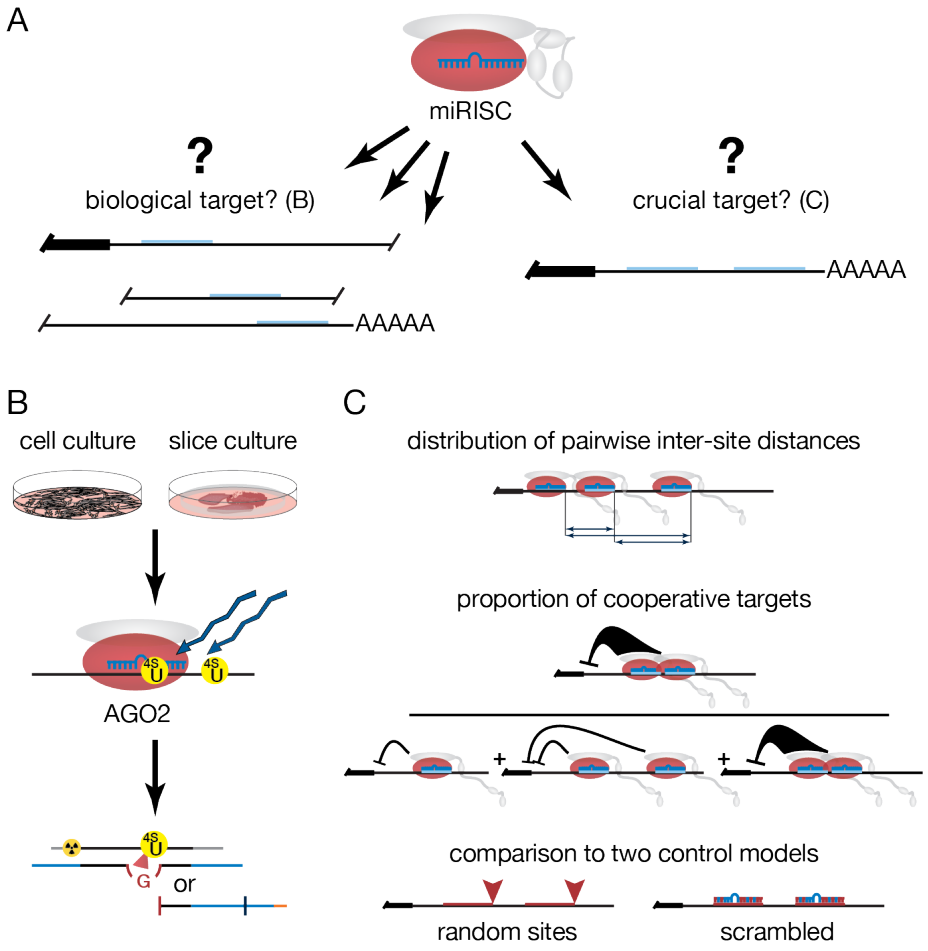

FIGURE 8.1. Schematic representation of the design of this project aiming at the molecular and computational characterization of miRNA/target interactions in general and more specifically within cardiac cells. A: depiction of the objectives which do not only included the comprehensive experimental identification of biological interactions between miRNA-guided miRISCs and regulated targets (biological targets), but also the computational analysis of selection criteria to determine biologically crucial target transcripts (crucial targets); B: experimental strategy consisting of the application of two different AGO CLIP approaches to cardiac material (PAR-CLIP with cultured rat cells and PAR-CLIP with cultured human tissue); C: computational approach consisting of a theoretical analysis of the parameters: genome-wide distribution of miRNA binding site distances (distribution of pairwise inter-site distances) and fraction of all targets with miRNA binding sites in cooperativity-permitting distance (proportion of cooperative targets); comparison to two control models: randomly defined target sites within the same 3′-UTR sequence data (random sites), predicted binding sites of scrambled miRNA-like sequences not matching to known miRNAs (scrambled). See main text for additional information.

9 PAR-CLIP WITH PRIMARY CARDIAC CELLS

The PAR-CLIP method [151] describes one of several CLIP protocols that can be used to profile miRISC-associated transcripts [152] (see Section 4.5 PAR-CLIP). Thereby, PAR-CLIP relies on the incorporation of photo-activatable nucleoside analogs (such as 4SU) into nascent RNA during transcription. Subsequently, labeled RNA can be cross-linked more efficiently to close-by (interacting) proteins by UV irradiation. Long-wave UV light (365 nm) introduces a covalent linkage between an activatable nucleotide analog and a proximal amino acid residue preserving biological contacts. Through ImmunoPrecipitation (IP) of proteins that are part of the miRISC, covalently linked miRNA and mRNA species can be isolated. The protein fraction is digested and the RNA subjected to RT-based cDNA library generation required for high-throughput sequencing. Importantly, the cross-linked nucleotide analogs lead to an increased likelihood of reverse transcriptase to introduce specific base transitions (4SU: T-to-C) at these RNA positions. Hence, the higher error rate, probably due to the more bulky nucleotides, indicates RNA positions engaged in covalent amino acid contacts. Ideally, these specific transitions should not only allow to distinguish cross-linked target mRNA from background non-target sequences, but also to identify miRISC binding sites on target mRNA at a nucleotide resolution.

9.1 PREPARATION: PAR-CLIP ADAPTATION TO PRIMARY CARDIAC CELLS

To establish PAR-CLIP for primary cardiac cells, a number of method-specific requirements had to be considered, especially with respect to the decision whether a certain cell type is at all suitable. These included to investigate how well mRNA can be labeled in cultured cardiac cells using the photo-reactive nucleoside 4SU, how efficiently the UV-induced cross-linking is achieved, to which degree the RNA has to be digested, and how the native miRISC can be isolated without the use of an epitope-tagged protein component as described in the original protocol [151]. The latter represents a crucial issue as primary cardiac cells are (even though biologically more relevant) very limited compared to cultured cell lines and protein components of interest cannot easily be over-expressed artificially. In the following, the results obtained for adapting the individual PAR-CLIP protocol steps to the use of primary cardiac cells are detailed.

9.1.1 INPUT MATERIAL

To analyze the heart-specific targetome of important miRNA candidates, human cardiac cells would be the preferred material. For obvious reasons, primary human cardiac cells or tissue are rarely available and such samples would be genetically different from each other. Thus, primary cardiac cells of rodents

like Adult Mouse Cardiac Myocytes (AMCM) and Adult Mouse Cardiac Fibroblasts (AMCF) or those of adult rats (Adult Rat Cardiac Myocytes (ARCM) and Adult Rat Cardiac Fibroblasts (ARCF)) are used as a model system to study myocardial mechanisms. Due to an expected higher yield of the latter, rat cardiac cells were preferred.
Nearly pure fractions of primary CM and CF can be prepared by an anterograde heart perfusion protocol [309] (see Section 7.3). Yield-wise, ~4×10^6 ARCM and ~10×10^6 ARCF have been obtained per adult rat heart. In weight, ~10 mg fresh ARCM or ~2 mg of ARCM cultured on laminin-coated plates have been isolated per heart.

9.1.2 4SU LABELING

As mentioned, specific to the PAR-CLIP protocol is the prior labeling of cellular RNA with photo-activatable nucleoside analogs. In this approach, 4-thio(S)-Uridine (4SU) was chosen as a suitable substrate. Since rodent cardiac cells have not been used for PAR-CLIP before, the 4SU incorporation rate into the RNA of such cultured primary cells had to be determined first. For this, initially total RNA samples were sent to the Tuschl Lab, where an established protocol involving HPLC analysis was applied to quantitatively measure the 4SU integration [151, 14]. ARCM cultured on laminin-coated dishes for 16 h showed an incorporation rate (replacement of U by 4SU) of ~2% and ~25% for supplementation of the growth medium with 0.1 mM and 1 mM 4SU, respectively. Another experiment in which ARCM were incubated for 4 h in solution within a 15 ml Falcon tube and growth medium containing 1 mM 4SU at 37°C led to only 0.3% 4SU incorporation.

9.1.3 UV CROSS-LINKING

To assess the efficiency of UV cross-linking the amount of RNA (radioactively labeled) that was covalently linked to the protein of interest was determined by Photo-Stimulated Luminescence of a corresponding western blot. Ideally, one would apply the UV impulse that gives ~70% of the maximum signal [70].
For the PAR-CLIP protocol, long-wave UV light (365 nm) has to be used to establish covalently linked AGO/RNA complexes. However, this has not been tested for primary cardiac cells before. Initially, AMCM were isolated and cultured on laminin-coated plates with 4SU-supplemented medium (0.1 mM) for 16 h. Cell were harvested directly or after irradiation with long-wave UV of 0.2 (original protocol: 0.15 [151]) or 2.0 J/cm². After PNK-mediated phosphorylation of RNA 5'-OH ends with ^{32}P-γ-ATP, RNA of immunoprecipitates was visualized by western blotting and Photo-Stimulated Luminescence image (PLS) recording (see Figure 9.1A). As there was no obvious difference detectable from the PLS, different UV conditions and a more specific labeling approach were applied. Short-wave UV (254 nm) of various intensities as well as other potential UV sources were compared. The RNA was labeled by a radioactive linker (P-TL3) ligated with T4 RNA Ligase 1 (see Figure 9.1B). Due to another inconclusive result and in order to prevent extensive use of animals, a more general experiment with virtually unlimitedly available HEK cells (also used by the original publi-

cation [151]) was performed comparing different HIgh-Throughput Sequencing of RNA isolated by CLIP (HITS-CLIP) (254 nm) and PAR-CLIP (365 nm) UV intensities (see Figure 9.2). As the inconsistency remained (without UV stronger signal than with irradiation), unspecific radioactive labeling was considered as a possible reason and tested for by comparing a third labeling strategy. Using total heart cell suspensions of adult rats, precipitated RNA was radioactively labeled with either ^{32}P-γ-ATP (PNK, see Figure 9.3A), ^{32}P-TL3 (T4 RNA Ligase 1, see Figure 9.3B) or using a pre-adenylylated Ap^{32}p-TL3 in an approach without adding ATP catalyzed by T4 RNA Ligase 2 truncated K227Q with reduced lysyl adenylation activity (see Figure 9.3C, for sequences see Table 6.7 Linker). The results of the third labeling strategy were probably more conclusive but the approach has not been followed up as the preparation of the radioactive Ap^{32}p-TL3 involved extensive handling of high-dosage radioactive substances.

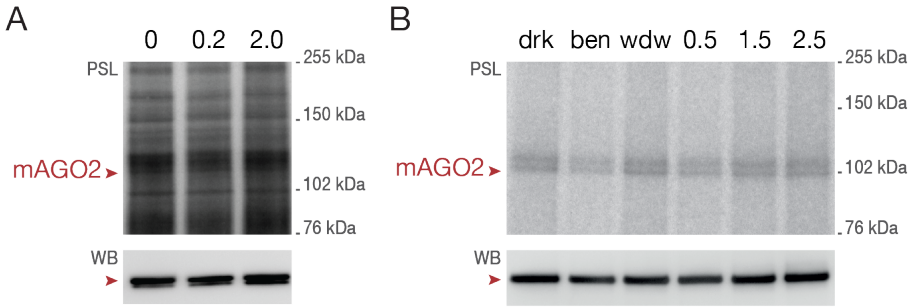

FIGURE 9.1. UV cross-linking of adult mouse cells. A: comparison of 0, 0.2 and 2.0 J/cm² at 365 nm, previously labeled with 0.1 mM 4SU for 16 h. Photo-Stimulated Luminescence image (PLS) and Western Blot (WB) of AMCM IP. IP: anti-mAGO2 (2D4), RNase: no, RNA detection: ^{32}P-γ-ATP (PNK), protein detection: anti-mAGO2 (2D4); B: comparison of different irradiation conditions (drk: darkness, ben: bench light, wdw: day light) and 0.5, 1.5 and 2.5 J/cm² at 254 nm. PLS and WB of AM total heart IP. IP: anti-mAGO2 (2D4), RNase: no, RNA detection: P-TL3 (T4 RNA Ligase 1), protein detection: anti-mAGO2 (2D4).

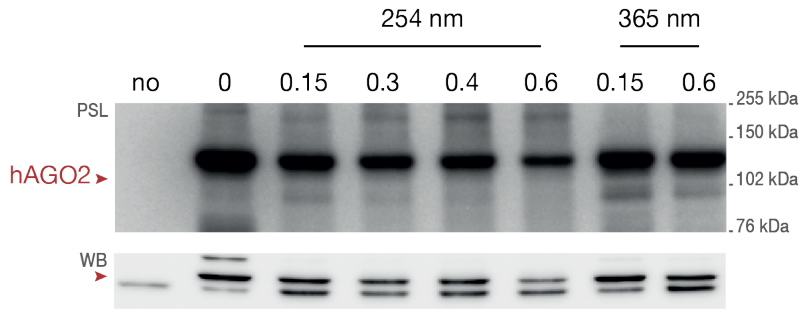

FIGURE 9.2. UV cross-linking of HEK cells. Comparison of 0 and 0.15, 0.3, 0.4, 0.6 J/cm² at 254 nm (254 nm) and 0.15, 0.6 J/cm² at 365 nm (365 nm), cells cross-linked at 365 nm were previously labeled with 0.1 mM 4SU for 16 h. Photo-Stimulated Luminescence images (PLS) and Western Blots (WB) of HEK cell or no lysate (no) IP. IP: anti-hAGO2 (11A9), RNase: RNase T1 (1 U/µl, 100 U/µl), RNA detection: ^{32}P-γ-ATP (PNK), protein detection: anti-hAGO2 (11A9).

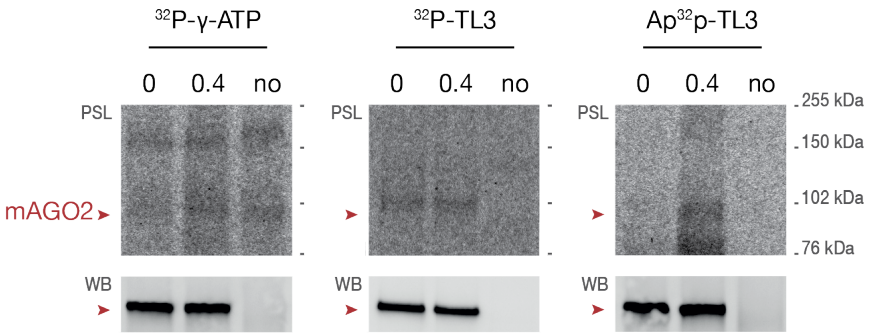

FIGURE 9.3. RNA detection by different radioactive labeling strategies. Comparison of radioactive labeling with ^{32}P-γ-ATP (PNK), ^{32}P-TL3 (T4 RNA Ligase 1) and Ap^{32}p-TL3 (T4 RNA Ligase 2 truncated K227Q). Always: comparison of 0 and 0.4 J/cm² at 254 nm. Photo-Stimulated Luminescence image (PLS) and Western Blot (WB) of AR total heart or no lysate (no) IP (three separate membranes). IP: anti-mAGO2 (2D4), RNase: RNase I (1 mU/µl), protein detection: anti-mAGO2 (2D4).

9.1.4 RNASE TREATMENT

Following cross-linking, cells have to be lysed to start with partial RNA digest, the next step of the PAR-CLIP protocol.
In initial experiments, adult rat total heart cell lysate was used to compare the effect of different RNase T1 concentrations prior to IP and RNA detection with ^{32}P-γ-ATP (see Figure 9.4). As no difference has been apparent between the results, again HEK cells were employed as a more general model. In an experiment comparing different RNase T1 concentrations as well as the results of no lysate or no antibody for the IP (see Figure 9.5), differences in the amount of the detectable RNA signal depending on the applied input could be observed. However, no difference has been detectable regarding an expected differential spreading of the bands within the expected size range (above ~110 kDa of AGO2/miRNA) in relation to the applied different RNase concentrations.

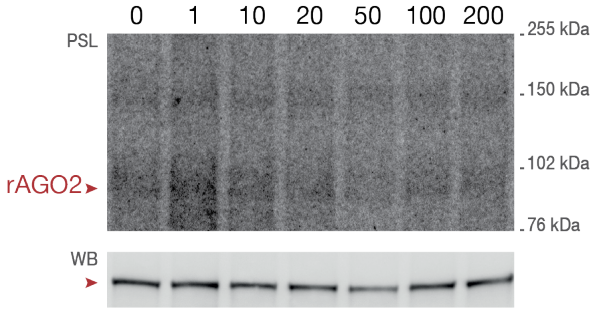

FIGURE 9.4. RNase-mediated digest with adult rat cells. Comparison of different RNase concentrations (0, 1, 10, 20, 50, 100 and 200 U/µl) at a single digestion step with RNase T1 prior to IP. Photo-Stimulated Luminescence image (PLS) and Western Blot (WB) of AR total heart IP. IP: anti-mAGO2 (2D4), UV irradiation: 0.3 J/cm² at 254 nm, RNA detection: ^{32}P-γ-ATP (PNK), protein detection: anti-mAGO2 (2D4).

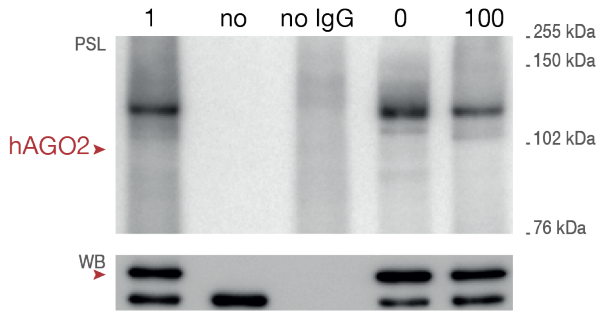

FIGURE 9.5. RNase-mediated digest with HEK cells. Comparison of different RNase concentrations (0, 1 and 100 U/µl) at a single digestion step with RNase T1 prior to IP. Photo-Stimulated Luminescence image (PLS) and Western Blot (WB) of HEK cell or no lysate (no) IP. IP: anti-hAGO2 (11A9) or no antibody (no IgG), UV irradiation: 0.3 J/cm² at 254 nm, RNA detection: ^{32}P-γ-ATP (PNK), protein detection: anti-hAGO2 (11A9).

9.1.5 AGO2 ANTIBODY AND IP CONDITIONS

One factor that strongly affects the success of a CLIP protocol is the efficiency with which the RBP of interest can be immunoprecipitated. For rodent AGO2, a strong cross-reactivity of antibodies has been observed. In an initial experiment, four different AGO antibodies were compared for their precipitation efficiency regarding rat AGO2 (see Figure 9.6). Anti-mAGO2 2D4 is a commercially available antibody against mouse AGO2 with cross-reactivity to rat and hamster. A second (MA2) and a third (5A5) anti-mAGO2 were kindly provided by the O'Carroll Lab and the Meister Lab, respectively. The fourth antibody (PAN) is commercially available and recommended against all mouse, rat and human AGO paralogs (anti-AGO1-4 H-300). A second selection of antibodies including the best performing 2D4 was tested under different IP washing conditions (see Figure 9.7A). As 2D4 again achieved the best results, IP conditions were further optimized for this antibody by comparing different incubation times and different bead volumes for equal IP inputs (see Figure 9.7B).

9.1.6 ESTIMATION OF INPUT MATERIAL

The typical scale of a PAR-CLIP experiment, according to the original protocol [151], has been a HEK cell pellet of ~3 ml. However, these cells contained epitope-tagged AGO proteins stably expressed from a strong CMV promoter [236]. Based on own results, per each 15 cm cell culture plate a pellet volume of ~60 µl cells and an amount of ~1 mg total protein can be expected. Thus, about 50 15 cm culture plates and about 50 mg total protein might have been applied per experiment in the original study. Per adult rat heart, ~1 mg of ARCM and ~1.3 mg of ARCF total protein can be estimated. Consequently, to reach an amount of ~50 mg total protein, about 50 adult rats would be required.

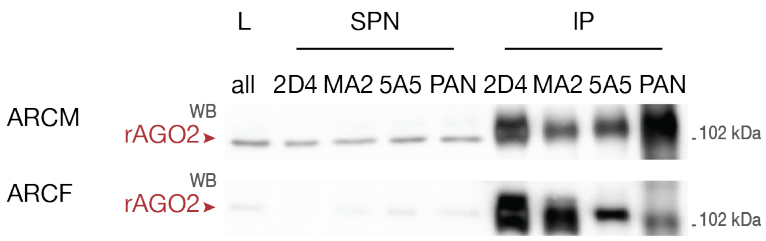

FIGURE 9.6. Mouse and rat AGO2 antibodies. Comparison of rat AGO2 IP efficiency in cardiac myocytes (ARCM) and cardiac fibroblasts (ARCF) using different AGO antibodies. Always: comparison of IP antibodies anti-mAGO2 (2D4), anti-mAGO2 kindly provided by the O'Carroll Lab (MA2), anti-mAGO2 hybridoma supernatant kindly provided by the Meister Lab (5A5) and anti-AGO1-4 (PAN). Western Blot (WB) of adult rat cell IP, L: 1% of IP input lysate, SPN: 1% of IP supernatant, IP: 66% of IP output. Lysis buffer: PAR-CLIP Lysis Buffer, IP input: ~0.75 mg per condition, beads per protein: ~13 µl/mg, IP incubation: 4 h, washing: 6 × PAR-CLIP Lysis Buffer, elution: NuPAGE Loading Buffer, protein detection: anti-AGO2 (C34C6).

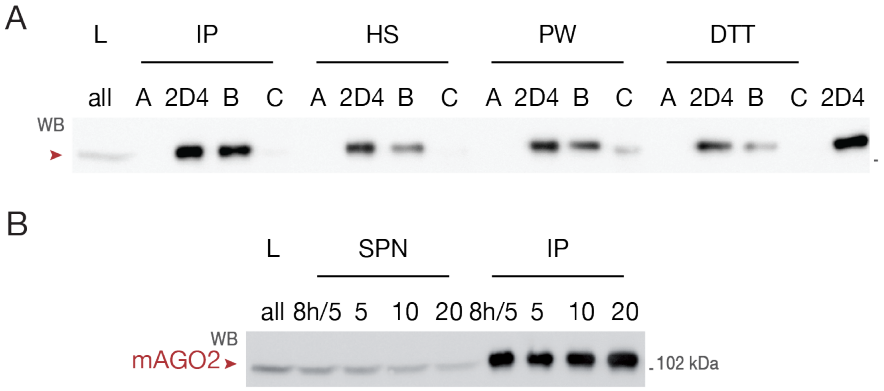

FIGURE 9.7. Mouse and rat AGO2 IP conditions. A: buffer stability of different AGO antibodies. Comparison of IP antibodies anti-hAGO2 (11A9, A), anti-mAGO2 (2D4), anti-mAGO2 hybridoma supernatant kindly provided by the Meister Lab (6F4, B) and anti-AGO2 (C34C6, C) under different washing conditions: 6 × PAR-CLIP Lysis Buffer (LB), 6 × IP Wash Buffer (300 mM NaCl, IP), 6 × High Salt Wash Buffer (500 mM NaCl, HS), 6 × Phosphatase Wash Buffer (0 mM NaCl, PW) and 6 × PNK Buffer supplemented with 5 mM DTT (DTT). Western Blot (WB) of NIH/3T3 cell IP, L: 5% of IP input lysate, SPN: 5% of IP supernatant, IP: 100% of IP output. Lysis buffer: PAR-CLIP Lysis Buffer, IP input: ~2 mg per condition, beads per protein: ~5 µl/mg, IP incubation: 4 h, elution: NuPAGE Loading Buffer, protein detection: anti-AGO2 (C34C6); B: mAGO2 IP efficiency. Comparison of different IP incubation times: 8 h (indicated) and 4 h (for all other samples) and different bead volumes used per mg total protein applied: 5, 10 and 20 µl/mg. WB of NIH/3T3 cell IP, L: 5% of IP input lysate, SPN: 5% of IP supernatant, IP: 100% of IP output. IP: anti-mAGO2 (2D4), Lysis buffer: PAR-CLIP Lysis Buffer, IP input: ~2 mg per condition, washing: 6 × PAR-CLIP Lysis Buffer, elution: NuPAGE Loading Buffer, protein detection: anti-AGO2 (C34C6).

9.2 CLIP STUDY: PAR-CLIP WITH ARCM AND ARCF

For the first preparative PAR-CLIP experiment, a total of 13 adult rat hearts has been applied. Cells were separated in ARCM and ARCF with a total protein

amount of ~13 and ~17 mg, respectively (see Figure 9.8A and Table 11.1). Upon cDNA library preparation at the Tuschl Lab, only the ARCM sample showed a reasonable amount of DNA after test PCR amplification and could thus be sent for sequencing. However, the quality of the obtained read library was rather poor and could not be evaluated.

A second PAR-CLIP study was conducted with 82 rat hearts providing a total protein amount of ~81 (ARCM) and ~109 mg (ARCF, see Figure 9.8B and Table 11.1). However, compared to the first experiment, not only less stringent IP washing conditions (150 instead of 300 mM NaCl), but also a more mild RNA digest were applied. After SDS-PAGE there were no clear rAGO2 bands detectable. To further purify the precipitate from unbound RNA, the gel was plotted on a nitrocellulose membrane. Additionally, it was confirmed that denaturing protein elution was effective by preparing another gel with a second eluate of the same beads.

Several other PAR-CLIP studies of primary cultured cells as well as HITS-CLIP experiments with fresh cardiac cells were prepared and the isolated RNA sent for library preparation to the Tuschl Lab. However, in each case the material has not been sufficient to obtain a sequenceable cDNA library.

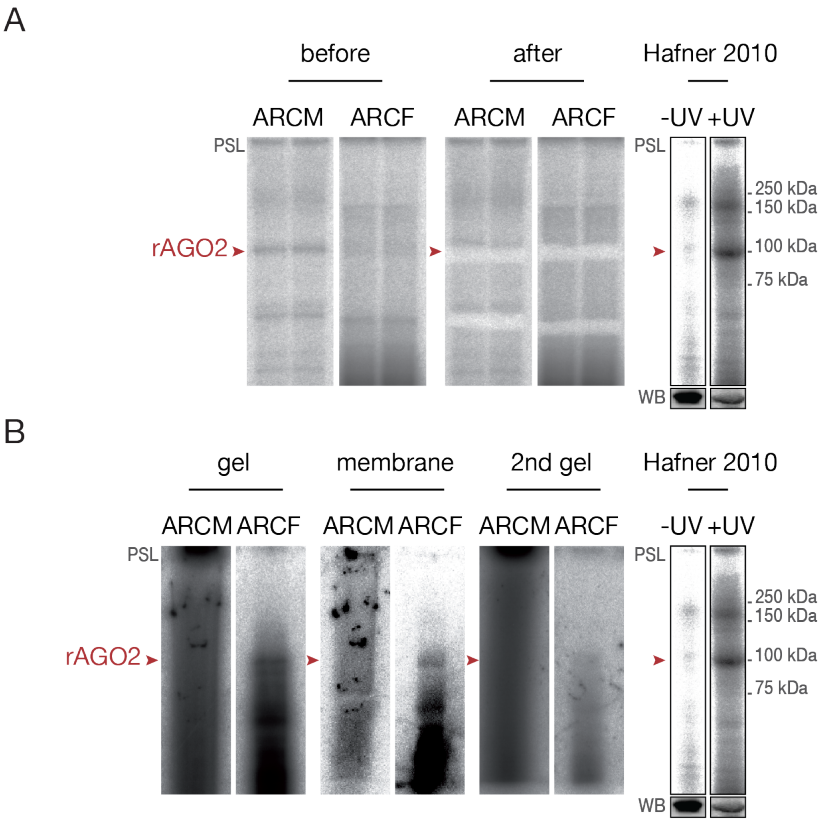

FIGURE 9.8. PAR-CLIP studies with adult rat primary cardiac cells. A: PAR-CLIP with 13 adult rat hearts. Comparison of the polyacrylamide gel (same gel) before and after cutting the region at the expected height of rat AGO2 with [151] Figure 5A (Flag/HA-hAGO2). Photo-Stimulated Luminescence images (PLS) obtained at the polyacrylamide gel purification step of the PAR-CLIP protocol. Input: ~13/17 mg (ARCM/ARCF), beads: 96 µl, IP: anti-mAGO2 (2D4), Lysis buffer: PAR-CLIP Lysis Buffer (300 mM NaCl), UV irradiation: 0.15 J/cm² at 254 nm, RNase: RNase T1 (1 U/µl, 100 U/µl), RNA detection: ^{32}P-γ-ATP (PNK); B: PAR-CLIP with 82 adult rat hearts. Comparison of the polyacrylamide gel, the western blots (membrane) after blotting the first gel and of a second polyacrylamide gel (2nd gel) prepared by loading a second denaturing eluate from the same beads with [151] Figure 5A (Flag/HA-hAGO2). PLS obtained at the polyacrylamide gel purification step of the PAR-CLIP protocol. Input: ~81/109 mg (ARCM/ARCF), beads: 96/240 µl (ARCM/ARCF), IP: anti-mAGO2 (2D4), Lysis buffer: PAR-CLIP Lysis Buffer, UV irradiation: 0.15 J/cm² at 254 nm, RNase: RNase T1 (1 U/µl), RNA detection: ^{32}P-γ-ATP (PNK).

10 PAR-CLIP WITH HUMAN SLICE CULTURES

Even though rodent heart cells offer a well-studied cardiac model system, certainly experimental results cannot be transferred one to one to the human myocardium. Thus, human heart tissue is highly advantageous, but also almost impossible to access.
However, it has been shown that vital tissue slices of about 300 µm thickness can be prepared from human ventricular myocardium without sacrificing organotypic characteristics. Such slices were derived from surgical specimens and preserved in an organotypic culture for more than 28 days [46].
As this offers enough time to potentially label newly synthesized RNA with 4SU, it was aimed for a hAGO2 PAR-CLIP study.

10.1 PREPARATION: PAR-CLIP ADAPTATION TO MYOCARDIAL SLICES

PAR-CLIP with native hAGO2 has already been published for HEK cells using anti-hAGO2 (11A9) [217]. Thus, establishing a protocol for human myocardial tissue slices predominantly involved the examination of 4SU labeling and RNA cross-linking efficiency for such slice cultures.

10.1.1 INPUT MATERIAL

The complex cellular and sub-cellular composition of adult human heart tissue accounting for its functionality is nearly impossible to reproduce by any model system. Thus, using human cardiac tissue to find out about the heart-specific targetome of interesting miRNA candidates is highly desirable.
Human myocardial tissue slices were prepared in cooperation with the Dendorfer Lab according to an optimized protocol [46] (see Section 7.3). The number and quality of slices available per experiment highly depends on the size and health of the surgical specimens that are obtained.

10.1.2 4SU LABELING

Since human myocardial tissue slices have never been used for PAR-CLIP before, first of all the photo-activatable nucleoside analog (4SU) incorporation rate into nascent RNA had to be determined under their specific culturing conditions.
A comparative method to detect the extent of 4SU incorporation consists in the specific biotinylation of carbon-bonded sulfhydryl groups (thiols) in the RNA samples compared and visualization on a membrane using streptavidin-coupled HRP and ECL detection reagent [92] (see Section 7.1). Applying this approach, the 4SU incorporation into HEK cell RNA after treating the cells as described in the original protocol [151] was compared with incorporation

into RNA of human tissue slices after different 4SU concentrations and labeling times (see Figure 10.1). For each condition, not only the results of the dot-blot assay, but also a representative section of the slices treated by a standard cell viability test (MTT) is depicted. Thereby, the yellow tetrazole 3-(4,5-diMethylThiazol-2-yl)-2,5-diphenylTetrazolium bromide (MTT) is reduced by oxidoreductases to its purple formazan indicating metabolically active (living) cells [293]. Increasing the 4SU concentration within the Slice Culture Medium to 10 mM and more resulted in adverse (DMSO-independent) effects with respect to cell viability (yellow areas). A longer incubation time at a lower 4SU concentration (5 mM) allowed for a relatively efficient 4SU integration while avoiding obvious cellular damage.
Furthermore, labeled RNA samples were sent to the Tuschl Lab for HPLC analysis to quantitatively determine 4SU incorporation. The fraction of sent RNA samples that could be measured showed a 4SU integration of 0.5 and 0.7% at 0.5 mM, 0.7 and 1.2% at 1 mM, 1.4 and 2.5% at 5 mM and 1.3% at 20 mM 4SU with 16 h of incubation.
HEK cells labeled according to the original protocol typically show an incorporation of ~4% 4SU [151, 14].

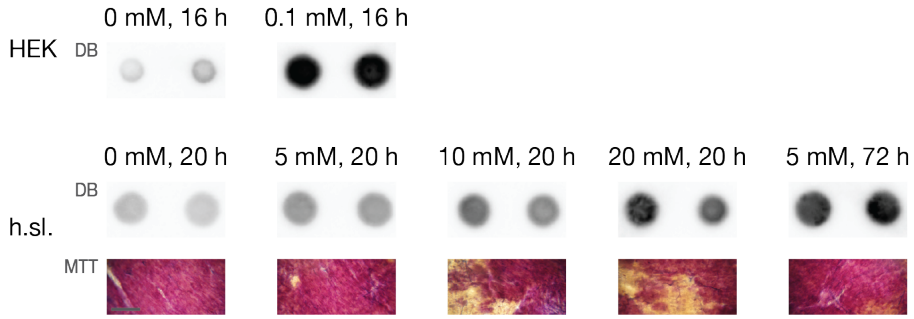

FIGURE 10.1. 4SU labeling efficiency of human cells and tissue. Comparison of 4SU incorporation into RNA of cultured HEK cells (HEK) and human myocardial tissue slices (h.sl.) at different 4SU concentrations and incubation times: HEK cells not (0 mM, 16 h) or labeled according to the original protocol [151] (0.1 mM, 16 h) and human slices incubated at 5, 10 or 20 mM for 20 h and 5 mM 4SU for 72 h (one medium change after 24 h) were compared. 4SU incorporation was visualized by a Dot-Blot (DB) approach including thiol-biotinylation and subsequent detection by streptavidin-coupled HRP and ECL reagent (see Section 7.1); cell viability was examined using a standard colorimetric assay (MTT, only for human slices), gray bar indicates a distance of 1 mm.

10.1.3 UV CROSS-LINKING

As the original protocol described the UV irradiation step for a single layer of HEK cells [151], the cross-linking efficiency of sliced cardiac tissue (300 µm) was examined using twice the intensity published for HEK cells (see Figure 10.2).
After standard PNK-mediated RNA labeling with radioactive ^{32}P-γ-ATP, however, there was again no obvious difference detectable between samples with-

out prior cross-linking and such irradiated with short or long-wave UV before harvesting (compare Figure 9.1 and 9.2).

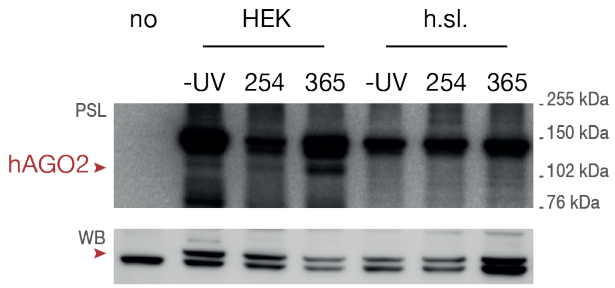

FIGURE 10.2. UV cross-linking of human cells and tissue. Comparison of no irradiation (-UV), 0.3 J/cm² at 254 nm (254), and 0.3 J/cm² at 365 nm (365) with previous 4SU labeling (HEK: 0.1 mM, 16 h and human slices: 5 mM, 20 h). Photo-Stimulated Luminescence image (PLS) and Western Blot (WB) of HEK cell (HEK) or human slice (h.sl.) IP and without lysate incubation (no). IP: anti-hAGO2 (11A9), RNase T1 (1 U/µl, 50 U/µl), RNA detection: ^{32}P-γ-ATP (PNK), protein detection: anti-hAGO2 (11A9).

10.1.4 RNASE TREATMENT

RNase T1-mediated fragmentation of RNA precipitated from human cell lysates has already been approached while preparing the first PAR-CLIP study with primary cardiac cells (compare Figure 9.5).

10.1.5 AGO2 ANTIBODY AND IP CONDITIONS

Anti-hAGO2 (11A9) is an effective monoclonal antibody specifically immunoprecipitating human AGO2 [348], which has been applied successfully in a hAGO2 PAR-CLIP study [217]. However, different IP lysis buffers were compared to affirm optimal conditions (see Figure 10.3).

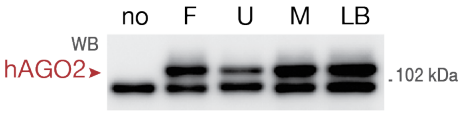

FIGURE 10.3. Human AGO2 IP conditions. Comparison of different lysis buffers on IP efficiency using anti-hAGO2 (11A9): Flag Lysis Buffer (F), Ule Lysis Buffer [221] (U), Meister Lysis Buffer [348] (M) and PAR-CLIP Lysis Buffer [151] (LB). Western Blot (WB) of HEK cell IP and without lysate incubation (no). IP input: ~2 mg per condition, beads per protein: ~5 µl/mg, IP incubation: 4 h, washing: 6 × PAR-CLIP Lysis Buffer, elution: NuPAGE Loading Buffer, protein detection: anti-hAGO2 (11A9).

It has been shown that hAGO2 can be efficiently eluted from anti-hAGO2 (11A9) using a competing peptide of 16 amino acids resembling parts of the N-terminus of hAGO2 [348] (for sequence see Table 6.7 Elution peptide). Different hAGO2 elution strategies were tested to determine their individual purities (depicted for a larger kDa area, see Figure 10.4). These variations of competi-

tive peptide elutions were compared to the denaturing elution approach using NuPAGE Loading Buffer.

FIGURE 10.4. Competitive hAGO2 elution. Comparison of different IP elution strategies: denaturing NuPAGE Loading Buffer (LDS, al) or competitive with a 16 amino acids peptide resembling the N-terminus of hAGO2 (4 µg/µl) at 600 rpm and 25°C for 90 min [348] (peptide, el); elution volume equaled bead volume; for the peptide elution different elution temperatures (4°C), times (overnight, o.n.) and peptide concentrations (8 µg/µl, 2x) were compared; further the yields of a second (el2) competitive and a third (rm) denaturing elution step were analyzed. Western Blot (WB) of of HEK cell IP. IP: anti-hAGO2 (11A9), IP input: ~1 mg per condition, beads per protein: ~15 µl/mg, IP incubation: 4 h, washing: 6 × PAR-CLIP Lysis Buffer, protein detection: anti-hAGO2 (11A9).

10.1.6 ESTIMATION OF INPUT MATERIAL

Albeit rarely being the case, if material from human heart explants is available, the sample size is by far more preferable than that of small mouse or rat hearts. With a yield of ~100 to 300 µg total protein per slice and assuming that a typical PAR-CLIP experiment requires a total protein input of ~50 mg, about 250 slices would be necessary to obtain a meaningful read library. However, the size and viability of individual tissue slices can vary greatly. Further, this estimation neglects important differences between HEK and cultured tissue cells such as the rate of metabolism, 4SU labeling efficiency or UV light accessibility. Hence, an initial test-CLIP study was set up to better estimate the amount of slices required.

10.2 CLIP STUDY: TEST-CLIP WITH HUMAN CELLS AND TISSUE

The test-CLIP dedicated to estimate the amount of cellular material needed in order to obtain a comprehensive sequencing library did not only comprise two myocardial tissue slice samples, but also three iCLIP and three PAR-CLIP samples meant as a reference with increasing amounts of HEK cell inputs (see Table 11.1). All eight samples were subjected to competitive peptide elution. However, a control western blot with equal amounts of input per IP was prepared to monitor the elution efficiency (see Figure 10.5). Unexpectedly, upon library preparation of the actual samples and test PCR amplification there has been no detectable amount of DNA, preventing continuation with high-throughput sequencing.

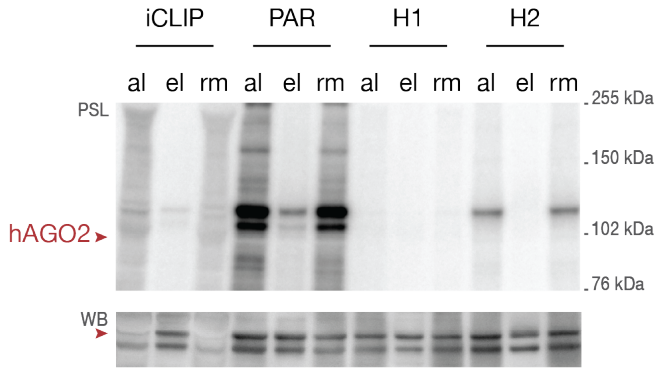

FIGURE 10.5. Test-CLIP with human cells and tissue. Comparison of IP and elution efficiency with denaturing (al), competitive peptide [348] (el) and a second (rm) denaturing elution of the peptide eluted samples. Control Photo-Stimulated Luminescence image (PLS) and Western Blot (WB) of iCLIP and PAR-CLIP (PAR) with HEK cells and PAR-CLIP with myocardial slices of two human hearts (H1 and H2). Input: ~2 mg per condition, beads: 10 µl per condition, IP: anti-hAGO2 (11A9), Lysis buffer: PAR-CLIP Lysis Buffer, UV irradiation: 0.3 J/cm² at 254 nm (iCLIP) or 0.3 J/cm² at 365 nm with previous labeling with 0.1 mM 4SU for 16 h (PAR) or 5 mM 4SU for 72 h with one medium change after 24 h (H1 and H2), RNase T1 (1 U/µl, 100 U/µl), RNA detection: ^{32}P-γ-ATP (PNK), protein detection: anti-hAGO2 (11A9).

11 SUMMARY OF THE EXPERIMENTAL FINDINGS

In the following, the findings of the experimental part of this PhD project are summarized and placed in context with literature-based expectations.
Prior to conducting CLIP, it is indispensable to adapt and optimize the protocol for the cellular system of choice. Based on the individual CLIP approach, this may include strategies to efficiently gain the cellular input material, label RNA with photo-activatable nucleoside analogs, cross-link RNA bases to specific amino acids within the binding protein of interest, partially digest the RNA of covalently connected protein/RNA complexes, and to find the best possible conditions for immunoprecipitation of the target complexes.
In the course of this project, two different strategies have been pursued. First, the PAR-CLIP approach was adapted to primary cardiac cells (rather than cultured cell lines). And second, the PAR-CLIP protocol was applied to human myocardial slice cultures.

11.1 PAR-CLIP WITH PRIMARY CARDIAC CELLS

In a first approach, the PAR-CLIP protocol developed for a human cell line that allows for the inducible expression of FLAG/HA-hAGO1-4 from a CMV promoter [151] was aimed to be adapted to primary cardiac cells such as CM and CF (see Section 9).

INPUT MATERIAL Adult rat cardiac cells were chosen as an available alternative to human cells to study the transcriptome-wide targetome of rAGO2-containing miRISCs in primary CM and CF.

4SU LABELING 4SU was selected as a PAR-CLIP-required photo-activatable ribonucleoside. Efficient labeling of cellular RNA is essential for successful cross-linking using long-wave UV light (365 nm). Published studies have achieved ~4% 4SU incorporation (relative to the total U content) [151]. Only the incorporation rate into ARCM RNA has been measured by direct HPLC analysis. Interestingly, a ten-fold higher 4SU concentration in the growth medium, compared to the original protocol [151], increased the amount of incorporated 4SU accordingly: 0.1 mM, ~2% and 1 mM 4SU, ~25%. However, already above 4SU concentrations of only 0.05 mM an inhibition of the production and processing of rRNA has been detected [54], which was accompanied by tumor suppressor gene induction and an anti-proliferative effect. Hence, it is important to keep in mind that 4SU labeling potentially influences the cellular metabolism and thus the final targetome data.

UV CROSS-LINKING The required irradiation intensity to covalently link RNA to the RBP of interest varies dramatically for different proteins and proto-

cols published (see Table 4.1 #4, HITS-CLIP, mAGO2, 0.004 J/cm² [245] or #15, PAR-CLIP, GLD-1, 2 J/cm² [198]). Cross-linking efficiency of certain RNA binding domains may depend on factors such as the spatial orientation of photo-activated nucleotide orbitals and the structural availability of reactive amino acids [70, 219] (see Section 4.5 PAR-CLIP). Thus, UV irradiation needs to be optimized for each RBP individually.
Published strategies to compare the amount of bound RNA through radioactive phosphorylation and subsequent analysis on a Photo-Stimulated Luminescence image (PLS) led to inconclusive results: cross-linking tests with either adult mouse cells (see Figure 9.1) or human cultured cells (see Figure 9.2) showed no obvious difference for samples irradiated at different intensities or even not exposed to any UV light.
Similarly, an RNA labeling method based on ligation rather than phosphorylation which is supposed to be more RNA-specific [70, 291] did not clarify this issue. In this second approach, the PNK-mediated transfer of ^{32}P from the γ position of ^{32}P-γ-ATP to hydroxyl groups (possibly also to protein-derived phosphorylation sites) was replaced by a T4 Ligase 1-catalyzed ligation of 5′-phosphoryl-terminated linkers (5′-^{32}P-TL3) to 3′-hydroxyl-terminated RNA fragments. T4 RNA Ligase 1-mediated phosphodiester bond formation results from three consecutive nucleotidyl transfers. In theory, upon activation of the enzyme with ATP (pppA) forming a covalent intermediate (ligase-(lysyl-N)-pA), AMP (pA) is expected to be transferred to the 5′-^{32}P of the TL3 linker (3′ ddC to prevent circularization) yielding the adenylylated intermediate (Ap^{32}p-TL3), which could then be attacked by the RNA 3′-OH ends to form labeled RNA esters, while releasing pA [414]. However, albeit the background signal appeared to have been reduced, the radioactive signal did not seem to differ for UV-irradiated and untreated samples (see Figure 9.1B and 9.3 middle). Maybe the 5′-^{32}P-TL3 could somehow unspecifically but strongly (NuPAGE Loading Buffer persistent) attach to the AGO2 complexes, with the double band in Figure 9.1B occurring due to unspecific sticking at either empty or miRNA-loaded protein complexes [291].
For small RNA cDNA library preparation, T4 RNA Ligase 1 is sometimes replaced by a truncated version of T4 RNA Ligase 2 in 3′-linker ligation [150]. This modified enzyme exhibits reduced adenylyltransferase activity [440] and therefore promises to cause less undesired ligation products. Interestingly, RNA detection using that enzyme and Ap^{32}p-TL3 resulted in a more expected picture (see Figure 9.3C) with a noticeable difference between the cross-linked and the untreated sample. Cross-linking with 0.4 J/cm² at 254 nm appeared to increase the amount of co-precipitated RNA. Due to the exposure to high-dosage radioactivity, this experiment has not been repeated for different UV intensities or a PAR-CLIP approach with previous labeling and irradiation at long-wave UV.
Surprisingly, neither published results of cross-linking according to the PAR-CLIP protocol (compare, e. g., [151] Figure 5A, FLAG/HA-hAGO1-4, 4SU: 0.1 mM, 16 h, UV: 0.15 J/cm² at 365 nm, ^{32}P-γ-ATP) nor of cross-linking with short-wave UV (compare, e. g., [245] Figure 1a, mAGO2, UV: 0.004 J/cm² at 254 nm, ^{32}P-γ-ATP) could be reproduced.

While comparing individual western blots of AGO2 with the belonging PLS, it should be considered that ~25 nucleotides of attached RNA account for approximately 8 kDa in addition to the molecular weight of the precipitated protein [14]. The length of the cross-linked RNA fragments depends on the intensity of the partial RNA digestion step. In theory, for AGO CLIP, two populations of cross-linked complexes are expected upon electrophoretic size separation: one at about 110 kDa reflecting the AGO/miRNA complexes and a second at about 130 kDa corresponding to AGO/miRNA/mRNA complexes [70, 291].

RNASE TREATMENT Similar to UV cross-linking, the intensity of the RNase-mediated digest is estimated by the radioactive RNA signal on the PLS. The difference is that not the signal intensity but the spread of the corresponding bands would be considered. A comparison of high versus low concentrations of RNase can be used to achieve an optimal RNA fragment size (compare, e. g., [400] Figure 2B/C, NOVA1, RNase A, high: 2 mU/µl, low: 0.04 mU/µl or [219] Figure 10.2, HNRNPC, RNase I, high: 20 mU/µl, low: 1 mU/µl). However, as for the cross-linking, no real difference between high or low RNase concentrations could be observed from the PLS of adult rat cell lysates digested with RNase T1 (see Figure 9.4). A test with cultured human cells resulted in a slightly more expected picture, though only when considering the different IP inputs (see Figure 9.5).

AGO2 ANTIBODY AND IP CONDITIONS Optimizing the conditions of protein IP is one of the most essential hurdles to be taken for successful application of a CLIP protocol to other RBPs or cellular systems. A balance between efficient precipitation and high purity has to be found by optimizing the salt and detergent stringency. The most efficient precipitation of rat AGO2 has been observed for the cross-reactive anti-mAGO2 (2D4, see Figures 9.6 and 9.7A). However, compared to the anti-Flag used for the original protocol [151], anti-mAGO2 is less resistant to high salt washing conditions. Thus, a salt concentration of only about 150 mM had to be used for IP washing (instead of up to 500 mM). A longer IP incubation time (8 h versus 4 h) or a higher amount of beads per total protein (5 versus 10 or 20 µl/mg) improved IP efficiency only marginally (see Figure 9.7B).

ESTIMATION OF INPUT MATERIAL The actual amount of input material (measured, e. g., in terms of total protein per IP) that is needed to perform a successful CLIP study is neither easy to obtain from literature nor easy to transfer to a different cellular system.
The original protocol indicates a typical pellet volume of 3 ml HEK cells per experiment [151]. An own estimation showed that per ~80% confluent 15 cm cell culture plate a pellet of about 60 µl HEK cells (accounting for a total protein content of ~1 mg after lysis) can be expected. Thus, a total of approximately 50 15 cm plates (~50 mg total protein) might have been used by the authors per each PAR-CLIP experiment (see Table 4.1 #12). Even though the cells employed for the original experiment stably over-expressed (strong CMV promoter) epitope-tagged AGO proteins [236, 151], similar input amounts were used successfully at a PAR-CLIP study of native hAGO2 in unmodified HEK cells [217] (see Table

4.1 #13). PAR-CLIP with about 10^9 EBV-positive lymphoblastoid cells (assuming about 20×10^6 cells per plate, ca. 50 15 cm plates per experiment) has been used to identify the viral and cellular targetome of tagged and native hAGO2 [373] (see Table 4.1 #16). For comparison, PAR-CLIP of ELAVL1 in HeLa cells was performed with 60 to 100 15 cm plates (assuming ~60 µl and ~1 mg per plate, ca. 3.6 to 6 ml pellet and 60 to 100 mg total protein) per condition [239] (see Table 4.1 #14) Another study precipitating GLD-1-GFP/Flag from *Caenorhabditis elegans* employed about 250,000 worms per experiment [198] (see Table 4.1 #15). To meet the apparent demand for high cell numbers, in a first step the protocol was adapted to use quantitatively more available cardiac cells from rat, rather than mouse hearts. In terms of total protein to be expected from one adult rat heart, the lysate of the ARCM fraction accounts for ~1 mg and that of the ARCF contains ~1.3 mg total protein.

CLIP STUDY Both preparative PAR-CLIP studies with either 13 or 82 adult rat hearts (see Table 11.1) did not yield evaluable sequencing results. For the first experiment, a total protein input of ~13 mg (ARCM) and ~17 mg (ARCF) may not have sufficed to isolate a proper amount of RNA for cDNA library preparation. The second experiment was based on a more than six-fold increased input amount (ARCM: ~81 mg, ARCF: ~109 mg). Here, the failure may be explained by the more mild RNA digestion in combination with reduced washing stringency compared to the previous study and thus too large and immobile complexes. RNase-mediated digest and IP washing was reduced in the hope to obtain higher amounts of co-isolated RNAs. However, this may have resulted in large protein/RNA complexes which could not be separated during gel electrophoresis, but remained within the loading pocket of the gel (see Figure 9.8B). Blotting of the gel on a membrane in order to get rid of misleading, non-covalently attached RNAs as well as a second denaturing elution from the same beads did not provide a remedy.

11.2 PAR-CLIP WITH HUMAN SLICE CULTURES

In a second approach, the PAR-CLIP protocol was aimed to be applied to human myocardial tissue cultures (slices of surgical specimens) preservable in culture [46] and thus theoretically amenable to 4SU labeling.

INPUT MATERIAL Human heart tissue is not only qualitatively much more relevant for detecting the transcriptome-wide targetome of important miRNA candidates, but also quantitatively it is certainly of higher yield than rodent hearts. However, both measures are highly fluctuating and largely dependent on the patient's kind and state of cardiac disease. Further, cell type-specific miRNA targetomes cannot readily be unraveled from whole tissue analyses (see Section 3.3).

4SU LABELING To estimate the 4SU labeling ability of myocardial slices, preliminary tests based on the relative incorporation into nascent RNA compared to a positive HEK cell control have been conducted (see Figure 10.1). At similar

labeling time as for the cell culture, evident labeling has only been detected after a 100- to 200-fold increase of employed 4SU concentrations. This did not only cause high consumption of valuable resources, but such levels of 4SU also seem to be toxic to the cells, as observed from a standard cell viability test (MTT assay). It should be noted, however, that this assay indicates metabolically active cells only (purple). Living but not active cells cannot be distinguished from dead ones (yellow). Simultaneous decrease in 4SU concentration and increase in labeling time (5 mM, 72 h) ameliorated the apparent toxic effect. Nevertheless, this 4SU concentration is still hundred-fold increased over the level above which adverse effects have been detected [54], potentially influencing the miRISC-regulated targetome.

UV CROSS-LINKING To induce the photo-activatable nucleoside enhanced cross-linking of RNA to interacting hAGO2, long-wave UV irradiation (365 nm) of sufficient intensity needs to reach the point of interaction. Adult CM accounting for most of the weight of a human myocardial slices are of cylindrical shape with a length of ~100 µm and a diameter of about 10 to 25 µm. Accordingly, a tissue slice of 300 µm comprises about 3 to 30 cell layers. To account for this increase, a doubling of the intensity used in the original protocol has been applied. The observed marginal difference between untreated and cross-linked slices (see Figure 10.2) appears, however, more likely to be the result of indistinctive PNK-mediated ^{32}P-γ-ATP labeling than being attributable to different amounts of co-precipitated RNA (see above).

RNASE TREATMENT Based on the results of the second PAR-CLIP study with primary rat cardiac cells where too mild RNase conditions may have caused inseparable protein/RNA complexes, it was returned to the conditions of the original protocol by performing two consecutive RNA digestion steps (before and after IP) using RNase T1 (1 and 100 U/µl, 22°C, 15 min).

AGO2 ANTIBODY AND IP CONDITIONS For native hAGO2 IP, different lysis buffers have been compared (see Figure 10.3). As the buffer used by the developers of the antibody [348] is of very similar content and showed a comparable IP efficiency to the one of the PAR-CLIP technique [151], it was decided to stay with the latter (PAR-CLIP Lysis Buffer). Human AGO2 has been shown to compete with a 16 amino acids peptide resembling its N-terminus for association with anti-hAGO2 [348]. One of the published competitive elution conditions (4 µg/µl peptide, 600 rpm, 25°C, 90 min [348]) has been confirmed as most effective (see Figure 10.4) and was thus chosen for the PAR-CLIP study with human slice cultures.

ESTIMATION OF INPUT MATERIAL A reasonable estimation of the amount of human tissue slices required to produce a sequenceable cDNA library and an evaluable data set was hindered by a couple of undetermined parameters such as the healthiness of an obtained specimen, the cells' remaining rate of metabolism and hence the ability to label nascent RNA with 4SU, UV penetrability of the slices and the like. For that reason, a preliminary PAR-CLIP experiment comparing a certain amount of slices with different inputs of HEK cells

was set up to obtain a better estimation of the amount of human myocardial tissue required for conducting a successful preparative study.

CLIP STUDY Within this project, only one such pilot experiment could be carried out. For that, two samples of a defined amount of slices (65 each) derived from two human hearts were compared to different input amounts of HEK cells used for either short-wave UV iCLIP or long-wave UV PAR-CLIP after previous 4SU labeling (see Table 11.1). More particularly, PAR-CLIP with the obtained total protein input of the two heart samples (6 and 18 mg) was compared to iCLIP and PAR-CLIP with HEK cell lysates of three different protein amounts (18, 36 and 72 mg). As the precipitate of all samples (eight in total) was eluted competitively, a control western blot was prepared (see Figure 10.5). For that, equal amounts of protein input (~2 mg) and beads (10 µl) were used per IP. Each sample was first eluted competitively using the same conditions as for the actual experiment. Subsequently, the beads were subjected to a second denaturing elution to test for the remaining protein fraction. The western blot appears to indicate an underestimation of the total protein input for the short-wave UV treated HEK cell IP (iCLIP). All the more interesting appears the corresponding PLS. Compared to the PAR-CLIP sample, which nicely shows the previously described doublet [70, 291] corresponding to hAGO2 complexed with either only miRNAs (lower band) or miRNAs and target RNA fragments (upper band), almost no RNA seems to have been cross-linked in the iCLIP sample. This appears to have been the case for both human heart samples, too. Even though detectable on a protein level (western blot), the peptide eluted fractions do not show any visible amount of complexed RNA (PLS). For cDNA library preparation, all eight samples were reverse transcribed individually using primers carrying a unique base quartet (barcode) and subsequently combined to a single sample. The success of 3'-linker (App-L3) ligation and Reverse Transcription (RT) as well as of the following cDNA size selection by gel purification, their circularization and subsequent linearization has not been controlled.
Electrophoresis of the test PCR showed no DNA band, even after 34 cycles of amplification. Since it appears likely, at least from the PAR-CLIP samples using HEK cells, that some RNA should have been obtainable, one or more of the numerous enzymatic reactions during library preparation might have failed. The only difference compared to the original protocol [219] consisted in the use of T4 RNA Ligase 2 truncated K227Q instead of T4 RNA Ligase 1 for the App-L3 ligation, which might work more specific but may also be less efficient. SuperScript® III Reverse Transcriptase, CircLigase™ II ssDNA Ligase, FastDigest BamHI and the AccuPrime SuperMix I as well as the oligos (CutOligo, P5/P3 Solexa) have all been stored for more than one year but not beyond their expiration dates. Possibly, pausing in-between RT and PCR amplification for over 24 h has not been ideal [291]. Detailed control experiments using additional input material would have been required to solve that issue. However, for conducting further PAR-CLIP studies with human myocardial slices, the first question which needs to be addressed might be how the RNA can be successfully labeled and cross-linked to miRISC complexes (see Section 14.2).

#	PROTOCOL	RBP	CELLS
1	PAR-CLIP	rAGO2	ARCM
2	PAR-CLIP	rAGO2	ARCF
3	PAR-CLIP	rAGO2	ARCM
4	PAR-CLIP	rAGO2	ARCF
5	iCLIP	hAGO2	HEK293
6	iCLIP	hAGO2	HEK293
7	iCLIP	hAGO2	HEK293
8	PAR-CLIP	hAGO2	HEK293
9	PAR-CLIP	hAGO2	HEK293
10	PAR-CLIP	hAGO2	HEK293
11	PAR-CLIP	hAGO2	human heart tissue
12	PAR-CLIP	hAGO2	human heart tissue

TABLE 11.1. Summary of CLIP studies conducted in the course of this PhD project. RNase T1 (T1), RNase I (I), protein G Dynabeads® (beads), total protein input (tot. prot.), denaturing NuPAGE Loading Buffer elution (#1-4, denat.), competitive peptide elution (16 amino acids hAGO2 peptide, #7-14, comp.).

#	4SU LABELING	UV [J/CM²]	RNASE [U/µL]	ANTIBODY	BEADS	INPUT	TOT. PROT.	ELUTION
1	0.1 mM, 16 h	365 nm: 0.15	T1: 1 + 100	anti-mAGO2 (2D4)	96 µl	20 × 10 cm (13 AR)	13 mg	denat.
2	0.1 mM, 16 h	365 nm: 0.15	T1: 1 + 100	anti-mAGO2 (2D4)	96 µl	39 × 15 cm (13 AR)	17 mg	denat.
3	0.1 mM, 16 h	365 nm: 0.15	T1: 1	anti-mAGO2 (2D4)	96 µl	98 × 10 cm (82 AR)	81 mg	denat.
4	0.1 mM, 16 h	365 nm: 0.15	T1: 1	anti-mAGO2 (2D4)	240 µl	174 × 15 cm (82 AR)	109 mg	denat.
5	no	365 nm: 0.3	T1: 1 + 100	anti-hAGO2 (11A9)	90 µl	20 × 15 cm HEK293	18 mg	comp.
6	no	365 nm: 0.3	T1: 1 + 100	anti-hAGO2 (11A9)	180 µl	40 × 15 cm HEK293	36 mg	comp.
7	no	365 nm: 0.3	T1: 1 + 100	anti-hAGO2 (11A9)	360 µl	80 × 15 cm HEK293	72 mg	comp.
8	0.1 mM, 16 h	365 nm: 0.3	T1: 1 + 100	anti-hAGO2 (11A9)	90 µl	20 × 15 cm HEK293	18 mg	comp.
9	0.1 mM, 16 h	365 nm: 0.3	T1: 1 + 100	anti-hAGO2 (11A9)	180 µl	40 × 15 cm HEK293	36 mg	comp.
10	0.1 mM, 16 h	365 nm: 0.3	T1: 1 + 100	anti-hAGO2 (11A9)	360 µl	80 × 15 cm HEK293	72 mg	comp.
11	5 mM, 72 h	365 nm: 0.3	T1: 1 + 100	anti-hAGO2 (11A9)	90 µl	65 slices	18 mg	comp.
12	5 mM, 72 h	365 nm: 0.3	T1: 1 + 100	anti-hAGO2 (11A9)	30 µl	65 slices	6 mg	comp.

(cont.)

12 DISTANCE ANALYSIS OF MIRNA BINDING SITES

A second computational part of the present project aimed at the theoretical analysis of miRISC cooperativity as a concept of miRNA-mediated target regulation.
Interactions between miRISCs and their targets are deemed to be highly combinatorial (see Section 2.6). One miRNA species may not only target many different mRNA transcripts, but also various types of miRNAs may potentially regulate a common mRNA target. In the latter case, three different scenarios are theoretically conceivable. First, the individual binding sites may lie very close to each other with even overlapping sites. Second, they could be far away or, third, they may be directly adjacent to each other. In the first case, when they are very close, different miRISCs may not be able to bind at once on a single mRNA. Also if the sites are very far away from each other, binding miRISCs may not be able to directly interact beneficially. For both cases, the consequence would be a rather independent (non-cooperative) mode of miRISC-mediated target regulation (see Figure 2.7A). Conversely, adjacent sites, as in the third case, may allow for a cooperative mode of miRISC binding (see Figure 2.7B).
Binding cooperativity means that the binding of one component will enhance the binding of another. The result will be that these two events cause a stronger effect than the sum of two individual and independent binding events (see Section 2.6). Even though experimental data concerning that issue for miRISC interaction are rare, all studies emphasize the importance of the distance between miRISC binding sites in order to cause cooperative regulation. Thereby, very often the reported inter-site distance required for miRISC cooperativity (measured, e. g., on the mRNA from the nucleotide opposite of the 5′-end of the first miRNA to the nucleotide across the 5′-end of the second miRNA) encircles the length of a miRNA (see Figure 2.7C and Table 2.1).
If binding cooperativity between miRISCs was indeed biologically relevant and maybe even required for effective target repression, one might expect a transcriptome-wide enrichment of miRNA binding sites in cooperativity-permitting adjacency. Thus, the first aim was to perform a global computational analysis of miRNA binding site positioning.

12.1 DISTRIBUTION OF PAIRWISE INTER-SITE DISTANCES

To comprehensively analyze pairwise distances between miRNA binding sites, a transcriptome-wide set of target sites was needed. For this, the prediction algorithm *TargetScan* (release 6.2) [246, 142, 127] was applied (see Section 7.4).
In a first approach, distances between multiple potential binding sites on a certain target 3′-UTR were measured for single miRNAs. The results for all human 3′-UTRs and all miRNAs considered were combined in a frequency distribution of pairwise distances. This could now be compared to random controls. Two

types of control models were set up. First, starting positions of control sites were picked randomly within the 3'-UTR data to obtain a set of completely shuffled binding sites. The obtained distance distribution was subtracted from the one of the predicted target sites leading to a difference in frequency of a certain inter-site distance plotted against this distance (see Figure 12.1A). Second, scrambled sequences reflecting the length of a miRNA but not matching to the sequence of any existing miRNA were used to predict control target sites and to compare the resulting pairwise inter-site distances distribution (see Figure 12.1B). Interestingly, the comparison to both control models showed an enrichment of the differential frequency of distances within the cooperativity-permitting range (15 to 26 nucleotides, see Section 7.4). In contrast, distances above the indicated zone (see Figure 12.1 brown area) seemed to occur with similar frequencies for real miRNA binding sites and the control groups.

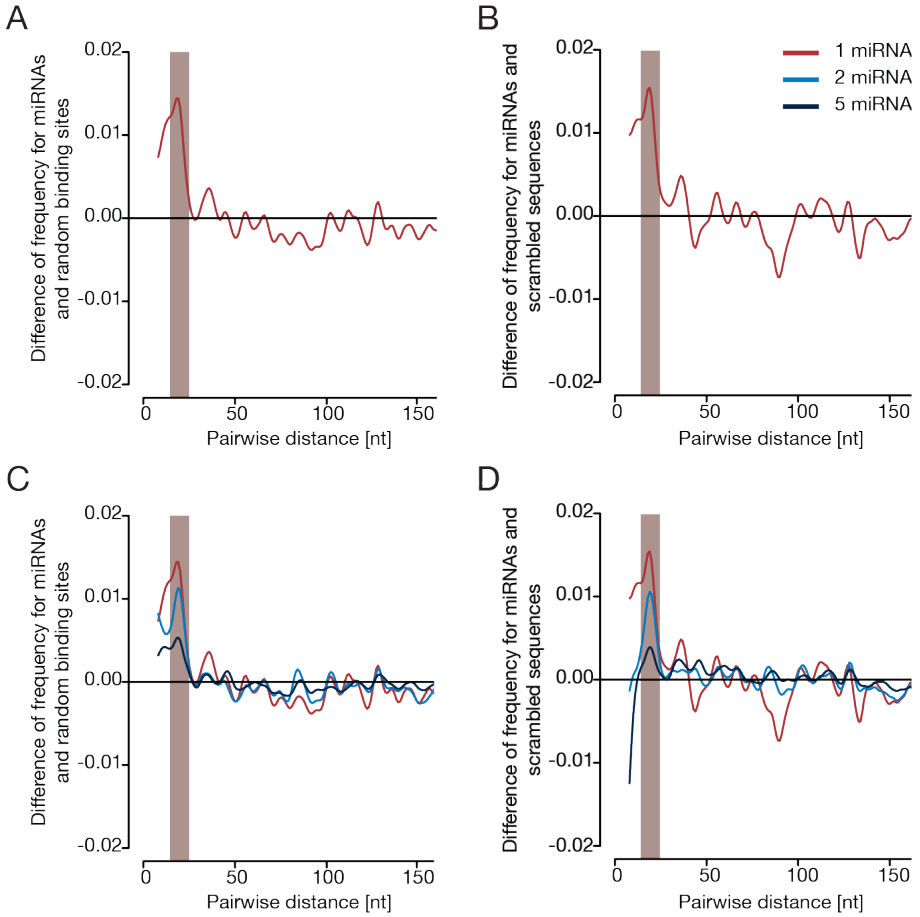

FIGURE 12.1. Difference in distributions of pairwise inter-site distances. A: comparison for one miRNA species and random binding sites. B: comparison for one miRNA species and binding sites of scrambled sequences. C: comparison for groups of miRNA species and random binding sites. D: comparison for groups of miRNA species and binding sites of scrambled sequences. The brown area reflects the nucleotide distance in which adjacent binding sites would be expected (15 to 26 nucleotides, see Section 7.4).

However, biological miRNA-mediated target regulation is rather complex. One target transcript is likely to be regulated by a group of different miRNA-loaded miRISCs. Thus, in a second approach not only one miRNA but groups of multiple miRNA species were used to determine inter-site distances. Groups of two or five miRNAs were sampled randomly (1,000 ×, without recurrence) and the pairwise distances were calculated for these ensembles. Again, the distance distributions were compared to those of the two control models analyzed accordingly. A similar enrichment within the cooperativity range was observed indicating that miRNA binding sites are more often located adjacently than expected by chance (see Figure 12.1C,D).

12.2 VALIDATION BY EXPERIMENTAL DATA

The distance data based on *TargetScan* prediction of miRNA binding sites was evaluated by both, binding sites determined by an alternative prediction algorithm (*miRanda/mirSVR*, release August 2010, [194, 33, 32]) and published experimentally identified target sets obtained by either HITS-CLIP or PAR-CLIP. Figure 12.2 summarizes the results. Importantly, this diagram depicts the proportion of cooperative targets (fraction of 3'-UTRs with miRNA binding sites in cooperativity-permitting distance) rather than a pairwise distance distribution. Again, results for individual miRNAs as well as groups of two or five miRNA species were compared. Out of statistical reasons, the fraction of cooperatively regulated targets expectedly increased for larger groups of miRNAs. But, interestingly, it increased relatively more for real miRNA binding sites determined by both of the predictions (TargetScan, miRanda) or based on the experimental data sets (HITS-CLIP, PAR-CLIP) when compared to the two control models (random sites, scrambled).

12.3 VALIDATION BY ANALYSIS OF FUNCTIONAL RELEVANCE

If miRISC cooperativity was indeed a common principle for effective target regulation, it could implicate that miRISC binding sites are enriched in cooperativity-permitting distance (see above). However, if appropriate, this may apply even more for miRNAs which are functionally related as, for example, when acting within the same cell or tissue or when being regulated in the same disease context.

To address the first point, binding site distances of miRNAs co-expressed within one tissue and miRNAs not expressed within that tissue (fetched from the *mimiRNA* database [343]) were analyzed to determine the corresponding fractions of cooperative targets. Interestingly, this proportion was indeed increased for targets regulated by groups of co-expressed miRNAs compared to targets of a control set of miRNAs not expressed within the respective tissue (see Figure 12.3).

The second issue was tested by similar analysis of miRNAs co-regulated (or not) in different diseases (retrieved from the *PhenomiR* database [349]). Again, related miRNAs showed an enrichment of target sites within cooperativity-permitting distance.

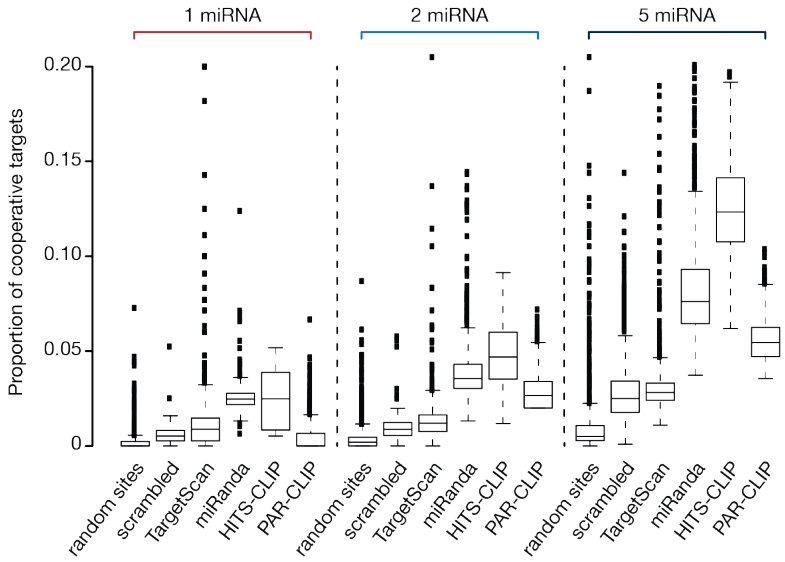

FIGURE 12.2. Validation of *in silico* results by experimental data. Comparison of the fraction of potentially cooperative targets per total targets. Analysis of the fraction of 3′-UTRs with miRNA binding sites in cooperativity-permitting distance of computationally predicted (TargetScan, miRanda), experimentally identified (HITS-CLIP, PAR-CLIP), and control target sites (random sites, scrambled). The proportion of cooperative targets is plotted for single miRNAs and sampled groups of two and five miRNAs. Except for the PAR-CLIP data of a single miRNA species, the mean is always higher for existing miRNAs than for either of the control models (p-value $< 2.2 \times 10^{-16}$, tested with a one-sided Wilcoxon rank-sum test).

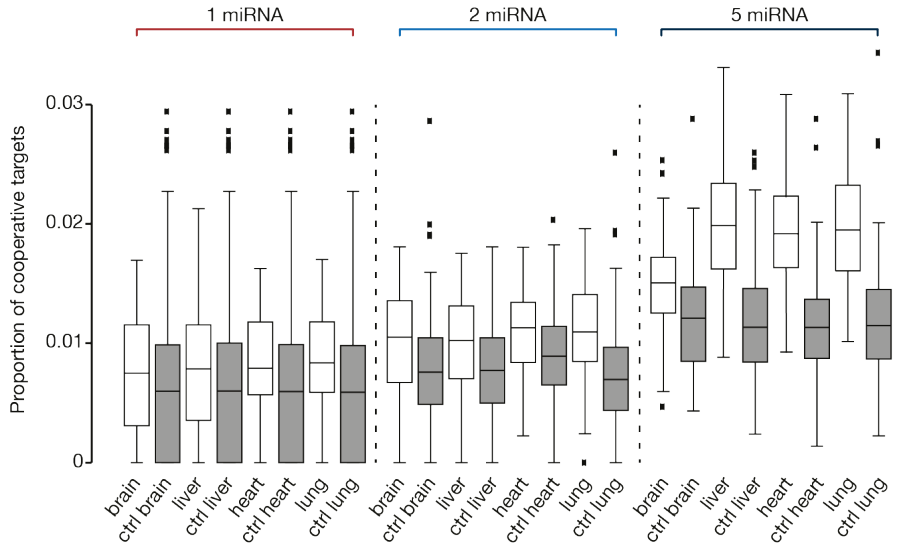

FIGURE 12.3. Validation by analysis of co-expressed miRNAs. Comparison of the fraction of potentially cooperative targets for miRNAs expressed in four exemplary tissues (white) compared with a control set of miRNAs not expressed within the respective tissue (gray). Targeting within the cooperativity-permitting distance is over-represented for co-expressed single miRNAs or groups of two or five miRNA species (p-value $< 2.2 \times 10^{-16}$, tested with a one-sided Wilcoxon rank-sum test).

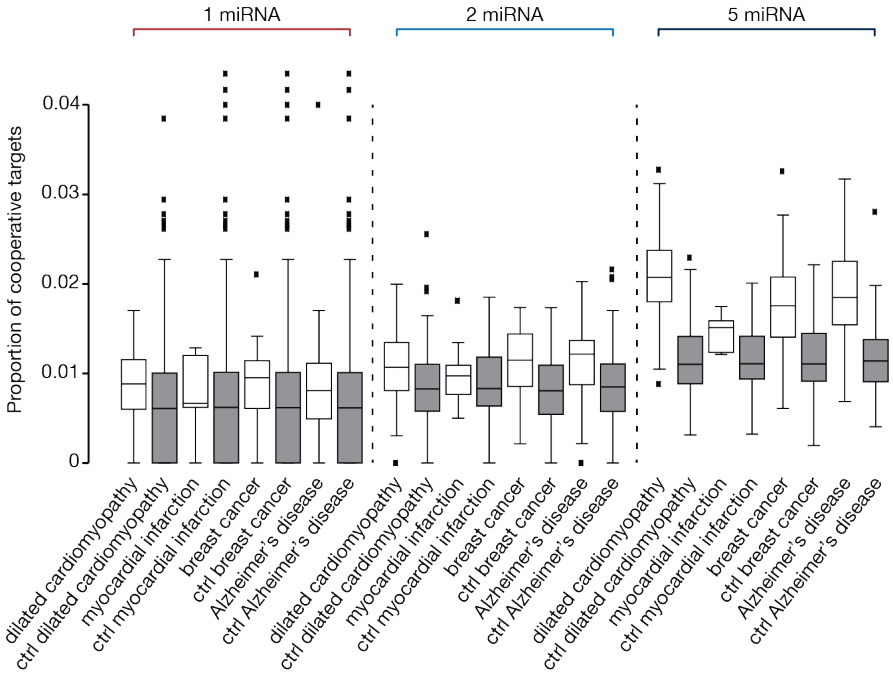

FIGURE 12.4. Validation by analysis of co-regulated miRNAs. Comparison of the fraction of potentially cooperative targets for miRNAs regulated in four exemplary disease contexts (white) compared with a control set of miRNAs not regulated within the respective disease (gray). Targeting within the cooperativity-permitting distance is over-represented for co-regulated single miRNAs or groups of two or five miRNA species (p-value $< 2.2 \times 10^{-16}$, tested with a one-sided Wilcoxon rank-sum test).

13 SUMMARY OF THE COMPUTATIONAL RESULTS

In what follows, the results of the computational part of this PhD project are briefly summarized.
To approach a major unresolved question in the miRNA field, namely whether miRISC cooperativity can be referred to as a common principle of miRNA-mediated target regulation, a comprehensive theoretical analysis based on inter-site distances was performed on published data.

13.1 DISTRIBUTION OF PAIRWISE INTER-SITE DISTANCES

If spatial proximity of binding sites would allow for cooperative binding of multiple miRISCs to a common transcript and thus synergistic repression of this target, inter-sites distances may be non-randomly distributed but globally enriched within such a cooperativity-permitting adjacency. As a starting point to answer the above question, this assumption was tested. Therefore, a transcriptome-wide analysis of the distribution of pairwise inter-site distances between miRNA target sites has been performed. Comparing the obtained distribution to those of two kinds of random control models revealed that target transcripts with more than one miRISC binding site (within their 3′-UTR) more often carry these sites in a cooperativity-permitting distance (15 to 26 nucleotides, see Section 7.4 and Table 2.1) than the controls. Interestingly, the differential distributions peak at a distance of ~21 nucleotides (about the length of one miRNA), reflecting binding of two miRISCs in direct adjacency. The same applied for considering two or five different miRNA species and their corresponding binding sites at a time, indicating that also under biologically more relevant conditions (combinatorial targeting) miRISC biding sites are more often located side by side than expected by chance. The enrichment was statistically tested by a Wilcoxon rank-sum test resulting in a p-value $< 2.2 \times 10^{-16}$, which is the smallest value that can be displayed using *R* [331].

13.2 VALIDATION BY EXPERIMENTAL DATA

However, global enrichment of adjacent binding sites would in principal be neither necessary nor sufficient to confirm the concept of miRISC cooperativity for effective target regulation. Moreover, the first analysis was solely based on potentially erroneous prediction data. Therefore, the *TargetScan*-based distance analysis was extended by also considering data obtained on the basis of an alternative *in silico* approach (*miRanda/mirSVR*) as well as high-confidence target data derived from CLIP experiments. With that, it was tested for a second criterion, the proportion of targets featuring at least two binding sites within close distance. The significant enrichment of the fraction of 3′-UTRs with miRISC

binding sites in cooperativity-permitting proximity compared to the randomized control setups (Wilcoxon rank-sum test, p-value $< 2.2 \times 10^{-16}$) adds evidence to the concept of miRISC cooperativity for effective target regulation. Interestingly, the measured proportion of cooperative targets can reach values of over 20% (see Figure 12.2 outliers). As anticipated, this value increased for considering more than one miRNA species. However, based on comparison to the control groups, it increased more than statistically expected.

13.3 VALIDATION BY ANALYSIS OF FUNCTIONAL RELEVANCE

A nearby strategy to validate the findings was based on the assumption that if miRISC cooperativity was biologically relevant, functionally related miRNAs should tend to regulate relatively more targets with binding sites in cooperativity-permitting neighborhood. Both, miRNAs co-expressed within the same tissue (*mimiRNA*) and miRNAs co-regulated in the same disease pathway (*PhenomiR*) showed a relative enrichment of miRISC binding cooperativity-allowing targets (Wilcoxon rank-sum test, p-value $< 2.2 \times 10^{-16}$) pointing towards a functional relevance of a concerted or even cooperative way of miRNA-mediated target regulation.

IV

DISCUSSION

14 DISCUSSION OF THE EXPERIMENTAL FINDINGS

In the following, the results of the experimental part of this PhD project as well as theoretical implications and practical applications are discussed.

14.1 SCIENTIFIC CONTRIBUTION OF THE CLIP STUDIES

In summary, the volume of information gathered for the field of AGO CLIP research by this PhD project leaves room for a multitude of questions which remain to be answered.
So far, the vast majority of CLIP studies were carried out using cell lines as input material. Since the function of RBPs, as the miRISC, is expected to be highly context-dependent, such studies allow for mechanistic but rather limited functional insight. Thus, this project first contributes by an adaption of the cell culture-optimized PAR-CLIP protocol to biologically more relevant primary cardiac cells and the precipitation of native rAGO2. This allows for the isolated consideration of the CM- or CF-specific miRISC targetome under physiological AGO2 levels. Admittedly, culturing of primary cardiac cells to perform 4SU labeling might bias the results and high amounts of input material are difficult to obtain.
Second, for cDNA library preparation, the protocol was switched from PAR-CLIP to iCLIP. According to the latter protocol, barcode-based RT primer avoid amplification artifacts. Further, one of the inefficient inter-molecular sequencing adaptor ligation steps is replaced with a more efficient intra-molecular circularization reaction. Even though it cannot make use of the PAR-CLIP characteristic cross-link indicatory T-to-C mutations introduced by reverse transcriptase, the iCLIP library preparation protocol allows for capturing the much more frequent events [384] at which reverse transcriptase drops off at the cross-linked base of the template strand. Such truncated cDNAs would be lost during the PAR-CLIP library preparation but can be used herewith to position the cross-link at nucleotide resolution (compare Section 4.5 iCLIP).
Third, the project demonstrated that cultivatable human tissue slices are in principle accessible for PAR-CLIP studies. Use of human material certainly increases the relevance of the results of future PAR-CLIP experiments. However, as for primary cells, culturing and 4SU labeling-induced alterations have to be considered. Further, it might not be trivial to draw conclusions on the native targetome from samples of patients suffering from different and often blinded kinds of heart disease.

14.2 OPTIMIZATION POTENTIAL AND FUTURE PERSPECTIVES

To meet a publishable standard, further experiments will be required.

INPUT MATERIAL With respect to the input material, a cell type-specific miRISC targetome based on the isolated examination of CM, CF and maybe also Endothelial Cells (EC) seems desirable. However, most rewarding appears the further development of the cultivation, labeling and cross-linking of human myocardial tissue slices.

4SU LABELING In case of PAR-CLIP, Uracil PhosphoRibosylTransferase (UPRT)-mediated cell type-specific labeling may represent an interesting development prospect. Introduction of this special uracil/uridine converting enzyme form *Toxoplasma gondii* into metazoan cells of interest (which naturally do not express this enzyme) enables the cells to couple the modified nucleobase 4-thio-uracil to ribose-5-phosphate and thus to incorporate it into nascent RNA [74]. The expression of UPRT from a neuronal-specific promoter in *Drosophila melanogaster* fed with 4-thio-uracil, in combination with thio-biotin coupling, has been used to isolate cell type-specific RNA [283]. In theory, a similar approach could be used to introduce cell type-specific cross-links in complex tissues [14] such as the heart.
Another potential extension would be pulsed 4SU labeling to disclose the temporal order of different RNA processing steps and to study the dynamic changes of miRISC targetomes.
Moreover, one may further purify the miRISC immunoprecipitates by isolating only biotinylated RNA upon thio-biotin coupling with streptavidin-conjugated magnetic beads [92, 332, 361].
However, 4SU-mediated side effects should be controlled for. For example, treatment of a human uveal melanoma cell line with 4-thio-uridine monophosphate concentrations of only 6 µM and 150 µM over a period of 24 h resulted in approximately 20 and 45% cell loss, respectively [206]. Furthermore, it has been shown that 4SU concentrations of only 50 µM (half the amount used in the original PAR-CLIP protocol [151]) can interfere with 47 S rRNA biosynthesis, induce nucleoplasmic translocation of nucleolar nucleophosmin and activate tumor suppressor p53, all indicating a nucleolar stress response. To avoid biased results of 4SU labeling experiments, the authors recommend that metabolic integrity regarding, e. g., functional ribosome biogenesis and intact cell cycle should be monitored [54].

UV CROSS-LINKING In order to provide clarity with respect to the UV cross-linking efficiency and to elucidate the origin of all bands within a certain PLS, one of the published protocols may be followed exactly using the very same cells, antibodies and remaining conditions. Further, an RNA labeling assay adding everything except PNK could help to understand the unexpected ^{32}P-γ-ATP labeling results and may reveal unspecific phosphorylation of direct AGO phosphorylation sites. Moreover, to reach a real *in situ* cross-link, it might be preferable to first shock-freeze a tissue of interest in liquid nitrogen, slice or grind it, and keep it frozen during UV irradiation [291]. As for the labeling, it should be controlled for adverse side effects such as UV-damaged RNA or intra-molecular RNA cross-linking.

RNASE TREATMENT Since the type of RNase mediating partial RNA digestion may bias a specific RBP's footprint, cleavage by alkaline hydrolysis could be worth to consider [291].

AGO2 ANTIBODY AND IP CONDITIONS AGO IP represents one of the most critical steps when aiming to obtain sufficient amounts of co-isolated (cross-linked) RNA. Hence, more efficient precipitation of AGO2 by an antibody of higher affinity would certainly be desirable. Albeit monoclonal antibodies offer consistent performance, also polyclonal alternatives possessing higher avidity and thus allowing for more efficient precipitation and more stringent purification should be considered. To minimize potential background, the amount of antibody used should be titrated just below fully depleting the RBP of interest from the supernatant. Ideally, technical replicates with two or more different AGO antibodies would be prepared to point out misleading unspecific signals. Access to negative (such as AGO2 knock-out cells) and positive (for example purified AGO2) controls for comparison could also prove useful in the identification of unassigned bands [291].
Besides, IP efficiency might benefit from conducting the partial RNA digestion step prior to centrifugation of the input cell lysates [221] to avoid loss due to sedimentation of too large complexes.
Replacing the gel or membrane purification step after the IP with a competitive AGO elution buys a higher yield, but at the expense of two disadvantages. First, it does not allow for a pre-selection of the length of cross-linked RNA fragments within the optimal size range (25 to 30 nucleotides without the linker sequences, compare Section 4.5 Considerations). Second, it increases the fraction of always co-precipitated non-cross-linked RNAs potentially compromising the results. In case of seeking optimal specificity, it may thus be reassessed. However, the more efficient miRISCs can be isolated, the less input material will be required.

LIBRARY PREPARATION The second critical step, and maybe even most important in the whole protocol, appears to be ligation of the linker sequences to the CLIP-obtained RNA fragments during cDNA library preparation. Not only that it can be a source of severe bias [153, 448], it is also highly ineffective (see Section 15.2). In a long term perspective, ligation-independent cloning could provide a remedy against this issue [291].
Another major disadvantage of cDNA library preparation is the large number of sequential reactions which are conducted without the possibility to directly control success of individual experiments. Although additional amount of input material may have to be accepted, it seems advisable to verify intermediate stages of the protocol. For instance, the amount of isolated RNA (RNA extraction), successful ligation of the 3'-linkers (using a spiked-in primer template for PCR verification), RT (complementary PCR primers) etc. could be analyzed. To assess the amount of unspecifically isolated background RNA carried through a library preparation of a CLIP study, AGO CLIP may be compared to the results of another RBP CLIP experiment with an unrelated but similarly abundant RBP [14].

Beyond that, CLIP studies with simultaneous candidate miRNA over-expression or inhibition [258] could be interesting. However, potentially detrimental perturbation of the endogenous stoichiometry should be considered [208].
Alternative experimental miRNA target identification strategies, such as the analysis of miRNA/mRNA chimeras (CLASH [162]) are discussed below (see Section 15.4).

15 DISCUSSION OF THE EXPERIMENTAL APPROACH

In this chapter, the experimental approach of profiling of miRISC-associated targets upon covalent cross-linking is discussed. Advantages and disadvantages are pointed out and different CLIP approaches are compared. Finally, experimental validation strategies and alternative methods to identify the miRISC targetome are briefly addressed.

15.1 ASSETS OF THE CLIP APPROACH

CLIP methods combine UV cross-linking of RBPs to respective target RNA with rigorous purification as well as partial digestion schemes and subsequent high-throughput sequencing of derived cDNA libraries.
Thereby, cross-linking allows for a high specificity of the detected targetome. Not only that a snapshot of *in vivo* contacts can be preserved throughout a denaturing purification protocol, it also introduces sequence mutations permitting to separate true signal from non-cross-linked noise.
Partial RNA digest leaves an RBP footprint on the full-length target transcripts and thus allows for a precise localization of the binding sites upon alignment of the sequenced fragments to the reference sequence data. Besides, the above mentioned cross-link indicatory mutations enable to pinpoint RBP binding sites with nucleotide resolution.
CLIP technologies allow for comprehensive transcriptome-wide studies of the targetome of individual RBPs or large complexes such as the miRISC. This feature is particularly advantageous for miRNA research. First, cross-linking increases the dynamic range of the profiling of associated transcripts by also detecting more transiently bound targets or such of lower affinity. As miRISC binding specificity is highly complex and even rather transient interaction could be biologically relevant, *in situ* cross-linking enables to capture otherwise undetected contacts. Second, CLIP methods have the potential to detect thousands of target sites in a single experiment. As it is often not sufficient to determine whether a miRNA interacts with a particular mRNA, but important to define the full landscape of interactions, transcriptome-wide assays are highly favorable. Only by revealing the combined effect of multiple miRISCs on several common and different mRNA targets, miRNA-mediated regulation can be fully understood and possibly be positively influenced.

15.2 WEAKNESSES OF THE CLIP PROTOCOLS

The benefit of a genome-wide identification of high-confidence RBP target sites provided by the CLIP approach has to be weighed against some drawbacks (compare Section 4.5 Considerations):

CLIP studies constitute laborious protocols with numerous steps at which precious input material may get lost. In case of PAR-CLIP experiments, sufficient RNA labeling with photo-activatable nucleosides is required. However, the incorporation rate of modified nucleosides is rather low (~4% 4SU relative to U under optimal conditions [151, 14]) and factors such as slow cellular metabolism or *in vivo* administration may additionally compromise labeling efficiency. Moreover, RNA labeling with modified photo-activatable ribonucleosides may provoke cellular stress potentially influencing post-transcriptional gene regulation [54] and thereby the identified targetome. Due to its nucleotide specificity, sequences rich in the respective component may preferentially be cross-linked and thus be over-represented in the corresponding sequencing library.
Generally, in terms of cross-linking, it cannot be excluded that a particular sequence and thus the spatial arrangement of nucleotides as compared to closeby and cross-linkable amino acids, for example within the miRISC, biases the cross-linking efficiency and thereby the final targetome. Further, excess UV irradiation may heat the cells or tissue and potentially cause misleading RNA mutations. Furthermore, UV-mediated cross-linking is rather incomplete. For irradiation with short-wave UV (254 nm), the efficiency of establishing a covalent linkage between nucleic acids and a binding protein has been shown to lie between only 2 and 7% [122].
Efficiency of the subsequent IP depends on the availability of a high affinity antibody with resistant binding throughout sequential re-buffering, on-bead reactions, and multiple washing steps. In case of SDS-PAGE or subsequent western blotting, RNA recovery from the gel or nitrocellulose membrane reflects a serious source of loss.
However, most material may get lost during cDNA library preparation. First, only ~50% of RNA fragments are ligated to a linker oligo at each ligation reaction [291]. Hence, in case of conventional 3'- and 5'-linker ligation, about 75% of input RNA will not carry both linker sequences, though they are required for Reverse Transcription (RT) and PCR amplification. Second, in more than 80% in which reverse transcriptase has to transcribe a cross-linked nucleotide, the enzyme probably fails, drops off, and leaves a truncated cDNA which will as well not be amplified and thus not be sequenced [384].
Regarding data evaluation, it needs to be considered that even the cross-link indicatory increased frequency of reverse transcriptase errors at the cross-linked nucleotide position (provided that, e. g., 4SU has been incorporated and successful cross-linking to a nearby amino acid took place) is not completely reliable. HITS-CLIP-mediated CIMS only arise in 7 to 22% (depending on the individual RBP) [291]. PAR-CLIP-induced T-to-C mutations could be detected in 50 to 70% of sequence reads corresponding to a cross-linked RBP binding site [151, 14]. Additionally, it should be noted that non-experimental sequence mutations can be encountered which cannot easily be distinguished from cross-link indicatory transitions. Potential sources of mis-interpretation may be sequencing errors intrinsic to currently available high-throughput sequencing platforms [441], contamination with non-cross-linked but ubiquitary external RNA (for instance from recombinantly produced enzymes) with by chance high similarity to any sub-sequence of the reference data or pre-existing genetic variations such as SNPs [368]. Also mutations introduced by UV damage of the RNA can

lead to false-positive hits during data evaluation. Certainly, existing evaluation strategies account for part of the problems for instance by removing all reads which can be aligned to external genomic sequences and exhaustive alignment of short reads to selected genomes before the analysis [209], only considering binding sites occurring in sense orientation of annotated regions [239] or employing other computational models [368].
In summary, however, to reach statistical significance the amount of starting material required per each CLIP study is rather high. This is probably one of the reasons why to date the vast majority of CLIP studies was carried out in easily accessible cell lines. However, using this approach the insights into the circumstances that prevail *in vivo* or in specific disease contexts may be finite. Since the protocols are additionally expensive in research time and money, it might be seducing to cut down on the number of certainly required replicates. However, they are of particular importance as plenty of enzymatic reactions increase the risk of unpredictable bias, with RNase-mediated digest [217] and linker ligation [153, 448] being the most prominent candidates. Even IP may influence the final outcome given the substantial background that may be introduced with certain antibodies [291]. Over-amplification of the cDNA library prior to sequencing is another potential source of bias. It invariably favors the predominance of certain sequences and thus leads to a reduced sample complexity [291]. Besides, in contrast to protein/DNA interactions, RNA targets feature a much higher dynamic range regarding their abundance. Hence, the peak hight of clustered reads is not only a function of the RBP's affinity to the respective site but also dependent on the expression level of the target transcripts. Together with the mentioned bias due to variable 4SU labeling and UV cross-linking efficiency as well as due to potentially different nuclease stability of the RNA fragments, even in case of high amounts of starting material, the complexity of current cDNA libraries does not allow for a quantification of RBP interaction at individual RNA binding sites. However, to quantify and thereby weigh certain interactions would be highly desirable.
Finally, all CLIP studies of miRISC-associated RNAs still have the limitation that they identify target mRNA regions which are usually not specific for a particular miRNA and thus do not allow for the determination of direct miRNA/mRNA interaction partners. They narrow down the search space for miRNA target sites, but they do not entirely avoid their prediction. Hence, target identification faces the same obstacles as computational predictors (compare Section 4.2 and 4.5 Considerations).

15.3 PAR-CLIP VS. OTHER CLIPS

Despite the high similarity between short-wave UV CLIP (such as HITS-CLIP or iCLIP) and long-wave UV (PAR-) CLIP technologies, both approaches provide certain advantages and disadvantages. Previous incorporation of photoactivatable ribonucleosides such as 4SU into nascent RNA (PAR-CLIP) increases, to a certain extent, UV cross-linking efficiency and may thus allow for a more comprehensive target identification. Upon cross-linking, the modified nucleotides are also differently reverse transcribed. Thus, introduced specific

base transitions indicate regions within or close to RBP binding sites. This not only allows for the determination of the binding site at a high resolution, but also makes it possible to perform a qualitative ranking of identified binding sites. Cross-linked target signal can directly be separated from the background noise of unspecifically co-isolated RNA.
However, only newly synthesized RNA can be labeled with photo-reactive nucleosides and thus only metabolically active cells are available for this approach. Further, it seems difficult to preform the labeling with larger organisms (such as mice) *in vivo* or with archived clinical specimens. Moreover, the incorporated thiolated nucleotides may influence gene expression and cellular metabolism with potential bias on the identified binding sites [54].
Besides, cDNA library preparation according to the original PAR-CLIP protocol is dependent on two inefficient RNA linker ligations and loses all information on reverse transcriptase drop off events at the cross-link position. Here, the iCLIP library preparation protocol, which replaces one of the ligations with a more efficient intra-molecular circularization reaction to capture prematurely truncated cDNAs may be favorably.

15.4 EXPERIMENTAL VALIDATION

Importantly, also the miRISC target data generated by CLIP studies is not free of errors and has to be validated. Next to replicate experiments, determined interactions should be verified by complementary methods. Certainly, successfully implemented approaches for the confirmation of miRNA/mRNA interactions reaching from individual and sensitive reporter assays to large-scale multiplex formats have own assumptions, strengths and weaknesses (compare Section 4.6).
A recently developed and highly convincing approach to comprehensively detect the cellular miRISC targetome with high-confidence represents CLASH [228, 162] (compare Section 4.6 CLASH). During a CLASH study, the two strands of partially base-paired miRNA/mRNA duplexes (associated to a miRISC) are ligated together (end to end) and are then recovered as chimeric cDNAs. Thereby, an inter-molecular linkage is established allowing for the direct matching of miRNA/mRNA interaction partners. However, chimeric reads of ligated miRNA/mRNA hybrids have only been observed in 1% of all precipitated ternary AGO/miRNA/mRNA complexes. Similarly to HITS-CLIP or iCLIP, the original CLASH protocol is further based on short-wave UV cross-linking (including the mentioned low efficiency and potential bias) and, as for PAR-CLIP, library preparation includes two adapter ligation steps. This indicates that the amount of input material needed to obtain a high coverage cDNA library and sequencing data which detects miRNA/mRNA chimeras with sufficient statistical significance might be quite high. Consequently, the application of this method to analyze the targetome of primary cells or to perform quantitative studies might remain difficult. A combination with single molecule RNA sequencing techniques [356] may provide a remedy [220].

15.5 COMPUTATIONAL VALIDATION

Besides, to understand the complete picture of cell type-specific post-transcriptional gene regulation, the development of advanced computational methods, e. g., modeling of the concerted binding of multiple RBPs in the whole network of regulated target transcripts, may be required [220].

Taken together, the experimental approach of applying CLIP techniques to comprehensively identify miRNA targets in the cardiac system has been promising but proved to be challenging. Future studies may benefit from the rapid progress in this field of research.

16 DISCUSSION OF THE COMPUTATIONAL ANALYSIS

In what follows, the results of the computational part of this PhD project are discussed and future applications suggested.

16.1 INTERPRETATION OF THE RESULTS

The second part of this project theoretically addressed the question whether miRISC binding cooperativity based on adjacent miRNA target sites can be referred to as a common principle of miRNA-mediated target regulation. In case of a positive answer, the presence of binding sites in cooperativity-permitting distance could provide a valuable criterion to predict the biologically most relevant target candidates. Assessment of miRISC/target interactions based on their cellular relevance is of high importance to shed light on the complex thicket of miRNA-dependent cellular networks.
A transcriptome-wide computational analysis of miRISC binding site positioning revealed that adjacent binding sites are indeed enriched in mRNA 3′-UTRs compared to randomized controls when conducted on published data of predicted as well as experimentally identified target sites. Further, functionally related miRNAs in terms of co-expression within a specific tissue or co-regulation in the same disease context appeared to regulate a higher number of targets via adjacent interaction sites potentially giving rise to miRISC binding cooperativity. Therefore, targets possessing binding sites in cooperativity-permitting distance may indeed be indicatory of enhanced regulation and would thus classify as potentially being more crucial within the regulation of cellular processes.

16.2 LIMITATIONS

Biological relevance, however, is something which can only be satisfactorily elucidated experimentally. The impact of the combined activity of multiple miRNAs rather than of only a single candidate needs to be analyzed in its cellular context as it may as well be an individual rather than global phenomenon.

16.3 FUTURE APPLICATIONS

To start further research in this area, one could make use of the web application *miRco* [341], a tool to predict potentially cooperative miRNA interactions and their mRNA targets based on binding site distances. For a given set of mRNAs and miRNAs, *miRco* detects groups of miRNA binding sites that fulfill the user set cooperativity-permitting distance criterion. For example, a recent study at the Engelhardt Lab analyzed most abundant pro-hypertrophic miRNAs in CM [189] using *miRco* for revealing pairwise miRNA combinations potentially

regulating their targets cooperatively. Experimental reporter assays are now in progress to detect the impact of simultaneous AAV-mediated over-expression of interesting miRNA combinations on the hypertrophic growth of neonatal rat CM.

16.4 OUTLOOK

Despite new insights, the concept of miRISC cooperativity in miRNA-mediated target regulation is still in its infancy. The exact mechanisms and their dependencies on, e. g., different AGO subtypes, other potential effector proteins or the sequence context around the miRISC binding sites remain to be disclosed. Not only that potentially also other RBPs could contribute to a cooperative binding model, also other parameters such as local secondary structures of the target RNAs etc. might have to be considered.
Understanding the complex interplay of miRNAs in genetic networks will be of high interest for therapeutic as well as experimental applications involving miRNAs. For instance, adverse side effects may be reduced by administration of miRNA mixtures of lower individual dosage. Further, combinations of miRNAs may also improve biochemical protocols. For example, the concerted activity of multiple miRNAs has been applied to facilitate the reprogramming of CF into CM-like cells [187].

Taken together, this theoretical part added evidence to positively answer the afore raised question. Binding cooperativity of miRISCs could be a wide-spread phenomenon that may play an important role in miRNA-mediated regulation of gene expression. Thus, inter-site distance might prove as a predictor to identify most relevant targets as well as most effective miRNA combinations to revise the screws of certain systems of interest.

17 FINAL CONSIDERATIONS

Between transcription and translation, eukaryotic gene expression is extensively controlled by interaction of the transcripts with various RBPs. Post-transcriptional gene regulation comprises a wide range of different events such as alternative splicing, poly-adenylation, editing, nuclear export, sequestration, stability modulation, and ultimately translation. Thereby, a plurality of regulatory levels can control the steps and rates of the progress. Hence, next to the determination of transcription factor cascades, more and more importance is ascribed to the elucidation of the complex and powerful post-transcriptional gene regulation networks.

Of particular interest in that context are the mechanisms and functions mediated by miRNAs. Repressive miRISCs establish a supplementary regulation system buffering against variation and imparting robustness to gene regulation. This provides them with a key role as regulators of gene expression at sites distant from the transcriptional activities within the nucleus. Recent years have witnessed a dramatic development of miRNA research and it still displays an emerging field of study. Ultimately, this can be attributed back to the fact that miRNAs interact on targets with a minimal degree of base pairing allowing them to potentially control numerous transcripts within the same or different metabolic pathways and thus coordinate whole cellular responses. Therefore, they represent a class of molecules with a high potential for use as diagnostic tools and therapeutic targets in modern molecular therapy of human diseases [266, 375, 431]. However, the mechanistic features of miRNA-guided target regulation also pose a significant challenge for elucidating biologically relevant miRISC/mRNA interactions by bioinformatic prediction. Hence, in order to identify individual target genes as well as whole signaling pathways regulated as the basis for developing new diagnostic and therapeutic strategies, complementary wet lab techniques are eagerly awaited.

The advent of deep-sequencing technologies and their combination with RBP-specific top-down CLIP methods has paved the way for comprehensively mapping interaction sites of RBPs and large regulatory complexes such as the miRISC on their RNA targets. These methods have the potential to transcriptome-wide identify hundreds of thousands of binding sites of a particular RBP in a single experiment. This is of particular importance as individual miRNA-mediated effects on target gene expression are often low. The combined impact of small alterations in the expression of multiple targets rather than a strong change in a single target gene may be responsible for the phenotypic outcome of miRNA-mediated regulation. Thereby the entire system is highly complex. For example, over 2,500 mature human miRNA sequences have been identified so far and each miRNA may regulate hundreds of target genes.

Nevertheless, identification of the whole network of interacting RNA species

and RBPs is not trivial. All currently available experimental target identification methods are subject to a certain degree of bias. In principle, CLIP techniques only narrow down the sequence space of potential miRNA sites to *bona fide* AGO footprints for target site predictions. Thus, when arriving at this point, they suffer from the same problem which is that all predictions are based on insufficient prior knowledge regarding the exact interaction rules.

An intertwined and iterative collaboration between bioinformatic predictions and experimental methods seems inevitable to reach better predictions and gain a better understanding of the mechanisms governing miRNA-mediated target regulation [271]. Advanced experimental approaches for identifying unconventional miRNA/mRNA pairing rules (such as CLASH [162]) will be needed. Further, to assure that found interactions reflect those that occur cell type-specifically *in vivo*, such system-wide experiments need to be performed with primary cells and tissues. Besides, currently obtained complexity of cDNA libraries derived from CLIP experiments may not be sufficient to draw quantitative conclusions. However, such information would be highly desirable especially against the background of spatiotemporal dynamic expression of miRNAs. Single molecule RNA sequencing for real-time monitoring of cross-linked positions has been proposed [220]. The combination with additional transcriptome-wide data revealing target abundance, stability, or secondary structure might further allow for the evaluation of the physiologically most relevant contacts. A recent study combining PAR-CLIP data with mamma carcinoma patients' expression data allowed for an advanced prediction of regulatory miRNAs and revealed potential therapeutic targets and prognostic markers of breast cancer [119].

With regard to the target sites, it should also be considered that, for example, about one half of the human transcripts undergo alternative cleavage and poly-adenylation generating multiple distinct transcripts with different 3′-UTRs [396]. Apparently, the 3′-UTR sequences of housekeeping genes are substantially shortened, possibly to avoid complementarity to the plethora of regulatory miRISCs within the cell [380].

However, miRISC binding events also seem to frequently occur at transcript sites other than the 3′-UTRs. CLIP studies revealed thousands of miRNA binding sites within the 5′-UTRs, exons, and even introns. It seems tantalizing to investigate the functional relevance of these sites and to find out whether, for instance, miRISC binding within alternatively spliced exons confers isoform-specific silencing and whether SNPs residing within miRISC binding sites and thus potentially modulating miRNA-mediated regulation may have disease-associated consequences [43]. For intronic sites it will be interesting whether and with which effect AGO proteins interact with primary transcripts in the nucleus.

With respect to AGO proteins as the major component of the miRISCs, even though being under intensive research for over one decade, there are still considerable gaps in understanding their function on a molecular level. Further structural elucidation of the AGO-containing miRISCs will be necessary to draw a more precise picture of essential processes such as how these complexes find their target sites, how they can be removed when repression is relieved [275] and how they might be able to undergo binding cooperativity at adjacent

target sites.
Moreover, to gain global insight into cell-specific post-transcriptional gene regulation, it will be required to evaluate the complete picture of the position and distribution of all RBP binding sites throughout the whole transcriptome. Recently, several studies highlighted the interaction of miRISCs with other RNA binding proteins [186, 190, 379]. Data integration of large-scale bottom-up strategies such as cross-linked RNA bait studies [20, 62] as well as advanced computational modeling of the competitive and combinatorial RNA binding of the complete set of regulatory RBPs [220] may take us closer to the goal of obtaining an exact picture of the highly complex post-transcriptional regulatory circuits.
Finally, also the concept of binding cooperativity will have to be extended to all RBPs and even feedback loops involving miRNA-regulating transcription factors may need to be considered in order to understand and predict powerful switches in eukaryotic regulation of translation.

All this will be required as the basis for subsequent studies aimed at the development of innovative miRNA-dependent diagnostic and therapeutic strategies.

V

APPENDIX

ACKNOWLEDGMENTS

This journey was filled with the exceptional guidance and generous companionship of many to whom I owe a heavy debt of gratitude.
I would like to take the opportunity to acknowledge the contribution of canny captains, well-organized bosuns, able seamen (and -women), skillful surgeons as well as warm-hearted carpenters, talented musicians, hearty cooks, and not to be forgotten of all the 'powder rodents'.
My first and special thanks certainly go to Stefan Engelhardt for welcoming me as a member of his research crew and sending me on this adventure in his lab. Daring during any engagement and with the type of personality required to steer the course while keeping an eye on all shipboard activity, I look upon him with respect as not only my doctoral but also fatherly adviser. Thank you very much.
Next, I am immensely grateful to Fabian Theis for cordially receiving me as an exotic biochemist in his computational research team. My admiration applies not only to his intellectual guidance and the excellent bioinformatic infrastructure, but especially to the companionable environment created by him and his group members. Beyond, plenty of extracurricular retreat activities such as alpine jogging and freestyle skiing on cross-country ski will remain unforgotten. Thank you for all!
I have further received great support from Bernhard Laggerbauer enthusiastically tutoring this project although he always had a busy schedule. Throughout my PhD work he constantly sought to keep me on an even keel, suggested important control experiments, strove to detect gaps in my arguments and let me benefit from numerous discussions. Thanks a lot.
Very particular thanks are owed to Martin Preusse who not only shares first authorship on our publication [341] for which he carried out extensive computational analyses, but also his flat, his ideas, his books, his music, and his life with me. I thank you with all my heart for your unending encouragement and for providing unconditional shelter each time the wind is knocked out of my sails. Thumbs up!
Regarding the manuscript, I would also like to thank Heiko Lickert, Nikola Müller, Carsten Marr and Dominik Lutter for helpful discussions and careful proofreading.
Furthermore, it has been a privilege to work in the lab of Thomas Tuschl who kindly invited me to spend a very encouraging and just amazing time in New York City. I am very much indebted to his staff members, in particular Kemal Akat, for introducing me to the secrets of the PAR-CLIP protocol, generously sharing insights and ideas, performing time consuming experiments as collaborators, and taking keen interest on making my stay an outstanding experience.
Another occasion leaving unforgettable impressions has certainly been the EMBO practical course on small non-coding RNA in Heidelberg, extraordinarily led by Vladimir Benes. Here, I happened to meet Oliver Meikar to whom I would also like to convey my sincere gratitude, not only for explaining me how

one gets splinted ligation to work, but also for providing new perspectives on the way of life in general. He always reminds me how important it is to ask 'why?'.

Coming to the actual crew, I am grateful to all of you, past and present fellows, for generating such a pleasant working atmosphere and wonderful camaraderie extending beyond the lab.

Maybe I should start with and heartily thank those without whom chaos might reside and we would probably all sink under the weight of paper work. Michaela Hennig, Hannelore Brand, and unforgettable heart and soul of the office, Brigitte Dick, thank you all for saving us from most of the administrative hassle!

Further, I would like to express my great appreciation for the generous support from our skilled postdocs. Stanislas Werfel not only helped me to clone a virus and needle mouse tails, but also saved my life multiple times as threatened by, for instance, a tick attack or a closed door of the radioactivity lab. Special thanks definitely go to my Breton baymate Fabrice Jaffré, whose clear mind and dissenting ideas made every conversation valuable. Thank you for your opinion, humor, and friendship! Yassine Sassi supported my research by his tireless expertise, constructive comments, warm encouragement, and Tunisian delicacies. Exactly the same applies to Deepak Ramanujam replacing Tunisian with Indian culinary delights. I thank Olympia Bikou for sharing her astonishing medical insight.

Part of the output of this project is owed to incalculable hours spent with my labmates during seminars, coffee, table football games, and outdoor pursuits. I would like to express my special thanks to Simon Leierseder for his scientific correctness and his profound expertise regarding microscopy and statistical analysis. Assuredly, without the girls it would not have been half the fun. I look up to Claudia Jentzsch for her classy spirit and for jumping first into the floods of the Eisbach, thank Petra Göbel and Megha Saraiya for increasing our average degree in fashionability tremendously (although I better keep silent about Petra's influence on the quality of music we inevitably had to listen to in the lab), I am grateful to Jayavarshni Ganesan for making me not always be the last one standing in the lab, appreciate Andrea Ahles for her extraordinary loyalty and sympathy, acknowledge Laura Hinz for being great in every respect, and want to point out Kathleen Meyer for the equilibrating time-outs at calm waters like the beautiful Osterseen. Surely though, I very much enjoyed the company of Thomas Hartmann, a master of ultimate frisbee, Michael Regn, a master of onions and chili peppers, Petros Avramopoulos, unnecessary to mention his Greek parentage, and the medical specialists Maximilian Fischer, Laurenz Grüter, Florian Scheufele and Stephan Skawran.

Beyond, I owe my profound gratitude to Lucia Koblitz for performing surgery on countless mice and rats, to Kornelija Sakac for echocardiography of my test mice, and I am indebted to Sabine Brummer for helping me with the radioactivity matters. It should also not go unmentioned how supportive Astrid Vens managed the ordering of all lab supplies and how perfectly she organized all other affairs such as, for example, excellent parties. Besides, I would like to express my sincerely thanks to our ship's carpenter Norbert Ertl, able to fix everything (even broken bicycles).

This work was generously funded by the Studienstiftung des Deutschen Volkes and the Boehringer Ingelheim Fonds. Thank you for the support. It should be emphasized that there is hardly any more reasonable choice than wasting money on research projects.
With respect to the typesetting, I have to acknowledge the kindness of André Miede allowing public access to the LaTeX bundle `classicthesis`, which has been adapted for this thesis.
I definitely cannot finish without thanking my family and friends. I am deeply grateful to my parents for their personal support. In principle, it was them who initially incited me to do a doctorate. (Please direct complaints accordingly!) As they almost became family, I would also like to thank Annemarie and Josef Mittermeier for their support with the best chocolate truffles ever. Finally, I need to put on record my appreciation and gratitude to all who provided distraction, encouragements, and perhaps most of all, patience and must thus be counted as genuine friends. Thank you very much indeed!

No thanks goes to the canteen caterer, the night watchman, and the leaf blower.

BIBLIOGRAPHY

[1] Abdellatif, M. Differential Expression of MicroRNAs in Different Disease States. *Circulation research 110*, 4 (2012), 638–50.

[2] Addo-Quaye, C., Eshoo, T. W., Bartel, D. P., and Axtell, M. J. Endogenous siRNA and miRNA targets identified by sequencing of the Arabidopsis degradome. *Current biology : CB 18*, 10 (2008), 758–62.

[3] Ai, J., Zhang, R., Li, Y., Pu, J., Lu, Y., Jiao, J., Li, K., Yu, B., Li, Z., Wang, R., Wang, L., Li, Q., Wang, N., Shan, H., Li, Z., and Yang, B. Circulating microRNA-1 as a potential novel biomarker for acute myocardial infarction. *Biochemical and biophysical research communications 391*, 1 (2010), 73–7.

[4] Alexiou, P., Maragkakis, M., Papadopoulos, G. L., Reczko, M., and Hatzigeorgiou, A. G. Lost in translation: an assessment and perspective for computational microRNA target identification. *Bioinformatics (Oxford, England) 25*, 23 (2009), 3049–55.

[5] Amaral, P. P., and Mattick, J. S. Noncoding RNA in development. *Mammalian genome : official journal of the International Mammalian Genome Society 19*, 7-8 (2008), 454–92.

[6] Ambros, V. The functions of animal microRNAs. *Nature 431*, 7006 (2004), 350–5.

[7] Ambros, V., Lee, R., Lavanway, A., Williams, P., and Jewell, D. MicroRNAs and Other Tiny Endogenous RNAs in C. elegans. *Current Biology 13* (2003), 807–818.

[8] Ameres, S. L., Martinez, J., and Schroeder, R. Molecular basis for target RNA recognition and cleavage by human RISC. *Cell 130*, 1 (2007), 101–12.

[9] Anders, G., Mackowiak, S. D., Jens, M., Maaskola, J., Kuntzagk, A., Rajewsky, N., Landthaler, M., and Dieterich, C. doRiNA: a database of RNA interactions in post-transcriptional regulation. *Nucleic acids research 40*, Database issue (2012), D180–6.

[10] Anderson, P., and Kedersha, N. RNA granules. *The Journal of cell biology 172*, 6 (2006), 803–8.

[11] Aravin, A. a., Hannon, G. J., and Brennecke, J. The Piwi-piRNA pathway provides an adaptive defense in the transposon arms race. *Science (New York, N.Y.) 318*, 5851 (2007), 761–4.

[12] Aravin, A. a., Lagos-Quintana, M., Yalcin, A., Zavolan, M., Marks, D., Snyder, B., Gaasterland, T., Meyer, J., and Tuschl, T. The small

RNA profile during Drosophila melanogaster development. *Developmental cell 5*, 2 (2003), 337–50.

[13] ARAVIN, A. A., NAUMOVA, N. M., TULIN, A. V., VAGIN, V. V., ROZOVSKY, Y. M., AND GVOZDEV, V. A. Double-stranded RNA-mediated silencing of genomic tandem repeats and transposable elements in the D. melanogaster germline. *Current biology : CB 11*, 13 (2001), 1017–27.

[14] ASCANO, M., HAFNER, M., CEKAN, P., GERSTBERGER, S., AND TUSCHL, T. Identification of RNA-protein interaction networks using PAR-CLIP. *Wiley interdisciplinary reviews. RNA 3*, 2 (2012), 159–77.

[15] ASOKAN, A., CONWAY, J. C., PHILLIPS, J. L., LI, C., HEGGE, J., SINNOTT, R., YADAV, S., DIPRIMIO, N., NAM, H.-J., AGBANDJE-MCKENNA, M., MCPHEE, S., WOLFF, J., AND SAMULSKI, R. J. Reengineering a receptor footprint of adeno-associated virus enables selective and systemic gene transfer to muscle. *Nature biotechnology 28*, 1 (2010), 79–82.

[16] AVNER, P., AND HEARD, E. X-chromosome inactivation: counting, choice and initiation. *Nature reviews. Genetics 2*, 1 (2001), 59–67.

[17] BABIARZ, J. E., RUBY, J. G., WANG, Y., BARTEL, D. P., AND BLELLOCH, R. Mouse ES cells express endogenous shRNAs, siRNAs, and other Microprocessor-independent, Dicer-dependent small RNAs. *Genes & development 22*, 20 (2008), 2773–85.

[18] BAEK, D., VILLÉN, J., SHIN, C., CAMARGO, F. D., GYGI, S. P., AND BARTEL, D. P. The impact of microRNAs on protein output. *Nature 455*, 7209 (2008), 64–71.

[19] BAILEY, T. L., BODEN, M., BUSKE, F. A., FRITH, M., GRANT, C. E., CLEMENTI, L., REN, J., LI, W. W., AND NOBLE, W. S. MEME SUITE: tools for motif discovery and searching. *Nucleic acids research 37*, Web Server issue (2009), W202–8.

[20] BALTZ, A., MUNSCHAUER, M., SCHWANHÄUSSER, B., VASILE, A., MURAKAWA, Y., SCHUELER, M., YOUNGS, N., PENFOLD-BROWN, D., DREW, K., MILEK, M., WYLER, E., BONNEAU, R., SELBACH, M., DIETERICH, C., AND LANDTHALER, M. The mRNA-Bound Proteome and Its Global Occupancy Profile on Protein-Coding Transcripts. *Molecular Cell 46*, 5 (2012), 674–690.

[21] BANERJEE, I., FUSELER, J. W., PRICE, R. L., BORG, T. K., AND BAUDINO, T. A. Determination of cell types and numbers during cardiac development in the neonatal and adult rat and mouse. *American journal of physiology. Heart and circulatory physiology 293*, 3 (2007), H1883–91.

[22] BARTEL, D. P. MicroRNAs: target recognition and regulatory functions. *Cell 136*, 2 (2009), 215–33.

[23] BARTEL, D. P., AND CHEN, C.-Z. Micromanagers of gene expression: the potentially widespread influence of metazoan microRNAs. *Nature reviews. Genetics 5*, 5 (2004), 396–400.

[24] Bauer, D. F. Constructing Confidence Sets Using Rank Statistics. *Journal of the American Statistical Association 67*, 339 (1972), 687–690.

[25] Baxter, D., McInnes, I. B., and Kurowska-Stolarska, M. Novel regulatory mechanisms in inflammatory arthritis: a role for microRNA. *Immunology and cell biology 90*, 3 (2012), 288–92.

[26] Behlke, M. a. Progress towards in vivo use of siRNAs. *Molecular therapy : the journal of the American Society of Gene Therapy 13*, 4 (2006), 644–70.

[27] Behm-Ansmant, I., Rehwinkel, J., Doerks, T., Stark, A., Bork, P., and Izaurralde, E. mRNA degradation by miRNAs and GW182 requires both CCR4:NOT deadenylase and DCP1:DCP2 decapping complexes. *Genes & development 20*, 14 (2006), 1885–98.

[28] Beitzinger, M., Peters, L., Zhu, J. Y., Kremmer, E., and Meister, G. Identification of human microRNA targets from isolated argonaute protein complexes. *RNA biology 4*, 2 (2007), 76–84.

[29] Berezikov, E., Chung, W.-J., Willis, J., Cuppen, E., and Lai, E. C. Mammalian mirtron genes. *Molecular cell 28*, 2 (2007), 328–36.

[30] Bernstein, E., Caudy, a. a., Hammond, S. M., and Hannon, G. J. Role for a bidentate ribonuclease in the initiation step of RNA interference. *Nature 409*, 6818 (2001), 363–6.

[31] Bernstein, E., Kim, S. Y., Carmell, M. a., Murchison, E. P., Alcorn, H., Li, M. Z., Mills, A. a., Elledge, S. J., Anderson, K. V., and Hannon, G. J. Dicer is essential for mouse development. *Nature genetics 35*, 3 (2003), 215–7.

[32] Betel, D., Koppal, A., Agius, P., Sander, C., and Leslie, C. Comprehensive modeling of microRNA targets predicts functional non-conserved and non-canonical sites. *Genome biology 11*, 8 (2010), R90.

[33] Betel, D., Wilson, M., Gabow, A., Marks, D. S., and Sander, C. The microRNA.org resource: targets and expression. *Nucleic acids research 36*, Database issue (2008), D149–53.

[34] Béthune, J., Artus-Revel, C. G., and Filipowicz, W. Kinetic analysis reveals successive steps leading to miRNA-mediated silencing in mammalian cells. *EMBO reports 13*, 8 (2012), 716–23.

[35] Beuvink, I., Kolb, F. a., Budach, W., Garnier, A., Lange, J., Natt, F., Dengler, U., Hall, J., Filipowicz, W., and Weiler, J. A novel microarray approach reveals new tissue-specific signatures of known and predicted mammalian microRNAs. *Nucleic acids research 35*, 7 (2007), e52.

[36] Bhattacharyya, S. N., Habermacher, R., Martine, U., Closs, E. I., and Filipowicz, W. Relief of microRNA-mediated translational repression in human cells subjected to stress. *Cell 125*, 6 (2006), 1111–24.

[37] Blencowe, B. J., Ahmad, S., and Lee, L. J. Current-generation high-throughput sequencing: deepening insights into mammalian transcriptomes. *Genes & development 23*, 12 (2009), 1379–86.

[38] Bohnsack, M. T., Czaplinski, K., and Gorlich, D. Exportin 5 is a RanGTP-dependent dsRNA-binding protein that mediates nuclear export of pre-miRNAs. *RNA (New York, N.Y.) 10*, 2 (2004), 185–91.

[39] Bohnsack, M. T., Martin, R., Granneman, S., Ruprecht, M., Schleiff, E., and Tollervey, D. Prp43 bound at different sites on the pre-rRNA performs distinct functions in ribosome synthesis. *Molecular cell 36*, 4 (2009), 583–92.

[40] Bohr, C., Hasselbalch, K., and Krogh, A. Ueber einen in biologischer Beziehung wichtigen Einfluss, den die Kohlensäurespannung des Blutes auf dessen Sauerstoffbindung übt1. *Skandinavisches Archiv Für Physiologie 16*, 2 (1904), 402–412.

[41] Boland, A., Huntzinger, E., Schmidt, S., Izaurralde, E., and Weichenrieder, O. Crystal structure of the MID-PIWI lobe of a eukaryotic Argonaute protein. *Proceedings of the National Academy of Sciences of the United States of America 108*, 26 (2011), 10466–71.

[42] Borchert, G. M., Lanier, W., and Davidson, B. L. RNA polymerase III transcribes human microRNAs. *Nature structural & molecular biology 13*, 12 (2006), 1097–101.

[43] Boudreau, R. L., Jiang, P., Gilmore, B. L., Spengler, R. M., Tirabassi, R., Nelson, J. a., Ross, C. a., Xing, Y., and Davidson, B. L. Transcriptome-wide Discovery of microRNA Binding Sites in Human Brain. *Neuron* (2013), 1–12.

[44] Bousquet, M., Harris, M. H., Zhou, B., and Lodish, H. F. MicroRNA miR-125b causes leukemia. *PNAS* (2010), 2–7.

[45] Bracken, C. P., Szubert, J. M., Mercer, T. R., Dinger, M. E., Thomson, D. W., Mattick, J. S., Michael, M. Z., and Goodall, G. J. Global analysis of the mammalian RNA degradome reveals widespread miRNA-dependent and miRNA-independent endonucleolytic cleavage. *Nucleic acids research 39*, 13 (2011), 5658–68.

[46] Brandenburger, M., Wenzel, J., Bogdan, R., Richardt, D., Nguemo, F., Reppel, M., Hescheler, J., Terlau, H., and Dendorfer, A. Organotypic slice culture from human adult ventricular myocardium. *Cardiovascular research 93*, 1 (2012), 50–9.

[47] Braun, J. E., Huntzinger, E., Fauser, M., and Izaurralde, E. GW182 proteins directly recruit cytoplasmic deadenylase complexes to miRNA targets. *Molecular cell 44*, 1 (2011), 120–33.

[48] Brennecke, J., Aravin, A. a., Stark, A., Dus, M., Kellis, M., Sachidanandam, R., and Hannon, G. J. Discrete small RNA-generating loci

as master regulators of transposon activity in Drosophila. *Cell 128*, 6 (2007), 1089–103.

[49] Brennecke, J., Stark, A., Russell, R. B., and Cohen, S. M. Principles of microRNA-target recognition. *PLoS biology 3*, 3 (2005), e85.

[50] Brimacombe, R., Stiege, W., Kyriatsoulis, A., and Maly, P. Intra-RNA and RNA-protein cross-linking techniques in Escherichia coli ribosomes. *Methods in enzymology 164* (1988), 287–309.

[51] Broderick, J. a., Salomon, W. E., Ryder, S. P., Aronin, N., and Zamore, P. D. Argonaute protein identity and pairing geometry determine cooperativity in mammalian RNA silencing. *RNA* (2011), 1858–1869.

[52] Brown, R. D., Ambler, S. K., Mitchell, M. D., and Long, C. S. The cardiac fibroblast: therapeutic target in myocardial remodeling and failure. *Annual review of pharmacology and toxicology 45*, 1 (2005), 657–87.

[53] Burge, C. B., Tuschl, T., and Sharp, P. A. Splicing of precursors to mRNAs by the spliceosomes. In *The RNA World, 2nd Ed.: The Nature of Modern RNA Suggests a Prebiotic RNA World*. 1999, ch. 20, pp. 525–560.

[54] Burger, K., Mühl, B., Kellner, M., Rohrmoser, M., Gruber-Eber, A., Windhager, L., Friedel, C. C., Dölken, L., and Eick, D. 4-thiouridine inhibits rRNA synthesis and causes a nucleolar stress response. *RNA biology 10*, 10 (2013).

[55] Burnett, J. C., Rossi, J. J., and Tiemann, K. Current progress of siRNA/shRNA therapeutics in clinical trials. *Biotechnology journal 6*, 9 (2011), 1130–46.

[56] Burroughs, A. M., Ando, Y., de Hoon, M. L., Tomaru, Y., Suzuki, H., Hayashizaki, Y., and Daub, C. O. Deep-sequencing of human Argonaute-associated small RNAs provides insight into miRNA sorting and reveals Argonaute association with RNA fragments of diverse origin. *RNA Biology 8*, 1 (2011), 158–177.

[57] Bushati, N., and Cohen, S. M. microRNA functions. *Annual review of cell and developmental biology 23* (2007), 175–205.

[58] Cabili, M. N., Trapnell, C., Goff, L., Koziol, M., Tazon-Vega, B., Regev, A., and Rinn, J. L. Integrative annotation of human large intergenic noncoding RNAs reveals global properties and specific subclasses. *Genes & development 25*, 18 (2011), 1915–27.

[59] Callis, T. E., Pandya, K., Seok, H. Y., Tang, R.-h., Tatsuguchi, M., Huang, Z.-p., Chen, J.-f., Deng, Z., Gunn, B., Shumate, J., Willis, M. S., Selzman, C. H., and Wang, D.-z. MicroRNA-208a is a regulator of cardiac hypertrophy and conduction in mice. *The Journal of clinical investigation 119*, 9 (2009), 2772–86.

[60] Carè, A., Catalucci, D., Felicetti, F., Bonci, D., Addario, A., Gallo, P., Bang, M.-L., Segnalini, P., Gu, Y., Dalton, N. D., Elia, L., Latronico, M. V. G., Hø ydal, M., Autore, C., Russo, M. a., Dorn, G. W., Ellingsen, O., Ruiz-Lozano, P., Peterson, K. L., Croce, C. M., Peschle, C., and Condorelli, G. MicroRNA-133 controls cardiac hypertrophy. *Nature medicine 13*, 5 (2007), 613–8.

[61] Carthew, R. W., and Sontheimer, E. J. Origins and Mechanisms of miRNAs and siRNAs. *Cell 136*, 4 (2009), 642–55.

[62] Castello, A., Fischer, B., Eichelbaum, K., Horos, R., Beckmann, B. M., Strein, C., Davey, N. E., Humphreys, D. T., Preiss, T., Steinmetz, L. M., Krijgsveld, J., and Hentze, M. W. Insights into RNA Biology from an Atlas of Mammalian mRNA-Binding Proteins. *Cell* (2012), 1–14.

[63] Chan, S.-P., and Slack, F. J. And now introducing mammalian mirtrons. *Developmental cell 13*, 5 (2007), 605–7.

[64] Chang, J., Nicolas, E., Marks, D., Sander, C., Lerro, A., Buendia, M. A., Xu, C., Mason, W. S., Moloshok, T., Bort, R., Zaret, K. S., and Taylor, J. M. miR-122, a mammalian liver-specific microRNA, is processed from hcr mRNA and may downregulate the high affinity cationic amino acid transporter CAT-1. *RNA biology 1*, 2 (2004), 106–13.

[65] Chekulaeva, M., Mathys, H., Zipprich, J. T., Attig, J., Colic, M., Parker, R., and Filipowicz, W. miRNA repression involves GW182-mediated recruitment of CCR4-NOT through conserved W-containing motifs. *Nature structural & molecular biology 18*, 11 (2011), 1218–26.

[66] Cheloufi, S., Dos Santos, C. O., Chong, M. M. W., and Hannon, G. J. A dicer-independent miRNA biogenesis pathway that requires Ago catalysis. *Nature 465*, 7298 (2010), 584–9.

[67] Chen, B., Yun, J., Kim, M. S., Mendell, J. T., and Xie, Y. PIPE-CLIP: a comprehensive online tool for CLIP-seq data analysis. *Genome biology 15*, 1 (2014), R18.

[68] Cheng, Y., Ji, R., Yue, J., Yang, J., Liu, X., Chen, H., Dean, D. B., and Zhang, C. MicroRNAs are aberrantly expressed in hypertrophic heart: do they play a role in cardiac hypertrophy? *The American journal of pathology 170*, 6 (2007), 1831–40.

[69] Cheng, Y., Tan, N., Yang, J., Liu, X., Cao, X., He, P., Dong, X., Qin, S., and Zhang, C. A translational study of circulating cell-free microRNA-1 in acute myocardial infarction. *Clinical science (London, England : 1979) 119*, 2 (2010), 87–95.

[70] Chi, S. W., Zang, J. B., Mele, A., and Darnell, R. B. Argonaute HITS-CLIP decodes microRNA-mRNA interaction maps. *Nature 460*, 7254 (2009), 479–86.

[71] Chien, K. R. Stress pathways and heart failure. *Cell 98*, 5 (1999), 555–8.

[72] Chou, C.-H., Lin, F.-M., Chou, M.-T., Hsu, S.-D., Chang, T.-H., Weng, S.-L., Shrestha, S., Hsiao, C.-C., Hung, J.-H., and Huang, H.-D. A computational approach for identifying microRNA-target interactions using high-throughput CLIP and PAR-CLIP sequencing. *BMC genomics 14 Suppl 1*, Suppl 1 (2013), S2.

[73] Cifuentes, D., Xue, H., Taylor, D. W., Patnode, H., Mishima, Y., Cheloufi, S., Ma, E., Mane, S., Hannon, G. J., Lawson, N. D., Wolfe, S. a., and Giraldez, A. J. A novel miRNA processing pathway independent of Dicer requires Argonaute2 catalytic activity. *Science (New York, N.Y.) 328*, 5986 (2010), 1694–8.

[74] Cleary, M. D. *Cell type-specific analysis of mRNA synthesis and decay in vivo with uracil phosphoribosyltransferase and 4-thiouracil.*, 1 ed., vol. 448. Elsevier Inc., 2008.

[75] Consortium, T. E. P. The ENCODE (ENCyclopedia Of DNA Elements) Project. *Science (New York, N.Y.) 306*, 5696 (2004), 636–40.

[76] Corcoran, D. L., Georgiev, S., Mukherjee, N., Gottwein, E., Skalsky, R. L., Keene, J. D., and Ohler, U. PARalyzer: Definition of RNA binding sites from PAR-CLIP short-read sequence data. *Genome Biology 12*, 8 (2011), R79.

[77] Cullen, B. R. Transcription and processing of human microRNA precursors. *Molecular cell 16*, 6 (2004), 861–5.

[78] da Costa Martins, P. a., Bourajjaj, M., Gladka, M., Kortland, M., van Oort, R. J., Pinto, Y. M., Molkentin, J. D., and De Windt, L. J. Conditional dicer gene deletion in the postnatal myocardium provokes spontaneous cardiac remodeling. *Circulation 118*, 15 (2008), 1567–76.

[79] D'Alessandra, Y., Devanna, P., Limana, F., Straino, S., Di Carlo, A., Brambilla, P. G., Rubino, M., Carena, M. C., Spazzafumo, L., De Simone, M., Micheli, B., Biglioli, P., Achilli, F., Martelli, F., Maggiolini, S., Marenzi, G., Pompilio, G., and Capogrossi, M. C. Circulating microRNAs are new and sensitive biomarkers of myocardial infarction. *European heart journal 31*, 22 (2010), 2765–73.

[80] Davis, E., Caiment, F., Tordoir, X., Cavaillé, J., Ferguson-Smith, A., Cockett, N., Georges, M., and Charlier, C. RNAi-mediated allelic trans-interaction at the imprinted Rtl1/Peg11 locus. *Current biology : CB 15*, 8 (2005), 743–9.

[81] de Saint Exupéry, A. *Le Petit Prince*. Gallimard, 1943.

[82] De Santa, F., Barozzi, I., Mietton, F., Ghisletti, S., Polletti, S., Tusi, B. K., Muller, H., Ragoussis, J., Wei, C.-L., and Natoli, G. A large fraction of extragenic RNA pol II transcription sites overlap enhancers. *PLoS biology 8*, 5 (2010), e1000384.

[83] Derry, M. C., Yanagiya, a., Martineau, Y., and Sonenberg, N. Regulation of poly(A)-binding protein through PABP-interacting proteins. *Cold Spring Harbor symposia on quantitative biology 71* (2006), 537–43.

[84] Didiano, D., and Hobert, O. Perfect seed pairing is not a generally reliable predictor for miRNA-target interactions. *Nature structural & molecular biology 13*, 9 (2006), 849–51.

[85] Didiano, D., and Hobert, O. Molecular architecture of a miRNA-regulated 3' UTR. *RNA (New York, N.Y.) 14*, 7 (2008), 1297–317.

[86] Diederichs, S., and Haber, D. a. Dual role for argonautes in microRNA processing and posttranscriptional regulation of microRNA expression. *Cell 131*, 6 (2007), 1097–108.

[87] Diederichs, S., Jung, S., Rothenberg, S. M., Smolen, G. a., Mlody, B. G., and Haber, D. a. Coexpression of Argonaute-2 enhances RNA interference toward perfect match binding sites. *Proceedings of the National Academy of Sciences of the United States of America 105*, 27 (2008), 9284–9.

[88] Ding, Y., Tang, Y., Kwok, C. K., Zhang, Y., Bevilacqua, P. C., and Assmann, S. M. In vivo genome-wide profiling of RNA secondary structure reveals novel regulatory features. *Nature* (2013).

[89] Djuranovic, S., Nahvi, A., and Green, R. miRNA-mediated gene silencing by translational repression followed by mRNA deadenylation and decay. *Science (New York, N.Y.) 336*, 6078 (2012), 237–40.

[90] Doench, J. G., Petersen, C. P., and Sharp, P. a. siRNAs can function as miRNAs. *Genes & development 17*, 4 (2003), 438–42.

[91] Doench, J. G., and Sharp, P. a. Specificity of microRNA target selection in translational repression. *Genes & development 18*, 5 (2004), 504–11.

[92] Dölken, L., Ruzsics, Z., Rädle, B., Friedel, C. C., Zimmer, R., Mages, J., Hoffmann, R., Dickinson, P., Forster, T., Ghazal, P., and Koszinowski, U. H. High-resolution gene expression profiling for simultaneous kinetic parameter analysis of RNA synthesis and decay. *RNA (New York, N.Y.) 14*, 9 (2008), 1959–72.

[93] Dong, S., Cheng, Y., Yang, J., Li, J., Liu, X., Wang, X., Wang, D., Krall, T. J., Delphin, E. S., and Zhang, C. MicroRNA expression signature and the role of microRNA-21 in the early phase of acute myocardial infarction. *The Journal of biological chemistry 284*, 43 (2009), 29514–25.

[94] Dorn, G. W., Robbins, J., and Sugden, P. H. Phenotyping hypertrophy: eschew obfuscation. *Circulation research 92*, 11 (2003), 1171–5.

[95] Dorsett, Y., and Tuschl, T. siRNAs: applications in functional genomics and potential as therapeutics. *Nature reviews. Drug discovery 3*, 4 (2004), 318–29.

[96] Drinnenberg, I. a., Weinberg, D. E., Xie, K. T., Mower, J. P., Wolfe, K. H., Fink, G. R., and Bartel, D. P. RNAi in budding yeast. *Science (New York, N.Y.) 326*, 5952 (2009), 544–50.

[97] Dueck, A., Ziegler, C., Eichner, A., Berezikov, E., and Meister, G. microRNAs associated with the different human Argonaute proteins. *Nucleic acids research 40*, 19 (2012), 9850–62.

[98] Duisters, R. F., Tijsen, A. J., Schroen, B., Leenders, J. J., Lentink, V., van der Made, I., Herias, V., van Leeuwen, R. E., Schellings, M. W., Barenbrug, P., Maessen, J. G., Heymans, S., Pinto, Y. M., and Creemers, E. E. miR-133 and miR-30 regulate connective tissue growth factor: implications for a role of microRNAs in myocardial matrix remodeling. *Circulation research 104*, 2 (2009), 170–8, 6p following 178.

[99] Easow, G., Teleman, A. a., and Cohen, S. M. Isolation of microRNA targets by miRNP immunopurification. *RNA (New York, N.Y.) 13*, 8 (2007), 1198–204.

[100] Ebert, M. S., Neilson, J. R., and Sharp, P. A. MicroRNA sponges: competitive inhibitors of small RNAs in mammalian cells. *Nature methods 4*, 9 (2007), 721–6.

[101] Ecker, J. R., and Davis, R. W. Inhibition of gene expression in plant cells by expression of antisense RNA. *Proceedings of the National Academy of Sciences of the United States of America 83*, 15 (1986), 5372–6.

[102] Eiring, A. M., Harb, J. G., Neviani, P., Garton, C., Oaks, J. J., Spizzo, R., Liu, S., Schwind, S., Santhanam, R., Hickey, C. J., Becker, H., Chandler, J. C., Andino, R., Cortes, J., Hokland, P., Huettner, C. S., Bhatia, R., Roy, D. C., Liebhaber, S. a., Caligiuri, M. a., Marcucci, G., Garzon, R., Croce, C. M., Calin, G. a., and Perrotti, D. miR-328 functions as an RNA decoy to modulate hnRNP E2 regulation of mRNA translation in leukemic blasts. *Cell 140*, 5 (2010), 652–65.

[103] El-Shami, M., Pontier, D., Lahmy, S., Braun, L., Picart, C., Vega, D., Hakimi, M.-A., Jacobsen, S. E., Cooke, R., and Lagrange, T. Reiterated WG/GW motifs form functionally and evolutionarily conserved ARGONAUTE-binding platforms in RNAi-related components. *Genes & development 21*, 20 (2007), 2539–44.

[104] Elbashir, S. M. RNA interference is mediated by 21- and 22-nucleotide RNAs. *Genes & Development 15*, 2 (2001), 188–200.

[105] Elia, L., Contu, R., Quintavalle, M., Varrone, F., Chimenti, C., Russo, M. A., Cimino, V., De Marinis, L., Frustaci, A., Catalucci, D., and Condorelli, G. Reciprocal regulation of microRNA-1 and insulin-like growth factor-1 signal transduction cascade in cardiac and skeletal muscle in physiological and pathological conditions. *Circulation 120*, 23 (2009), 2377–85.

[106] Eliceiri, G. L. Small nucleolar RNAs. *Cellular and molecular life sciences : CMLS 56*, 1-2 (1999), 22–31.

[107] Elkayam, E., Kuhn, C.-D., Tocilj, A., Haase, A. D., Greene, E. M., Hannon, G. J., and Joshua-Tor, L. The structure of human argonaute-2 in complex with miR-20a. *Cell 150*, 1 (2012), 100–10.

[108] Ender, C., Krek, A., Friedländer, M. R., Beitzinger, M., Weinmann, L., Chen, W., Pfeffer, S., Rajewsky, N., and Meister, G. A human snoRNA with microRNA-like functions. *Molecular cell 32*, 4 (2008), 519–28.

[109] Engelhardt, S. Beta-adrenergic receptors in heart failure. *Heart failure clinics 1*, 2 (2005), 183–91.

[110] Erhard, F., Dolken, L., Jaskiewicz, L., and Zimmer, R. PARma: identification of microRNA target sites in Argonaute PAR-CLIP data. *Genome biology 14*, 7 (2013), R79.

[111] Eulalio, A., Behm-Ansmant, I., and Izaurralde, E. P bodies: at the crossroads of post-transcriptional pathways. *Nature reviews. Molecular cell biology 8*, 1 (2007), 9–22.

[112] Eulalio, A., Huntzinger, E., and Izaurralde, E. Getting to the root of miRNA-mediated gene silencing. *Cell 132*, 1 (2008), 9–14.

[113] Eulalio, A., Huntzinger, E., and Izaurralde, E. GW182 interaction with Argonaute is essential for miRNA-mediated translational repression and mRNA decay. *Nature structural & molecular biology 15*, 4 (2008), 346–53.

[114] Eulalio, A., Rehwinkel, J., Stricker, M., Huntzinger, E., Yang, S.-F., Doerks, T., Dorner, S., Bork, P., Boutros, M., and Izaurralde, E. Target-specific requirements for enhancers of decapping in miRNA-mediated gene silencing. *Genes & development 21*, 20 (2007), 2558–70.

[115] Fabian, M. R., Cieplak, M. K., Frank, F., Morita, M., Green, J., Srikumar, T., Nagar, B., Yamamoto, T., Raught, B., Duchaine, T. F., and Sonenberg, N. miRNA-mediated deadenylation is orchestrated by GW182 through two conserved motifs that interact with CCR4-NOT. *Nature structural & molecular biology 18*, 11 (2011), 1211–7.

[116] Fabian, M. R., Mathonnet, G., Sundermeier, T., Mathys, H., Zipprich, J. T., Svitkin, Y. V., Rivas, F., Jinek, M., Wohlschlegel, J., Doudna, J. a., Chen, C.-Y. a., Shyu, A.-B., Yates, J. R., Hannon, G. J., Filipowicz, W., Duchaine, T. F., and Sonenberg, N. Mammalian miRNA RISC recruits CAF1 and PABP to affect PABP-dependent deadenylation. *Molecular cell 35*, 6 (2009), 868–80.

[117] Fabian, M. R., and Sonenberg, N. The mechanics of miRNA-mediated gene silencing: a look under the hood of miRISC. *Nature structural & molecular biology 19*, 6 (2012), 586–93.

[118] Farazi, T. a., Juranek, S. a., and Tuschl, T. The growing catalog of small RNAs and their association with distinct Argonaute/Piwi family members. *Development (Cambridge, England) 135*, 7 (2008), 1201–14.

[119] Farazi, T. a., Ten Hoeve, J. J., Brown, M., Mihailovic, A., Horlings, H. M., van de Vijver, M. J., Tuschl, T., and Wessels, L. F. Identification of distinct miRNA target regulation between breast cancer molecular subtypes using AGO2-PAR-CLIP and patient datasets. *Genome biology 15*, 1 (2014), R9.

[120] Farh, K. K.-H., Grimson, A., Jan, C., Lewis, B. P., Johnston, W. K., Lim, L. P., Burge, C. B., and Bartel, D. P. The widespread impact of mammalian MicroRNAs on mRNA repression and evolution. *Science (New York, N.Y.) 310*, 5755 (2005), 1817–21.

[121] Favre, A., Saintomé, C., Fourrey, J. L., Clivio, P., and Laugâa, P. Thionucleobases as intrinsic photoaffinity probes of nucleic acid structure and nucleic acid-protein interactions. *Journal of photochemistry and photobiology. B, Biology 42*, 2 (1998), 109–24.

[122] Fecko, C. J., Munson, K. M., Saunders, A., Sun, G., Begley, T. P., Lis, J. T., and Webb, W. W. Comparison of femtosecond laser and continuous wave UV sources for protein-nucleic acid crosslinking. *Photochemistry and photobiology 83*, 6 (2007), 1394–404.

[123] Filipowicz, W., Bhattacharyya, S. N., and Sonenberg, N. Mechanisms of post-transcriptional regulation by microRNAs: are the answers in sight? *Nature reviews. Genetics 9*, 2 (2008), 102–14.

[124] Fire, A., Xu, S., Montgomery, M. K., Kostas, S. A., Driver, S. E., and Mello, C. C. Potent and specific genetic interference by double-stranded RNA in Caenorhabditis elegans. *Nature 391*, 6669 (1998), 806–11.

[125] Flicek, P., Ahmed, I., Amode, M. R., Barrell, D., Beal, K., Brent, S., Carvalho-Silva, D., Clapham, P., Coates, G., Fairley, S., Fitzgerald, S., Gil, L., García-Girón, C., Gordon, L., Hourlier, T., Hunt, S., Juettemann, T., Kähäri, A. K., Keenan, S., Komorowska, M., Kulesha, E., Longden, I., Maurel, T., McLaren, W. M., Muffato, M., Nag, R., Overduin, B., Pignatelli, M., Pritchard, B., Pritchard, E., Riat, H. S., Ritchie, G. R. S., Ruffier, M., Schuster, M., Sheppard, D., Sobral, D., Taylor, K., Thormann, A., Trevanion, S., White, S., Wilder, S. P., Aken, B. L., Birney, E., Cunningham, F., Dunham, I., Harrow, J., Herrero, J., Hubbard, T. J. P., Johnson, N., Kinsella, R., Parker, A., Spudich, G., Yates, A., Zadissa, A., and Searle, S. M. J. Ensembl 2013. *Nucleic acids research 41*, Database issue (2013), D48–55.

[126] Frank, F., Sonenberg, N., and Nagar, B. Structural basis for 5′-nucleotide base-specific recognition of guide RNA by human AGO2. *Nature 465*, 7299 (2010), 818–22.

[127] Friedman, R. C., Farh, K. K.-H., Burge, C. B., and Bartel, D. P. Most mammalian mRNAs are conserved targets of microRNAs. *Genome research 19*, 1 (2009), 92–105.

[128] Fukunaga, T., Ozaki, H., Terai, G., Asai, K., Iwasaki, W., and Kiryu, H. CapR: revealing structural specificities of RNA-binding protein target recognition using CLIP-seq data. *Genome Biology 15*, 1 (2014), R16.

[129] Gaidatzis, D., van Nimwegen, E., Hausser, J., and Zavolan, M. Inference of miRNA targets using evolutionary conservation and pathway analysis. *BMC bioinformatics 8* (2007), 69.

[130] Galgano, A., Forrer, M., Jaskiewicz, L., Kanitz, A., Zavolan, M., and Gerber, A. P. Comparative analysis of mRNA targets for human PUF-family proteins suggests extensive interaction with the miRNA regulatory system. *PloS one 3*, 9 (2008), e3164.

[131] Ganesan, J., Ramanujam, D., Sassi, Y., Ahles, A., Jentzsch, C., Werfel, S., Leierseder, S., Loyer, X., Giacca, M., Zentilin, L., Thum, T., Laggerbauer, B., and Engelhardt, S. MiR-378 controls cardiac hypertrophy by combined repression of mitogen-activated protein kinase pathway factors. *Circulation 127*, 21 (2013), 2097–106.

[132] Gantier, M. P., McCoy, C. E., Rusinova, I., Saulep, D., Wang, D., Xu, D., Irving, A. T., Behlke, M. a., Hertzog, P. J., Mackay, F., and Williams, B. R. G. Analysis of microRNA turnover in mammalian cells following Dicer1 ablation. *Nucleic acids research 39*, 13 (2011), 5692–703.

[133] Garofalo, M., Romano, G., Di Leva, G., Nuovo, G., Jeon, Y.-J., Ngankeu, A., Sun, J., Lovat, F., Alder, H., Condorelli, G., Engelman, J. A., Ono, M., Rho, J. K., Cascione, L., Volinia, S., Nephew, K. P., and Croce, C. M. EGFR and MET receptor tyrosine kinase-altered microRNA expression induces tumorigenesis and gefitinib resistance in lung cancers. *Nat Med 18*, 1 (2012), 74–82.

[134] Geekiyanage, H., and Chan, C. MicroRNA-137/181c Regulates Serine Palmitoyltransferase and In Turn Amyloid Â , Novel Targets in Sporadic Alzheimer's Disease. *Journal of Neuroscience 31*, 41 (2011), 14820–14830.

[135] German, M. a., Pillay, M., Jeong, D.-H., Hetawal, A., Luo, S., Janardhanan, P., Kannan, V., Rymarquis, L. a., Nobuta, K., German, R., De Paoli, E., Lu, C., Schroth, G., Meyers, B. C., and Green, P. J. Global identification of microRNA-target RNA pairs by parallel analysis of RNA ends. *Nature biotechnology 26*, 8 (2008), 941–6.

[136] Ghildiyal, M., and Zamore, P. D. Small silencing RNAs: an expanding universe. *Nature reviews. Genetics 10*, 2 (2009), 94–108.

[137] Gilbert, W. Origin of life: The RNA world. *Nature 319*, 6055 (1986), 618–618.

[138] Go, A. S., Mozaffarian, D., Roger, V. L., Benjamin, E. J., Berry, J. D., Borden, W. B., Bravata, D. M., Dai, S., Ford, E. S., Fox, C. S., Franco, S., Fullerton, H. J., Gillespie, C., Hailpern, S. M., Heit, J. a., Howard, V. J., Huffman, M. D., Kissela, B. M., Kittner, S. J., Lackland, D. T., Lichtman, J. H., Lisabeth, L. D., Magid, D., Marcus, G. M., Marelli, A., Matchar, D. B., McGuire, D. K., Mohler, E. R., Moy, C. S., Mussolino, M. E., Nichol, G., Paynter, N. P., Schreiner, P. J., Sorlie, P. D., Stein, J., Turan, T. N., Virani, S. S., Wong, N. D., Woo, D., and Turner, M. B. Executive summary: heart disease and stroke statistics–2013 update: a report from the American Heart Association. *Circulation 127*, 1 (2013), 143–52.

[139] Goldstrohm, A. C., Hook, B. a., Seay, D. J., and Wickens, M. PUF proteins bind Pop2p to regulate messenger RNAs. *Nature structural & molecular biology 13*, 6 (2006), 533–9.

[140] Granneman, S., Kudla, G., Petfalski, E., and Tollervey, D. Identification of protein binding sites on U3 snoRNA and pre-rRNA by UV cross-linking and high-throughput analysis of cDNAs. *Proceedings of the National Academy of Sciences of the United States of America 106*, 24 (2009), 9613–8.

[141] Gregory, R. I., Chendrimada, T. P., Cooch, N., and Shiekhattar, R. Human RISC couples microRNA biogenesis and posttranscriptional gene silencing. *Cell 123*, 4 (2005), 631–40.

[142] Grimson, A., Farh, K. K.-H., Johnston, W. K., Garrett-Engele, P., Lim, L. P., and Bartel, D. P. MicroRNA targeting specificity in mammals: determinants beyond seed pairing. *Molecular cell 27*, 1 (2007), 91–105.

[143] Grosshans, H., and Filipowicz, W. Molecular biology: the expanding world of small RNAs. *Nature 451*, 7177 (2008), 414–6.

[144] Grün, D., Wang, Y.-L., Langenberger, D., Gunsalus, K. C., and Rajewsky, N. microRNA target predictions across seven Drosophila species and comparison to mammalian targets. *PLoS computational biology 1*, 1 (2005), e13.

[145] Guerrier-Takada, C., Gardiner, K., Marsh, T., Pace, N., and Altman, S. The RNA moiety of ribonuclease P is the catalytic subunit of the enzyme. *Cell 35*, 3 Pt 2 (1983), 849–57.

[146] Gunawardane, L. S., Saito, K., Nishida, K. M., Miyoshi, K., Kawamura, Y., Nagami, T., Siomi, H., and Siomi, M. C. A slicer-mediated mechanism for repeat-associated siRNA 5′ end formation in Drosophila. *Science (New York, N.Y.) 315*, 5818 (2007), 1587–90.

[147] Guo, H., Ingolia, N. T., Weissman, J. S., and Bartel, D. P. Mammalian microRNAs predominantly act to decrease target mRNA levels. *Nature 466*, 7308 (2010), 835–40.

[148] Haase, A. D., Jaskiewicz, L., Zhang, H., Lainé, S., Sack, R., Gatignol, A., and Filipowicz, W. TRBP, a regulator of cellular PKR and HIV-1 virus expression, interacts with Dicer and functions in RNA silencing. *EMBO reports 6*, 10 (2005), 961–7.

[149] Haecker, I., Gay, L. a., Yang, Y., Hu, J., Morse, A. M., McIntyre, L. M., and Renne, R. Ago HITS-CLIP expands understanding of Kaposi's sarcoma-associated herpesvirus miRNA function in primary effusion lymphomas. *PLoS pathogens 8*, 8 (2012), e1002884.

[150] Hafner, M., Landgraf, P., Ludwig, J., Rice, A., Ojo, T., Lin, C., Holoch, D., Lim, C., and Tuschl, T. Identification of microRNAs and other small regulatory RNAs using cDNA library sequencing. *Methods (San Diego, Calif.) 44*, 1 (2008), 3–12.

[151] Hafner, M., Landthaler, M., Burger, L., Khorshid, M., Hausser, J., Berninger, P., Rothballer, A., Ascano, M., Jungkamp, A.-C., Munschauer, M., Ulrich, A., Wardle, G. S., Dewell, S., Zavolan, M., and Tuschl, T. Transcriptome-wide identification of RNA-binding protein and microRNA target sites by PAR-CLIP. *Cell 141*, 1 (2010), 129–41.

[152] Hafner, M., Lianoglou, S., Tuschl, T., and Betel, D. Genome-wide identification of miRNA targets by PAR-CLIP. *Methods* (2012).

[153] Hafner, M., Renwick, N., Brown, M., Mihailović, A., Holoch, D., Lin, C., Pena, J. T. G., Nusbaum, J. D., Morozov, P., Ludwig, J., Ojo, T., Luo, S., Schroth, G., and Tuschl, T. RNA-ligase-dependent biases in miRNA representation in deep-sequenced small RNA cDNA libraries. *RNA (New York, N.Y.) 17*, 9 (2011), 1697–712.

[154] Haley, B., and Zamore, P. D. Kinetic analysis of the RNAi enzyme complex. *Nature structural & molecular biology 11*, 7 (2004), 599–606.

[155] Hamilton, a. J. A Species of Small Antisense RNA in Posttranscriptional Gene Silencing in Plants. *Science 286*, 5441 (1999), 950–952.

[156] Han, J., Lee, Y., Yeom, K.-H., Nam, J.-W., Heo, I., Rhee, J.-K., Sohn, S. Y., Cho, Y., Zhang, B.-T., and Kim, V. N. Molecular basis for the recognition of primary microRNAs by the Drosha-DGCR8 complex. *Cell 125*, 5 (2006), 887–901.

[157] Hannon, G. J., Rivas, F. V., Murchison, E. P., and Steitz, J. a. The expanding universe of noncoding RNAs. *Cold Spring Harbor symposia on quantitative biology 71* (2006), 551–64.

[158] Hansen, T. B., Jensen, T. I., Clausen, B. H., Bramsen, J. B., Finsen, B., Damgaard, C. K., and Kjems, J. r. Natural RNA circles function as efficient microRNA sponges. *Nature 495*, 7441 (2013), 384–8.

[159] Hansen, T. B., Wiklund, E. D., Bramsen, J. B., Villadsen, S. B., Statham, A. L., Clark, S. J., and Kjems, J. r. miRNA-dependent gene silencing involving Ago2-mediated cleavage of a circular antisense RNA. *The EMBO journal 30*, 21 (2011), 4414–22.

[160] Haraguchi, T., Ozaki, Y., and Iba, H. Vectors expressing efficient RNA decoys achieve the long-term suppression of specific microRNA activity in mammalian cells. *Nucleic acids research 37*, 6 (2009), e43.

[161] Hatfield, S. D., Shcherbata, H. R., Fischer, K. a., Nakahara, K., Carthew, R. W., and Ruohola-Baker, H. Stem cell division is regulated by the microRNA pathway. *Nature 435*, 7044 (2005), 974–8.

[162] Helwak, A., Kudla, G., Dudnakova, T., and Tollervey, D. Mapping the Human miRNA Interactome by CLASH Reveals Frequent Noncanonical Binding. *Cell 153*, 3 (2013), 654–65.

[163] Hendrickson, D. G., Hogan, D. J., Herschlag, D., Ferrell, J. E., and Brown, P. O. Systematic identification of mRNAs recruited to argonaute 2 by specific microRNAs and corresponding changes in transcript abundance. *PloS one 3*, 5 (2008), e2126.

[164] Hendrickson, D. G., Hogan, D. J., McCullough, H. L., Myers, J. W., Herschlag, D., Ferrell, J. E., and Brown, P. O. Concordant regulation of translation and mRNA abundance for hundreds of targets of a human microRNA. *PLoS biology 7*, 11 (2009), e1000238.

[165] Hentze, M. W., and Preiss, T. Circular RNAs: splicing's enigma variations. *The EMBO journal 32*, 7 (2013), 923–5.

[166] Heymans, S., Hirsch, E., Anker, S. D., Aukrust, P., Balligand, J.-L., Cohen-Tervaert, J. W., Drexler, H., Filippatos, G., Felix, S. B., Gullestad, L., Hilfiker-Kleiner, D., Janssens, S., Latini, R., Neubauer, G., Paulus, W. J., Pieske, B., Ponikowski, P., Schroen, B., Schultheiss, H.-P., Tschöpe, C., Van Bilsen, M., Zannad, F., McMurray, J., and Shah, A. M. Inflammation as a therapeutic target in heart failure? A scientific statement from the Translational Research Committee of the Heart Failure Association of the European Society of Cardiology. *European journal of heart failure 11*, 2 (2009), 119–29.

[167] Hill, J. a., Karimi, M., Kutschke, W., Davisson, R. L., Zimmerman, K., Wang, Z., Kerber, R. E., and Weiss, R. M. Cardiac Hypertrophy Is Not a Required Compensatory Response to Short-Term Pressure Overload. *Circulation 101*, 24 (2000), 2863–2869.

[168] Hill, J. a., and Olson, E. N. Cardiac plasticity. *The New England journal of medicine 358*, 13 (2008), 1370–80.

[169] Hong, X., Hammell, M., Ambros, V., and Cohen, S. M. Immunopurification of Ago1 miRNPs selects for a distinct class of microRNA targets. *Proceedings of the National Academy of Sciences of the United States of America 106*, 35 (2009), 15085–90.

[170] Houwing, S., Kamminga, L. M., Berezikov, E., Cronembold, D., Girard, A., van den Elst, H., Filippov, D. V., Blaser, H., Raz, E., Moens, C. B., Plasterk, R. H. a., Hannon, G. J., Draper, B. W., and Ketting, R. F.

A role for Piwi and piRNAs in germ cell maintenance and transposon silencing in Zebrafish. *Cell 129*, 1 (2007), 69–82.

[171] Hsu, S.-D., Chu, C.-H., Tsou, A.-P., Chen, S.-J., Chen, H.-C., Hsu, P. W.-C., Wong, Y.-H., Chen, Y.-H., Chen, G.-H., and Huang, H.-D. miRNAMap 2.0: genomic maps of microRNAs in metazoan genomes. *Nucleic acids research 36*, Database issue (2008), D165–9.

[172] Hu, Q., Tanasa, B., Trabucchi, M., Li, W., Zhang, J., Ohgi, K. a., Rose, D. W., Glass, C. K., and Rosenfeld, M. G. DICER- and AGO3-dependent generation of retinoic acid-induced DR2 Alu RNAs regulates human stem cell proliferation. *Nature structural & molecular biology 19*, 11 (2012), 1168–75.

[173] Humphreys, D. T., Westman, B. J., Martin, D. I. K., and Preiss, T. MicroRNAs control translation initiation by inhibiting eukaryotic initiation factor 4E/cap and poly(A) tail function. *Proceedings of the National Academy of Sciences of the United States of America 102*, 47 (2005), 16961–6.

[174] Hunter, M. P., Ismail, N., Zhang, X., Aguda, B. D., Lee, E. J., Yu, L., Xiao, T., Schafer, J., Lee, M.-L. T., Schmittgen, T. D., Nana-Sinkam, S. P., Jarjoura, D., and Marsh, C. B. Detection of microRNA expression in human peripheral blood microvesicles. *PloS one 3*, 11 (2008), e3694.

[175] Huntzinger, E., Braun, J. E., Heimstädt, S., Zekri, L., and Izaurralde, E. Two PABPC1-binding sites in GW182 proteins promote miRNA-mediated gene silencing. *The EMBO journal 29*, 24 (2010), 4146–60.

[176] Huntzinger, E., and Izaurralde, E. Gene silencing by microRNAs: contributions of translational repression and mRNA decay. *Nature reviews. Genetics 12*, 2 (2011), 99–110.

[177] Hutvágner, G., McLachlan, J., Pasquinelli, a. E., Bálint, E., Tuschl, T., and Zamore, P. D. A cellular function for the RNA-interference enzyme Dicer in the maturation of the let-7 small temporal RNA. *Science (New York, N.Y.) 293*, 5531 (2001), 834–8.

[178] Hutvagner, G., and Simard, M. J. Argonaute proteins: key players in RNA silencing. *Nature reviews. Molecular cell biology 9*, 1 (2008), 22–32.

[179] Hutvágner, G., and Zamore, P. D. A microRNA in a multiple-turnover RNAi enzyme complex. *Science (New York, N.Y.) 297*, 5589 (2002), 2056–60.

[180] Hwang, H.-W., Wentzel, E. a., and Mendell, J. T. A hexanucleotide element directs microRNA nuclear import. *Science (New York, N.Y.) 315*, 5808 (2007), 97–100.

[181] Ikeda, S., He, A., Kong, S. W., Lu, J., Bejar, R., Bodyak, N., Lee, K.-H., Ma, Q., Kang, P. M., Golub, T. R., and Pu, W. T. MicroRNA-1 negatively regulates expression of the hypertrophy-associated calmodulin and Mef2a genes. *Molecular and cellular biology 29*, 8 (2009), 2193–204.

[182] Ikeda, S., Kong, S. W., Lu, J., Bisping, E., Zhang, H., Allen, P. D., Golub, T. R., Pieske, B., and Pu, W. T. Altered microRNA expression in human heart disease. *Physiological genomics 31*, 3 (2007), 367–73.

[183] Inagaki, K., Fuess, S., Storm, T. a., Gibson, G. a., Mctiernan, C. F., Kay, M. a., and Nakai, H. Robust systemic transduction with AAV9 vectors in mice: efficient global cardiac gene transfer superior to that of AAV8. *Molecular therapy : the journal of the American Society of Gene Therapy 14*, 1 (2006), 45–53.

[184] Iwasaki, S., Kobayashi, M., Yoda, M., Sakaguchi, Y., Katsuma, S., Suzuki, T., and Tomari, Y. Hsc70/Hsp90 chaperone machinery mediates ATP-dependent RISC loading of small RNA duplexes. *Molecular cell 39*, 2 (2010), 292–9.

[185] Izaurralde, E. Elucidating the temporal order of silencing. *EMBO reports 13*, 8 (2012), 662–3.

[186] Jacobsen, A., Wen, J., Marks, D. S., and Krogh, A. Signatures of RNA binding proteins globally coupled to effective microRNA target sites. *Genome research 20*, 8 (2010), 1010–9.

[187] Jayawardena, T. M., Egemnazarov, B., Finch, E. a., Zhang, L., Payne, J. A., Pandya, K., Zhang, Z., Rosenberg, P., Mirotsou, M., and Dzau, V. J. MicroRNA-mediated in vitro and in vivo direct reprogramming of cardiac fibroblasts to cardiomyocytes. *Circulation research 110*, 11 (2012), 1465–73.

[188] Jeck, W. R., Sorrentino, J. a., Wang, K., Slevin, M. K., Burd, C. E., Liu, J., Marzluff, W. F., and Sharpless, N. E. Circular RNAs are abundant, conserved, and associated with ALU repeats. *RNA (New York, N.Y.) 19*, 2 (2013), 141–57.

[189] Jentzsch, C., Leierseder, S., Loyer, X., Flohrschütz, I., Sassi, Y., Hartmann, D., Thum, T., Laggerbauer, B., and Engelhardt, S. A phenotypic screen to identify hypertrophy-modulating microRNAs in primary cardiomyocytes. *Journal of molecular and cellular cardiology* (2011).

[190] Jiang, P., and Coller, H. Functional Interactions Between microRNAs and RNA Binding Proteins. *MicroRNA 1*, 1 (2012), 70–79.

[191] Jinek, M., and Doudna, J. a. A three-dimensional view of the molecular machinery of RNA interference. *Nature 457*, 7228 (2009), 405–12.

[192] Jinek, M., Fabian, M. R., Coyle, S. M., Sonenberg, N., and Doudna, J. a. Structural insights into the human GW182-PABC interaction in microRNA-mediated deadenylation. *Nature structural & molecular biology 17*, 2 (2010), 238–40.

[193] Johannes, G., Carter, M. S., Eisen, M. B., Brown, P. O., and Sarnow, P. Identification of eukaryotic mRNAs that are translated at reduced cap

binding complex eIF4F concentrations using a cDNA microarray. *Proceedings of the National Academy of Sciences of the United States of America 96*, 23 (1999), 13118–23.

[194] John, B., Enright, A. J., Aravin, A., Tuschl, T., Sander, C., and Marks, D. S. Human MicroRNA targets. *PLoS biology 2*, 11 (2004), e363.

[195] Johnson, C. D., Esquela-Kerscher, A., Stefani, G., Byrom, M., Kelnar, K., Ovcharenko, D., Wilson, M., Wang, X., Shelton, J., Shingara, J., Chin, L., Brown, D., and Slack, F. J. The let-7 microRNA represses cell proliferation pathways in human cells. *Cancer research 67*, 16 (2007), 7713–22.

[196] Johnson, S. M., Grosshans, H., Shingara, J., Byrom, M., Jarvis, R., Cheng, A., Labourier, E., Reinert, K. L., Brown, D., and Slack, F. J. RAS is regulated by the let-7 microRNA family. *Cell 120*, 5 (2005), 635–47.

[197] Jordan, S. D., Krüger, M., Willmes, D. M., Redemann, N., Wunderlich, F. T., Brönneke, H. S., Merkwirth, C., Kashkar, H., Olkkonen, V. M., Böttger, T., Braun, T., Seibler, J., and Brüning, J. C. Obesity-induced overexpression of miRNA-143 inhibits insulin-stimulated AKT activation and impairs glucose metabolism. *Nature cell biology 13*, 4 (2011), 434–46.

[198] Jungkamp, A.-C., Stoeckius, M., Mecenas, D., Grün, D., Mastrobuoni, G., Kempa, S., and Rajewsky, N. In Vivo and Transcriptome-wide Identification of RNA Binding Protein Target Sites. *Molecular Cell 44*, 5 (2011), 828–840.

[199] Kahvejian, A., Svitkin, Y. V., Sukarieh, R., M'Boutchou, M.-N., and Sonenberg, N. Mammalian poly(A)-binding protein is a eukaryotic translation initiation factor, which acts via multiple mechanisms. *Genes & development 19*, 1 (2005), 104–13.

[200] Kaikkonen, M. U., Lam, M. T. Y., and Glass, C. K. Non-coding RNAs as regulators of gene expression and epigenetics. *Cardiovascular research 90*, 3 (2011), 430–40.

[201] Karginov, F. V., Cheloufi, S., Chong, M. M. W., Stark, A., Smith, A. D., and Hannon, G. J. Diverse endonucleolytic cleavage sites in the mammalian transcriptome depend upon microRNAs, Drosha, and additional nucleases. *Molecular cell 38*, 6 (2010), 781–8.

[202] Karginov, F. V., Conaco, C., Xuan, Z., Schmidt, B. H., Parker, J. S., Mandel, G., and Hannon, G. J. A biochemical approach to identifying microRNA targets. *Proceedings of the National Academy of Sciences of the United States of America 104*, 49 (2007), 19291–6.

[203] Kawamata, T., and Tomari, Y. Making RISC. *Trends in biochemical sciences 35*, 7 (2010), 368–76.

[204] Kedde, M., Strasser, M. J., Boldajipour, B., Oude Vrielink, J. a. F., Slanchev, K., le Sage, C., Nagel, R., Voorhoeve, P. M., van Duijse, J., Ø rom, U. A., Lund, A. H., Perrakis, A., Raz, E., and Agami, R. RNA-binding protein Dnd1 inhibits microRNA access to target mRNA. *Cell 131*, 7 (2007), 1273–86.

[205] Keene, J. D., Komisarow, J. M., and Friedersdorf, M. B. RIP-Chip: the isolation and identification of mRNAs, microRNAs and protein components of ribonucleoprotein complexes from cell extracts. *Nature protocols 1*, 1 (2006), 302–7.

[206] Kemény-Beke, a., Berényi, E., Facskó, a., Damjanovich, J., Horváth, a., Bodnár, a., Berta, a., and Aradi, J. Antiproliferative effect of 4-thiouridylate on OCM-1 uveal melanoma cells. *European journal of ophthalmology 16*, 5 (2006), 680–5.

[207] Kertesz, M., Iovino, N., Unnerstall, U., Gaul, U., and Segal, E. The role of site accessibility in microRNA target recognition. *Nature genetics 39*, 10 (2007), 1278–84.

[208] Khan, A. a., Betel, D., Miller, M. L., Sander, C., Leslie, C. S., and Marks, D. S. Transfection of small RNAs globally perturbs gene regulation by endogenous microRNAs. *Nature biotechnology 27*, 6 (2009), 549–55.

[209] Khorshid, M., Rodak, C., and Zavolan, M. CLIPZ: a database and analysis environment for experimentally determined binding sites of RNA-binding proteins. *Nucleic acids research 39*, Database issue (2011), D245–52.

[210] Khvorova, A., Reynolds, A., and Jayasena, S. D. Functional siRNAs and miRNAs exhibit strand bias. *Cell 115*, 2 (2003), 209–16.

[211] Kim, H. H., Kuwano, Y., Srikantan, S., Lee, E. K., Martindale, J. L., and Gorospe, M. HuR recruits let-7/RISC to repress c-Myc expression. *Genes & development 23*, 15 (2009), 1743–8.

[212] Kim, T.-K., Hemberg, M., Gray, J. M., Costa, A. M., Bear, D. M., Wu, J., Harmin, D. a., Laptewicz, M., Barbara-Haley, K., Kuersten, S., Markenscoff-Papadimitriou, E., Kuhl, D., Bito, H., Worley, P. F., Kreiman, G., and Greenberg, M. E. Widespread transcription at neuronal activity-regulated enhancers. *Nature 465*, 7295 (2010), 182–7.

[213] Kim, V. N. MicroRNA biogenesis: coordinated cropping and dicing. *Nature reviews. Molecular cell biology 6*, 5 (2005), 376–85.

[214] Kim, V. N. Small RNAs just got bigger: Piwi-interacting RNAs (piRNAs) in mammalian testes. *Genes & development 20*, 15 (2006), 1993–7.

[215] Kim, V. N., Han, J., and Siomi, M. C. Biogenesis of small RNAs in animals. *Nature reviews. Molecular cell biology 10*, 2 (2009), 126–39.

[216] Kiriakidou, M., Tan, G. S., Lamprinaki, S., De Planell-Saguer, M., Nelson, P. T., and Mourelatos, Z. An mRNA m7G cap binding-like

motif within human Ago2 represses translation. *Cell 129*, 6 (2007), 1141–51.

[217] KISHORE, S., JASKIEWICZ, L., BURGER, L., HAUSSER, J., KHORSHID, M., AND ZAVOLAN, M. A quantitative analysis of CLIP methods for identifying binding sites of RNA-binding proteins. *Nature methods 8*, 7 (2011), 559–64.

[218] KIVIOJA, T., VÄHÄRAUTIO, A., KARLSSON, K., BONKE, M., ENGE, M., LINNARSSON, S., AND TAIPALE, J. Counting absolute numbers of molecules using unique molecular identifiers. *Nature methods 9*, 1 (2012), 72–4.

[219] KÖNIG, J., MCGLINCY, N. J., AND ULE, J. *Tag-Based Next Generation Sequencing*. Wiley-VCH Verlag GmbH & Co. KGaA, Weinheim, Germany, 2011.

[220] KÖNIG, J., ZARNACK, K., LUSCOMBE, N. M., AND ULE, J. Protein-RNA interactions: new genomic technologies and perspectives. *Nature reviews. Genetics 13*, 2 (2011), 77–83.

[221] KÖNIG, J., ZARNACK, K., ROT, G., CURK, T., KAYIKCI, M., ZUPAN, B., TURNER, D. J., LUSCOMBE, N. M., AND ULE, J. iCLIP reveals the function of hnRNP particles in splicing at individual nucleotide resolution. *Nature Structural & Molecular Biology 17*, 7 (2010), 909–916.

[222] KOZOMARA, A., AND GRIFFITHS-JONES, S. miRBase: integrating microRNA annotation and deep-sequencing data. *Nucleic acids research 39*, Database issue (2011), D152–7.

[223] KREK, A., GRÜN, D., POY, M. N., WOLF, R., ROSENBERG, L., EPSTEIN, E. J., MACMENAMIN, P., DA PIEDADE, I., GUNSALUS, K. C., STOFFEL, M., AND RAJEWSKY, N. Combinatorial microRNA target predictions. *Nature genetics 37*, 5 (2005), 495–500.

[224] KROL, J., LOEDIGE, I., AND FILIPOWICZ, W. The widespread regulation of microRNA biogenesis, function and decay. *Nature reviews. Genetics 11*, 9 (2010), 597–610.

[225] KRUGER, K., GRABOWSKI, P. J., ZAUG, A. J., SANDS, J., GOTTSCHLING, D. E., AND CECH, T. R. Self-splicing RNA: autoexcision and autocyclization of the ribosomal RNA intervening sequence of Tetrahymena. *Cell 31*, 1 (1982), 147–57.

[226] KRÜTZFELDT, J., KUWAJIMA, S., BRAICH, R., RAJEEV, K. G., PENA, J., TUSCHL, T., MANOHARAN, M., AND STOFFEL, M. Specificity, duplex degradation and subcellular localization of antagomirs. *Nucleic acids research 35*, 9 (2007), 2885–92.

[227] KRÜTZFELDT, J., RAJEWSKY, N., BRAICH, R., RAJEEV, K. G., TUSCHL, T., MANOHARAN, M., AND STOFFEL, M. Silencing of microRNAs in vivo with 'antagomirs'. *Nature 438*, 7068 (2005), 685–9.

[228] Kudla, G., Granneman, S., Hahn, D., Beggs, J. D., and Tollervey, D. Cross-linking, ligation, and sequencing of hybrids reveals RNA-RNA interactions in yeast. *Proceedings of the National Academy of Sciences of the United States of America 108*, 24 (2011), 10010–5.

[229] Kumar, A. The silent defense: micro-RNA directed defense against HIV-1 replication. *Retrovirology 4* (2007), 26.

[230] Kuo, M. H., and Allis, C. D. In vivo cross-linking and immunoprecipitation for studying dynamic Protein:DNA associations in a chromatin environment. *Methods (San Diego, Calif.) 19*, 3 (1999), 425–33.

[231] Kuzuoglu-Öztürk, D., Huntzinger, E., Schmidt, S., and Izaurralde, E. The Caenorhabditis elegans GW182 protein AIN-1 interacts with PAB-1 and subunits of the PAN2-PAN3 and CCR4-NOT deadenylase complexes. *Nucleic acids research 40*, 12 (2012), 5651–65.

[232] Kwak, P. B., and Tomari, Y. The N domain of Argonaute drives duplex unwinding during RISC assembly. *Nature structural & molecular biology 19*, 2 (2012), 145–51.

[233] Lagos-Quintana, M., Rauhut, R., Lendeckel, W., and Tuschl, T. Identification of novel genes coding for small expressed RNAs. *Science (New York, N.Y.) 294*, 5543 (2001), 853–8.

[234] Lal, A., Navarro, F., Maher, C. a., Maliszewski, L. E., Yan, N., O'Day, E., Chowdhury, D., Dykxhoorn, D. M., Tsai, P., Hofmann, O., Becker, K. G., Gorospe, M., Hide, W., and Lieberman, J. miR-24 Inhibits cell proliferation by targeting E2F2, MYC, and other cell-cycle genes via binding to "seedless" 3'UTR microRNA recognition elements. *Molecular cell 35*, 5 (2009), 610–25.

[235] Lal, A., Thomas, M. P., Altschuler, G., Navarro, F., O'Day, E., Li, X. L., Concepcion, C., Han, Y.-C., Thiery, J., Rajani, D. K., Deutsch, A., Hofmann, O., Ventura, A., Hide, W., and Lieberman, J. Capture of microRNA-bound mRNAs identifies the tumor suppressor miR-34a as a regulator of growth factor signaling. *PLoS genetics 7*, 11 (2011), e1002363.

[236] Landthaler, M., Gaidatzis, D., Rothballer, A., Chen, P. Y., Soll, S. J., Dinic, L., Ojo, T., Hafner, M., Zavolan, M., and Tuschl, T. Molecular characterization of human Argonaute-containing ribonucleoprotein complexes and their bound target mRNAs. *RNA (New York, N.Y.) 14*, 12 (2008), 2580–96.

[237] Langendorff, O. Untersuchungen am überlebenden Säugethierherzen. *Pflüger, Archiv für die Gesammte Physiologie des Menschen und der Thiere 61*, 6 (1895), 291–332.

[238] Lau, N. C., Lim, L. P., Weinstein, E. G., and Bartel, D. P. An abundant class of tiny RNAs with probable regulatory roles in Caenorhabditis elegans. *Science (New York, N.Y.) 294*, 5543 (2001), 858–62.

[239] LEBEDEVA, S., JENS, M., THEIL, K., SCHWANHÄUSSER, B., SELBACH, M., LANDTHALER, M., AND RAJEWSKY, N. Transcriptome-wide Analysis of Regulatory Interactions of the RNA-Binding Protein HuR. *Molecular cell* (2011).

[240] LEE, R. C., AND AMBROS, V. An extensive class of small RNAs in Caenorhabditis elegans. *Science (New York, N.Y.) 294*, 5543 (2001), 862–4.

[241] LEE, R. C., FEINBAUM, R. L., AND AMBROS, V. The C. elegans heterochronic gene lin-4 encodes small RNAs with antisense complementarity to lin-14. *Cell 75*, 5 (1993), 843–54.

[242] LEE, Y., AHN, C., HAN, J., CHOI, H., KIM, J., YIM, J., LEE, J., PROVOST, P., RÅ DMARK, O., KIM, S., AND KIM, V. N. The nuclear RNase III Drosha initiates microRNA processing. *Nature 425*, 6956 (2003), 415–9.

[243] LEE, Y., HUR, I., PARK, S.-Y., KIM, Y.-K., SUH, M. R., AND KIM, V. N. The role of PACT in the RNA silencing pathway. *The EMBO journal 25*, 3 (2006), 522–32.

[244] LEE, Y., KIM, M., HAN, J., YEOM, K.-H., LEE, S., BAEK, S. H., AND KIM, V. N. MicroRNA genes are transcribed by RNA polymerase II. *The EMBO journal 23*, 20 (2004), 4051–60.

[245] LEUNG, A. K. L., YOUNG, A. G., BHUTKAR, A., ZHENG, G. X., BOSSON, A. D., NIELSEN, C. B., AND SHARP, P. A. Genome-wide identification of Ago2 binding sites from mouse embryonic stem cells with and without mature microRNAs. *Nature structural & molecular biology 18*, 2 (2011), 237–44.

[246] LEWIS, B. P., BURGE, C. B., AND BARTEL, D. P. Conserved seed pairing, often flanked by adenosines, indicates that thousands of human genes are microRNA targets. *Cell 120*, 1 (2005), 15–20.

[247] LEWIS, B. P., SHIH, I.-H., JONES-RHOADES, M. W., BARTEL, D. P., AND BURGE, C. B. Prediction of mammalian microRNA targets. *Cell 115*, 7 (2003), 787–98.

[248] LI, W., ASOKAN, A., WU, Z., VAN DYKE, T., DIPRIMIO, N., JOHNSON, J. S., GOVINDASWAMY, L., AGBANDJE-MCKENNA, M., LEICHTLE, S., REDMOND, D. E., MCCOWN, T. J., PETERMANN, K. B., SHARPLESS, N. E., AND SAMULSKI, R. J. Engineering and selection of shuffled AAV genomes: a new strategy for producing targeted biological nanoparticles. *Molecular therapy : the journal of the American Society of Gene Therapy 16*, 7 (2008), 1252–60.

[249] LIAN, S. L., LI, S., ABADAL, G. X., PAULEY, B. A., FRITZLER, M. J., AND CHAN, E. K. L. The C-terminal half of human Ago2 binds to multiple GW-rich regions of GW182 and requires GW182 to mediate silencing. *RNA (New York, N.Y.) 15*, 5 (2009), 804–13.

[250] LICATALOSI, D. D., AND DARNELL, R. B. RNA processing and its regulation: global insights into biological networks. *Nature reviews. Genetics 11*, 1 (2010), 75–87.

[251] Licatalosi, D. D., Mele, A., Fak, J. J., Ule, J., Kayikci, M., Chi, S. W., Clark, T. a., Schweitzer, A. C., Blume, J. E., Wang, X., Darnell, J. C., and Darnell, R. B. HITS-CLIP yields genome-wide insights into brain alternative RNA processing. *Nature 456*, 7221 (2008), 464–9.

[252] Lim, L. P., Lau, N. C., Garrett-Engele, P., Grimson, A., Schelter, J. M., Castle, J., Bartel, D. P., Linsley, P. S., and Johnson, J. M. Microarray analysis shows that some microRNAs downregulate large numbers of target mRNAs. *Nature 433*, 7027 (2005), 769–73.

[253] Lin, S.-y., Johnson, S. M., Abraham, M., Vella, M. C., Pasquinelli, A., Gamberi, C., Gottlieb, E., and Slack, F. J. The C elegans hunchback homolog, hbl-1, controls temporal patterning and is a probable microRNA target. *Developmental cell 4*, 5 (2003), 639–50.

[254] Lingel, A., Simon, B., Izaurralde, E., and Sattler, M. Nucleic acid 3'-end recognition by the Argonaute2 PAZ domain. *Nature structural & molecular biology 11*, 6 (2004), 576–7.

[255] Linsley, P. S., Schelter, J., Burchard, J., Kibukawa, M., Martin, M. M., Bartz, S. R., Johnson, J. M., Cummins, J. M., Raymond, C. K., Dai, H., Chau, N., Cleary, M., Jackson, A. L., Carleton, M., and Lim, L. Transcripts targeted by the microRNA-16 family cooperatively regulate cell cycle progression. *Molecular and cellular biology 27*, 6 (2007), 2240–52.

[256] Liu, J., Carmell, M. a., Rivas, F. V., Marsden, C. G., Thomson, J. M., Song, J.-J., Hammond, S. M., Joshua-Tor, L., and Hannon, G. J. Argonaute2 is the catalytic engine of mammalian RNAi. *Science (New York, N.Y.) 305*, 5689 (2004), 1437–41.

[257] Liu, N., Bezprozvannaya, S., Williams, A. H., Qi, X., Richardson, J. A., Bassel-Duby, R., and Olson, E. N. microRNA-133a regulates cardiomyocyte proliferation and suppresses smooth muscle gene expression in the heart. *Genes & development 22*, 23 (2008), 3242–54.

[258] Loeb, G. B., Khan, A. a., Canner, D., Hiatt, J. B., Shendure, J., Darnell, R. B., Leslie, C. S., and Rudensky, A. Y. Transcriptome-wide miR-155 binding map reveals widespread noncanonical microRNA targeting. *Molecular cell 48*, 5 (2012), 760–70.

[259] Lohse, M. J., Engelhardt, S., and Eschenhagen, T. What is the role of beta-adrenergic signaling in heart failure? *Circulation research 93*, 10 (2003), 896–906.

[260] Long, D., Lee, R., Williams, P., Chan, C. Y., Ambros, V., and Ding, Y. Potent effect of target structure on microRNA function. *Nature structural & molecular biology 14*, 4 (2007), 287–94.

[261] Lowes, B. D., Minobe, W., Abraham, W. T., Rizeq, M. N., Bohlmeyer, T. J., Quaife, R. A., Roden, R. L., Dutcher, D. L., Robertson, A. D.,

VOELKEL, N. F., BADESCH, D. B., GROVES, B. M., GILBERT, E. M., AND BRISTOW, M. R. Changes in gene expression in the intact human heart. Downregulation of alpha-myosin heavy chain in hypertrophied, failing ventricular myocardium. *The Journal of clinical investigation 100*, 9 (1997), 2315–24.

[262] LU, S., AND CULLEN, B. R. Adenovirus VA1 noncoding RNA can inhibit small interfering RNA and MicroRNA biogenesis. *Journal of virology 78*, 23 (2004), 12868–76.

[263] LUDMAN, A. J., YELLON, D. M., AND HAUSENLOY, D. J. Cardiac preconditioning for ischaemia: lost in translation. *Disease models & mechanisms 3*, 1-2 (2010), 35–8.

[264] LUND, E., AND DAHLBERG, J. E. Substrate selectivity of exportin 5 and Dicer in the biogenesis of microRNAs. *Cold Spring Harbor symposia on quantitative biology 71* (2006), 59–66.

[265] MA, J.-B., YE, K., AND PATEL, D. J. Structural basis for overhang-specific small interfering RNA recognition by the PAZ domain. *Nature 429*, 6989 (2004), 318–22.

[266] MACK, G. S. MicroRNA gets down to business. *Nature biotechnology 25*, 6 (2007), 631–8.

[267] MACRAE, I. J., MA, E., ZHOU, M., ROBINSON, C. V., AND DOUDNA, J. A. In vitro reconstitution of the human RISC-loading complex. *Proceedings of the National Academy of Sciences of the United States of America 105*, 2 (2008), 512–7.

[268] MANIATAKI, E., AND MOURELATOS, Z. A human, ATP-independent, RISC assembly machine fueled by pre-miRNA. *Genes & development 19*, 24 (2005), 2979–90.

[269] MARCHLER-BAUER, A., LU, S., ANDERSON, J. B., CHITSAZ, F., DERBYSHIRE, M. K., DEWEESE-SCOTT, C., FONG, J. H., GEER, L. Y., GEER, R. C., GONZALES, N. R., GWADZ, M., HURWITZ, D. I., JACKSON, J. D., KE, Z., LANCZYCKI, C. J., LU, F., MARCHLER, G. H., MULLOKANDOV, M., OMELCHENKO, M. V., ROBERTSON, C. L., SONG, J. S., THANKI, N., YAMASHITA, R. A., ZHANG, D., ZHANG, N., ZHENG, C., AND BRYANT, S. H. CDD: a Conserved Domain Database for the functional annotation of proteins. *Nucleic acids research 39*, Database issue (2011), D225–9.

[270] MARTIN, K. C., AND EPHRUSSI, A. mRNA localization: gene expression in the spatial dimension. *Cell 136*, 4 (2009), 719–30.

[271] MATICZKA, D., LANGE, S. J., COSTA, F., AND BACKOFEN, R. GraphProt: modeling binding preferences of RNA-binding proteins. *Genome Biology 15*, 1 (2014), R17.

[272] MATTICK, J. S. Non-coding RNAs: the architects of eukaryotic complexity. *EMBO reports 2*, 11 (2001), 986–91.

[273] McKinsey, T. A., and Olson, E. N. Toward transcriptional therapies for the failing heart: chemical screens to modulate genes. *The Journal of clinical investigation 115*, 3 (2005), 538–46.

[274] Meisenheimer, K. M., Meisenheimer, P. L., and Koch, T. H. Nucleoprotein photo-cross-linking using halopyrimidine-substituted RNAs. *Methods in enzymology 318* (2000), 88–104.

[275] Meister, G. Argonaute proteins: functional insights and emerging roles. *Nature Reviews Genetics*, June (2013).

[276] Meister, G., Landthaler, M., Patkaniowska, A., Dorsett, Y., Teng, G., and Tuschl, T. Human Argonaute2 mediates RNA cleavage targeted by miRNAs and siRNAs. *Molecular cell 15*, 2 (2004), 185–97.

[277] Meister, G., Landthaler, M., Peters, L., Chen, P. Y., Urlaub, H., Lührmann, R., and Tuschl, T. Identification of novel argonaute-associated proteins. *Current biology : CB 15*, 23 (2005), 2149–55.

[278] Meister, G., and Tuschl, T. Mechanisms of gene silencing by double-stranded RNA. *Nature 431*, 7006 (2004), 343–9.

[279] Melvin, W. T., Milne, H. B., Slater, a. a., Allen, H. J., and Keir, H. M. Incorporation of 6-thioguanosine and 4-thiouridine into RNA. Application to isolation of newly synthesised RNA by affinity chromatography. *European journal of biochemistry / FEBS 92*, 2 (1978), 373–9.

[280] Memczak, S., Jens, M., Elefsinioti, A., Torti, F., Krueger, J., Rybak, A., Maier, L., Mackowiak, S. D., Gregersen, L. H., Munschauer, M., Loewer, A., Ziebold, U., Landthaler, M., Kocks, C., le Noble, F., and Rajewsky, N. Circular RNAs are a large class of animal RNAs with regulatory potency. *Nature 495*, 7441 (2013), 333–8.

[281] Milek, M., Wyler, E., and Landthaler, M. Transcriptome-wide analysis of protein-RNA interactions using high-throughput sequencing. *Seminars in cell & developmental biology 23*, 2 (2011), 206–212.

[282] Mili, S., and Steitz, J. a. Evidence for reassociation of RNA-binding proteins after cell lysis: implications for the interpretation of immunoprecipitation analyses. *RNA (New York, N.Y.) 10*, 11 (2004), 1692–4.

[283] Miller, M. R., Robinson, K. J., Cleary, M. D., and Doe, C. Q. TU-tagging: cell type-specific RNA isolation from intact complex tissues. *Nature methods 6*, 6 (2009), 439–41.

[284] Miranda, K. C., Huynh, T., Tay, Y., Ang, Y.-S., Tam, W.-L., Thomson, A. M., Lim, B., and Rigoutsos, I. A pattern-based method for the identification of MicroRNA binding sites and their corresponding heteroduplexes. *Cell 126*, 6 (2006), 1203–17.

[285] Mishima, Y., Giraldez, A. J., Takeda, Y., Fujiwara, T., Sakamoto, H., Schier, A. F., and Inoue, K. Differential regulation of germline mRNAs

in soma and germ cells by zebrafish miR-430. *Current biology : CB 16*, 21 (2006), 2135–42.

[286] MODZELEWSKI, A. J., HOLMES, R. J., HILZ, S., GRIMSON, A., AND COHEN, P. E. AGO4 regulates entry into meiosis and influences silencing of sex chromosomes in the male mouse germline. *Developmental cell 23*, 2 (2012), 251–64.

[287] MOFFAT, J., AND SABATINI, D. M. Building mammalian signalling pathways with RNAi screens. *Nature reviews. Molecular cell biology 7*, 3 (2006), 177–87.

[288] MOLKENTIN, J. D., LU, J. R., ANTOS, C. L., MARKHAM, B., RICHARDSON, J., ROBBINS, J., GRANT, S. R., AND OLSON, E. N. A calcineurin-dependent transcriptional pathway for cardiac hypertrophy. *Cell 93*, 2 (1998), 215–28.

[289] MONTGOMERY, R. L., HULLINGER, T. G., SEMUS, H. M., DICKINSON, B. A., SETO, A. G., LYNCH, J. M., STACK, C., LATIMER, P. A., OLSON, E. N., AND VAN ROOIJ, E. Therapeutic inhibition of miR-208a improves cardiac function and survival during heart failure. *Circulation 124*, 14 (2011), 1537–47.

[290] MOORE, M. J., AND PROUDFOOT, N. J. Pre-mRNA processing reaches back to transcription and ahead to translation. *Cell 136*, 4 (2009), 688–700.

[291] MOORE, M. J., ZHANG, C., GANTMAN, E. C., MELE, A., DARNELL, J. C., AND DARNELL, R. B. Mapping Argonaute and conventional RNA-binding protein interactions with RNA at single-nucleotide resolution using HITS-CLIP and CIMS analysis. *Nature protocols 9*, 2 (2014), 263–93.

[292] MORETTI, F., KAISER, C., ZDANOWICZ-SPECHT, A., AND HENTZE, M. W. PABP and the poly(A) tail augment microRNA repression by facilitated miRISC binding. *Nature structural & molecular biology 19*, 6 (2012), 603–8.

[293] MOSMANN, T. Rapid colorimetric assay for cellular growth and survival: application to proliferation and cytotoxicity assays. *Journal of immunological methods 65*, 1-2 (1983), 55–63.

[294] MOSS, E. G., LEE, R. C., AND AMBROS, V. The cold shock domain protein LIN-28 controls developmental timing in C. elegans and is regulated by the lin-4 RNA. *Cell 88*, 5 (1997), 637–46.

[295] MUKHERJEE, N., CORCORAN, D. L., NUSBAUM, J. D., REID, D. W., GEORGIEV, S., HAFNER, M., ASCANO, M., TUSCHL, T., OHLER, U., AND KEENE, J. D. Integrative Regulatory Mapping Indicates that the RNA-Binding Protein HuR Couples Pre-mRNA Processing and mRNA Stability. *Molecular cell 43*, 3 (2011), 327–339.

[296] MUKHERJI, S., EBERT, M. S., ZHENG, G. X. Y., TSANG, J. S., SHARP, P. A., AND VAN OUDENAARDEN, A. MicroRNAs can generate thresholds in target gene expression. *Nature genetics 43*, 9 (2011), 854–9.

[297] Munschauer, M., Schueler, M., Dieterich, C., and Landthaler, M. High-resolution profiling of protein occupancy on polyadenylated RNA transcripts. *Methods (San Diego, Calif.)* (2013).

[298] Nag, A. C. Study of non-muscle cells of the adult mammalian heart: a fine structural analysis and distribution. *Cytobios 28*, 109 (1980), 41–61.

[299] Nakanishi, K., Weinberg, D. E., Bartel, D. P., and Patel, D. J. Structure of yeast Argonaute with guide RNA. *Nature 486*, 7403 (2012), 368–74.

[300] Nakao, K., Minobe, W., Roden, R., Bristow, M. R., and Leinwand, L. a. Myosin heavy chain gene expression in human heart failure. *The Journal of clinical investigation 100*, 9 (1997), 2362–70.

[301] Napoli, C., Lemieux, C., and Jorgensen, R. Introduction of a Chimeric Chalcone Synthase Gene into Petunia Results in Reversible Co-Suppression of Homologous Genes in trans. *The Plant cell 2*, 4 (1990), 279–289.

[302] Nielsen, C. B., Shomron, N., Sandberg, R., Hornstein, E., Kitzman, J., and Burge, C. B. Determinants of targeting by endogenous and exogenous microRNAs and siRNAs. *RNA (New York, N.Y.) 13*, 11 (2007), 1894–910.

[303] Niu, Z., Li, A., Zhang, S. X., and Schwartz, R. J. Serum response factor micromanaging cardiogenesis. *Current opinion in cell biology 19*, 6 (2007), 618–27.

[304] Noland, C. L., Ma, E., and Doudna, J. a. siRNA repositioning for guide strand selection by human Dicer complexes. *Molecular cell 43*, 1 (2011), 110–21.

[305] Nolde, M. J., Saka, N., Reinert, K. L., and Slack, F. J. The Caenorhabditis elegans pumilio homolog, puf-9, is required for the 3'UTR-mediated repression of the let-7 microRNA target gene, hbl-1. *Developmental biology 305*, 2 (2007), 551–63.

[306] Nottrott, S., Simard, M. J., and Richter, J. D. Human let-7a miRNA blocks protein production on actively translating polyribosomes. *Nature structural & molecular biology 13*, 12 (2006), 1108–14.

[307] Ø rom, U. A., Derrien, T., Beringer, M., Gumireddy, K., Gardini, A., Bussotti, G., Lai, F., Zytnicki, M., Notredame, C., Huang, Q., Guigo, R., and Shiekhattar, R. Long noncoding RNAs with enhancer-like function in human cells. *Cell 143*, 1 (2010), 46–58.

[308] O'Carroll, D., Mecklenbrauker, I., Das, P. P., Santana, A., Koenig, U., Enright, A. J., Miska, E. a., and Tarakhovsky, A. A Slicer-independent role for Argonaute 2 in hematopoiesis and the microRNA pathway. *Genes & development 21*, 16 (2007), 1999–2004.

[309] O'Connell, T., Ni, Y., Lin, K., Han, H., and Yan, Z. Isolation and Culture of Adult Mouse Cardiac Myocytes for Signaling Studies. *AfCS Research Reports 1*, 5 (2003), 1–9.

[310] Olsen, P. H., and Ambros, V. The lin-4 regulatory RNA controls developmental timing in Caenorhabditis elegans by blocking LIN-14 protein synthesis after the initiation of translation. *Developmental biology 216*, 2 (1999), 671–80.

[311] Ono, K., Kuwabara, Y., and Han, J. MicroRNAs and cardiovascular diseases. *The FEBS journal 278*, 10 (2011), 1619–33.

[312] Pacak, C. a., Mah, C. S., Thattaliyath, B. D., Conlon, T. J., Lewis, M. a., Cloutier, D. E., Zolotukhin, I., Tarantal, A. F., and Byrne, B. J. Recombinant adeno-associated virus serotype 9 leads to preferential cardiac transduction in vivo. *Circulation research 99*, 4 (2006), e3–9.

[313] Pace, C. N., Heinemann, U., Hahn, U., and Saenger, W. Ribonuclease T1: Struktur, Funktion und Stabilität. *Angewandte Chemie 103*, 4 (1991), 351–369.

[314] Pan, Q., Shai, O., Lee, L. J., Frey, B. J., and Blencowe, B. J. Deep surveying of alternative splicing complexity in the human transcriptome by high-throughput sequencing. *Nature genetics 40*, 12 (2008), 1413–5.

[315] Papadopoulos, G. L., Reczko, M., Simossis, V. a., Sethupathy, P., and Hatzigeorgiou, A. G. The database of experimentally supported targets: a functional update of TarBase. *Nucleic acids research 37*, Database issue (2009), D155–8.

[316] Parker, J. S., Roe, S. M., and Barford, D. Structural insights into mRNA recognition from a PIWI domain-siRNA guide complex. *Nature 434*, 7033 (2005), 663–6.

[317] Parker, R., and Sheth, U. P bodies and the control of mRNA translation and degradation. *Molecular cell 25*, 5 (2007), 635–46.

[318] Parker, R., and Song, H. The enzymes and control of eukaryotic mRNA turnover. *Nature structural & molecular biology 11*, 2 (2004), 121–7.

[319] Pasquinelli, A. E. MicroRNAs and their targets: recognition, regulation and an emerging reciprocal relationship. *Nature reviews. Genetics 13*, 4 (2012), 271–82.

[320] Pasquinelli, a. E., Reinhart, B. J., Slack, F., Martindale, M. Q., Kuroda, M. I., Maller, B., Hayward, D. C., Ball, E. E., Degnan, B., Müller, P., Spring, J., Srinivasan, a., Fishman, M., Finnerty, J., Corbo, J., Levine, M., Leahy, P., Davidson, E., and Ruvkun, G. Conservation of the sequence and temporal expression of let-7 heterochronic regulatory RNA. *Nature 408*, 6808 (2000), 86–9.

[321] Pedersen, I. M., Cheng, G., Wieland, S., Volinia, S., Croce, C. M., Chisari, F. V., and David, M. Interferon modulation of cellular microRNAs as an antiviral mechanism. *Nature 449*, 7164 (2007), 919–22.

[322] Peters, L., and Meister, G. Argonaute proteins: mediators of RNA silencing. *Molecular cell 26*, 5 (2007), 611–23.

[323] Petersen, C. P., Bordeleau, M.-E., Pelletier, J., and Sharp, P. a. Short RNAs repress translation after initiation in mammalian cells. *Molecular cell 21*, 4 (2006), 533–42.

[324] Petri, S., Dueck, A., Lehmann, G., Putz, N., Rüdel, S., Kremmer, E., and Meister, G. Increased siRNA duplex stability correlates with reduced off-target and elevated on-target effects. *RNA (New York, N.Y.) 17*, 4 (2011), 737–49.

[325] Piñol Roma, S., Adam, S. A., Choi, Y. D., and Dreyfuss, G. Ultraviolet-induced cross-linking of RNA to proteins in vivo. *Methods in enzymology 180*, 1981 (1989), 410–8.

[326] Pillai, R. S., Artus, C. G., and Filipowicz, W. Tethering of human Ago proteins to mRNA mimics the miRNA-mediated repression of protein synthesis. *RNA (New York, N.Y.) 10*, 10 (2004), 1518–25.

[327] Pillai, R. S., Bhattacharyya, S. N., Artus, C. G., Zoller, T., Cougot, N., Basyuk, E., Bertrand, E., and Filipowicz, W. Inhibition of translational initiation by Let-7 MicroRNA in human cells. *Science (New York, N.Y.) 309*, 5740 (2005), 1573–6.

[328] Pinder, B. D., and Smibert, C. a. microRNA-independent recruitment of Argonaute 1 to nanos mRNA through the Smaug RNA-binding protein. *EMBO reports*, November (2012), 1–7.

[329] Ponting, C. P., Oliver, P. L., and Reik, W. Evolution and functions of long noncoding RNAs. *Cell 136*, 4 (2009), 629–41.

[330] Powell, T., and Twist, V. W. A rapid technique for the isolation and purification of adult cardiac muscle cells having respiratory control and a tolerance to calcium. *Biochemical and biophysical research communications 72*, 1 (1976), 327–33.

[331] R Core Team. R: A Language and Environment for Statistical Computing, 2013.

[332] Rabani, M., Levin, J. Z., Fan, L., Adiconis, X., Raychowdhury, R., Garber, M., Gnirke, A., Nusbaum, C., Hacohen, N., Friedman, N., Amit, I., and Regev, A. Metabolic labeling of RNA uncovers principles of RNA production and degradation dynamics in mammalian cells. *Nature biotechnology 29*, 5 (2011), 436–42.

[333] Rajewsky, N., and Socci, N. D. Computational identification of microRNA targets. *Developmental biology 267*, 2 (2004), 529–35.

[334] Rao, P. K., Toyama, Y., Chiang, H. R., Gupta, S., Bauer, M., Medvid, R., Reinhardt, F., Liao, R., Krieger, M., Jaenisch, R., Lodish, H. F., and Blelloch, R. Loss of cardiac microRNA-mediated regulation leads to dilated cardiomyopathy and heart failure. *Circulation research 105*, 6 (2009), 585–94.

[335] Reczko, M., Maragkakis, M., Alexiou, P., Grosse, I., and Hatzigeorgiou, A. G. Functional microRNA targets in protein coding sequences. *Bioinformatics (Oxford, England) 28*, 6 (2012), 771–6.

[336] Rehmsmeier, M., Steffen, P., Hochsmann, M., and Giegerich, R. Fast and effective prediction of microRNA/target duplexes. *RNA (New York, N.Y.) 10*, 10 (2004), 1507–17.

[337] Rehwinkel, J., Natalin, P., Stark, A., Brennecke, J., Cohen, S. M., and Izaurralde, E. Genome-wide analysis of mRNAs regulated by Drosha and Argonaute proteins in Drosophila melanogaster. *Molecular and cellular biology 26*, 8 (2006), 2965–75.

[338] Reinhart, B. J., Slack, F. J., Basson, M., Pasquinelli, a. E., Bettinger, J. C., Rougvie, a. E., Horvitz, H. R., and Ruvkun, G. The 21-nucleotide let-7 RNA regulates developmental timing in Caenorhabditis elegans. *Nature 403*, 6772 (2000), 901–6.

[339] Ren, X.-P., Wu, J., Wang, X., Sartor, M. a., Qian, J., Jones, K., Nicolaou, P., Pritchard, T. J., and Fan, G.-C. MicroRNA-320 is involved in the regulation of cardiac ischemia/reperfusion injury by targeting heat-shock protein 20. *Circulation 119*, 17 (2009), 2357–66.

[340] Riley, K. J., Rabinowitz, G. S., Yario, T. a., Luna, J. M., Darnell, R. B., and Steitz, J. a. EBV and human microRNAs co-target oncogenic and apoptotic viral and human genes during latency. *The EMBO journal 31*, 9 (2012), 2207–21.

[341] Rinck, A., Preusse, M., Laggerbauer, B., Lickert, H., Engelhardt, S., and Theis, F. J. The human transcriptome is enriched for miRNA-binding sites located in cooperativity-permitting distance. *RNA biology 10*, 7 (2013), 1125–35.

[342] Ritchie, W., Flamant, S., and Rasko, J. E. J. Predicting microRNA targets and functions: traps for the unwary. *Nature methods 6*, 6 (2009), 397–8.

[343] Ritchie, W., Flamant, S., and Rasko, J. E. J. mimiRNA: a microRNA expression profiler and classification resource designed to identify functional correlations between microRNAs and their targets. *Bioinformatics (Oxford, England) 26*, 2 (2010), 223–7.

[344] Robb, G. B., and Rana, T. M. RNA helicase A interacts with RISC in human cells and functions in RISC loading. *Molecular cell 26*, 4 (2007), 523–37.

[345] Rohr, S. Cardiac fibroblasts in cell culture systems: myofibroblasts all along? *Journal of cardiovascular pharmacology 57*, 4 (2011), 389–99.

[346] Rouskin, S., Zubradt, M., Washietl, S., Kellis, M., and Weissman, J. S. Genome-wide probing of RNA structure reveals active unfolding of mRNA structures in vivo. *Nature* (2013).

[347] Ruby, J. G., Jan, C. H., and Bartel, D. P. Intronic microRNA precursors that bypass Drosha processing. *Nature 448*, 7149 (2007), 83–6.

[348] Rüdel, S., Flatley, A., Weinmann, L., Kremmer, E., and Meister, G. A multifunctional human Argonaute2-specific monoclonal antibody. *RNA (New York, N.Y.) 14*, 6 (2008), 1244–53.

[349] Ruepp, A., Kowarsch, A., Schmidl, D., Buggenthin, F., Brauner, B., Dunger, I., Fobo, G., Frishman, G., Montrone, C., and Theis, F. J. PhenomiR: a knowledgebase for microRNA expression in diseases and biological processes. *Genome biology 11*, 1 (2010), R6.

[350] Saetrom, P. l., Heale, B. S. E., Snø ve, O., Aagaard, L., Alluin, J., and Rossi, J. J. Distance constraints between microRNA target sites dictate efficacy and cooperativity. *Nucleic acids research 35*, 7 (2007), 2333–42.

[351] Saini, H. K., Griffiths-Jones, S., and Enright, A. J. Genomic analysis of human microRNA transcripts. *Proceedings of the National Academy of Sciences of the United States of America 104*, 45 (2007), 17719–24.

[352] Salzman, J., Chen, R. E., Olsen, M. N., Wang, P. L., and Brown, P. O. Cell-type specific features of circular RNA expression. *PLoS genetics 9*, 9 (2013), e1003777.

[353] Salzman, J., Gawad, C., Wang, P. L., Lacayo, N., and Brown, P. O. Circular RNAs are the predominant transcript isoform from hundreds of human genes in diverse cell types. *PloS one 7*, 2 (2012), e30733.

[354] Sayed, D., Hong, C., Chen, I.-Y., Lypowy, J., and Abdellatif, M. MicroRNAs play an essential role in the development of cardiac hypertrophy. *Circulation research 100*, 3 (2007), 416–24.

[355] Sayed, D., Rane, S., Lypowy, J., He, M., Chen, I.-Y., Vashistha, H., Yan, L., Malhotra, A., Vatner, D., and Abdellatif, M. MicroRNA-21 targets Sprouty2 and promotes cellular outgrowths. *Molecular biology of the cell 19*, 8 (2008), 3272–82.

[356] Schadt, E. E., Turner, S., and Kasarskis, A. A window into third-generation sequencing. *Human molecular genetics 19*, R2 (2010), R227–40.

[357] Schirle, N. T., and MacRae, I. J. The crystal structure of human Argonaute2. *Science (New York, N.Y.) 336*, 6084 (2012), 1037–40.

[358] Schmitter, D., Filkowski, J., Sewer, A., Pillai, R. S., Oakeley, E. J., Zavolan, M., Svoboda, P., and Filipowicz, W. Effects of Dicer and Argonaute down-regulation on mRNA levels in human HEK293 cells. *Nucleic acids research 34*, 17 (2006), 4801–15.

[359] Schueler, M., Munschauer, M., Gregersen, L. H., Finzel, A., Loewer, A., Chen, W., Landthaler, M., and Dieterich, C. Differential protein occupancy profiling of the mRNA transcriptome. *Genome biology 15*, 1 (2014), R15.

[360] Schug, J., McKenna, L. B., Walton, G., Hand, N., Mukherjee, S., Essuman, K., Shi, Z., Gao, Y., Markley, K., Nakagawa, M., Kameswaran, V., Vourekas, A., Friedman, J. R., Kaestner, K. H., and Greenbaum, L. E. Dynamic recruitment of microRNAs to their mRNA targets in the regenerating liver. *BMC genomics 14* (2013), 264.

[361] Schwanhäusser, B., Busse, D., Li, N., Dittmar, G., Schuchhardt, J., Wolf, J., Chen, W., and Selbach, M. Global quantification of mammalian gene expression control. *Nature 473*, 7347 (2011), 337–42.

[362] Schwarz, D. S., Hutvágner, G., Du, T., Xu, Z., Aronin, N., and Zamore, P. D. Asymmetry in the assembly of the RNAi enzyme complex. *Cell 115*, 2 (2003), 199–208.

[363] Scott, M. S., and Ono, M. From snoRNA to miRNA: Dual function regulatory non-coding RNAs. *Biochimie 93*, 11 (2011), 1987–92.

[364] Selbach, M., Schwanhäusser, B., Thierfelder, N., Fang, Z., Khanin, R., and Rajewsky, N. Widespread changes in protein synthesis induced by microRNAs. *Nature 455*, 7209 (2008), 58–63.

[365] Shahi, P., Loukianiouk, S., Bohne-Lang, A., Kenzelmann, M., Küffer, S., Maertens, S., Eils, R., Gröne, H.-J., Gretz, N., and Brors, B. Argonaute–a database for gene regulation by mammalian microRNAs. *Nucleic acids research 34*, Database issue (2006), D115–8.

[366] Shin, C., Nam, J.-W., Farh, K. K.-H., Chiang, H. R., Shkumatava, A., and Bartel, D. P. Expanding the microRNA targeting code: functional sites with centered pairing. *Molecular cell 38*, 6 (2010), 789–802.

[367] Siddharthan, R., Siggia, E. D., and van Nimwegen, E. PhyloGibbs: a Gibbs sampling motif finder that incorporates phylogeny. *PLoS computational biology 1*, 7 (2005), e67.

[368] Sievers, C., Schlumpf, T., Sawarkar, R., Comoglio, F., and Paro, R. Mixture models and wavelet transforms reveal high confidence RNA-protein interaction sites in MOV10 PAR-CLIP data. *Nucleic acids research 40*, 20 (2012), e160.

[369] Silverman, I. M., Li, F., Alexander, A., Goff, L., Trapnell, C., Rinn, J. L., and Gregory, B. D. RNase-mediated protein footprint sequencing reveals protein-binding sites throughout the human transcriptome. *Genome biology 15*, 1 (2014), R3.

[370] Simon, B., Kirkpatrick, J. P., Eckhardt, S., Reuter, M., Rocha, E. a., Andrade-Navarro, M. a., Sehr, P., Pillai, R. S., and Carlomagno, T. Recognition of 2'-O-methylated 3'-end of piRNA by the PAZ domain of a Piwi protein. *Structure (London, England : 1993) 19*, 2 (2011), 172–80.

[371] Siomi, H., and Siomi, M. C. On the road to reading the RNA-interference code. *Nature 457*, 7228 (2009), 396–404.

[372] Siomi, M. C., Sato, K., Pezic, D., and Aravin, A. a. PIWI-interacting small RNAs: the vanguard of genome defence. *Nature reviews. Molecular cell biology 12*, 4 (2011), 246–58.

[373] Skalsky, R. L., Corcoran, D. L., Gottwein, E., Frank, C. L., Kang, D., Hafner, M., Nusbaum, J. D., Feederle, R., Delecluse, H.-J., Luftig, M. a., Tuschl, T., Ohler, U., and Cullen, B. R. The viral and cellular microRNA targetome in lymphoblastoid cell lines. *PLoS pathogens 8*, 1 (2012), e1002484.

[374] Slack, F. J., Basson, M., Liu, Z., Ambros, V., Horvitz, H. R., and Ruvkun, G. The lin-41 RBCC gene acts in the C. elegans heterochronic pathway between the let-7 regulatory RNA and the LIN-29 transcription factor. *Molecular cell 5*, 4 (2000), 659–69.

[375] Soifer, H. S., Rossi, J. J., and Saetrom, P. l. MicroRNAs in disease and potential therapeutic applications. *Molecular therapy : the journal of the American Society of Gene Therapy 15*, 12 (2007), 2070–9.

[376] Sonenberg, N., and Hinnebusch, A. G. Regulation of translation initiation in eukaryotes: mechanisms and biological targets. *Cell 136*, 4 (2009), 731–45.

[377] Song, J.-J., Smith, S. K., Hannon, G. J., and Joshua-Tor, L. Crystal structure of Argonaute and its implications for RISC slicer activity. *Science (New York, N.Y.) 305*, 5689 (2004), 1434–7.

[378] Song, R., Hennig, G. W., Wu, Q., Jose, C., Zheng, H., and Yan, W. Male germ cells express abundant endogenous siRNAs. *Proceedings of the National Academy of Sciences of the United States of America 108*, 32 (2011), 13159–64.

[379] Srikantan, S., Tominaga, K., and Gorospe, M. Functional interplay between RNA-binding protein HuR and microRNAs. *Current protein & peptide science 13*, 4 (2012), 372–9.

[380] Stark, A., Brennecke, J., Bushati, N., Russell, R. B., and Cohen, S. M. Animal MicroRNAs confer robustness to gene expression and have a significant impact on 3'UTR evolution. *Cell 123*, 6 (2005), 1133–46.

[381] Su, H., Meng, S., Lu, Y., Trombly, M. I., Chen, J., Lin, C., Turk, A., and Wang, X. Mammalian hyperplastic discs homolog EDD regulates miRNA-mediated gene silencing. *Molecular cell 43*, 1 (2011), 97–109.

[382] Su, H., Trombly, M. I., Chen, J., and Wang, X. Essential and overlapping functions for mammalian Argonautes in microRNA silencing. *Genes & development 23*, 3 (2009), 304–17.

[383] Suárez, Y., Fernández-Hernando, C., Yu, J., Gerber, S. a., Harrison, K. D., Pober, J. S., Iruela-Arispe, M. L., Merkenschlager, M., and Sessa, W. C. Dicer-dependent endothelial microRNAs are necessary for postnatal angiogenesis. *Proceedings of the National Academy of Sciences of the United States of America 105*, 37 (2008), 14082–7.

[384] Sugimoto, Y., König, J., Hussain, S., Zupan, B. ., Curk, T. ., Frye, M., and Ule, J. Analysis of CLIP and iCLIP methods for nucleotide-resolution studies of protein-RNA interactions. *Genome biology 13*, 8 (2012), R67.

[385] Taft, R. J., Glazov, E. A., Lassmann, T., Hayashizaki, Y., Carninci, P., and Mattick, J. S. Small RNAs derived from snoRNAs. *RNA (New York, N.Y.) 15*, 7 (2009), 1233–40.

[386] Takimoto, K., Wakiyama, M., and Yokoyama, S. Mammalian GW182 contains multiple Argonaute-binding sites and functions in microRNA-mediated translational repression. *RNA (New York, N.Y.) 15*, 6 (2009), 1078–89.

[387] Tam, O. H., Aravin, A. a., Stein, P., Girard, A., Murchison, E. P., Cheloufi, S., Hodges, E., Anger, M., Sachidanandam, R., Schultz, R. M., and Hannon, G. J. Pseudogene-derived small interfering RNAs regulate gene expression in mouse oocytes. *Nature 453*, 7194 (2008), 534–8.

[388] Tatsuguchi, M., Seok, H. Y., Callis, T. E., Thomson, J. M., Chen, J.-F., Newman, M., Rojas, M., Hammond, S. M., and Wang, D.-Z. Expression of microRNAs is dynamically regulated during cardiomyocyte hypertrophy. *Journal of molecular and cellular cardiology 42*, 6 (2007), 1137–41.

[389] Tay, Y., Zhang, J., Thomson, A. M., Lim, B., and Rigoutsos, I. MicroRNAs to Nanog, Oct4 and Sox2 coding regions modulate embryonic stem cell differentiation. *Nature 455*, 7216 (2008), 1124–8.

[390] Tenenbaum, S. a., Carson, C. C., Lager, P. J., and Keene, J. D. Identifying mRNA subsets in messenger ribonucleoprotein complexes by using cDNA arrays. *Proceedings of the National Academy of Sciences of the United States of America 97*, 26 (2000), 14085–90.

[391] Thomas, M., Lieberman, J., and Lal, A. Desperately seeking microRNA targets. *Nature structural & molecular biology 17*, 10 (2010), 1169–74.

[392] Thum, T., and Borlak, J. Isolation and cultivation of Ca2+ tolerant cardiomyocytes from the adult rat: improvements and applications. *Xenobiotica; the fate of foreign compounds in biological systems 30*, 11 (2000), 1063–77.

[393] Thum, T., Chau, N., Bhat, B., Gupta, S. K., Linsley, P. S., Bauersachs, J., and Engelhardt, S. Comparison of different miR-21 inhibitor chemistries in a cardiac disease model. *The Journal of clinical investigation 121*, 2 (2011), 461–2; author reply 462–3.

[394] Thum, T., Galuppo, P., Wolf, C., Fiedler, J., Kneitz, S., van Laake, L. W., Doevendans, P. a., Mummery, C. L., Borlak, J., Haverich, A., Gross, C.,

Engelhardt, S., Ertl, G., and Bauersachs, J. MicroRNAs in the human heart: a clue to fetal gene reprogramming in heart failure. *Circulation 116*, 3 (2007), 258–67.

[395] Thum, T., Gross, C., Fiedler, J., Fischer, T., Kissler, S., Bussen, M., Galuppo, P., Just, S., Rottbauer, W., Frantz, S., Castoldi, M., Soutschek, J., Koteliansky, V., Rosenwald, A., Basson, M. A., Licht, J. D., Pena, J. T. R., Rouhanifard, S. H., Muckenthaler, M. U., Tuschl, T., Martin, G. R., Bauersachs, J., and Engelhardt, S. MicroRNA-21 contributes to myocardial disease by stimulating MAP kinase signalling in fibroblasts. *Nature 456*, 7224 (2008), 980–4.

[396] Tian, B., Hu, J., Zhang, H., and Lutz, C. S. A large-scale analysis of mRNA polyadenylation of human and mouse genes. *Nucleic acids research 33*, 1 (2005), 201–12.

[397] Till, S., Lejeune, E., Thermann, R., Bortfeld, M., Hothorn, M., Enderle, D., Heinrich, C., Hentze, M. W., and Ladurner, A. G. A conserved motif in Argonaute-interacting proteins mediates functional interactions through the Argonaute PIWI domain. *Nature structural & molecular biology 14*, 10 (2007), 897–903.

[398] Tolia, N. H., and Joshua-Tor, L. Slicer and the argonautes. *Nature chemical biology 3*, 1 (2007), 36–43.

[399] Trapnell, C., Pachter, L., and Salzberg, S. L. TopHat: discovering splice junctions with RNA-Seq. *Bioinformatics (Oxford, England) 25*, 9 (2009), 1105–11.

[400] Ule, J., Jensen, K., Mele, A., and Darnell, R. B. CLIP: a method for identifying protein-RNA interaction sites in living cells. *Methods (San Diego, Calif.) 37*, 4 (2005), 376–86.

[401] Ule, J., Jensen, K. B., Ruggiu, M., Mele, A., Ule, A., and Darnell, R. B. CLIP identifies Nova-regulated RNA networks in the brain. *Science (New York, N.Y.) 302*, 5648 (2003), 1212–5.

[402] Urlaub, H., Hartmuth, K., and Lührmann, R. A two-tracked approach to analyze RNA-protein crosslinking sites in native, nonlabeled small nuclear ribonucleoprotein particles. *Methods (San Diego, Calif.) 26*, 2 (2002), 170–81.

[403] Valadi, H., Ekström, K., Bossios, A., Sjöstrand, M., Lee, J. J., and Lötvall, J. O. Exosome-mediated transfer of mRNAs and microRNAs is a novel mechanism of genetic exchange between cells. *Nature cell biology 9*, 6 (2007), 654–9.

[404] van Rooij, E., and Olson, E. N. MicroRNA therapeutics for cardiovascular disease: opportunities and obstacles. *Nature reviews. Drug discovery 11*, 11 (2012), 860–72.

[405] van Rooij, E., Quiat, D., Johnson, B. a., Sutherland, L. B., Qi, X., Richardson, J. a., Kelm, R. J., and Olson, E. N. A family of microRNAs encoded by myosin genes governs myosin expression and muscle performance. *Developmental cell 17*, 5 (2009), 662–73.

[406] van Rooij, E., Sutherland, L. B., Liu, N., Williams, A. H., McAnally, J., Gerard, R. D., Richardson, J. a., and Olson, E. N. A signature pattern of stress-responsive microRNAs that can evoke cardiac hypertrophy and heart failure. *Proceedings of the National Academy of Sciences of the United States of America 103*, 48 (2006), 18255–60.

[407] van Rooij, E., Sutherland, L. B., Qi, X., Richardson, J. a., Hill, J., and Olson, E. N. Control of stress-dependent cardiac growth and gene expression by a microRNA. *Science (New York, N.Y.) 316*, 5824 (2007), 575–9.

[408] van Rooij, E., Sutherland, L. B., Thatcher, J. E., DiMaio, J. M., Naseem, R. H., Marshall, W. S., Hill, J. a., and Olson, E. N. Dysregulation of microRNAs after myocardial infarction reveals a role of miR-29 in cardiac fibrosis. *Proceedings of the National Academy of Sciences of the United States of America 105*, 35 (2008), 13027–32.

[409] van Rossum, G., and de Boer, J. Interactively Testing Remote Servers Using the Python Programming Language. In *CWI Quarterly*. Amsterdam, 1991, pp. 283–303.

[410] Vasudevan, S. Functional validation of microRNA-target RNA interactions. *Methods (San Diego, Calif.) 58*, 2 (2012), 126–34.

[411] Vaucheret, H. Post-transcriptional small RNA pathways in plants: mechanisms and regulations. *Genes & development 20*, 7 (2006), 759–71.

[412] Vella, M. C., Choi, E.-Y., Lin, S.-Y., Reinert, K., and Slack, F. J. The C. elegans microRNA let-7 binds to imperfect let-7 complementary sites from the lin-41 3'UTR. *Genes & development 18*, 2 (2004), 132–7.

[413] Wagenmakers, A. J., Reinders, R. J., and van Venrooij, W. J. Cross-linking of mRNA to proteins by irradiation of intact cells with ultraviolet light. *European journal of biochemistry / FEBS 112*, 2 (1980), 323–30.

[414] Walker, G. C., Uhlenbeck, O. C., Bedows, E., and Gumport, R. I. T4-induced RNA ligase joins single-stranded oligoribonucleotides. *Proceedings of the National Academy of Sciences of the United States of America 72*, 1 (1975), 122–6.

[415] Wang, E. T., Sandberg, R., Luo, S., Khrebtukova, I., Zhang, L., Mayr, C., Kingsmore, S. F., Schroth, G. P., and Burge, C. B. Alternative isoform regulation in human tissue transcriptomes. *Nature 456*, 7221 (2008), 470–6.

[416] Wang, G.-K., Zhu, J.-Q., Zhang, J.-T., Li, Q., Li, Y., He, J., Qin, Y.-W., and Jing, Q. Circulating microRNA: a novel potential biomarker for early diagnosis of acute myocardial infarction in humans. *European heart journal 31*, 6 (2010), 659–66.

[417] Wang, T., Xie, Y., and Xiao, G. dCLIP: a computational approach for comparative CLIP-seq analyses. *Genome biology 15*, 1 (2014), R11.

[418] Wang, X., and Wang, X. Systematic identification of microRNA functions by combining target prediction and expression profiling. *Nucleic acids research 34*, 5 (2006), 1646–52.

[419] Wang, Y., Juranek, S., Li, H., Sheng, G., Tuschl, T., and Patel, D. J. Structure of an argonaute silencing complex with a seed-containing guide DNA and target RNA duplex. *Nature 456*, 7224 (2008), 921–6.

[420] Wang, Y., Sheng, G., Juranek, S., Tuschl, T., and Patel, D. J. Structure of the guide-strand-containing argonaute silencing complex. *Nature 456*, 7219 (2008), 209–13.

[421] Wang, Z. *MicroRNA Interference Technologies*. Springer Berlin Heidelberg, Berlin, Heidelberg, 2009.

[422] Wang, Z., Gerstein, M., and Snyder, M. RNA-Seq: a revolutionary tool for transcriptomics. *Nature reviews. Genetics 10*, 1 (2009), 57–63.

[423] Wang, Z., Kayikci, M., Briese, M., Zarnack, K., Luscombe, N. M., Rot, G., Zupan, B., Curk, T., and Ule, J. iCLIP Predicts the Dual Splicing Effects of TIA-RNA Interactions. *PLoS Biology 8*, 10 (2010), 16.

[424] Wells, S. E., Hillner, P. E., Vale, R. D., and Sachs, a. B. Circularization of mRNA by eukaryotic translation initiation factors. *Molecular cell 2*, 1 (1998), 135–40.

[425] Wienholds, E., Koudijs, M. J., van Eeden, F. J. M., Cuppen, E., and Plasterk, R. H. a. The microRNA-producing enzyme Dicer1 is essential for zebrafish development. *Nature genetics 35*, 3 (2003), 217–8.

[426] Wightman, B., Ha, I., and Ruvkun, G. Posttranscriptional regulation of the heterochronic gene lin-14 by lin-4 mediates temporal pattern formation in C. elegans. *Cell 75*, 5 (1993), 855–62.

[427] Winter, J., Jung, S., Keller, S., Gregory, R. I., and Diederichs, S. Many roads to maturity: microRNA biogenesis pathways and their regulation. *Nature cell biology 11*, 3 (2009), 228–34.

[428] Witkos, T. M., Koscianska, E., and Krzyzosiak, W. J. Practical Aspects of microRNA Target Prediction. *Current molecular medicine 11*, 2 (2011), 93–109.

[429] Wu, L., and Belasco, J. G. Let me count the ways: mechanisms of gene regulation by miRNAs and siRNAs. *Molecular cell 29*, 1 (2008), 1–7.

[430] Wu, L., Fan, J., and Belasco, J. G. Importance of translation and nonnucleolytic ago proteins for on-target RNA interference. *Current biology : CB 18*, 17 (2008), 1327–32.

[431] Wurdinger, T., and Costa, F. F. Molecular therapy in the microRNA era. *The pharmacogenomics journal 7*, 5 (2007), 297–304.

[432] Xiao, F., Zuo, Z., Cai, G., Kang, S., Gao, X., and Li, T. miRecords: an integrated resource for microRNA-target interactions. *Nucleic acids research 37*, Database issue (2009), D105–10.

[433] Yan, K. S., Yan, S., Farooq, A., Han, A., Zeng, L., and Zhou, M.-M. Structure and conserved RNA binding of the PAZ domain. *Nature 426*, 6965 (2003), 468–74.

[434] Yang, J.-H., Li, J.-H., Shao, P., Zhou, H., Chen, Y.-Q., and Qu, L.-H. starBase: a database for exploring microRNA-mRNA interaction maps from Argonaute CLIP-Seq and Degradome-Seq data. *Nucleic acids research 39*, Database issue (2011), D202–9.

[435] Yao, B., Li, S., Lian, S. L., Fritzler, M. J., and Chan, E. K. L. Mapping of Ago2-GW182 functional interactions. *Methods in molecular biology (Clifton, N.J.) 725* (2011), 45–62.

[436] Ye, Y., Hu, Z., Lin, Y., Zhang, C., and Perez-Polo, J. R. Downregulation of microRNA-29 by antisense inhibitors and a PPAR-gamma agonist protects against myocardial ischaemia-reperfusion injury. *Cardiovascular research 87*, 3 (2010), 535–44.

[437] Yekta, S., Shih, I.-H., and Bartel, D. P. MicroRNA-directed cleavage of HOXB8 mRNA. *Science (New York, N.Y.) 304*, 5670 (2004), 594–6.

[438] Yi, R., Qin, Y., Macara, I. G., and Cullen, B. R. Exportin-5 mediates the nuclear export of pre-microRNAs and short hairpin RNAs. *Genes & development 17*, 24 (2003), 3011–6.

[439] Yigit, E., Batista, P. J., Bei, Y., Pang, K. M., Chen, C.-C. G., Tolia, N. H., Joshua-Tor, L., Mitani, S., Simard, M. J., and Mello, C. C. Analysis of the C. elegans Argonaute family reveals that distinct Argonautes act sequentially during RNAi. *Cell 127*, 4 (2006), 747–57.

[440] Yin, S., Ho, C. K., and Shuman, S. Structure-function analysis of T4 RNA ligase 2. *The Journal of biological chemistry 278*, 20 (2003), 17601–8.

[441] Zagordi, O., Klein, R., Däumer, M., and Beerenwinkel, N. Error correction of next-generation sequencing data and reliable estimation of HIV quasispecies. *Nucleic acids research 38*, 21 (2010), 7400–9.

[442] Zekri, L., Huntzinger, E., Heimstädt, S., and Izaurralde, E. The silencing domain of GW182 interacts with PABPC1 to promote translational repression and degradation of microRNA targets and is required for target release. *Molecular and cellular biology 29*, 23 (2009), 6220–31.

[443] Zhang, C., and Darnell, R. B. Mapping in vivo protein-RNA interactions at single-nucleotide resolution from HITS-CLIP data. *Nature biotechnology 29*, 7 (2011), 607–14.

[444] Zhang, L., Ding, L., Cheung, T. H., Dong, M.-Q., Chen, J., Sewell, A. K., Liu, X., Yates, J. R., and Han, M. Systematic identification of C. elegans

miRISC proteins, miRNAs, and mRNA targets by their interactions with GW182 proteins AIN-1 and AIN-2. *Molecular cell 28*, 4 (2007), 598–613.

[445] Zhang, Y., Zhang, X.-O., Chen, T., Xiang, J.-F., Yin, Q.-F., Xing, Y.-H., Zhu, S., Yang, L., and Chen, L.-L. Circular intronic long noncoding RNAs. *Molecular cell 51*, 6 (2013), 792–806.

[446] Zhao, Y., Ransom, J. F., Li, A., Vedantham, V., von Drehle, M., Muth, A. N., Tsuchihashi, T., McManus, M. T., Schwartz, R. J., and Srivastava, D. Dysregulation of cardiogenesis, cardiac conduction, and cell cycle in mice lacking miRNA-1-2. *Cell 129*, 2 (2007), 303–17.

[447] Zhao, Y., Samal, E., and Srivastava, D. Serum response factor regulates a muscle-specific microRNA that targets Hand2 during cardiogenesis. *Nature 436*, 7048 (2005), 214–20.

[448] Zhuang, F., Fuchs, R. T., Sun, Z., Zheng, Y., and Robb, G. B. Structural bias in T4 RNA ligase-mediated 3'-adapter ligation. *Nucleic acids research 40*, 7 (2012), e54.

[449] Zimmer, H.-g. The Isolated Perfused Heart and Its Pioneers. *News in physiological sciences : an international journal of physiology produced jointly by the International Union of Physiological Sciences and the American Physiological Society 13*, August (1998), 203–210.

[450] Zisoulis, D. G., Lovci, M. T., Wilbert, M. L., Hutt, K. R., Liang, T. Y., Pasquinelli, A. E., and Yeo, G. W. Comprehensive discovery of endogenous Argonaute binding sites in Caenorhabditis elegans. *Nature structural & molecular biology 17*, 2 (2010), 173–9.